Bond of Reinforcing Bars to Steel Fiber Reinforced Concrete (SFRC)

Emilio José García Taengua

SUPERVISORS:
Dr. Pedro Serna Ros
Dr. José Rocío Martí Vargas

UNIVERSITAT POLITÈCNICA DE VALÈNCIA

Universitat Politècnica de València (Spain)

September 2013

Index

BOND OF REINFORCING BARS TO SFRC

Abstract, Resum, Resumen

Abstract

Abstract, Resum, Resumen

ABSTRACT

Abstract [English]

The use of steel fiber reinforced concrete (SFRC hereafter) is becoming more and more common. Building codes and recommendations are gradually including the positive effect of fibers on mechanical properties of concrete. How to take advantage of the higher ductility and energy absorption capacity of SFRC to reduce anchorage lengths when using fibers is not a straightforward issue.

Fibers improve bond performance because they confine reinforcement (playing a similar role to that of transverse reinforcement). Their impact on bond performance of concrete is really important in terms of toughness/ductility.

The study of previous literature has revealed important points of ongoing discussion regarding different issues, especially the following: a) whether the effect of fibers on bond strength is negligible or not, b) whether the effect of fibers on bond strength is dependent on any other factors such as concrete compressive strength or concrete cover, c) quantifying the effect of fibers on the ductility of bond failure (bond toughness). These issues have defined the objectives of this thesis.

A modified version of the Pull Out Test (POT hereafter) has been selected as the most appropriate test for the purposes of this research. The effect of a number of factors on bond stress–slip curves has been analyzed. The factors considered are: concrete compressive strength (between 30 MPa and 50 MPa), rebar diameter (between 8 mm and 20 mm), concrete cover (between 30 mm and 5 times rebar diameter), fiber content (up to 70 kg/m^3), and fiber slenderness and length.

The experimental program has been designed relying on the principles of statistical Design Of Experiments. This has allowed to select a reduced

number of combinations to be tested without any bias or loss of accuracy. A total of 81 POT specimens have been produced and tested.

An accurate model for predicting the mode of bond failure has been developed. It relates splitting probability to the factors considered. It has been proved that increasing fiber content restrains the risk of splitting failure. The favorable effect of fibers when preventing splitting failures has been revealed to be more important for higher concrete compressive strength values. Higher compressive strength values require higher concrete cover/diameter ratios for splitting failure to be prevented. Fiber slenderness and fiber length modify the effect of fiber content on splitting probability and therefore on minimum cover/diameter ratios required to prevent splitting failures. Two charts have been developed for estimating the minimum cover/ diameter ratio required to prevent splitting.

Predictive equations have been obtained for estimating bond strength and areas under the bond stress–slip curve as a function of the factors considered. Increasing fiber content has a slightly positive impact on bond strength, which is mainly determined by concrete compressive strength. On the contrary, fibers have a very important effect on the ductility of bond failure, just as well as concrete cover, as long as no splitting occurs.

Multivariate analysis has proved that bond stress corresponding to the onset of slippage behaves independently from the rest of the bond stress–slip curve. The effect of fibers and concrete compressive strength on bond stress values corresponding to the onset of slips is mainly attributable to their influence on the material mechanical properties. On the contrary, the effect of fibers and concrete cover on the rest of the bond stress–slip curve is due to their structural role.

Resum [Valencià]

La utilització del formigó reforçat amb fibres d'acer (SFRC d'ara endavant) és cada cop més habitual. La normativa i les recomanacions per al càlcul d'estructures de formigó estan introduint progressivament l'efecte positiu que tenen les fibres sobre les propietats mecàniques del formigó. Com aprofitar la major ductilitat i capacitat d'absorció d'energia del material per reduir les longituds d'ancoratge quan s'utilitzen fibres no és una qüestió evident.

Les fibres milloren la capacitat adherent del formigó perquè confinen l'armadura (jugant un paper semblant al de l'armadura transversal). El seu impacte sobre el comportament adherent del formigó és molt important sobretot quant a la ductilitat.

L'estudi de la literatura prèvia ha revelat punts clau on la discussió encara continua, especialment els següents: a) si l'efecte de les fibres sobre la tensió màxima d'adherència és o no negligible; b) si aquest efecte és o no independent del d'altres factors, com ara la resistència a compressió del formigó o el recobriment; c) la quantificació de l'efecte de les fibres sobre la ductilitat de l'esgotament de la capacitat adherent. Aquests aspectes han delimitat els objectius d'aquesta tesi.

Una versió modificada de l'assaig d'arrancament s'ha fet servir per haver-se vist que era el més adient als propòsits d'aquesta tesi. S'ha analitzat l'efecte d'una sèrie de factors sobre la corba tensió-lliscament. Els factors considerats han estat: resistència a compressió del formigó (entre 30 MPa i 50 MPa), diàmetre de l'armadura (entre 8 mm i 20 mm), recobriment (entre 30 mm i 5 vegades el diàmetre de l'armadura), el contingut en fibres (fins a 70 kg/m^3), i l'esbeltesa i longitud de les fibres.

El programa experimental s'ha dissenyat seguint els principis del disseny estadístic d'experiments. Això ha permés seleccionar un nombre reduït d'assajos a dur a terme en lloc de provar totes les combinacions possibles, i sense pèrdua de confiabilitat en les conclusions. S'han fabricat i assajat un total de 81 provetes d'arrancament.

S'ha formulat un model molt acurat per la predicció del mode d'esgotament per adherència. Aquest model relaciona la probabilitat de *splitting* amb els factors que s'han considerat. S'ha provat que augmentar el contingut en fibras redueix el risc de *splitting*. Aquest efecte favorable de les fibres adquireix major importància per a valors elevats de la resistència a compressió del formigó. Així, com més elevada siga la resistència a compressió, es necessita major relació recobriment/diàmetre per evitar que hi haja *splitting*. S'han desenvolupat dos àbacs per facilitar l'estimació de les relacions recobriment/diàmetre mínimes en cada cas per evitar que hi haja *splitting*.

S'han obtés equacions predictives per estimar la tensió màxima d'adherència i les àrees sota la corba tensió-lliscament en funció dels factors considerats. S'ha detectat que l'augment del contingut en fibres té un efecte moderat sobre la tensió màxima d'adherència, que està principalment determinada per la resistència a compressió. Per contra, les fibres tenen un efecte molt important sobre la ductilitat de l'esgotament de la capacitat adherent, igual que el recobriment, quan no hi ha *splitting*.

L'anàlisi multivariat de les corbes experimentals ha provat que la tensió corresponent a l'inici de lliscaments es comporta de forma independent a la resta de la corba tensió-lliscament. L'efecte de les fibres i la resistència a compressió sobre l'inici de lliscaments és atribuïble a la seua influència sobre les propietats del material. Per contra, l'efecte de les fibres i el recobriment sobre la resta de la corba tensió-lliscament és deguda a la seua contribució estructural.

Resumen [Español]

La utilización del hormigón reforzado con fibras de acero (en adelante, SFRC) es cada vez más habitual. La normativa y las recomendaciones constructivas para el cálculo de estructuras de hormigón están introduciendo progresivamente el efecto positivo que tienen las fibras sobre las propiedades mecánicas del hormigón. Cómo aprovechar la mayor ductilidad y capacidad de absorción de energía del material para reducir las longitudes de anclaje cuando se usan fibras no es una cuestión evidente.

Las fibras mejoran la capacidad adherente del hormigón porque confinan la armadura (jugando un papel parecido al del armado transversal). Su impacto sobre el comportamiento adherente del hormigón es muy importante en términos de ductilidad.

El estudio de la literatura previa ha revelado puntos clave donde la discusión sigue, especialmente los siguientes: a) si el efecto de las fibras sobre la tensión máxima de adherencia es o no despreciable; b) si este efecto es o no independiente del de otros factores, como la resistencia a compresión del hormigón o el recubrimiento; c) la cuantificación del efecto de las fibras sobre la ductilidad del fallo por adherencia. Estos aspectos han delimitado los objetivos de esta tesis.

Se ha recurrido a una versión modificada del ensayo de arrancamiento porque ha resultado la más adecuada a los propósitos de esta tesis. Se ha analizado el efecto de una serie de factores sobre la curva tensión adherente–deslizamiento. Los factores considerados han sido: resistencia a compresión del hormigón (entre 30 y 50 MPa), diámetro de la armadura (entre 8 mm y 20 mm), recubrimiento mecánico (entre 30 mm y 5 veces el diámetro de la armadura), el contenido en fibras (hasta 70 kg/m^3), y la esbeltez y longitud de las fibras.

El programa experimental se ha diseñado siguiendo los principios del diseño estadístico de experimentos. Esto ha permitido seleccionar un número reducido de ensayos a realizar en lugar de probar todas las combinaciones posibles, y sin pérdida de fiabilidad en las conclusiones. En total, se han fabricado y ensayado 81 probetas de arrancamiento.

Se ha formulado un modelo preciso para la predicción del modo de fallo por adherencia. Este modelo relaciona la probabilidad de estallido del recubrimiento con los factores considerados. Se ha probado que aumentar el contenido en fibras reduce el riesgo de estallido. Este efecto favorable de las fibras adquiere mayor importancia para valores elevados de la resistencia a compresión del hormigón. Así, cuanto mayor sea la resistencia a compresión del hormigón, mayor es la relación recubrimiento/diámetro necesaria para evitar el estallido del recubrimiento. Se han desarrollado dos ábacos que facilitan la estimación de los valores mínimos de la relación recubrimiento/diámetro para evitar el estallido del recubrimiento.

Se han obtenido ecuaciones predictivas para estimar la tensión máxima de adherencia y las áreas bajo la curva tensión adherente–deslizamiento en función de los factores considerados. Se ha detectado que el aumento del contenido en fibras tiene un efecto moderado sobre la tensión máxima de adherencia, básicamente determinada por la resistencia a compresión. Por el contrario, las fibras tienen un efecto muy importante sobre la ductilidad del fallo por adherencia, al igual que el recubrimiento, cuando no se da estallido del recubrimiento.

El análisis multivariante aplicado a las curvas experimentales ha probado que la tensión adherente correspondiente al inicio de deslizamientos en el extremo libre se comporta de forma independiente del resto de la curva. El efecto de las fibras y la resistencia a compresión sobre esta tensión se atribuye a su influencia sobre las propiedades del material. Por el contrario, el efecto de las fibras y el recubrimiento sobre el resto de la curva tensión adherente–deslizamiento se debe básicamente a su contribución en el plano estructural.

0| Introduction and Objectives

0| Introduction and Objectives

0.1 Background

Fibers have a positive effect on bond of reinforcement to concrete, even when low fiber contents are considered (Cairns & Plizzari 2004). Building codes and recommendations are gradually including the positive effect of fibers on mechanical properties of concrete. The Spanish code for structural concrete EHE-08 explicitly states that fibers improve bond capacity of concrete and that this can be taken into account when designing anchors and splices. Similar statements are found in the recommendations by other organisms (ACI-ASCE 2003, ACI 2011).

However, the positive effect of fibers is acknowledged but is not always explicitly introduced in formulations for anchorage/splice lengths. Considering that the use of non-conventional concretes, including steel fiber reinforced concrete (SFRC hereafter), is becoming more and more common (Serna et al. 2009, Shah & Ribakov 2011), it is likely that anchorage lengths are higher than necessary in most of the cases. How to take advantage of the higher ductility and energy absorption capacity of SFRC to reduce anchorage lengths when using fibers is not a straightforward issue. In this sense, several studies have been performed attempting to model the bond phenomenon and anchorage behavior in general (among the most significant ones: Darwin et al. 1996, Lundgren et al. 2000, Harajli et al. 2002, Russo et al. 2006, Russo et al. 2009, Tastani et al. 2009, Harajli et al. 2009, Cattaneo et al. 2009).

Fibers improve bond performance because they confine reinforcement (playing a similar role to that of the transverse reinforcement) and because they broaden the range of crack width values within which passive confinement remains active (Cairns & Plizzari 2004, Holschemacher & Weisse 2004). Although it is true that their influence on bond strength is of little importance, improvements in bond performance

of concrete are really important in terms of toughness/ductility of the material (García-Taengua et al. 2011, Dancygier & Katz 2011).

However, there are many aspects that call for continuing research effort in this area. For example, improvements in toughness/ductility of bond failure that are obtained by using fibers in concrete have not been quantified or dissociated from the effect of other factors such as compressive strength or the rebar diameter.

A central issue is whether the effect of fibers on bond depends on concrete compressive strength. In most of the studies only one or two variables are considered and their effect on bond is analyzed in a one-to-one fashion, without investigating if there is any synergy between them. It would be interesting, for example, to find out whether the effect of fibers on bond performance is the same regardless of the diameter of the rebar being anchored. In fact, there is some confusion in literature regarding the effect of rebar diameter on bond, since larger diameters increase the tendency to concrete cover splitting. Thus, another important issue is the study of the relationship between the presence of fibers and the concrete cover needed to prevent splitting failures. In fact, the effect of fibers on bond when there is splitting of the concrete cover proves to be very important (Harajli et al. 1995, 2002). On the contrary, it is not so important when concrete cover splitting does not occur: under such circumstances fibers affect bond failure ductility but not bond strength. The study how fibers determine mode of bond failure (if they do so), and how they are related to concrete compressive strength and rebar diameter in terms of probability that no cover splitting occurs are issues that have not been addressed in literature yet.

0.2 Objectives

- ☐ Deepening the knowledge of the phenomena involved in bond of reinforcement to Steel Fiber Reinforced Concrete, especially regarding the role of fibers in relation to cover splitting and its prevention.
- ☐ Carrying out an extensive experimental campaign comprising Pull Out Tests which entails a significant contribution to the corpus of experimental results available to the scientific community, aiming at the continuity of research on bond.
- ☐ Studying the effect of the factors considered (fiber geometry and content, concrete compressive strength, concrete cover, and rebar diameter) on bond capacity of concrete and on the ductility of bond failure.
- ☐ Studying the effect of fiber geometry, fiber content, and concrete compressive strength on minimum cover values needed to prevent splitting failures.
- ☐ Obtaining analytical expressions which prove useful to estimate bond strength and bond toughness as well as the splitting probability in terms of the factors considered.
- ☐ Applying the techniques of multivariate analysis to study the effect of the factors considered on bond stress–slip behavior.

1 | Steel Fiber Reinforced Concrete: an Introduction

Part I: State of the Art

1 | Steel Fiber Reinforced Concrete: an Introduction

PART I: STATE OF THE ART

1.1 Background

The Report on Fiber Reinforced Concrete reapproved in 2002 by the ACI Committee 544 (ACI 544.1R-96 hereafter), as well as some authors (like Naaman 2008) have outlined the history of developments leading to fiber reinforced concretes as they are nowadays.

The first serious studies assessing steel fibers potential as concrete reinforcement appeared in the 1960s. Since then, a very important research activity has been carried out on what eventually came to be known as steel fiber reinforced concrete (SFRC hereafter). Indeed their being used has generalized in such a way that talking of a large degree of introduction of SFRCs in construction is totally realistic.

Many properties of concrete are improved by fibers: compressive strength, tensile strength and behavior, fatigue behavior, cracking control, impact resistance, and fire resistance, among many others.

However, SFRCs have long been included in the category of 'special concretes' and this restricted their use to non-structural applications for years. As Di Prisco et al. (2009) point out, the use of SFRC for structural applications is still very limited with respect to its potentials (although it is continuously increasing) mainly due to the lack of international building codes for SFRC structural elements. Such situation has been particularly remarkable in Spain, where we are used to rely on official construction codes whose observance is a legal requirement.

For some years now SFRCs are being introduced in new codes and this is contributing to potentiate their use with a structural purpose in concrete members, i.e. partially or totally replacing the reinforcement. The Spanish code for structural concrete in its latest version (EHE-08 hereafter)

includes a specific appendix devoted in its entirety to fiber reinforced concretes, the *Appendix 14. Recommendations for the use of fiber reinforced concrete* (EHE-08 App. 14 hereafter). And ACI 318-11 code mentions fibers not in a separate and specific appendix but in some articles and commentaries throughout the text.

1.2 Definitions and General Aspects

EHE-08 App. 14 defines fiber reinforced concrete as any concrete including short, discrete and randomly distributed fibers, and allows their being used in general: in mass concrete, reinforced concrete, and prestressed concrete. Similarly, ACI 544.1R-96 defines fiber reinforced concrete as any 'concrete made primarily of hydraulic cements, aggregates, and discrete reinforcing fibers'.

Fibers are short elements with a small cross-section that can be randomly dispersed within the fresh concrete by means of conventional mixing techniques. They can be made with different materials (Figure 1.1). Although EHE-08 App. 14 mentions steel fibers, polymer fibers, and other inorganic fibers (like glass fibers), and states that the approach is general for all types of fibers, it underlines that the corpus of knowledge on which all expressions and provisions are based upon is that of steel fibers, these being the most usual type both in research and in applications. ACI 544.1R-96 defines steel fibers intended for reinforcing concrete as 'short, discrete lengths of steel having an aspect ratio (ratio of length to diameter) between 20 and 100, with any of several cross-sections, and that are sufficiently small to be randomly dispersed in an unhardened concrete mixture using usual mixing procedures'.

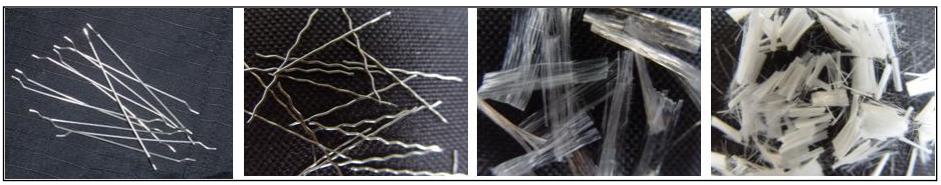

Figure 1.1. Different types of fibers. From left to right: steel (hook-end wire and deformed); polypropylene; poliester.

Fiber contents are referred to in terms of volume percentage or kilograms per cubic metre of concrete, kg/m^3. In the case of steel fibers, the approximate equivalence is 1% in volume = 78 kg/m^3.

Usually the distinction between microfibers and macrofibers is made (Rossi 1998). Microfibers are those whose diameter is not greater than 0.30 mm, and whose length is not greater than 10-12 mm. Macrofibers are those whose diameter is 0.30 mm or more, and whose length is greater than 10-12 mm.

Relatively new approaches in literature are concerned with SFRC varieties that require more specific definitions. The most relevant ones are steel fiber reinforced self-compacting concrete (SFRSCC hereafter), hybrid fiber reinforced concrete, and high-strength fiber reinforced concrete (HSFRC hereafter).

SFRSCC combines the advantages of self-compacting concrete (SCC hereafter) in the fresh state and shows an improved performance in the hardened state due to the addition of fibers (Grünewald 2004). Adding fibers to SCC has different implications that may lead to clear technical advantages in terms of the costs/benefits ratio (Pereira et al. 2008). The fluid properties of the fresh SCC formulations are beneficial for the homogeneous dispersion of fibers but, at the same time, steel fibers affect properties of fresh concrete. As a consequence, the design procedure to achieve self-compacting requirements highly depends on fibers content and their geometry. Several authors have studied the optimization of SFRSCC proportioning (Grünewald 2004, Pereira et al. 2008) and how the dispersion of fibers affects (and is affected by) mixture design (Prasanth et al. 2008).

Hybrid fiber reinforced concrete includes two or more types of fiber that make complementary contributions to the performance of a concrete mix (Lawler et al. 2001, 2005). The most usual case is that of a microfiber and macrofiber hybrid fiber reinforced concrete, although there are other possibilities like combining polymer and steel fibers. Such blends have proved to be highly effective at improving the material's performance, particularly strength and toughness, with respect to an equivalent one-type-fiber reinforced concrete with the same fiber

content. In addition to the synergistic effect, microfibers delay the formation of macrocracks and potentiate multiple microcracking instead, thus improving the durability of concrete.

High Strength SFRCs (HSFRCs) or cement reinforced composites when referring to fibered mortars (Aarup & Jensen 1998) are terms that refer to concretes or cementitious composites with high fiber contents, between 2% and 6% in volume. Such contents allow a very remarkable increase of the material's load-bearing capacity but substantially alter their granular skeleton, rheology, and proportioning with respect to SFRCs in general.

1.3 Components and Proportioning

SFRCs are made with the same components than traditional concretes with the exception of steel fibers.

There is only one remark to be made concerning water: seawater cannot be used. Although EHE-08 App. 14 does not provide any special remark about it, art. 27 of EHE-08 states that seawater can be used only for unreinforced concretes. This is not the case in SFRCs, where fibers are indeed a type of reinforcement. The guidelines provided by ACHE (2000) make this same remark.

In relation to fibers, steel fibers are the only ones covered by the scope of this thesis although fibers of different nature can be used as well. It is worth mentioning what Di Prisco et al. (2009) point out regarding the nature of fibers to be used: while high-modulus fibers are the most convenient to substitute (partially or totally) conventional reinforcement, low-modulus short fibers can be used as well to reduce shrinkage cracking and to enhance fire resistance. In fact, this is the case of hybrid fiber reinforced concretes (commented in section 1.2).

One more factor to consider when choosing fibers is their geometry: length, aspect ratio or slenderness (length/diameter), and shape. Fiber shape admits several possibilities (straight, deformed, crimped-end, etc) and has an important influence on bond of fibers to the matrix.

Fiber content mainly depends on the properties intended for SFRC. However, there are minimum and maximum limits to fiber content. According to ACI 544.1R-96, when aspect ratio is less than 50, the minimum fiber content required to have a significant effect on concrete flexural response is 0.5% in volume, i.e. 39 kg/m^3. Similarly EHE-08 App. 14 establishes a minimum fiber content of 20 kg/m^3 if fibers contribution is to be considered in structural calculations. On the other hand, the maximum fibers content is imposed by the workability of fresh concrete. The higher fiber content, the better mechanical properties of hardened concrete, but workability of fresh concrete is seriously affected by increasing fiber contents. The generally accepted upper limit is 100 kg/m^3. Furthermore, fiber contents higher than 100 kg/m^3 importantly affect the granular structure of concrete: this is the reason why EHE-08 App. 14 excludes SFRCs with fibers contents higher than 1.5% in volume (117 kg/m^3) when defining its scope. With all that, fiber contents are most usually between 0.5% and 1.5% in volume.

Adding fibers also affects fresh state behavior of concrete. In consequence, proportioning a SFRC requires certain modifications with respect to that of its unreinforced counterpart. In particular, the maximum aggregate size and the coarse aggregate/sand ratio must be reduced, and more superplasticizer is needed. These modifications are aimed to maintain an acceptable workability when fibers are added to the mix –in order not to hinder the production and casting of concrete.

Maximum aggregate size affects the potential mobility of fibers within the mix and, consequently, the homogeneity of their dispersion, as exemplified in Figure 1.2. It is generally accepted that the optimum value of this parameter should be that of half the length of the fibers used and not greater than 20 mm in any case. Furthermore, river aggregate is better than crushed aggregate, because the former makes the mix more workable than the latter for the same water/cement ratio.

Maximum aggregate size together with fiber content condition the amount of cement required for a certain workability. ACI 544.1R-96 provides usual ranks for proportioning parameters of SFRC depending on maximum aggregate size (Table 1.1). It is worth noting that recommended sand/coarse aggregate ratios for SFRC are bigger than

for conventional concrete. This is due to the needle-shaped geometry of fibers: this requires higher sand contents to maintain the maximum compactness in the granular skeleton.

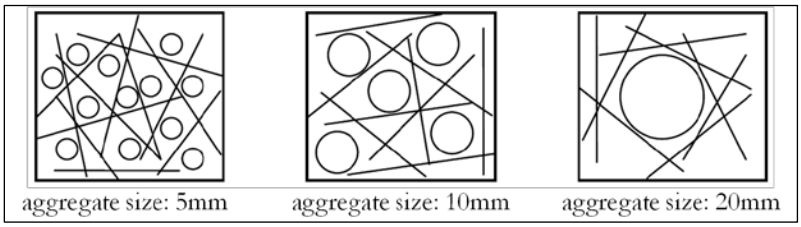

Figure 1.2. Effect of maximum aggregate size in the potential mobility of fibers in fresh concrete.

Table 1.1. Usual ranges for FRC components (ACI 544.1R-96).

Components	Max. aggregate size	
	10 mm	20 mm
Cement (kg/m³)	350-600	300-530
water / cement	0.35-0.45	0.35-0.50
sand / coarse aggr.	0.45-0.60	0.45-0.55
V_f (hooked-end)	0.4-1.0	0.3-0.8
V_f (plain)	0.8-2.0	0.6-1.6

Concerning superplasticizers, their use does not withdraw the need of controlling the amount of fibers added: balls of fibers are likely to form even when superplasticizers are used. Preliminary testing is always required with SFRC, as EHE-08 App. 14 states.

With respect to the volume of paste related to total volume, the usual range between 25% and 35% is increased to 30%-40% for SFRC in order to maintain the same workability. In consequence, SFRCs require greater powder contents. In particular, cement content is usually between 300 kg/m³ and 450 kg/m³.

Among the additions used with FRCs, the most usual ones are fly ash and silica fume. Both of them have a pozzolanic nature but, most importantly, they act as correctors of powders content as well. It has been shown that the beneficial effect of silica fume upon FRCs properties is mainly exercised through the improvement of the interfacial bond of fibers to

the hydrated cement matrix (see, for instance, Uygunoglu 2008). Usual contents (in percentage over cement weight) range between 4% and 8% for silica fume and between 20% and 35% for fly ash.

1.4 Fibers Contribution to Concrete Behavior

Talking about fibers contribution to concrete performance is generally referred to mechanical properties in opposition to their use with other purposes like the control of shrinkage cracking or the improvement of fire resistance. EHE-08 App. 14 states that fibers are used with a structural purpose when their contribution to concrete properties is taken into account in calculations concerning ultimate limit states or serviceability limit states, thus allowing the partial or total reduction of traditional reinforcement.

Di Prisco et al. (2009) have made some interesting remarks concerning the use of fibers with structural purposes. In relation to the possibility of reducing traditional reinforcement, they recall the need of structural redundancy: such reduction will be more important in structures with high degrees of redundancy.

It is important to bear in mind that fibers are not expected to modify the behavior of uncracked elements since fiber reinforcement mechanisms are mainly activated through crack development. As a matter of fact, in the uncracked state SFRC can be assumed to be a homogeneous and isotropic material (Di Prisco et al. 2009), while this assumption is totally untrue in the cracked state.

In the cracked state the effect of fibers is very significant and, according to Rossi (1998), must be regarded at two levels: non-structurally and structurally. The non-structural contribution of fibers is mainly exercised by short fibers and is related to their sewing effect, thus preventing crack widening and propagation. This effect is clearly related to serviceability limit states and is involved in situations like shrinkage microcracking or the first stages of tensile or flexural response. Under these circumstances

fibers bear stress resulting from non-structural phenomena –not directly related to the load-carrying capacity of the material. On the contrary, the structural contribution of fibers begins when microcracks develop further and cracks appear, then the load-carrying responsibility is partially or totally transferred to fibers. Under such circumstances, long fibers not only benefit durability (the sewing action of fibers favours multicracking and allows minimal crack widths) but significantly co-operate in carrying loads. This is the case of fibers contribution to the performance of members under tension or bending (Figure 1.3).

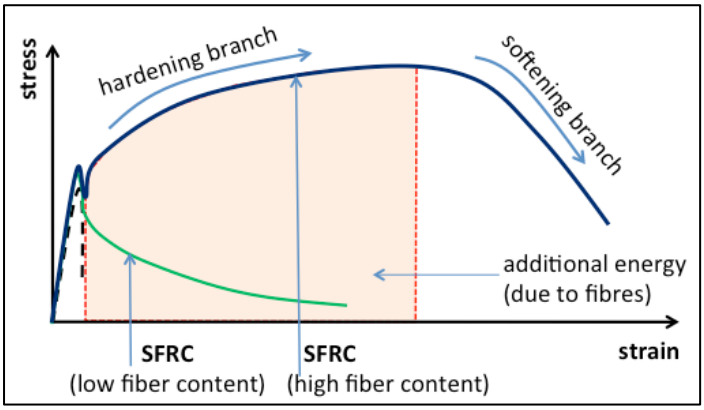

Figure 1.3. Structural contribution of fibers to flexural behavior.

Figure 1.3 shows the flexural stress-strain curves for two different fiber contents. The dotted line, which corresponds to the unreinforced concrete, shows a brittle failure once the cracking load is reached. The green line corresponds to SFRC with a relatively low fiber content: there is no such brittle failure but once the first crack occurs, load-carrying capacity is gradually decreased (softening behavior). The blue line represents the behavior of SFRC with an intermediate or relatively high fiber content: after the cracking load is reached, concrete not only goes on bearing load but fibers make it possible to bear increasing loads (hardening branch) until a maximum stress value (ultimate load) is reached in the postpeak region, which is higher than the cracking load. After that, load-carrying capacity gradually decreases (softening branch). Thanks to the contribution of fibers the material is capable of absorbing a great deal

of additional deformation energy (coloured region under the curve) when compared to its unreinforced countepart.

The frontier between softening behavior and hardening behavior depends on several factors, mainly: fiber geometry, fiber content, and the proportion of short fibers to long fibers (if that is the case). In relation to that, Di Prisco et al. (2009) have pointed out that residual strength (the load-carrying capacity in the postpeak region) depends significantly on the number of fibers crossing active cracks and on their orientation. Fibers are therefore to be selected on the basis of the type of member and the load conditions.

Curves in Figure 1.3 illustrate SFRC flexural response, but similar comments can be made in relation to its tensile behavior. However, the fact that a certain SFRC presents a hardening flexural behavior does not necessarily imply tensile behavior to be hardening as well. In consequence, a distinction is made between a primary classification of SFRCs according to tensile behavior and a secondary classification according to flexural response (Naaman 2008), as shown in Figure 1.4.

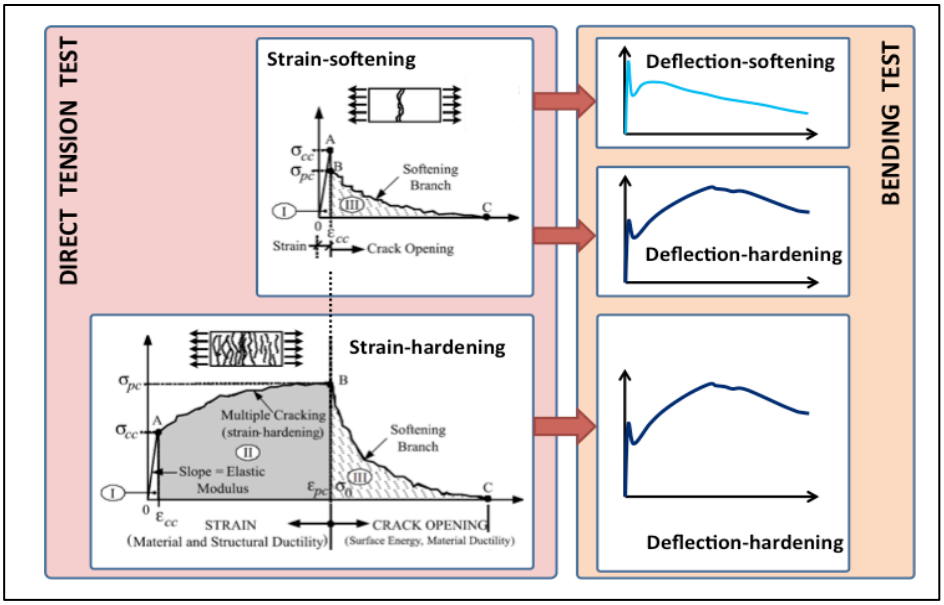

Figure 1.4. Types of tensile response and bending response of SFRCs (adapted from Naaman 2008).

In general terms, it can be said that strain-softening SFRCs exhibit crack localization immediately following first cracking: the critical crack keeps opening while other cracks relax, gradually unload and become narrower. Strain-hardening SFRCs, on the contrary, experience multiple cracking.

Some particular remarks can be made in relation to the contribution of fibers to hybrid SFRC performance (see, for instance, Yun et al. 2007). In a concrete reinforced with long fibers only, the role they play is a structural one and is reflected in the postpeak branch only. On the contrary, in a concrete reinforced with short fibers only, they delay the formation of cracks by preventing the growth of microcracks and therefore the peak load is increased, though slightly. However, once cracks have developed, short fibers are easily pulled out of the matrix and are therefore incapable of working structurally.

In hybrid SFRCs there is a combination of the two aforementioned effects, accompanied by a synergistic component which is not forcefully positive. As short fibers delay the contribution of long fibers, the post-peak region may be slightly affected if short fibers are added to a SFRC with long fibers (Yun et al. 2007), but it will be seriously affected (Figure 1.5) if part of the long fibers are replaced with short fibers (Lawler 2001, Lawler et al. 2005), although in both cases the peak load will be increased due to the presence of short fibers.

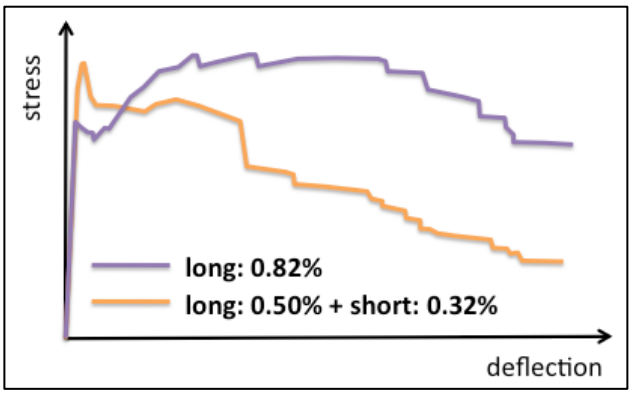

Figure 1.5. Flexural stress-deflection curves for different hybrid SFRCs (adapted from Lawler et al. 2005).

1.5 Fresh State Behavior

Rheology of SFRCs is significantly different from that of unreinforced conventional concretes, even if the fibers content is low. It is true that SFRCs, when the fibers content is low (20 – 30 kg/m^3), can be produced without any modification with respect to the equivalent unreinforced concrete. But when higher amounts of fibers are to be added to concrete, more exigent adjustments are required (as a consequence of the modification of rheology of concrete) to keep workability at proper levels.

The addition of fibers implies a loss of workability which is observed in a reduction of consistency (for instance, lesser slump values). Such loss depends on the fibers content and also on the slenderness of fibers: the higher the aspect ratio is, the more difficult the fibers dispersion. This is due to the tendency for fibers of long length (or small diameter) to cling to one another (Chung 2005).

The desired compromise is clearly the improvement of concrete properties in the hardened state without too much affecting workability. Consistency can be improved by considering the following three options in a balanced way: using superplasticisers; increasing the amount of water; and/or adding extra powders to make the fresh mix more stable, thus avoiding segregation.

The case of SFRSCC is worth mentioning, for the effect of fibers upon the rheology of fresh concrete is of capital importance. As a matter of fact, this particular has attracted a great deal of research interest in the recent years, together with that of dispersion of fibers.

Adding fibers to a SCC takes advantage of self-placeability and rheological stability to achieve a more uniform dispersion of fibers (Shah et al. 2008). However, as Vandewalle et al. (2008) have pointed out, this brings about important consequences: slump flow values decrease, and segregation of fibers is more likely to occur. Concerning this last aspect, Shah et al. (2008) have emphasized the importance of takint into account not only the mix resistance to static segregation of fibers, i.e.

when the mix is at rest, but also its resistance to dynamic segregation of fibers.

Grünewald's work in relation to SFRSCC (2004) has dealt with the rheology of this type of reinforced concrete, but the conclusions he comes to are applicable to SFRCs in general. Given a fiber content, the higher their slenderness, the higher VeBe times are, thus implying less workability. The synergic effect of maximum aggregate size and fiber content is also dealt with. The maximum fiber content that a SFRC mix can admit depends on the maximum aggregate size, if this 'maximum' content is defined as that implying the strongest reduction of consistency. Then, concretes whose maximum aggregate size is 20 mm are not likely to admit fiber contents greater than 4%, while mortars whose maximum aggregate size is 5 mm can admit considerably higher fiber contents, even 8% or 9% in volume.

With respect to this last issue of the maximum fibers content of a SFRC and the possibilities of its determination, different approaches have been proposed by a number of authors. De Larrard (1999) introduced in his Compressible Packing Model the concept of 'perturbation volume', through which the influence of fibers on the packing density of a given solid skeleton can be predicted. The perturbation volume depends on the aggregate particle diameter as well as on fiber content, length, and diameter. Another approach is that followed by Ferrara et al. (2008), who have proposed to perform the grading of the solid particle skeleton for the optimum packing density including fibers as a further aggregate fraction with 100% passing at an equivalent diameter defined through the specific surface area equivalence.

1.6 Compressive Behavior

The most important aspect of concrete compressive behavior is compressive strength, standardized to be measured at the age of 28 days and in cylindrical specimens (standard EN 12390-3:2009). Upon this parameter, the addition of fibers has proved to have a very slight effect. Figures 1.6 and 1.7 show results from different authors that come to this conclusion in relation to the compressive strength of concrete.

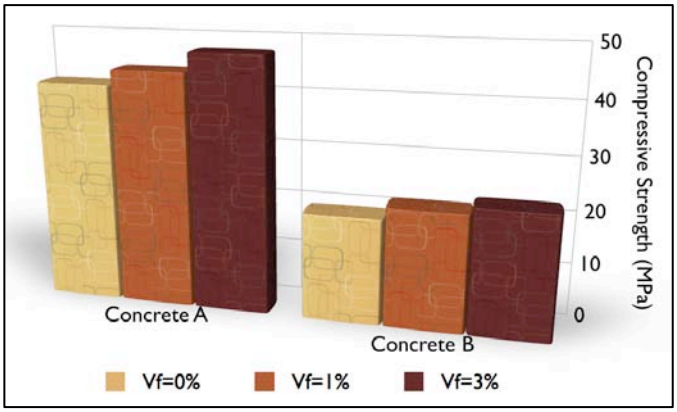

Figure 1.6. Compressive strength of concretes with different fibers contents (adapted from Kovács & Balázs, 2004).

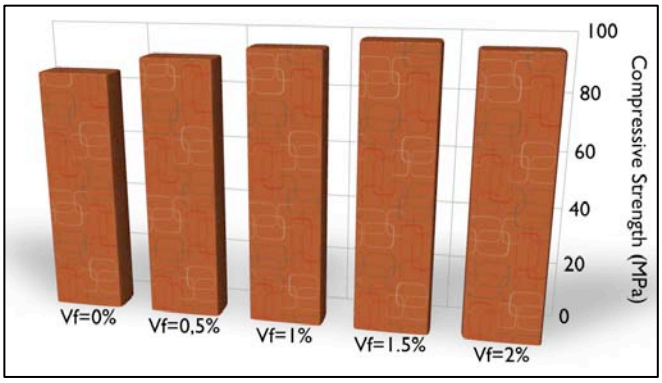

Figure 1.7. Compressive strength of concretes with different fibers contents (adapted from Song & Hwang, 2004).

In Figure 1.6, two concretes are considered, each with a clearly different compressive strength: concrete 'A' (compr. strength of about 40 MPa) and

concrete 'B' (compr. strength of about 20 MPa). As it can be seen, no matter the compressive strength of the unreinforced concrete is, adding fibers increases the compressive strength but no more than 15% when the fibers content is 3% in volume. Similarly, Figures 1.6 and 1.7 show that no concluding difference is observed between SFRCs with different fiber contents when these are not bigger than 2% in volume, or between them and their unreinforced counterparts. Fibers also improve the ductility of concrete in compression, and this is reflected in the slope of the postpeak branch of the curve, which is less step the higher is the fibers content, as can be seen in Figure 1.8.

Compressive behavior of fibered concretes presents certain specificities when two or more types of fibers are used. A good example is that of concretes reinforced with steel fibers and a relatively small amount of polypropylene fibers, what has been called a 'fibers cocktail' by König & Kützing (1999). Figure 1.8 compares the compressive stress-strain curve of a SFRC with 120 kg/m^3 of steel fibers (1.5% in volume) to that of its unreinforced counterpart (compressive strength of 120 MPa). It is observed that the addition of steel fibers increases ductility but rather slightly. But if 2 kg/m^3 of polypropylene fibers are added together with the 120 kg/m^3 of steel fibers, compressive behavior of concrete turns out to be much more ductile, as can be seen in Figure 1.9. The explanation is that polypropylene fibers, a very weak component (Young modulus of about 10,000 MPa), work as initiators of microcracks that spread and absorb energy before steel fibers are brought into play.

However, in low and normal strength concretes this increase in ductility is accompanied by a decrease in compressive strength, as can be seen in Figure 1.10. According to König & Kützing (1999), in low and normal strength concretes the matrix is more porous than in high strength concretes and this contributes to the absorption of energy in the same way polypropylene fibers do and therefore their use is not advantageous any more. Other authors (like Yun et al. 2007) have also observed this negative effect that reinforcement with the so-called fiber cocktails instead of steel fibers only has on the compressive strength of normal strength concretes.

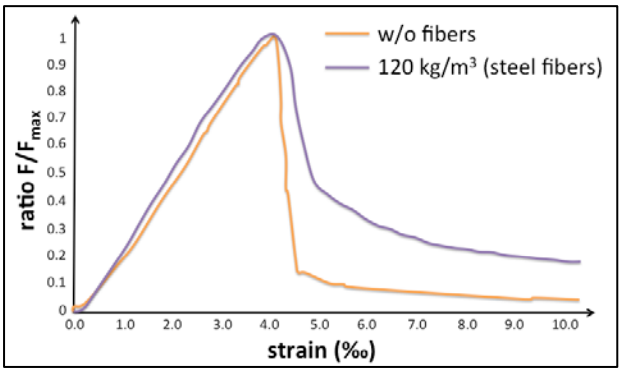

Figure 1.8. Effect of steel fibers on compressive stress-strain curve (adapted from König & Kützing 1999).

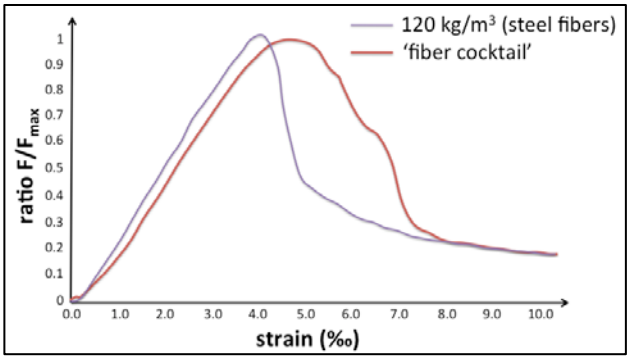

Figure 1.9. Effect of fibers 'cocktail' on compressive stress-strain curve (adapted from König & Kützing 1999).

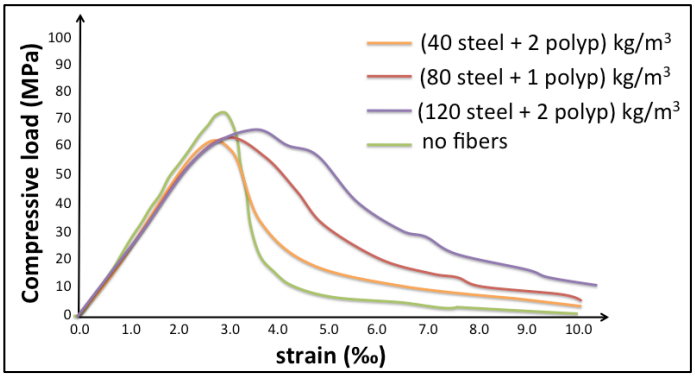

Figure 1.10. Effect of fiber cocktail on concrete compressive stress-strain curve (König & Kützing, 1999).

1.7 Tensile Behavior

According to Suwannakarn et al. (2008), the tensile behavior of a SFRC admits three different possibilities depending on the evolution of the cracking process it experiences with increasing tensile loads:

- Clearly strain-hardening behavior. In this case, a zone of influence develops around the notched section where multiple cracking occurs (Figure 1.11 left). As Naaman (2008) states, the stress-strain curve (Figure 1.11 right) of a strain-hardening SFRC starts with a step initial ascending branch up to the strain that corresponds to the occurrence of the first percolation crack. This is followed by a strain-hardening branch where multiple cracking develops. The end of this hardening branch leads to the maximum post-cracking stress, post-peak stress or, simply, the ultimate stress. At this point, one crack becomes critical and defines the onset of crack localization. Thereafter, the load-carrying capacity of the material drops gradually. No more cracks develop and only the critical crack will go on opening under increased straining while the others gradually unload and become narrower in width.

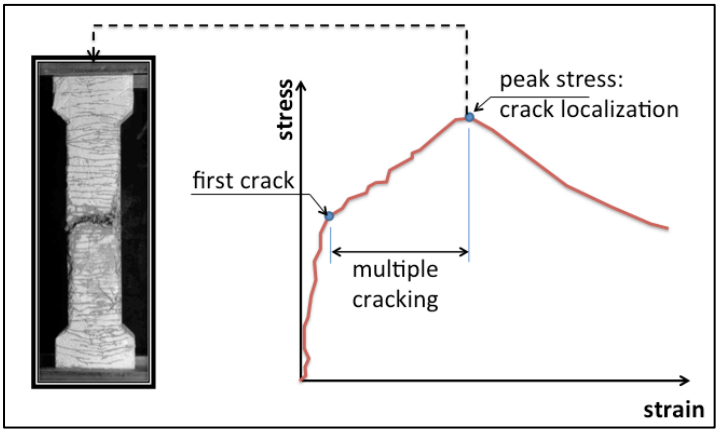

Figure 1.11. Clearly strain hardening behavior and specimen after failure (adapted from Naaman 2008).

- Clearly strain-softening behavior. The specimen shows a single localized crack instead of a zone where multiple cracking occurs

(Figure 1.12 right). In terms of the stress-strain curve (Figure 1.12 left), post-cracking load-carrying capacity drops significantly after the first crack.

☐ Transition behaviors (neither strain-softening nor strain-hardening). According to Suwannakarn et al. (2008), two more possibilities exist that may be referred to as transition cases, as shown in Figure 1.13.

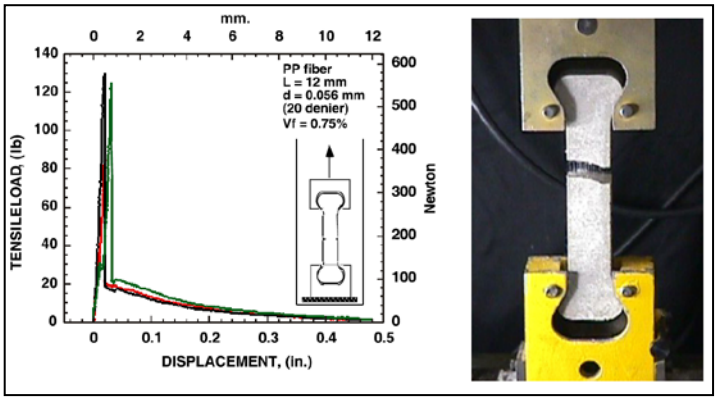

Figure 1.12. Clearly strain softening behavior and specimen after failure (source: Naaman 2008).

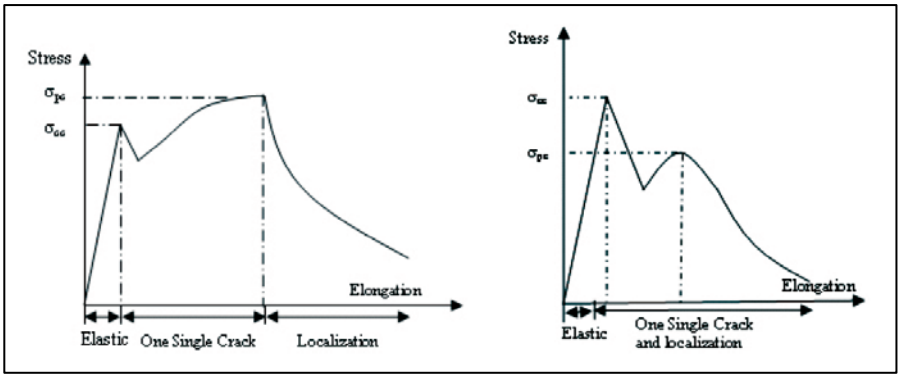

Figure 1.13. Strain-hardening (left) and strain-softening (right) behavior with single major crack (Suwannakarn et al. 2008).

Figure 1.14 shows the stress-strain curves of SFRCs with different fibers contents within the usual range for real applicacions, i.e. up to 1.5% in volume, and that for their unreinforced counterpart. As it can be seen, for

these fibers contents the tensile behavior is clearly strain-softening. Differently from what happens when under compresion, the addition of fibers does significantly increase the tensile strength of concrete, i.e. the stress corresponding to the first percolation crack or peak stress. According to ACI 544.1R-96, this strength is increased up to 40% in a SFRC when compared to its unreinforced counterpart when fibers volume fracion is 1.5%. In addition to the tensile strength, adding fibers also makes the material more ductile (the more the higher fibers content): the post-peak branch of the stress-strain curve presents a very reduced slope, being practically horizontal as can be seen in Figure 1.14, this in contrast with the brittle failure of unreinforced concrete.

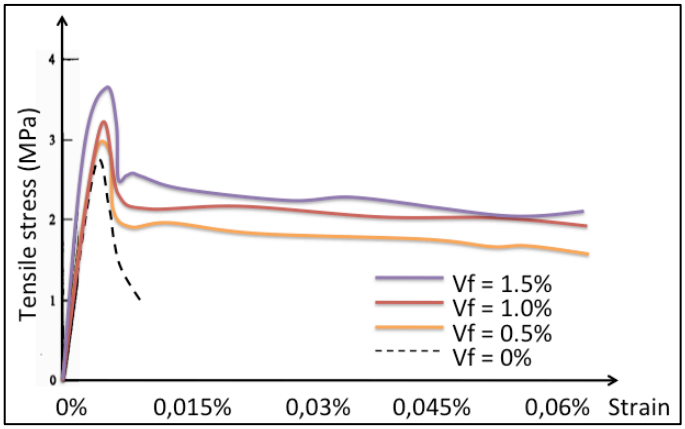

Figure 1.14. Examples of stress-strain curves from concretes with different fibers contents when under direct tension.

The splitting test is another way of approaching tensile behavior of concrete and it is indeed the commonest and mostly preferred way, given the difficulties that the execution of direct tension tests involves. As a consequence, conclusions drawn from splitting test results are more usual in literature than those from direct tension tests. Figures 1.15 and 1.16 show results from different authors that compare SFRCs with different fiber contents, and a clear increasing tendency in splitting strength is observed with increasing fibers contents. As a matter of fact, the increase observed in splitting strength when fibers are added to concrete is higher than that observed in direct tensile strength.

It can be noted in Figure 1.15 that splitting strength of a SFRC containing 1.5% of fibers is twice the splitting strength of its unreinforced counterpart. Similar conclusions can be drawn from the results plotted in Figure 1.16, where 1.5% of fibers represents an increase in splitting strength of about 85% when compared to unreinforced concrete.

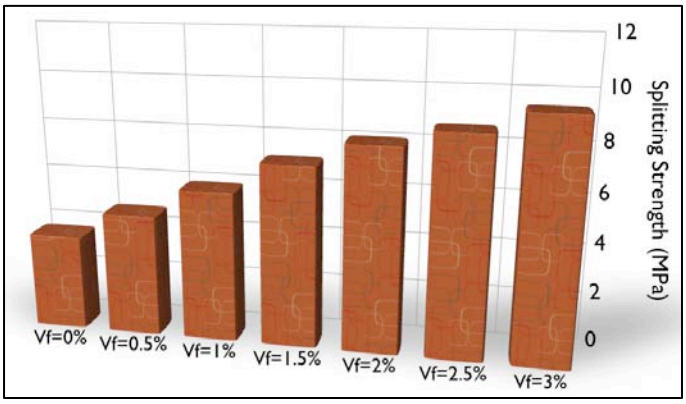

Figure 1.15. Splitting strength for different fiber contents (adapted from Kovács & Balázs 2004, Narayanan et al. 1987).

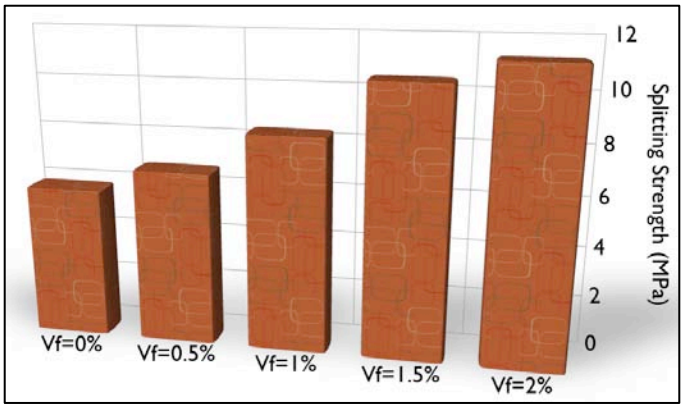

Figure 1.16. Splitting strength for different fiber contents (adapted from Song & Hwang 2004).

1.8 Flexural Behavior

Flexural behavior is the reference for comparative purposes when describing SFRCs, because it is in bending where the addition of fibers implies substantial improvement of SFRC performance. It is true that the contribution of fibers is very important in tension as well, but bending is related to most common applications, and that is the reason why SFRCs are best described in terms of their flexural response (Naaman 2008). The bending test can be said to fall in two groups: beam test and plate test, the former being the most usual one due to the simple setup when compared to the latter.

Beam tests are carried out on prismatic specimens and have been standardized in two different variants: depending on the number of points where load is applied, one can have the three-point or the four-point bending test, both shown in Figure 1.17. Furthermore, the specimen can be notched (the notch is executed in the midspan cross-section of the specimen) or unnotched.

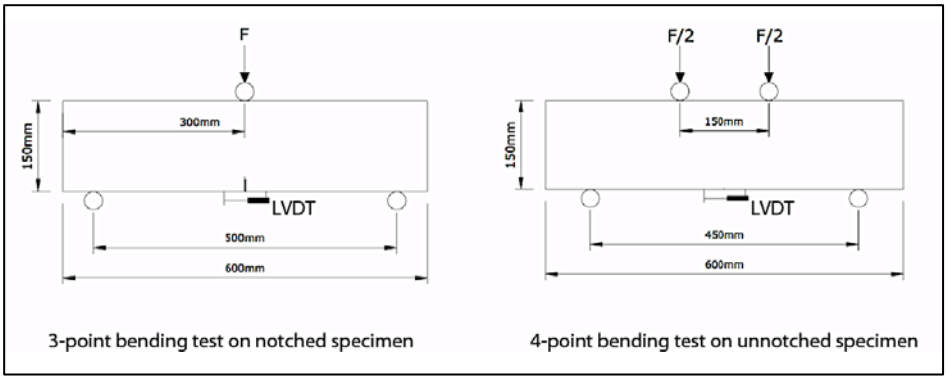

Figure 1.17. Three-point and four-point bending tests.

The maximum bending moment in the four-point test extends to all the cross-sections in the central third of the specimen, while in the three-point test the maximum bending moment exists only at the midspan cross-section. Having a notch the cross-section is reduced and thus, in the case of the three-point test, it makes the percolation crack originate at the

midspan cross-section, because it is there where the notch is and where the bending moment is maximum.

In Spain, EHE-08 App. 14 establishes that bending tests are to be carried out following the standard EN 14651. The result of the bending test is a curve presenting load vs crack mouth opening displacement (CMOD hereafter) like the one sketched in Figure 1.18. The following parameters are retained:

- ☐ Limit of proportionality (LOP hereafter), F_L.
- ☐ Load values F_1, F_2, F_3, and F_4, corresponding to crack widths of w_1=0.5mm, w_2=1.5mm, w_3=2.5mm, and w_4=3.5mm respectively.

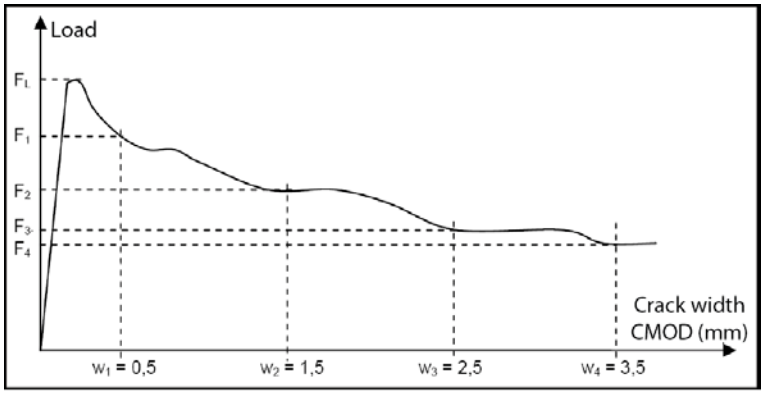

Figure 1.18. Typical load – CMOD curve from the bending test (source: EHE-08 App. 14).

The LOP is conditioned in the last instance by compressive strength of the cementitious matrix, and therefore is not significantly affected by fiber content within the usual range (contents up to 1.5% in volume). The part of the curve that follows LOP is usually referred to as the 'post-peak region', even when the bending behavior is strain-hardening (then, obviously the LOP is not the 'peak' or maximum load that the material is capable of carrying).

The value of the ultimate flexural strength, defined as the maximum flexural stress that the material is capable of carrying, depends basically on fiber content and fiber geometry. For low fiber contents, the post-peak branch of the stress – CMOD curve will be strain-softening, its slope

depending on the fibers content: in such cases the ultimate flexural strength will be that corresponding to the LOP. But for higher fibers contents, the post-peak branch can be descending with a very reduced slope, horizontal or may be even a strain-hardening one, this meaning that medium or high fibers contents can make the post-peak load-carrying capacity of concrete even higher than that corresponding to the LOP, i.e. the strength of the matrix (Figure 1.19). In such cases, the ultimate flexural strength of the material can double that corresponding to the LOP or be even greater.

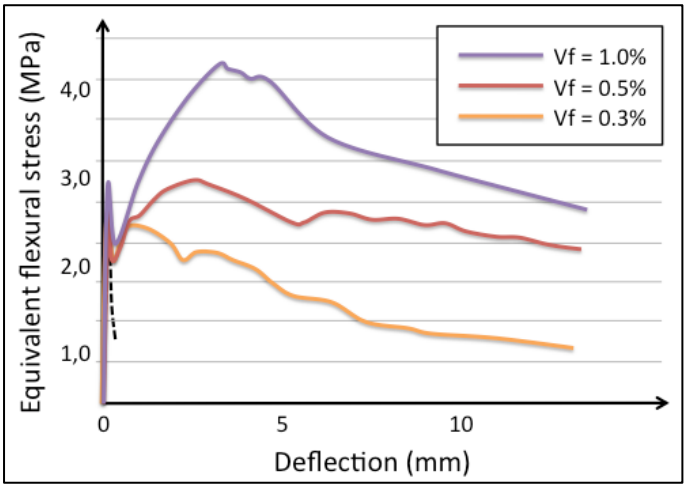

Figure 1.19. Stress – deflection curve for the same concrete with different fibers contents (curves obtained by the author).

Figure 1.20 illustrates how fibers make it possible for the material to have load-carrying capacity in the post-peak region. The image shown in Figure 1.20 is taken from a specimen right after being tested in bending, and it makes clear how fibers sew the crack and resist increasing levels of stress when the crack is opening, while the same concrete without fibers would have failed at the very moment the crack initiates.

Beam bending tests have usually been criticized for the considerable scatter their results present. Parmentier et al. (2008) state that one of the most significant restraints for using SFRCs in structural applications is the scatter of toughness parameters measured in laboratory, and underline that the test method is one of the most important sources of variation.

They point out that the coefficient of variation for test results are usually between 20% and 30% and come to the conclusion that it is much higher than in plate tests, where the usual values of the coefficient of variation are between 6% and 9%.

Figure 1.20. Sewing effect of fibers as observed in a cracked specimen right after being tested in bending.

Di Prisco et al. (2009) comment on some results by other authors they have compiled and show how high the scatter of the different parameters that are retained from beam bending test is: for a SFRC with 50kg/m^3 of 60mm-length fibers, the coefficient of variation is 27% for the equivalent flexural strength between crack widths of 0 mm and 0.6 mm ($f_{eq0-0.6}$), and 35% for that between crack widths of 0.6 mm and 3mm ($f_{eq0.6-3}$). Furthermore, they put the validity of notching the specimen into question and argue in favour of unnotched specimens: the notch may susbstract a significant bending resource of the specimen if part of the fibers cumulate in the bottom, as often happens.

Plate tests are the alternative to beam tests. The main reference is the ASTM standard C1550-10 for measuring the flexural response of SFRCs by means of centrally loaded panels relying on three supports. The scattering of the results is reduced when compared to beam bending tests, as shown in Figure 1.21, due to the following reasons:

- The volume of concrete involved in the failure mechanism is higher than in beam bending tests.

- Three radial cracks appear that propagate along three different directions, which generally form at internal angles of about 120°: any fiber orientation is generally averaged and the material can be better characterized as a homogeneous, isotropic material.

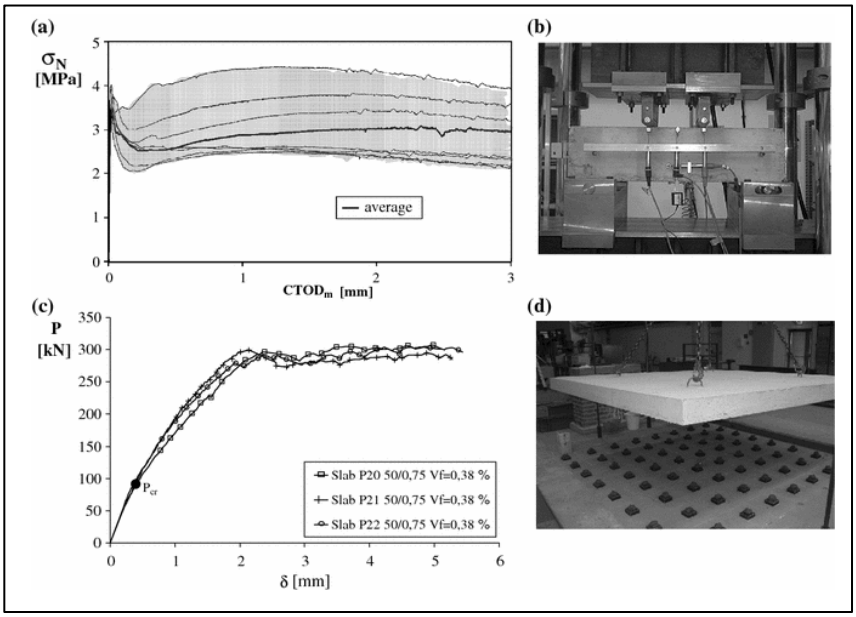

Figure 1.21. Setup of beam test and plate test and the scatter in their results exemplified (source: Di Prisco et al. 2009).

Pereira et al. (2009) comment on a different panel prototype for the flexural test, shown in Figure 1.22. This variation proposes a square plate specimen on eight supports and with a lightweight central region to be loaded at four points where deflection is measured. The number of supports comes to guarantee a high redundancy. Since steel fiber reinforcement is particularly efficient in structures with a redundant number of supports, where considerable stress redistribution occurs after the crack initiation, this test setup better reflects the behavior of SFRCs to be expected in real applications. The lightweight central region would be the 2D equivalent for the notch in beam tests. Since deflection is measured at four different points, four load-deflection curves are averaged to better reflect the material's behavior.

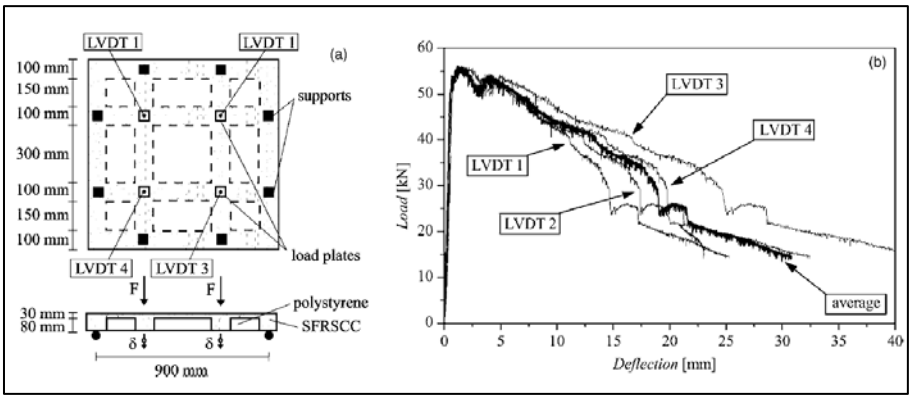

Figure 1.22. Variation of the plate test and example of load-deflection curves obtained (source: Pereira et al. 2009).

1.9 Shear Behavior

Adding steel fibers to concrete increases shear strength. More than twenty years ago, Narayanan & Darwish (1988) found out that for a fibers content of 1% in volume the increase in shear strength could reach the 30% with respect to the unreinforced counterpart. This has been confirmed by several other studies. For instance, more recently Dinh et al. (2008) have concluded that using steel hooked-end fibers in a volume fraction greater than or equal to 0.75% leads to a significant increase of shear strength of concrete beams. Their results indicate that a fiber volume fraction of 0.75% may be enough to replace the requirement of minimum stirrup reinforcement in the ACI 318-08 code. Fibers allowing a partial or total replacement of transverse reinforcement may allow concrete elements to be produced without stirrups, this meaning a reduction in the costs of production.

Steel fibers may present some potential advantages when used to partially or totally replace stirrups in beams:

- ☐ The randomly distribution of fibers within the volume of concrete leads to an average distance between fibers much more reduced than that between stirrups. As a consequence, for a certain load value, the crack width in a FRC will be smaller than in its equivalent without fibers and with stirrups.
- ☐ First crack stress and ultimate stress of concrete in tension are increased when fibers are added to the concrete.
- ☐ The friction component of shear strength is increased as a consequence of the pullout strength of fibers (the sewing effect of fibers increases friction between the two faces of a crack).

1.10 Durability

All rules of good practice regarding the durability of conventional reinforced concrete apply to SFRCs.

Probably one of the first concerns in relation to durability of SFRC may be that of corrosion. Requirements for cement content, compressive strength, maximum w/c ratio as well as minimum concrete cover values are specified by codes of practice to protect steel reinforcing bars from corrosion. But in the case of SFRCs, steel fibers are randomly distributed and some of them lie at the surface of concrete, i.e. directly exposed to environment: concrete cover for such fibers is effectively zero (Serna & Arango 2008), and this could be regarded as a special threat. However, in uncracked members made of concrete with a compressive strength at 28 days greater than 21 MPa corrosion affects only to fibers in the surface: there is no such thing as the propagation of corrosion to fibers within the volume of concrete more than 2.5 mm below the surface (ACI Committee 544). This is due to the fact that fibers are randomly dispersed within the matrix and contact each other very rarely: the electrical path necessary for the conduction of corrosion is not at all likely.

As a matter of fact, Serna & Arango (2008) confirmed that, in uncracked SFRC elements exposed to seawater, corrosion is limited to the specimen surface and does not penetrate into concrete deeper than 2 mm. Furthermore, they studied the behavior of cracked specimens (crack width being 0.5 mm) exposed to chlorides (seawater) regarding corrosion, and found out that in spite of corrosion being observed in some fibers, flexural strength was not weakened but, quite surprisingly, seemed to increase, probably due to the fact that fibers corrosion did not significantly affect their section but made their surface less smooth, this increasing their pullout strength.

EHE-08 App. 14 states that, in general, FRCs can be used in all exposition classes and, in addition, recognises that fibers improve concrete's resistance to erosion. With respect to the specific exposition classes concerned with chemical attacks to concrete, steel and

polypropylene fibers can be used but previous tests in order to confirm the absence of interaction between them and the chemical agents are required.

Further studies are still needed concerning the rules to be adopted in SFRC structures in relation to exposition classes, since the effect of fibers reducing crack width may result, for instance, in smaller concrete covers required in SFRC structures than those established for conventional concretes (Di Prisco et al. 2009). In the case of hybrid FRCs, as Lawler et al. (2005) have pointed out, microfibers modify crack development by delaying the formation of macrocracks, and this makes the material less permeable than other concretes when multiple cracking occurs, hence having durability improved.

One thing is very clear: durability benefits from the fibers effect of reducing crack width. Shah & Ferrara (2008) highlight how this effect of fibers to durability of concrete is even more positive in the case of SFRSCCs. Durability benefits not only from the fact that fibers reduce crack width but also from the higher compactness of the matrix when compared to conventional concrete or unreinforced SCC: together with crack widths being reduced thanks to the fibers, lower matrix porosity due to self-compactability makes SFRSCC a highly durable concrete in terms of water permeability and penetration of chlorides and/or aggressive substances in outdoor or chemically aggressive environments.

1.11 Production and Control

The mixing process is of essential importance to obtain a homogeneous and random distribution of fibers within the fresh concrete. When this may be a difficulty, the volume of the batch shall be reduced, the mixing time shall be increased, or a more powerful mixer shall be used (or a combination of the three possibilities).

The occurrence of fiber balls is always to be avoided. To do so, ACI Committee 544 makes the following recommendations: fibers should be poured to the mix once this is fluid enough, concretes are to be proportioned with enough fine aggregate, excessive transportation times are to be avoided, and fibers with high slenderness are to be avoided when possible. In those cases when relatively long transportation times are foreseen, the possibility of pouring fibers to the concrete once in the worksite has to be considered.

Fibers distribution and orientation are affected by a number of factors which are difficult to control (Di Prisco et al. 2009). The scatter of any parameter characterizing SFRC will always be increased by lack of homogeneity, which is further complicated by the well known negative effects of fibers on concrete workability. It is therefore very important to control fibers dispersion.

Fibers tend to orient themselves along the flow of concrete (Tenikella & Gettu 2008). This effect is especially favoured in the case of SFRSCC (Torrijos et al. 2008). When the flow of fresh concrete is basically unidirectional, there can be considerable benefits in having preferentially oriented fibers. Therefore the casting process needs to be conceived so that fresh concrete flows according to the directions of the principal tensile stresses that will develop when the structural element is in service (Shah & Ferrara 2008).

Fiber dispersion is a critical problem when fiber content is low (Chung 2005) but, on the contrary, the higher fiber content, the more likely to have a homogenous dispersion of fibers (Di Prisco 2009). There are different possibilities to analyze fiber dispersion within a structural element, namely (Shah & Ferrara 2008):

- Drilling small cores at different positions along the element, crushing the cores and then determining the fiber content in each core by means of counting.
- Measuring different electrical properties of SFRC (resistivity or capacity), for instance by means of the Alternate Current Impedance Spectroscopy.

The two aforementioned groups comprise a number of variants. For instance, Vandewalle et al. (2008) have taken further the first approach by using X ray. As shown in Figure 1.23, slices can be cut out of the SFRC specimen in different directions and then to look at the distribution of fibers in the slice by means of X ray. This not only makes the counting of fibers much easier, but also offers an insight into the orientation of fibers: a preferential orientation of fibers is observed when the specimen is parallel to flow direction (left) which is not observed when the specimen is cut out otherwise (right).

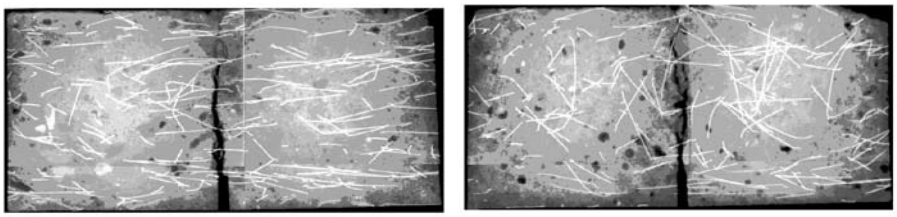

Figure 1.23. X-ray view: flow direction (left) vs not in flow direction (right) (Vandewalle et al. 2008).

Another approach is that of cutting out prismatic specimens from a SFRC slabs, according to different directions, to subject them to the beam bending test or to execute saw cuts on them in order to be able to count fibers in each section. For instance, Tanikella & Gettu (2008) did so in order to study fibers dispersion when SFRSCC is used to produce a slab. They observed that fibers tend to accumulate near the borders of the slab, where there are oriented parallel to the edges of the slab in clear coherence with the flow directions to be expected when casting such elements. This is called the 'wall effect'. According to Torrijos et al. (2008), it clearly depends on the relation between the dimensions of the mould and the length of the fibers used. Therefore, to minimize the wall effect in small slabs, it is better to use short fibers than long fibers.

2| Bond of Reinforcing Bars to Concrete

Part I: State of the Art

2| Bond of Reinforcing Bars to Concrete

PART I: STATE OF THE ART

2.1 Rebar-Concrete Interaction

Bond between reinforcement and concrete is most usually studied as a local phenomenon (i.e. puting aside structural conditionings that may interfere bond performance) and is approached as shown in Figure 2.1: a reinforcing bar embedded in a concrete specimen is subjected to a gradually increasing load pulling it out.

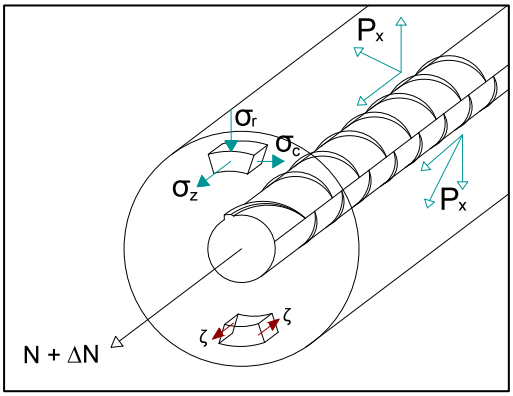

Figure 2.1. Bond of an embedded ribbed rebar (adapted from FIB Bulletin no.10, 2000).

Therefore bond is treated in codes by having this complex phenomenon reduced to shear stresses, or bond stresses, which develop in the steel-concrete interface to balance the pulling load. This has motivated the definition of a reference parameter, the average bond stress in the rebar-concrete interface assuming a uniform distribution along the embedded length of the rebar, as illustrated in Figure 2.2. This view is nuclear in the rationale behind the provisions for the bond tests, for instance beam-test (standard EN 36740), which aims at checking bond of

reinforcement to concrete (and its observance is mandatory according to the Spanish code for structural concrete).

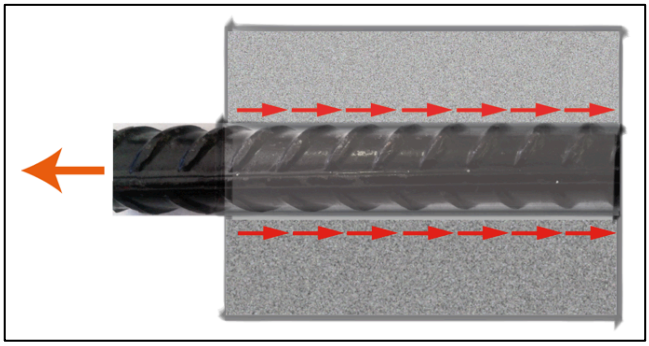

Figure 2.2. Hypothesis of uniform bond stress distribution.

Average bond stress (simply 'bond stress' hereafter) increases as the axial load increases. At the same time, the rebar is gradually pulled out of concrete and slips (relative displacement between rebar and concrete) develop. Therefore, a local law relating bond stress to slip values characterizes bond behaviour. Based on a wide experimental campaign was performed by Eligehausen et al. (1983) on short pull-out specimens, a relatively simple local bond–slip relationship for ribbed rebars in well confined concrete was developed and adopted in the Model Code (Fib, 2010), as shown in Figure 2.3.

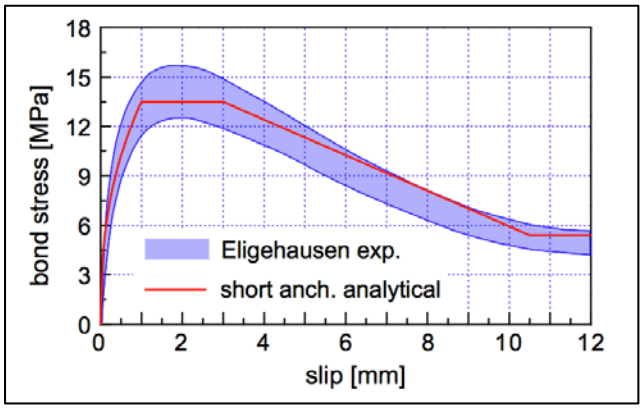

Figure 2.3. Bond-slip relationship and curves obtained by Eligehausen et al. (1983) (Mazzarolo et al. 2012).

In consequence, bond between reinforcement and concrete is commonly conceptualized as a shear stress, or bond stress, which is uniformly distributed over the surface of the rebar along the embedded length. Bond stress can be defined as the ratio between the rate of change in axial force along the rebar and the area of rebar surface over which this change takes place (Cairns & Plizzari 2003). However, this view is not accurate because of two reasons:

- ☐ Bond stresses are not uniformly distributed, as shown in Figure 2.4.
- ☐ There are other aspects besides bond stress to be considered, especially in the case of deformed, ribbed rebars (Cairns & Plizzari 2003, Bamonte & Gambarova Gambarova 2012), mainly related to radial stresses. Please note that, in the context of this thesis, rebars are always ribbed rebars unless said otherwise.

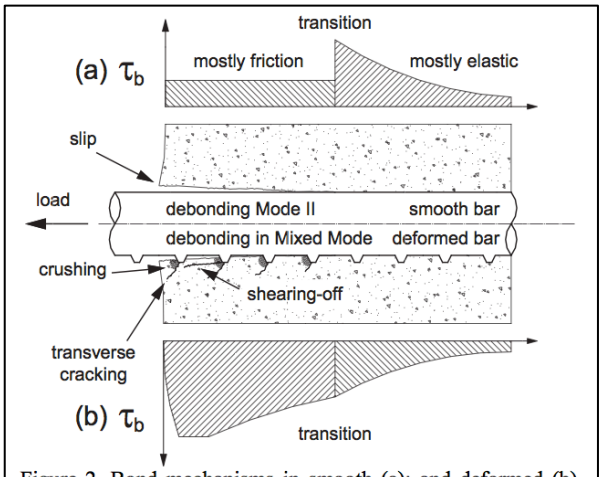

Figure 2. Bond mechanisms in smooth (a); and deformed (b) bars, from Bamonte and Gambarova, (2007).

Figure 2.4. Bond stress distribution in smooth (a) and ribbed (b) rebars (Gambarova 2012, Bamonte & Gambarova 2007).

A variety of test setups and methodologies to study bond can be found in literature, and can be divided into long specimen and short specimen tests (FIB 2000). However, pull out and pull in tests, in their different versions, constitute the main tool used to explore bond in concrete (Mazzarolo et al. 2012). Their main feature is that they are short

specimen tests, i.e. the embedment length imposes short anchorage conditions, and therefore rebars remain in the elastic range and bond stresses are approximated as constant, uniformly distributed. But even under these circumstances, bond stress distribution in a typical pullout test is not uniform (Abrishami & Mitchell 1996), as shown in Figure 2.5. Furthermore, bond stress distribution varies as slippage develops (FIB 2000).

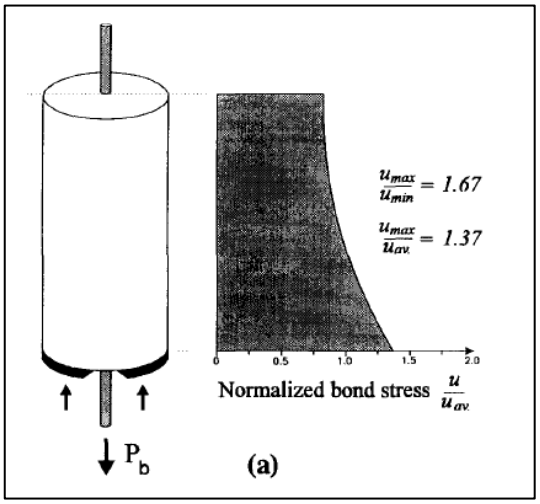

Figure 2.5. Bond stress distribution in a pull out test according to Abrishami & Mitchell (1996).

Besides the non-uniformity of bond stress distribution along the rebar, there are several aspects involved other than the average bond stress along the embedded length, as Figure 2.6 shows. The tensile load pulling the rebar out of concrete produces reaction forces which are exerted on the sorrounding concrete by ribs. These reactions can be decomposed in two components and therefore, the bond phenomenon involves:

- A shear component, parallel to the rebar axis, so that there are triaxially compressed concrete regions in front of each rib. This leads to the so-called bond stresses.
- A radial component, orthogonal to the shear component, which extends bond mechanisms to the surrounding concrete further than concrete between ribs.

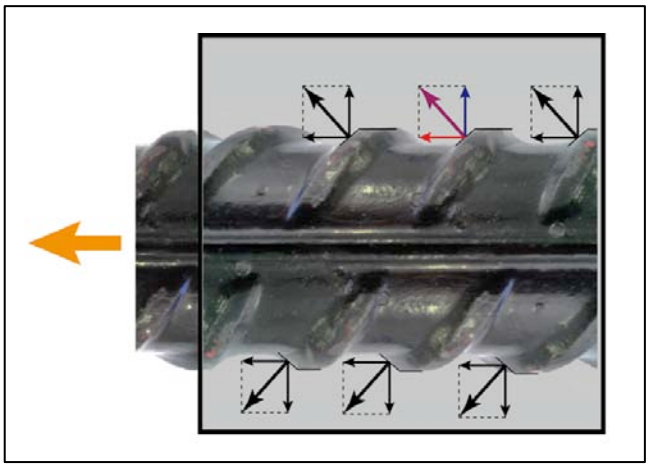

Figure 2.6. Decomposition of forces exerted by a ribbed rebar unto surrounding concrete.

STAGES OF REBAR-CONCRETE INTERACTION

Different stages can be distinguished in the rebar-concrete interaction as the tensile load pulling the rebar out is gradually increased (Gambarova et al. 1989, Bazant et al. 1995, FIB 2000). These stages are summarized in Figure 2.7.

- **STAGE 1**. When the average bond stress is below 80% of concrete tensile strength, bond between steel and concrete is simply due to the contact, i.e. friction forces appearing in the steel-concrete interface. In addition to the cohesive nature of these forces, chemical adhesion also plays a role. At this stage, there is strain compatibility between concrete and steel and therefore there is no relative displacement of the reinforcing bar with respect to concrete, i.e. there is no slip of the reinforcing bar.

- **STAGE 2**. When the average bond stress is increased over 80% of concrete tensile strength approximately (between 0.7 and 1.5 times concrete tensile strength, Gambarova et al. 1989), friction-natured, cohesive bond between steel and concrete is lost and strain compatibility is no longer possible. Then transverse microcracks originate at the ribs tips, and slippage of the rebar is initiated.

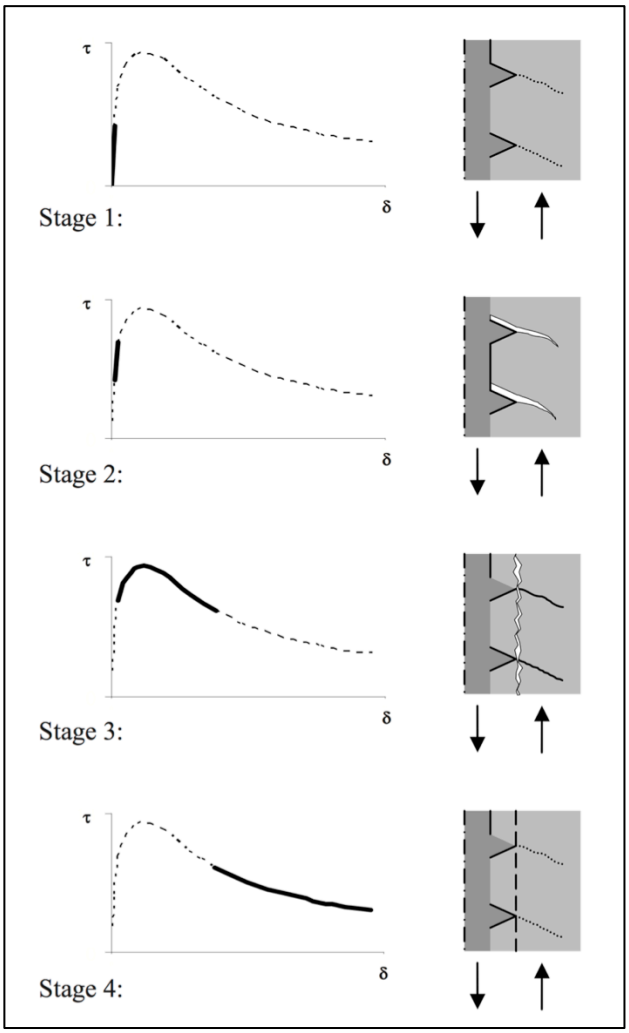

Figure 2.7. Stages in the development of bond (adapted from Auer & Stempniewski 2012).

- **STAGE 3.** For bond stress values between 1.0 and 3.0 times concrete tensile strength, wedging action by rebar ribs increases and as a result the first longitudinal cracks form. There is a relative displacement of the reinforcing bar with respect to concrete, and therefore slippage of the reinforcement begins. When this happens, reactions are developed from the rebar ribs onto the concrete, as shown in Figure 2.8. It is observed that these reactions have an

inclination due to the ribs form. Concrete between ribs is crushed by the development of these reactions. At the same time, the derived radial stresses are applied onto surrounding concrete and generate the so-called hoop stresses, as shown in Figure 2.8. As the load increases, these hoop stresses also increase and concrete tensile strength is also reached in the surrounding concrete. This leads to the phenomenon of transverse microcracking. The development of these microcracks are at the very basis of the loss of strain compatibility between steel and concrete: slip values increase as a result of the widening of these microcracks.

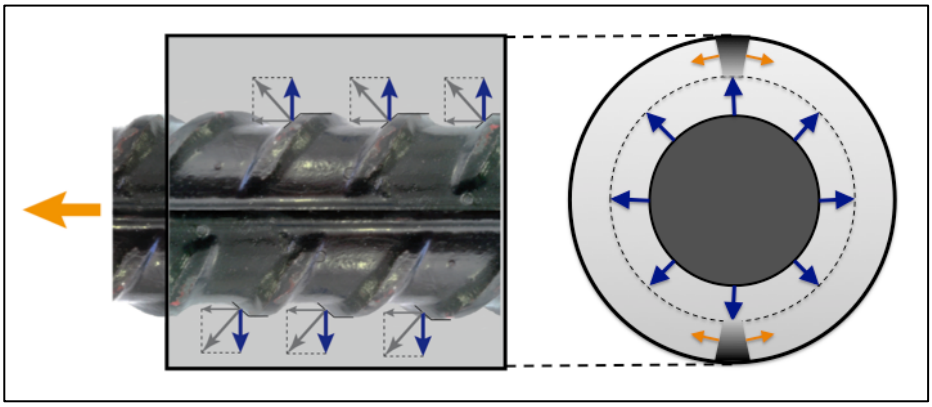

Figure 2.8. Radial stresses and derived hoop stresses in surrounding concrete.

☐ **STAGE 4.** Transverse cracking and longitudinal cracks go on developing: they keep on opening and reaching further following the load increase. As a result, slip values increase with bond stress values until the maximum bond stress, or bond strength, is reached. Bond stress–slip curves are characterized by postpeak softening behaviour, and slippage represents shear fracture (Bazant et al. 1995). Bond stress remains remarkable even at very large slip values in the postpeak region of the bond stress–slip curve (between 15% and 30% of concrete tensile strength for a slip of 0.3 times the rebar diameter, according to Gambarova et al. 1989). Eventually, bond behaviour tends to be dry-friction (Coulomb) type: concrete between ribs is crushed and sheared off with the rebar. However, this is not

necessarily how it ends. Different modes of failure will be dealt with in the next section of this chapter.

FACTORS AFFECTING BOND

Different factors affect bond between reinforcing bars and concrete. The latest report of ACI Committee 408 on bond of reinforcing bars in tension (ACI 2003) groups them in three categories: structural characteristics, reinforcing bar properties, and concrete properties. According to this classification criteria, a comprehensive list (though possibly not exhaustive) of factors affecting bond is presented (FIB 2000, ACI Committee 408 2003, Gambarova 2012):

- ☐ Structural characteristics:
  - Concrete cover.
  - Transverse reinforcement.
  - Active confinement.
  - Embedment, development, or splice length.
  - Bar spacing.
  - Rebar position when casting concrete.

- ☐ Reinforcing bar properties:
  - Rebar size, i.e. diameter.
  - Rebar yield strength, rebar yielding.
  - Rebar surface: epoxi-coated or not.
  - Rib height.
  - Rib spacing.

- ☐ Concrete properties:
  - Concrete compressive strength.
  - Aggregate type and quantity.
  - Tensile strength.
  - Use of lightweight aggregates.
  - Workability and use of workability admixtures.
  - Use of mineral admixtures.
  - Fiber reinforcement.
  - Consolidation adequacy.

- Use of vibration.

Sections 2.3 to 2.5 are devoted to the detailed description of how some of these factors affect bond performance of concrete, which are the most relevant ones in the context of this thesis, namely:

- ☐ Concrete compressive strength (section 2.3).
- ☐ Reinforcing bars, considering a variety of aspects, including the embedment length, which is a specially relevant topic directly related to the different test setups aimed at investigating bond (section 2.4).
- ☐ Confinement (section 2.5).

2.2 Modes of Failure

Bond failure can occur in two different major modes. One mode consists in splitting of concrete surrounding the rebar (splitting failure), and the other mode consists in having the rebar pulled out after the shear failure of the steel-concrete interface (pullout failure).

When concrete cover and/or transverse reinforcement are not sufficient (this will be addressed in detail in section 2.5), transverse cracks originated at the steel-concrete interface eventually reach concrete surface and if there is no transverse reinforcement capable of bearing the derived tensile stresses, bond capacity is totally lost. There are different possibilities of splitting depending on the relative position of the reinforcement and the shape of the element cross-section, as shown in Figure 2.9.

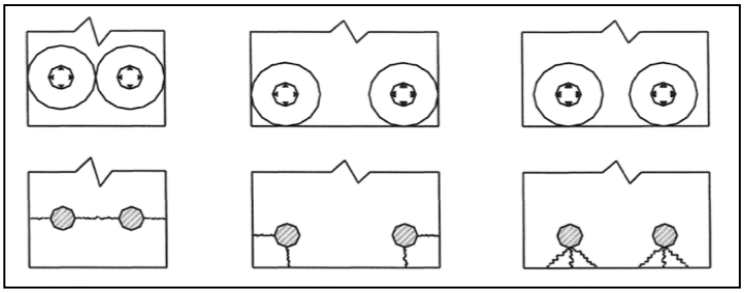

Figura 2.9. Splitting failures (FIB 2000).

If there is no transverse reinforcement, the occurence of splitting implies the total failure of the anchorage: bond stress drops to zero in a brittle failure, and a considerable slippage is observed at this time. On the contrary, if there is considerable amount of transverse reinforcement, splitting is not total but partial: stirrups are loaded when transverse cracks have developed and therefore they provide the anchorage with a residual bond strength. In general terms, it is assumed that splitting failures occur when concrete cover is less than approximately 2.5 or 3.0 times bar diameter (Cairns & Jones 1995). Splitting failures are caused by the tensile hoop stresses in the concrete surrounding the rebar as a result of the wedging action of rebar ribs (Bazant & Sener 1988). The consequence is that radial splitting cracks are formed, leading to a

sudden loss of bond capacity. Figures 2.10 and 2.11 are two photographs of a concrete specimen tested by the author, which experienced splitting failure. It is important to remark that the ribs profile is still visible on both faces of the splitting crack, as shown in Figure 2.11. This is so because bond failure was not a consequence of the concrete between ribs being crushed and then the shearing off of rebar and concrete, but by tensile failure of the surrounding concrete. This is distinctive of splitting failures.

Figure 2.10. Example of splitting failure.

Figure 2.11. Example of splitting failure (detail).

Pullout failures, on the other hand, occur when there is considerable confinement of concrete. The crushing of concrete between ribs defines a cylindrical frictional surface around the rebar (Bazant & Sener 1988), as

shown in Figure 2.12. As a consequence, when the rebar has experienced considerable slippage, crushed concrete has been extracted between ribs, as shown in Flgure 2.13. The shearing failure starts from the loaded end and then propagates toward the free end as one lug after another shears or crushes the concrete in front of the lug (Bazant & Sener 1988). After the shearing has progressed over the entire length of embedment of the bar, the force drops and then the remaining pullout is resisted only by friction.

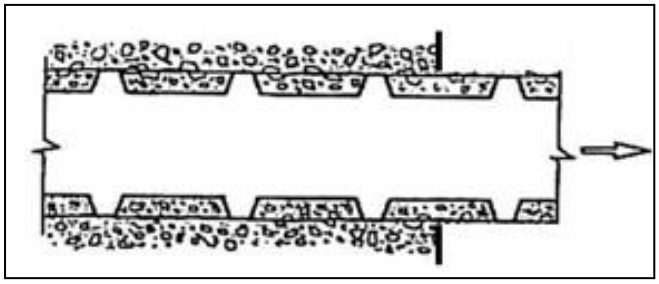

Figura 2.12 Pullout failure (FIB 2000).

Figure 2.13. Example of pullout failure (detail).

Because of its negative aspects, concrete splitting has been viewed by scholars and code-makers as something which has to be prevented or kept to a minimum, with the obvious consequence that bond behaviour after concrete splitting has been underestimated (Gambarova & Rosati 1997). A first reason is the widespread opinion that longitudinal splitting

is dangerous both for bond strength and for structural durability, since bar corrosion may start from the longitudinal cracks. According to this point of view, longitudinal splitting should be prevented, being incompatible with structural safety in the working load situation, and with structural strength in the ultimate load situation. However, the test results so far obtained by a number of authors that bonding can be highly efficient even under serious longitudinal cracking, on condition that suitable confinement action is applied (Gambarova et al. 1989).

2.3 Concrete Compressive Strength

As a result of the rebar-concrete interaction, concrete between ribs is compressed and tensile stresses develop in concrete surrounding the rebar. Therefore, concrete compressive strength and tensile strength are determining properties. Since concrete tensile strength is directly related to compressive strength, and considering that concrete compressive strength is generally assumed as the main parameter describing the material's performance, this section presents an overview of how this feature determines bond in concrete.

Several studies have confirmed that concrete compressive strength has a positive effect on bond, namely on bond strength (Chapman & Shah 1987, Hughes & Videla 1992, Harajli 2004, among many others). Furthermore, the growing interest in high strength concretes and ultra-high performance concretes has produced a continuous source of data in relation to bond of reinforcement to concrete confirming this positive effect. Figure 2.14 shows some results taken from Harajli (2004): it can be observed that bond strength is increased when concrete compressive strength increases.

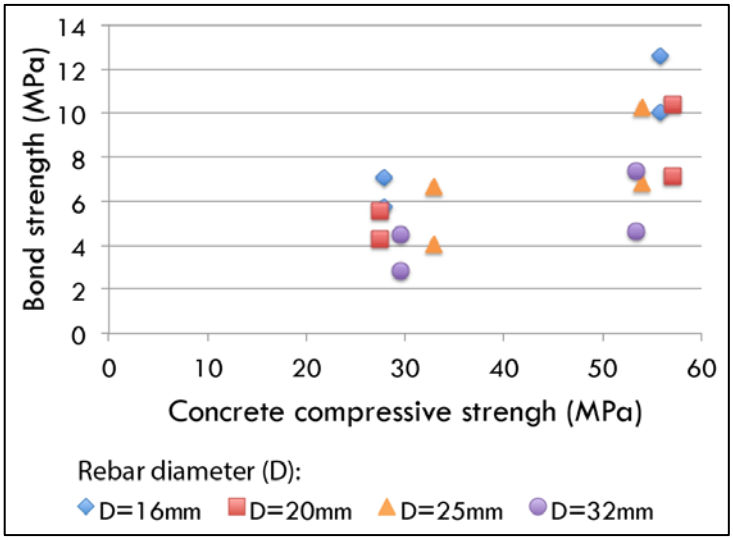

Figure 2.14. Relation between average bond strength and concrete compressive strength (data from Harajli 2004).

This trend is more clearly observed in Figures 2.15 and 2.16, which present the results obtained by Hughes & Videla (1992). They investigated bond in concrete at different testing ages and this produced bond strength data for a wide variety of concrete compressive strength values up to 35 MPa.

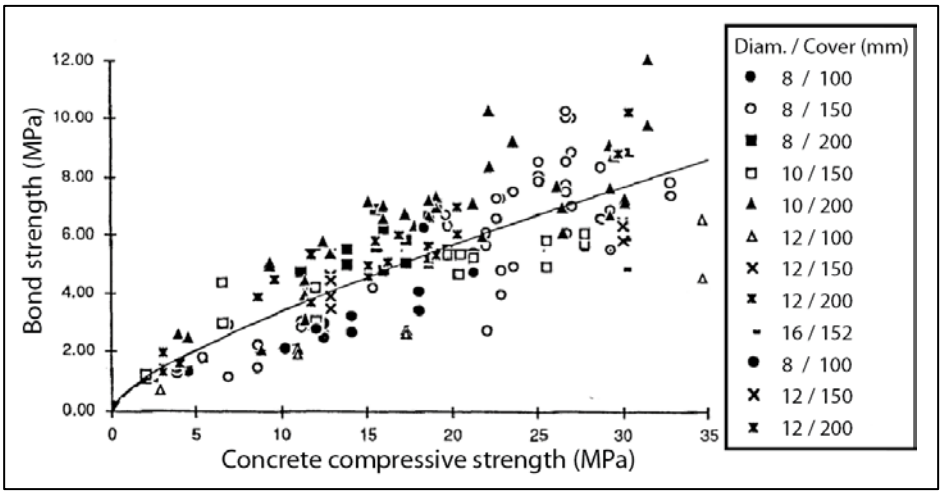

Figure 2.15. Bond strength vs concrete compressive strength (cube), adapted from Hughes & Videla (1992).

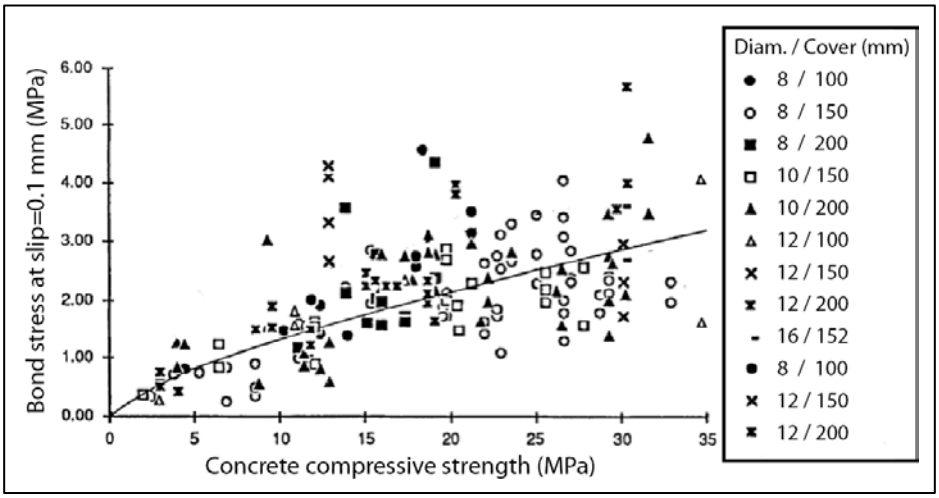

Figure 2.16. Bond stress at 0.1mm slip vs concrete compressive strength (cube), adapted from Hughes & Videla (1992).

It is also important to notice that the scatter of bond strength or bond stress values increases with concrete compressive strength, which is observed in Figure 2.14 and specially in Figures 2.15 and 2.16.

However, all these data are concerned with bond strength, but there are other parameters which have been neither so thoroughly investigated nor related to concrete compressive strength, specially failure ductility, i.e. the area under the bond stress–slip curve. Increasing concrete compressive strength values lead to higher areas under the curve, since not only bond strength but also the postpeak, softening branch of the bond stress–slip curve is affected, as noticed by Chapman & Shah (1987), as shown in Figure 2.17. These authors investigated the evolution of the relation between bond strength and compressive strength with respect to testing age, and presented some curves (Figure 2.17, right) for illustrative purposes, where the positive effect of increasing concrete compressive strength on bond failure ductility is clearly observed.

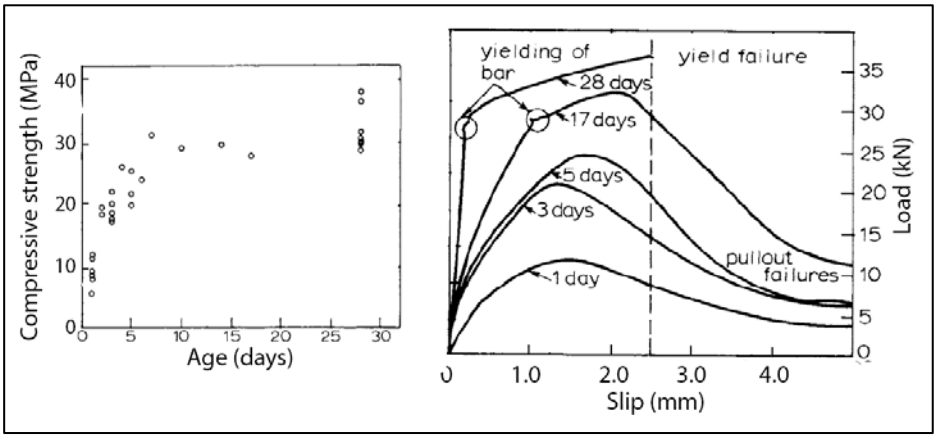

Figure 2.17. Variation of compressive strength with age (left) and pullout load–slip curves (right), adapted from Chapman & Shah (1987).

Chapman & Shah (1987) presented their results relating bond strength to concrete compressive strength and took into consideration the effect of confinement, embedment length, and rebar diameter in addition to that of concrete compressive strength when developing the fitting equations they finally proposed. Figure 2.18 shows their results for two different

embedment lengths (76 mm and 127 mm). In this case, no significative differences are found between the two sets of data. However, the effect of embedment length, or anchorage length, on bond strength has attracted extensive attention, and will be discussed in section 2.4.

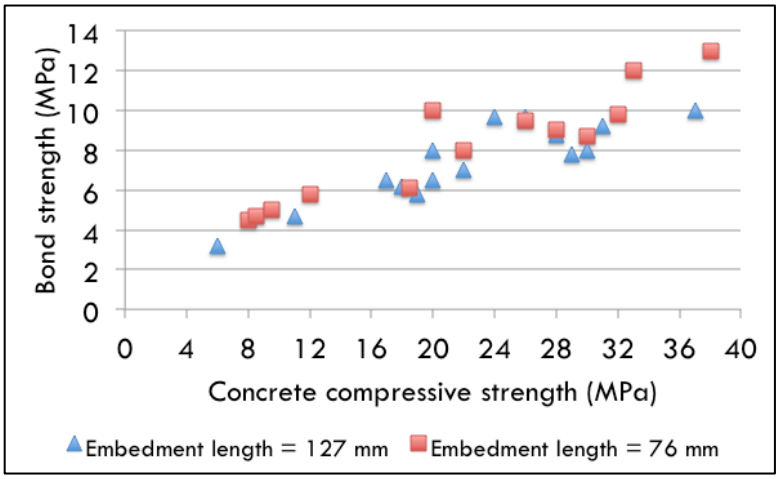

Figure 2.18. Bond strength vs concrete compressive strengh, based on data from Chapman & Shah (1987).

Finally, there is the issue of how concrete compressive strength values are taken into account concerning their relation with bond strength. Figures 2.15, 2.16 and 2.18 suggest that this relation is practically linear. However, Chapman & Shah (1987) use the square root of compressive strength in the equations they obtain for modelling bond strength. The report of ACI Committee 408 (ACI 2003) extensively discusses the different possibilities arising from studies carried out by different authors and concludes that the contribution of concrete quality to bond strength is best represented by concrete compressive strength to the 1/4 power, though this does not hold for those cases where transverse reinforcement is considered.

2.4 Reinforcing Bar

REBAR DIAMETER

There are several aspects dealing with reinforcement which have proved relevant to bond performance. Probably the most obvious one is rebar diameter. Bond strength has been found to be a linear function of rebar diameter. Higher diameters bring in higher bond stresses (Gambarova & Rosati 1997) and a higher risk of concrete cover splitting as well (Hughes & Videla 1992). More precisely, the total force developed at bond failure, i.e. when peak bond stress is achieved, is an increasing function of rebar area (Darwin et al. 1992, 1996). Maximum bond force, however, increases more slowly than the rebar area, which means that a longer embedment length is needed for a larger bar to fully develop a given bar stress. Therefore, in terms of bond stress, conventional wisdom suggests that it is desirable to use a larger number of small rebars rather than a smaller number of large bars (ACI Committee 408, 2003). This is clearly reflected in the expressions to determine the development length of reinforcing bars found in ACI 318 (2011), which are based on previous studies (mainly Darwin & Zuo 1996): development length is an increasing function of rebar diameter.

It is difficult to approach the effect of rebar diameter on bond strength in absolute terms, because varying rebar diameter modifies the frontier which separates pullout failures from splitting failures. Furthermore, parameters like concrete compressive strength or concrete cover are also involved in determining this frontier and affect bond strength as well. For instance, De Larrard et al. (1993) found out that increasing rebar diameter affected bond stresses but in different ways depending on concrete compressive strength. With all that, it is clear that the effect of rebar diameter on bond is not easily decoupled from the effect of other factors. Whatever the particular case, higher diameters imply higher forces to be anchored by the surrounding concrete. Therefore, if the material is capable of resisting these forces and the embedment length is enough to allow for their development, then higher bond stresses will

develop in the case of higher rebar diameters (Gambarova & Rosati 1997). However, it is usually observed that bond strength is decreased with increasing steel ratios, specially in those cases where concrete confinement is relatively limited (Ichinose et al. 2004), as is observed in Figures 2.19 and 2.20. This has been ascertained to be the consequence of a higher splitting tendency of concrete specimens in these cases (Hughes & Videla 1992, Ichinose et al. 2004).

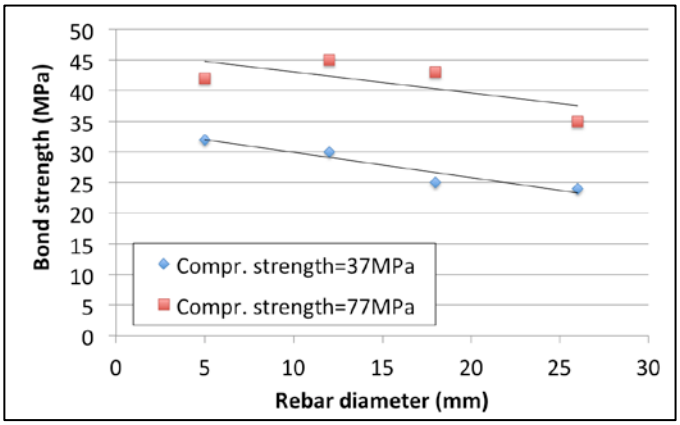

Figure 2.19 Bond strength vs rebar diameter (based on data from Bamonte & Gambarova 2007).

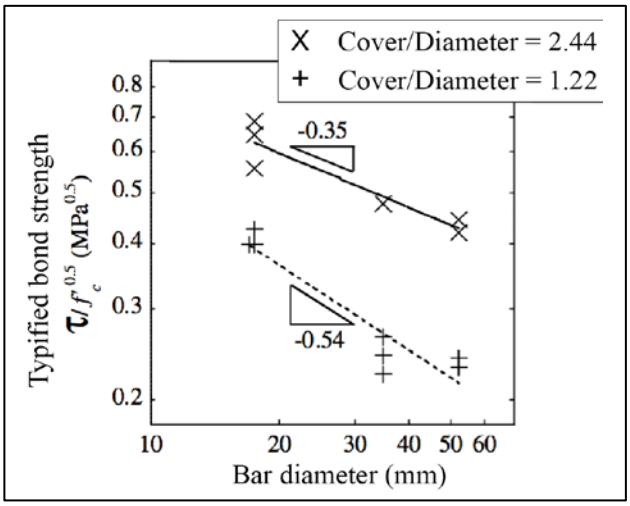

Figure 2.20. Bond strength vs rebar diameter, adapted from Ichinose et al. (2004).

REBAR YIELDING AND EMBEDMENT LENGTH

Embedment length is a matter of concern at both structural and local levels. At the structural level, i.e. real members in reinforced concrete structures, embedment length is directly related to the possibility of rebar yielding. In terms of local bond performance, there is the discussion of whether variations among different test setups regarding embedment lengths considered can affect experimental results.

When the anchorage length is long enough, which is the usual condition in real scale structural members, the reinforcing bars can be subjected to high stress levels and even to yielding before slip if enough confinement is provided. Then the lateral bar contraction influences the development of bond stresses and hence the frictional mechanism (Mazzarolo et al. 2012). In the latest version of the Model Code (FIB 2010), the influence of steel yielding on the bond stress–slip curve is explicitly considered, as shown in Figure 2.21, by means of a reduction factor depending on steel actual strain and steel mechanical properties.

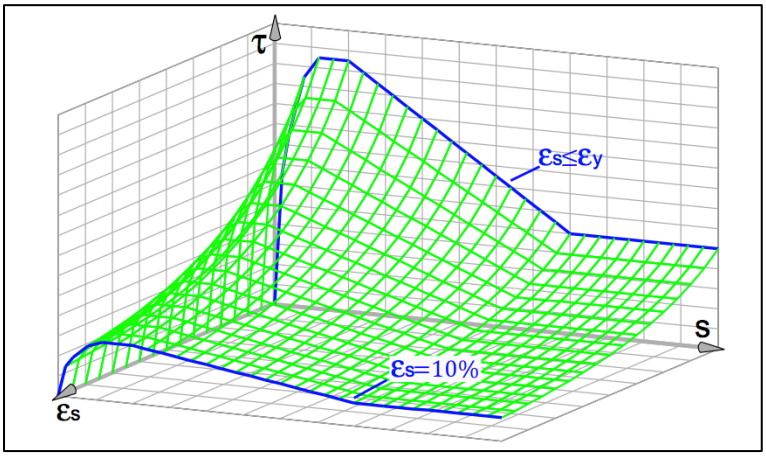

Figure 2.21. Effect of rebar yielding on bond stress–slip curve according to FIB Model Code.

However, there are also concerns with embedment length in the sphere of experimental research in relation to local bond laws. In terms of bond strength (which, as said, is the most widely studied parameter and taken as representative of bond performance), there is the question whether

varying the embedment length significantly affects bond strength values. Different authors have come to different conclusions.

Chapman & Shah (1987) noticed that the longer the embedment length, the smaller bond strength value obtained, as shown in Figure 2.22 for a rebar diameter of 10 mm. They argue that this is due to the actual bond stress distribution, which cannot be assumed to be constant. However, the decreasing trend in Figure 2.22 is not very clear: it seems rather a matter of scatter of the results. Figure 2.23 has been elaborated with results from these same authors, and it shows that the difference between the two embedment lengths they considered is not significant.

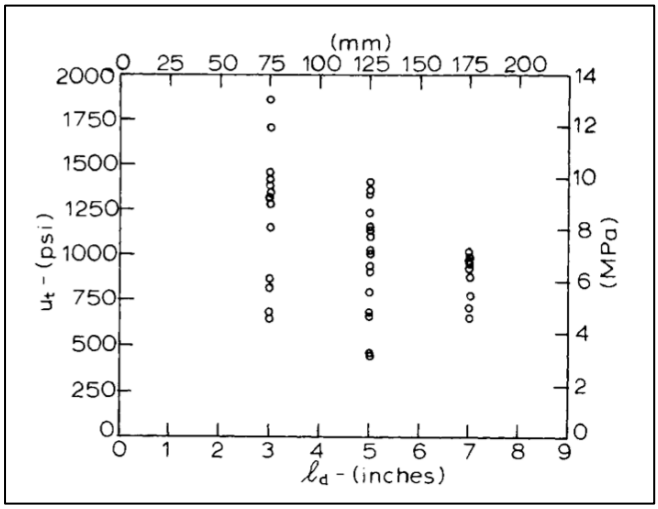

Figure 2.22. Bond strength vs embedment length (Chapman & Shah 1987).

As a matter of fact, other authors have come to the conclusion that embedment length makes no substantial difference when it comes to obtain bond strength values. For instance, Hughes & Videla (1992) conclude that the relation between bond failure load and embedment length is practically linear, regardless of rebar diameter or concrete cover: therefore bond strength is independent of the embedment length. In fact, the average bond strength shows little dependence on anchorage length. This is shown in Figure 2.24 for the case of 12-mm rebars. As the

anchorage length increases, the bond strength remains essentially the same for embedment lengths shorter than the development length.

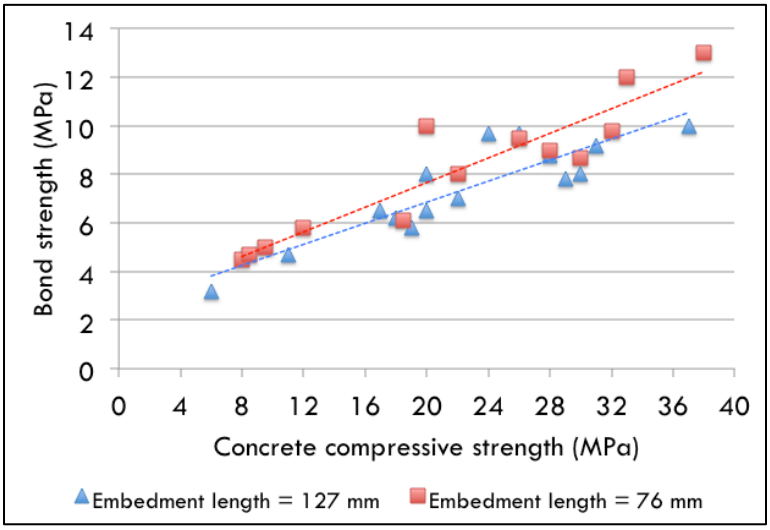

Figure 2.23. Bond strength vs concrete compressive strength for different embedment lengths, based on data from Chapman & Shah (1987).

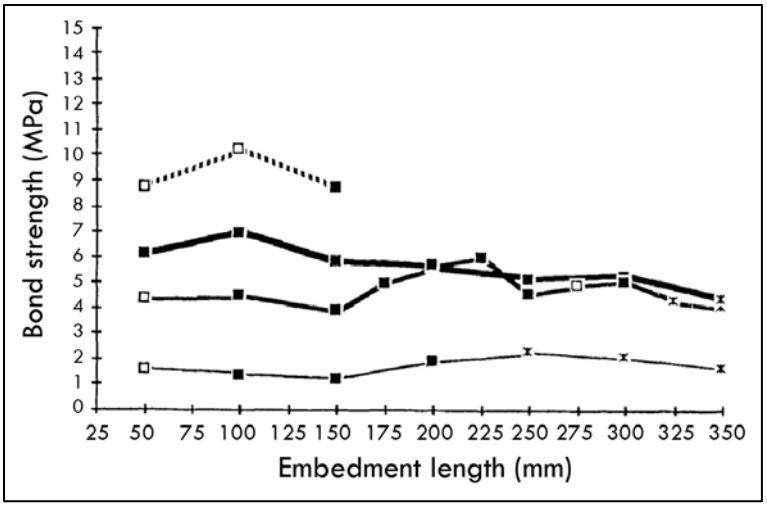

Figure 2.24. Bond strength vs embedment length for 12-mm rebars (Hughes & Videla 1992).

REBAR GEOMETRY

As outlined in section 2.1, rebar geometry in terms of ribs profile, rib height, angle of rib surface with respect to rebar axis, and rib spacing, is also a determining factor affecting bond performance. Different authors (Cairns & Jones 1995, Silva Filho et al. 2012, among others) have explored this topic by considering different types of reinforcing ribbed bars and by correlating parameters describing their geometry to bond strength.

To unify all of the aforementioned parameters (rib height, rib spacing, etc) into only one, representative index, a parameter which has been extensively used to quantify rebar geometry is the relative rib area or bond index (Soretz & Holzenbeim 1979, FIB 2000), which is defined as follows:

$$f_r = \frac{A_r}{\pi D s_r} \tag{2.1}$$

where: A_r is the area of the projection of a single rib on a plane perpedincular to the rebar axis, D is the rebar diameter, and s_r is the rib spacing.

Recently, Silva Filho et al. (2012) have considered rebars coming from different countries and have compared them in terms of their bond to concrete. These authors have characterized their geometry in a very precise way by means of 3D scanning, as shown in Figure 2.25. It is worth mentioning that rebars used in Spain (and therefore in the experimental campaign at the core of this thesis) are type 5.

When all other conditions are kept constant, bond strength values obtained vary depending on the rib pattern and rib dimensions of the rebar used (Cairns & Jones 1995, Hamad 1995, FIB 2000). This can be observed in Figure 2.26: variation depending on rebar geometry exists. However, with only one exception, all types of rebars considered by Silva Filho et al. (2012) lead to bond strength values which are scattered around an average value. Differences are not severe: the coefficient of variation is less than 12%. This is also observed in FIgure 2.27: bond

strength clearly tends to increase with the relative rib height, but almost all values are relatively clustered between 12 MPa and 16 MPa (for a rebar diameter of 12 mm). Therefore, it can be concluded that, as long as standardized rebars are used, differences in bond strength due to different rib patterns are not substantial.

Figure 2.25. Different rib patterns and geometries in reinforcing bars (Silva Filho et al. 2012).

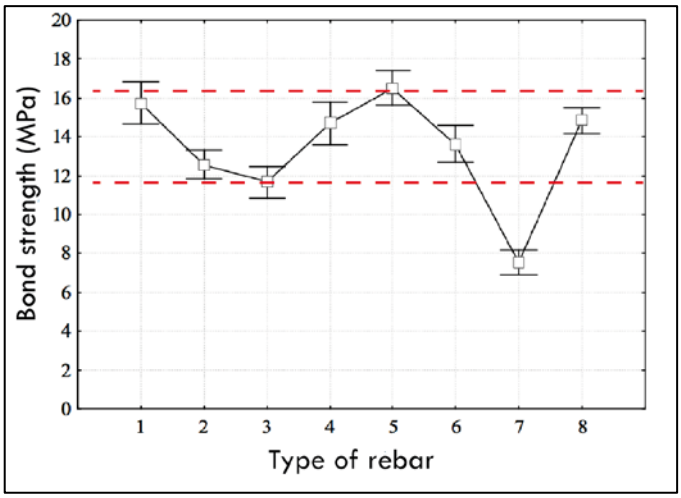

Figure 2.26. Bond strength values for different rib patterns (Silva Filho et al. 2012)

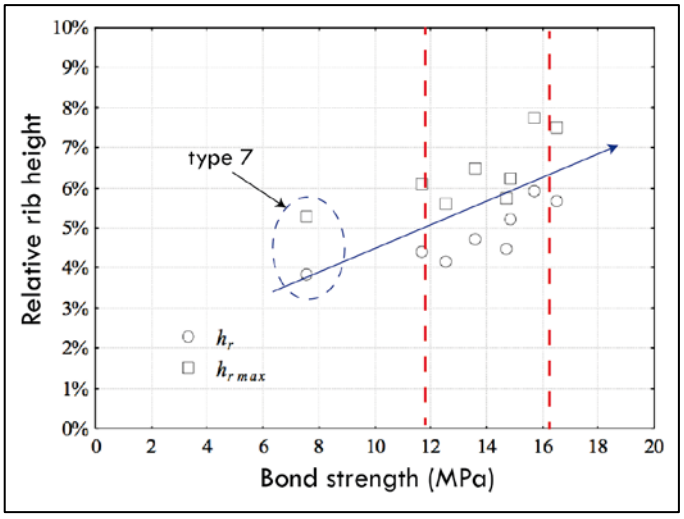

Figure 2.27. Relation between relative rib height and bond strength (source: Silva Filho et al. 2012)

2.5 Confinement

Concrete confinement can be defined as the restrainment of concrete transverse strains. This can be caused by either lateral pressure, or transverse reinforcement, or both. Concerning bond, more confinement in the anchorage region means higher bond capacity of concrete. A distinction is made between active and passive confinement:

- **ACTIVE CONFINEMENT**. It is the consequence of concrete being compressed by external forces, for instance reactions in supports or beam-column joints. Active confinement is therefore the result of forces being directly applied to the anchorage region. This type of confinement is not affected by cracks development in the anchorage and therefore is particularly effective in circumstances when concrete cover is prone to splitting.
- **PASSIVE CONFINEMENT**. Contrarily to active confinement, it is not the result of actions being applied on the anchorage regions, but the consequence of the constraining effect of concrete cover and transverse reinforcement. This constraining effect is progressively activated with the onset of bond stresses.

Figure 2.28 exemplifies active and passive confinement, showing three situations where confinement is present in different ways (Gambarova & Rosati 1997):

- (A): There is both active and passive confinement. The vertical reaction in the support is a source of active confinement, while the stirrups are a source of passive confinement.
- (B): There is only passive confinement acting on the splice shown, as a result of the stirrups.
- (C): There is only active confinement: the upper half of the anchorage region is confined by compressive stresses.

Confinement, either active or passive, plays a major role as a parameter affecting bond. Active confinement is more efficient than passive confinement particularly in situations prone to splitting, since the activation

of active confinement does not depend on the mobilization of bond stresses. On the other hand, passive confinement originates from concrete dilatancy, i.e. is progressively activated as bond stresses develop, and therefore is not so effective as active confinement in situations prone to splitting.

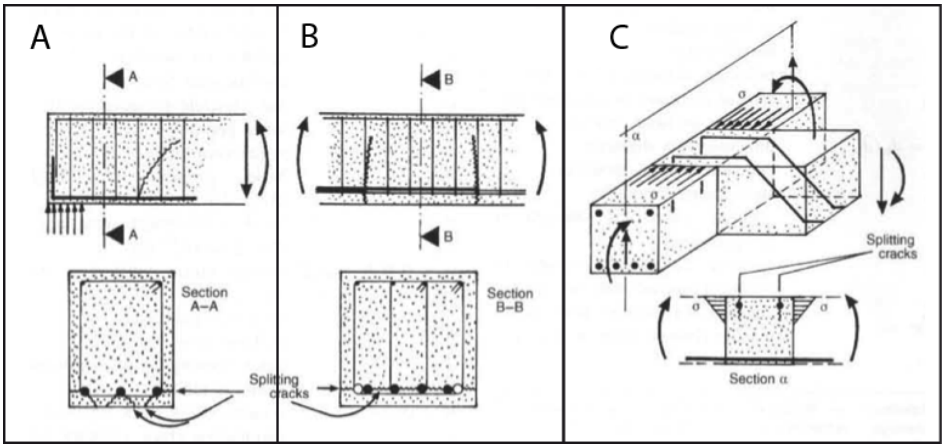

Figure 2.28. Examples of bond-confinement interaction (source: Gambarova & Rosati 1997).

The Model Code (FIB 2010)provides precise definitions for the extreme cases of unconfined concrete and well confined concrete, as follows:

- ☐ Concrete is unconfined when concrete cover is less than one time rebar diameter and when the total cross-sectional area of transverse reinforcement along the development length is less than 25% of the cross-sectional area of the longitudinal reinforcement.
- ☐ Concrete is assumed to be well confined in any of these situations:
    - Concrete cover is not less than five times rebar diameter, and the spacing between rebars is not less than ten times rebar diameter.
    - Total cross-sectional area of all transverse reinforcement along the development length is not less than the total cross-sectional area of the longitudinal reinforcement.
    - Transverse pressure is applied, not less than 7.5 MPa.

PASSIVE CONFINEMENT

It is generally assumed that the major concern regarding passive confinement is connected to the minimum values of transverse reinforcement or concrete cover in order to prevent concrete splitting (FIB 2000). It has been already mentioned in section 2.2 that the minimum concrete cover value to avoid splitting failures is approximately between 2.5 and 3.0 times rebar diameter (Cairns & Jones 1995, ACI 318-11). As a matter of fact, the confining effect of concrete cover is most usually typified by rebar diameter: concrete cover/diameter ratio is the reference parameter, because the effect of concrete cover is inversely related to rebar diameter: the bigger rebar diameter is, higher concrete cover is required to have the same degree of confinement.

Passive confinement includes not only the effect of concrete cover but also that of transverse reinforcement, and is treated in similar ways by different codes. For instance, the ACI 318-11 code defines the so-called confinement term, which simply adds the effect of transverse reinforcement to that of concrete cover/diameter ratio :

$$\frac{c_b + K_{tr}}{d_b} = \frac{c_b}{d_b} + \frac{K_{tr}}{d_b} \tag{2.2}$$

where: c_b is concrete cover, d_b is rebar diameter, and K_{tr} is the transverse reinforcement parameter, defined as follows:

$$K_{tr} = \frac{40A_{tr}}{sn} \tag{2.2}$$

where: A_{tr} is the area of transverse reinforcement, n is the number of bars being developed, and s is the spacing of transverse reinforcement.

The ACI 318-11 code establishes that the confinement term shall not be taken greater than 2.5 when used to determine the anchorage length. The reasons for the assumption of this limit on the confinement term are explicitly admitted in the commentary paragraphs of the code: when it is less than 2.5, splitting failures are likely to occur, and a pullout failure is expected for values above 2.5. However, the statement that follows this in the commentary section states: "an increase in cover or transverse

reinforcement is unlikely to increase the anchorage capacity". This statement seems to contradict the criteria regarding confinement found in the Model Code (FIB 2010), where this limit of no further positive gains in confinement is established at 5.0. Therefore, one must think that only security has motivated the aforementioned criterion found in the ACI 318-11 code.

Passive confinement affects bond performance in terms of bond strength and bond failure ductility as well (FIB 2000), not only in relation to the mode of bond failure. Bond strength increases as concrete cover increases, as shown in Figures 2.29 and 2.30.

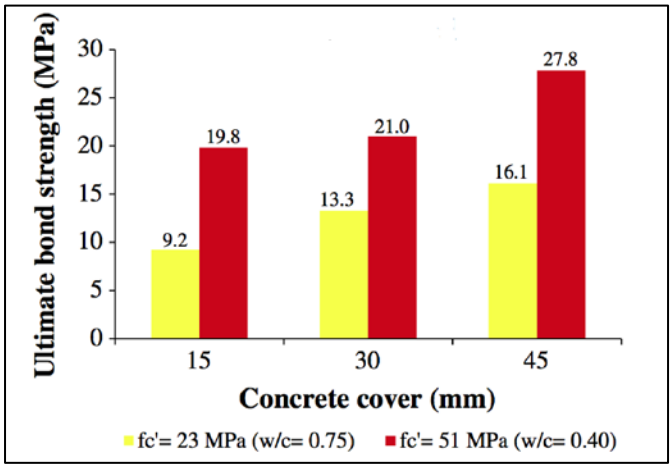

Figure 2.29. Bond strength vs cover (Yalciner et al. 2012).

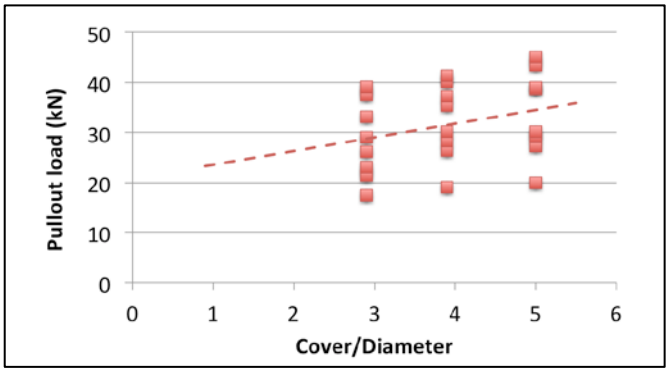

Figure 2.30. Pullout load vs cover/diameter ratio (based on data from Arel & Yacizi 2012).

The positive effect of concrete cover on bond strength is added to that of concrete compressive strength (Arel & Yacizi 2012), as shown in Figure 2.31.

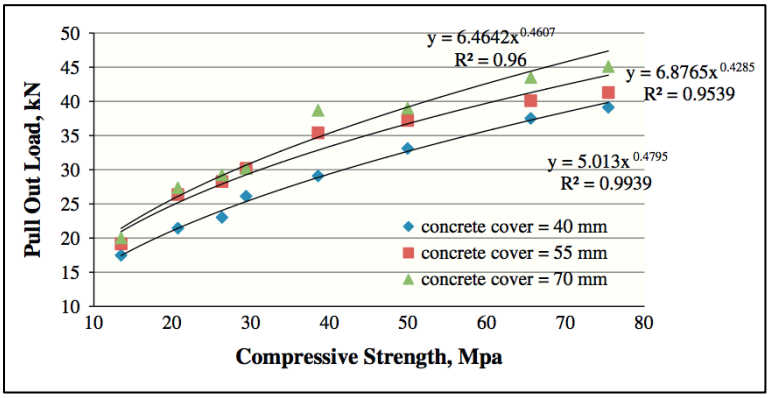

Figure 2.31. Pullout load vs compressive strength for different cover values, rebar diameter 14mm (Arel & Yacizi 2012).

Furthermore, bond stress–slip curves become steeper as concrete cover increases (FIB 2000), as shown in Figure 2.32: concrete confinement in the splice/development region improves the ductility of bond failure as well (García-Taengua et al. 2011).

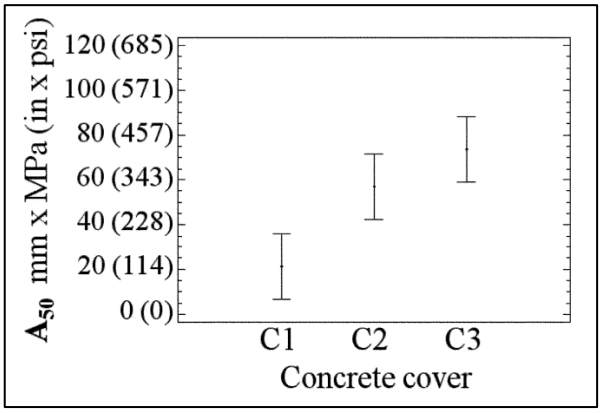

Figure 2.32. Bond ductility vs concrete cover (García-Taengua et al. 2011).

Passive confinement as considered in Figures 2.29 to 2.32 involves only concrete cover, but Harajli et al. (2004) conducted a research which

considered not only concrete cover but the effect of transverse reinforcement as well. They related bond strength to the values of the confinement term as defined by the ACI 318-11 code. Their results confirm the positive effect of transverse reinforcement on bond strength, as shown in Figure 2.33. Transverse reinforcement also improves ductility of bond failure, as shown in Figure 2.34.

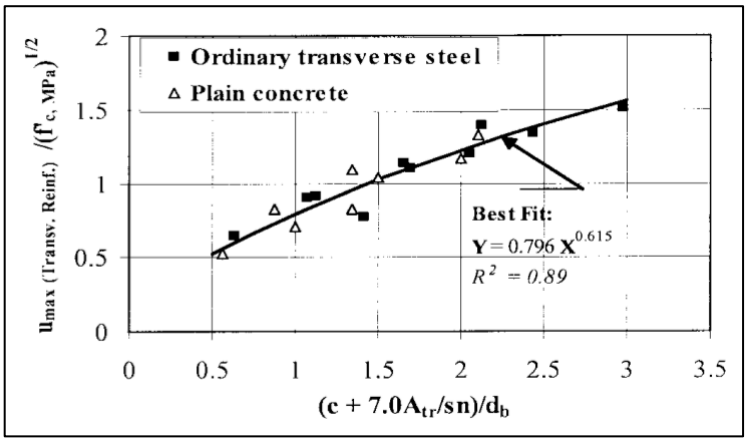

Figure 2.33. Typified bond strength vs confinement term (Harajli et al. 2004).

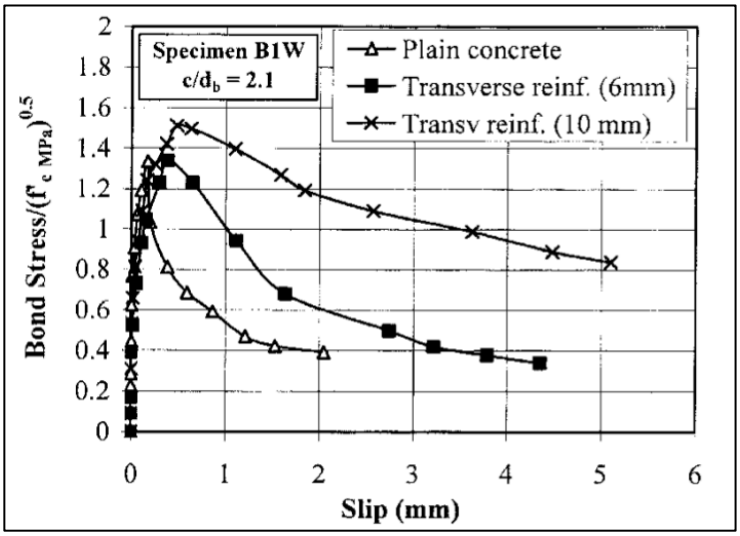

Figure 2.34. Typified bond–slip curves for concrete with and without transverse reinforcement (Harajli et al. 2004).

Harajli et al. (2004) also reported results showing how other sources of concrete confinement (addition of steel fibers among them, as will be discussed in the chapter 3) also have a positive effect on bond between reinforcing bars and concrete. Furthermore, the influence of other factors on the confining effect of concrete cover and/or transverse reinforcement has been explored by several authors (for instance, the interaction between the effect of silica fume content and passive confinement).

ACTIVE CONFINEMENT

Concerning active confinement, the crucial aspect is its role in the transition from a pullout failure to a splitting failure, because splitting failures are largely affected by different structural parameters (Tepfers 1973, Eligehausen 1979, Gambarova & Rosati 1997, Bamonte & Gambarova 2007, among others).

A number of investigations have been carried out to understand how reinforcing bars behave in terms of bond to concrete when active confinement, namely lateral pressure is applied. Robins & Standish (1984) found out that lateral pressure affects plain and deformed rebars in a different way. These differences have been related to the different failure modes in the cases of plain and ribbed rebars. With plain rebars, no splitting failure occurs: since there are no ribs, no radial stresses are induced in the concrete surrounding the rebar (Gambarova 2012). Test results obtained for plain rebars show a clear increasing trend of pullout strength with respect to lateral pressure (Robins & Standish 1984, Xu et al. 2012, among others). This is shown in Figure 2.35, where it can be observed as well that the increasing rate in bond strength with respect to lateral pressure is higher for higher rebar diameters.

The case is different for deformed rebars, as can be observed in Figure 2.36. For lateral pressure of about 30% of concrete compressive strength, splitting failure occurs (Robins & Standish 1984). When the lateral stress is increased beyond this value, there is a clear levelling off in ultimate load and concrete splitting does not occur. That is to say: in the case of plain rebars, lateral pressure increases bond strength, while in the case of deformed, ribbed rebars, lateral pressure prevents concrete splitting (Robins & Standish 1984), though a slight increase in bond strength is also detected (Xu et al. 2012), as shown in Figure 2.37.

Experimental results obtained by other authors (namely Gambarova & Rosati, 1997) agree with the aforementioned aspects findings. For example, Figure 2.38 comprises results from different authors relating bond strength to lateral pressure, and there is an inflection point for a lateral pressure value between 0.2 and 0.3 times concrete compressive strength. This result is coherent with previous findings (Robins & Standish

1984) and confirms that applying a lateral pressure of about 30% of concrete compressive strength avoids splitting. Furthermore, in Figure 2.38 it can be observed that bond strength values follow a slightly increasing trend after this inflection point, in agreement with Figure 2.37.

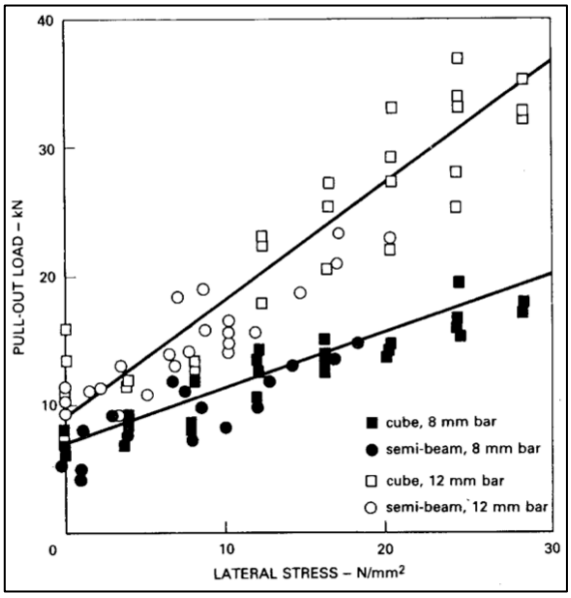

Figure 2.35. Pullout load vs lateral pressure applied, in the case of plain rebars (Robins & Standish 1984).

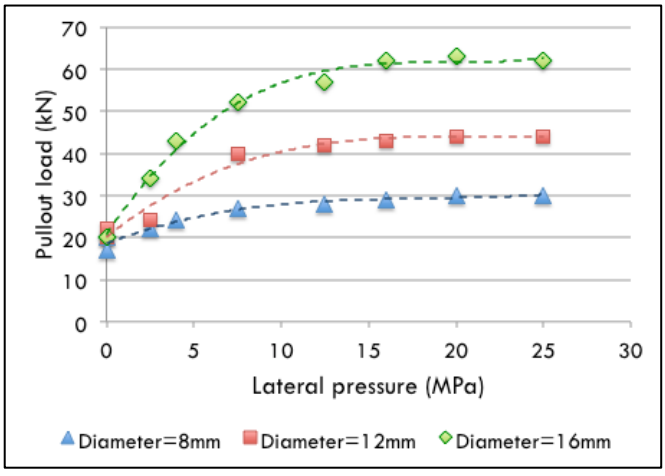

Figure 2.36. Pullout load vs lateral pressure for different rebar diameters (ribbed rebars) (Robins & Standish 1984).

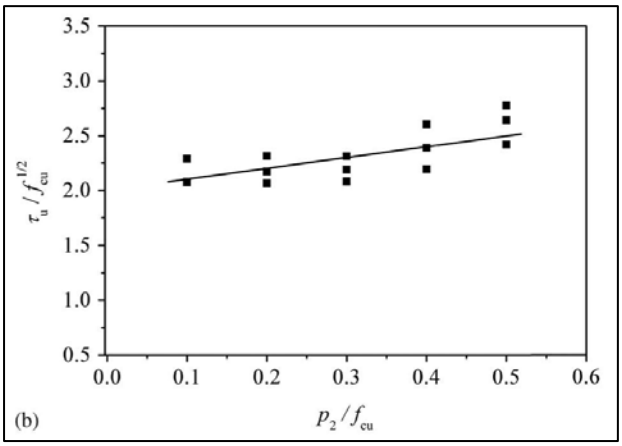

Figure 2.37. Typified bond strength vs lateral pressure for 16-mm ribbed rebars (Xu et al. 2012).

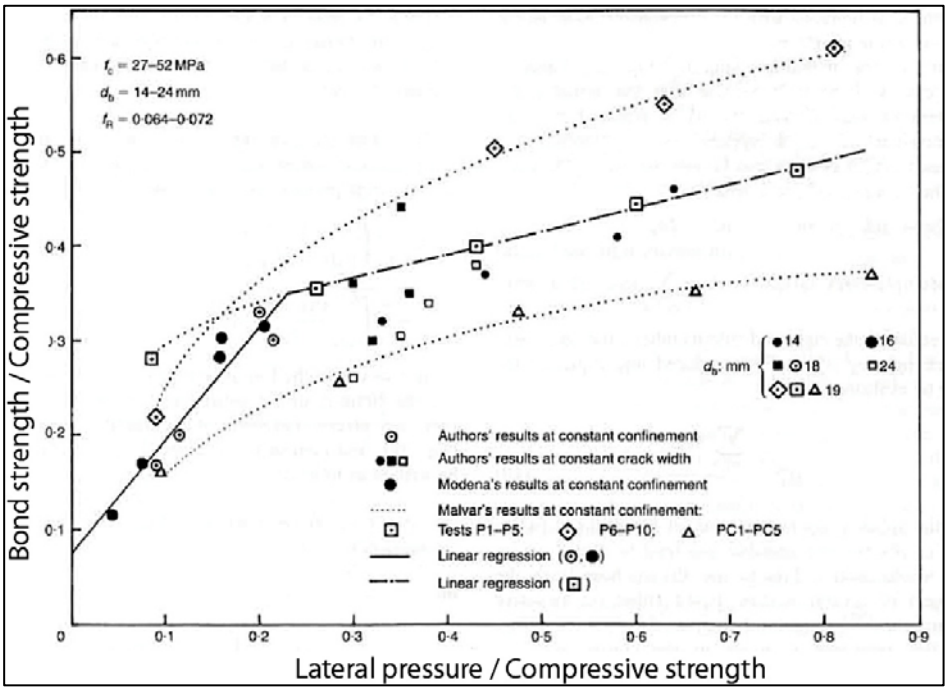

Figure 2.38. Bond strength vs confining pressure (Gambarova & Rosati 1997).

3| Effect of Fibers on Bond

Part I: State of the Art

3| Effect of Fibers on Bond

PART I: STATE OF THE ART

3.1 Contribution of Fibers to Bond Performance

As discussed in chapter 1, fibers are used to improve concrete characteristics related to tensile behavior by preventing crack growth and by enhancing mechanical behavior. Most important improvements include increase in toughness or energy absorption capacity, tensile strength, fatigue resistance, and ductility (Hamad et al. 2001). And, as described in chapter 2, bond of rebars to concrete take advantage of all these improvements when fibers are used.

Today, the beneficial effect of fibers on bond of rebars to concrete is something supported by and accepted in literature. It has also been introduced to codes. Proof of this is that the Spanish code EHE-08 specifically mentions the positive impact of fibers on bond in Annex 14 (article 69.5.1.1): "fibers improve anchorage performance whenever they are used with passive and active reinforcement". Plizzari & Cairns (2004) mention that this beneficial effect exists even for low fiber content and poorly confined situations. In relation to how fibers contribute to bond, Cairns & Plizzari (2004) point out that basically through two mechanisms: by confining reinforcement and by widening the range of crack width values this confinement remains activated.

Ezeldin & Balaguru (1989) concluded that the use of fibers improved postpeak behavior of concrete and therefore suggested their use to increase the ductility of bond failure. Cairns & Plizzari (2004) as well as Holschemacher & Weiße (2004) agree on pointing out that the most important achievement of fibers regarding bond is that they improve considerably the ductility of bond failure, and this is so even for low fiber contents. Harajli (1994) states that the presence of fibers can also imply a change in the mode of failure, leading to a ductile bond failure as

opposed to the brittle bond failure observed in plain, unconfined concrete.

It is therefore assumed that fibers improve postcrack ductility but do not modify bond strength, or only slightly if they do (Harajli 2007). Several findings until now support a limited confidence on the positive effect that fibers have on bond performance, and the tendency has been to restrict this positive impact of fibers to postpeak behaviour. It is true that a number of studies have concluded that fibers play a role very similar to that of transverse reinforcement in anchorage and splice regions, i.e. they confine concrete and control cracking (Harajli & Mabsout 2002, among others). However, other studies like that by Bischoff et al. (2004) conclude that the improvements are only partially attributable to a direct role of fibers in bond phenomena: wherever fibers are present, part of the tensile stresses is no longer to bare by longitudinal reinforcement, and then this reduction in rebar stresses is responsible for part of the improvement in bond capacity.

But the question whether fibers improve or not bond strength has also been discussed in relation to the test setup and test specimens used. A number of different test setups and methodologies have been proposed so far, but they can all be classified in two groups: short specimen tests and long specimen tests (FIB 2000). Short specimen tests and, in particular, the Pull Out Test, represent the commonest option when approaching bond and it will be the one dealt with in this thesis. However, several authors have observed discrepancies concerning the impact of fibers on bond strength values and have concluded that the source of these discrepancies is to be found at the level of test design. For instance, Hamad et al. (2001) performed a series of spliced beam tests and found out that fibers increase bond strength of reinforcement in tension. They argue that their results prove that bond tests using pullout specimens largely underestimate the effect of fibers and claim that beam tests provide more accurate results for bond strength. However, this debate is not over.

Another ongoing debate is concerned with the relationship between the mode of bond failure and the effect that fibers have on bond performance in general, and on bond strength in particular. Some studies

have concluded that the effect of fibers on bond is really significant only when there is concrete cover splitting (Harajli et al. 1995, Harajli & Mabsout 2002). However, most of the studies have analyzed together all their results in terms of bond strength regardless of their mode of failure, which probably needs some more data to clarify whether the impact of fibers on bond is of the same magnitude when there is splitting or not.

In any case, codes and provisions now consider the fibers contribution to bond. It has been already noted that the Spanish code EHE-08 explicitly states that fibers do improve bond, but leaves open the possibility of considering it in the calculations: "fibers improve anchorage conditions [...], and this may be taken into consideration when performing the corresponding calculations [...] as long as it is supported by experimental campaigns" (art. 69.5.1.1, Annex 14). Annex 14 does not add anything like a particular equation or modifying factors for the expressions to calculate the anchorage length in art. 69.5: Specific criteria for anchorage and splicing of reinforcement.

The Eurocode 2, meanwhile, does not mention anything about it, either in its provisions or its annexes.

The code ACI 318-11, although its section 3.5: Steel reinforcement in section 3: Materials regards steel fibers and states that they are allowed to resist shear in flexural elements only, it does not mention anything about their impact on bond in Chapter 12: Development and splices of reinforcement.

It is true that the report *ACI 408R-03 Bond and Development of Straight Reinforcing Bars in Tension* does consider fibers when they are added to concrete. In *Chapter 2: Factors affecting bond*, fibers are accounted for as a factor to be considered within the group of factors corresponding to "concrete properties", and reads: "The provisions in ACI 318 for the development of deformed bars are based on bond strengths that are governed by a splitting failure of the concrete around the bar [...].Theoretically, the use of FRC should improve resistance to splitting cracks and reduce required development lengths". But this document does not goes beyond this either: despite the aforementioned statements, it does neither propose corrective factors that could be applied to the

formulation in ACI 318-11 nor adopt any other approach to account for fibers contribution in development/splice length calculations. Moreover, this report by ACI Committee 408 follows an approach which is clearly targeted to bond in general. It reviews different formulations and data from different sources but does not constitute a supplement of ACI 318-11 for the practice of structural design regarding fibers and bond.

3.2 Overview of Experimental Approaches Found in Literature

This section aims at providing a comprehensive description of the different experimental approaches found in scientific literature dealing with bond of reinforcing bars to steel fiber reinforced concrete. A number of different aspects are considered under the generic naming of 'experimental approaches': what variables are considered, how different different mix designs are taken into account, and the objectives usually pursued.

As for the type of tests performed and the kind of test setup or structural elements used, pull-out tests constitute the most common option. By means of pull-out test, a bond stress–slip curve is to be obtained from each tested specimen. Then the analysis of experimental results is focused in the exploration of how fibers (as well as other factors) affect bond strength, and sometimes bond toughness as well.

Thus, the most usual approach can be summarized as the analysis of the effect of certain factors (including the amount and/or type of fibers) on certain variables (such as bond strength or the ductility of bond failure).

The factors normally considered are no more than two or three of the following:

- **FIBER CONTENT**. In virtually all cases, the fiber contents considered do not exceed 120 kg/m^3. And most of the times, the maximum amount that is considered is 60 kg/m^3. Such limitation seeks to restrict the amounts of fiber considered in research to the usual contents in

real applications. Thus, for instance, Dupont & Vandewalle (2002) compared concretes with fiber contents ranging between 20 kg/m^3 and 60 kg/m^3 to concrete without fibers. Meanwhile, Ezeldin & Balaguru (1989) considered fiber contents of 20 kg/m^3, 30 kg/m^3, 45 kg/m^3, and 60 kg/m^3, and Plizzari & Cairns (2004) compared concrete with 30 kg/m^3 to its unreinforced counterpart. There are few cases where higher fiber contents are considered, like the case of Harajli et al. (1995), who consider fiber contents up to 156 kg/m^3.

- **CONCRETE COMPRESSIVE STRENGTH**. In general terms, concre compressive strengths considered are usually between 50 MPa and 90 MPa. It is common to two concretes compared, one of 'normal' strength compared to a higher strength concrete (Reza & Rangan, 1998 or Holschemacher and Weiße, 2004). Thus, approaches like that followed by Ezeldin & Balaguru (1989), who consider concretes of 35 MPa and 76 MPa, that followed by Cairns & Plizzari (2004), who consider concretes of 50 MPa and 80 MPa, or that followed by Holschemacher & Weiße (2004), who compared a concrete of 30 MPa to a 90-MPa concrete, are examples of the most general scenario. No doubt this is motivated by the issue of how the effect of fibers on bond strength is affected by varying concrete strength, as will be discussed in the following section.

- **PASSIVE CONFINEMENT**: concrete cover and/or transverse reinforcement. Papers which consider different levels for passive confinement in their experiments follow one of the three general options described below:

    - On one hand, studies such as that by Dupont & Vandewalle (2002) or that by Reza & Rangan (1998) consider different situations of non-symmetrical concrete cover. For example, Figure 3.1 represents the three levels defined for concrete cover as defined by Vandewalle & Dupont (2002) in their study. Considering non-symmetrical concrete cover configurations is motivated by the most usual situation of reinforcement in structural concrete members, where reinforcing bars are rarely confined by the same concrete cover in all directions.

- Contrarily, other studies, such as that reported by Ezeldin & Balaguru (1989), consider concrete cover symmetrically with respect to the reinforcing bar.

- In other cases, instead of considering concrete cover as a factor, authors like Harajli et al. (1995) choose not to vary concrete cover and to introduce different levels of transverse reinforcement as a factor to control passive confinement. In the case of Harajli et al. (1995), the effect of passive confinement is restricted to the comparison of specimens with transverse reinforcement to specimens without transverse reinforcement. Other authors, such as Cairns & Plizzari (2004), go further and do not simply compare situations with transverse reinforcement to situations without, but also consider different diameters for the stirrups: 6mm, 8mm and 10mm in the case of Cairns & Plizzari (2004).

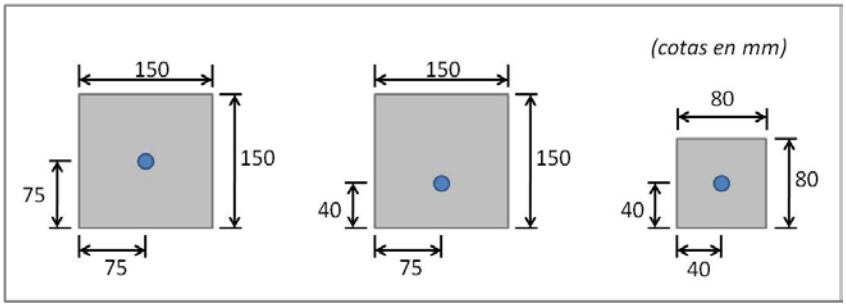

Figure 3.1. Concrete cover values as considered by Dupont & Vandewalle (2002).

☐ **REBAR DIAMETER**. The vast majority of investigations comprised in literature concerning bond of reinforcing bars to concrete consider different diameters of the rebar. Most of the studies have considered rebar diameters of 16 mm and below. Holschemacher & Weiße (2004), for example, considered diameters of 10 mm and 16 mm. However, there are several papers reporting results obtained with larger diameters, like those by Cairns & Plizzari (2004) (diameters of 20 mm and 24 mm) or Harajli et al. (1995) (diameters of 20 mm and 25 mm), for example. It can be said that most of the studies that focus

on local behavior by means of pull out tests consider rebar diameters not higher than 16 mm. On the contrary, experiments based on large specimen test setups like spliced beam test usually consider bigger rebar diameters as well.

3.3 Effect of Fibers on Bond Strength

As already mentioned in section 3.1, the addition of fibers to concrete improves the adhesion of the reinforcing steel. However, there are a variety of nuances thereon which will be discussed below.

First, it is necessary to precise what particular aspects of bond are improved by adding fibers. Dupont & Vandewalle (2002) conclude that the addition of fibers brings about no improvements in the ascending branch of the bond stress–slip curve or on bond strength: benefits are limited to the descending branch or postpeak region only, and they point out this effect is more important for higher concrete cover values. Harajli (1994) agrees noting this, and states that, unless a high fiber content is used, the presence of fibers has no impact on bond strength when compared to plain unconfined concrete.

However, some studies have concluded that the addition of fibers not only does not improve bond strength: fibers have been detected to slighly decrease bond strength in some occasions. Adding fibers may cause a reduction in bond strength of up to 30%, as concluded by Dancygier et al. 2010. The authors claim that this effect is likely to be caused by the fact that adding fibers prevented the proper compaction of concrete matrix around the rebar. It is true that fibers decrease workability of concrete mixes, as discussed in chapter 1, and that improper compaction might affect not only bond but all mechanical properties of concrete. However, it is important to take into account the scatter in the experimental results before drawing conclusions concerning bond strength. Experimental results obtained by Dancygier et al. (2010) are plotted in Figures 3.2 and 3.3 together with the error bars corresponding to the 95%-confidence intervals in each case. These confidence intervals have been calculated with the standard deviation

values provided by the authors. It is observed that confidence intervals overlap in all cases, and therefore the decrease observed in the bond strength values averaged from a number of specimens cannot be considered as definite.

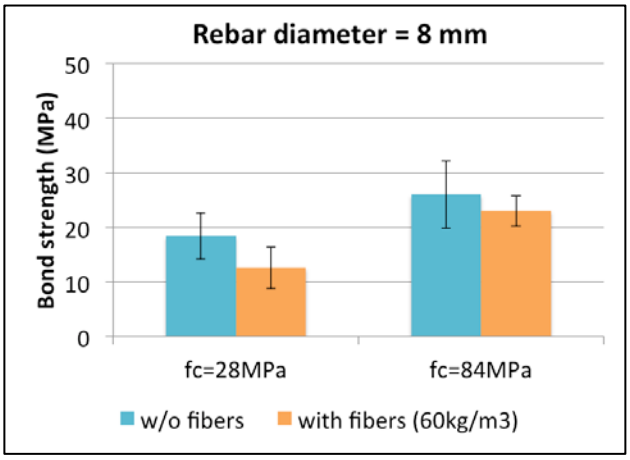

Figure 3.2. Bond strength vs concrete compressive strength and fiber content (based on data from Dancygier et al. 2010).

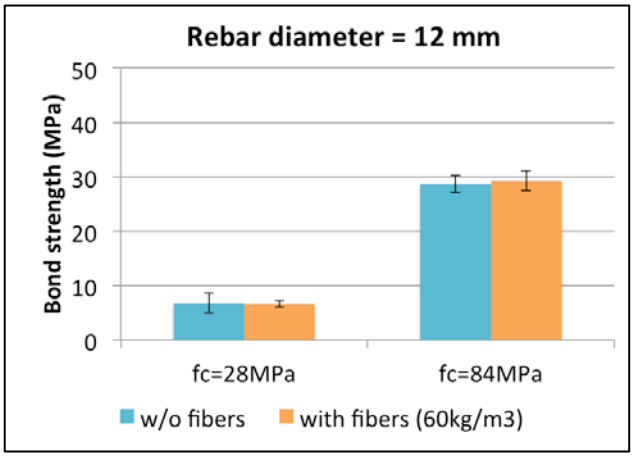

Figure 3.3. Bond strength vs concrete compressive strength and fiber content (based on data from Dancygier et al. 2010).

This analysis is coherent with what these same authors reported two years later (Dancygier & Katz 2012) as well as with the conclusions obtained by several other authors: adding fibers does not increase or decrease

bond strength. The addition of steel fibers hardly influences bond strength, as shown in Figure 3.4. In this Figure, values of the so-called bond ratio, i.e. the ratio between bond strength obtained for SFRC and bond strength obtained for the equivalent plain concrete, are shown. It can be seen that even a slight increase in bond strength is observed when fibers are added in most of the cases (Dancygier & Katz 2012).

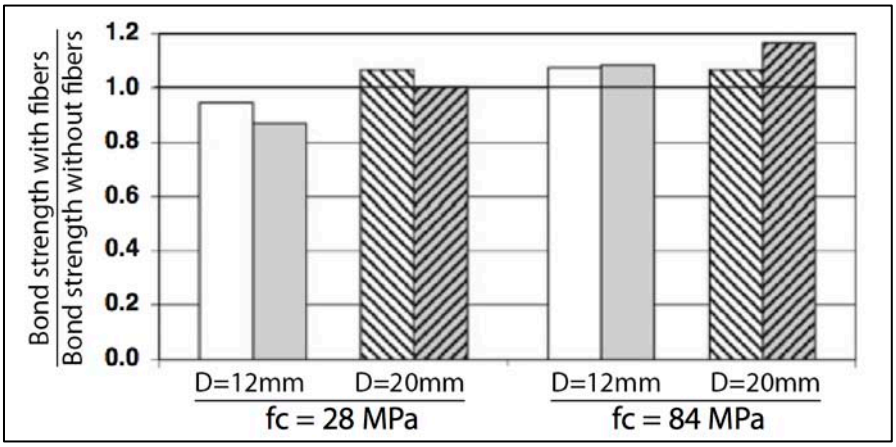

Figure 3.4. Bond ratio vs concrete compressive strength and rebar diameter (Dancygier & Katz 2012).

In this regard there has been much discussion in literature about whether the effect of fibers on bond depends on concrete compressive strength. It is observed in Figures 3.2 to 3.4 that different concrete compressive strength values are considered, and the effect of fibers is usually analyzed in these different scenarios.

The works of Ezeldin & Balaguru (1989), for instance, compared bond capacity of concretes with different compressive strengths, all of them reinforced with steel fibers. Their research considered two different fiber contents (30 kg/m^3 and 60 kg/m^3) and concluded that the effect of fibers on bond strength is practically negligible in normal strength concretes below 40 MPa.

Holschemacher & Weiße (2004) come to similar conclusions. That is why, in their opinion, it would not make sense to consider the contribution of

fibers in calculations for anchorage or splice length of reinforcement. They argue that in normal strength concrete the contribution of fibers to bond is almost negligible, and in high-strength concrete bond strength is good enough without fibers and therefore it is not worth taking into account the effect of the fibers.

However, we should not forget that Hamad et al. (2001) note that, following the results of their research, pull-out type tests probably underestimate the effect of fibers on bond strength. This may explain the discrepancies between the positions described above, and between values experimentally obtained by different authors. Because a number of studies have pointed out that fibers do increase bond strength. For instance, Harajli & Salloukh (1997) observed that adding 156 kg/m^3 of steel fibers increase bond strength up to 55% with respect to plain unconfined concrete. This is coherent with the results reported by Hamad et al. (2001), as shown in Figure 3.5, where there is a consistent increase in bond strength when fiber content is increased.

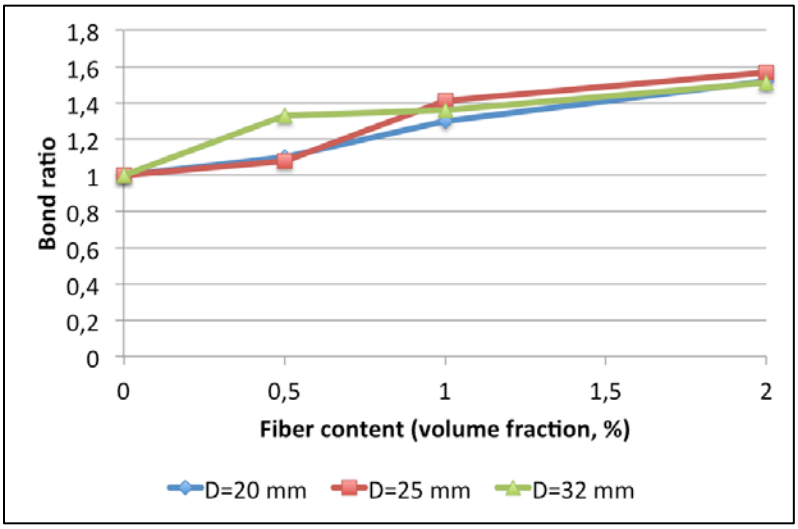

Figure 3.5. Bond ratio vs fiber content for different rebar diameters (based on data from Hamad et al. 2001).

Conclusions reached by Harajli et al. (2002) agree with those of Hamad et al. (2001) and Harajli & Salloukh (1997), as shown in Figure 3.6. The addition of steel fibers does not have an important effect on bond

strength for volume fractions below 0.5%. However, for higher fiber contents, it is observed that bond strength increases when fiber content is increased. The average increase in bond strength observed with was about 8%, 26%, and 33% for fiber contents of 0.5%, 1.0%, and 2.0% respectively (Harajli et al. 2002). It is also observed in Figure 3.6 that the positive effect of fibers on bond strength may have an upper limit, as the increasing rate of the bond ratio decreases with fiber content (red lines).

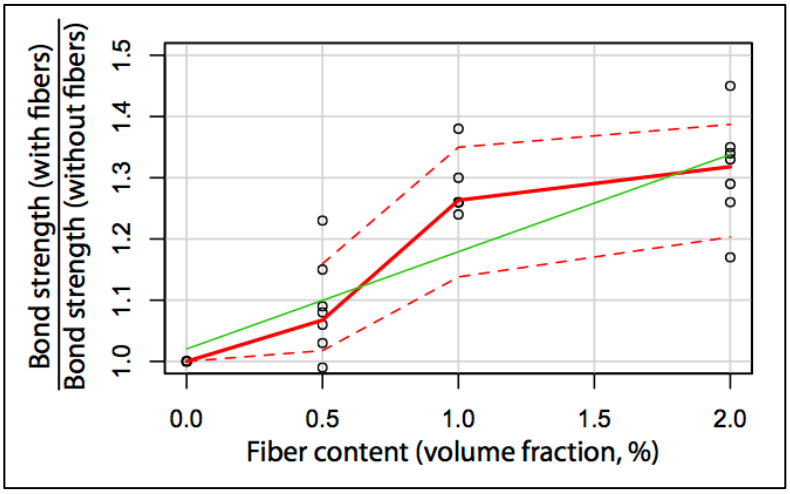

Figure 3.6. Bond ratio vs fiber content (based on data from Harajli et al. 2002).

To sum up, the issues concerning the effect that steel fibers have on bond of reinforcing bars to concrete, and particularly on bond strength, have not yet been totally resolved. This justifies the need for further research on this topic, and therefore the convenience and objectives of this thesis.

3.4 Structural Role of Fibers on Bond

Harajli et al. (1995) concluded that whether the effect of fibers on bond strength is significant or not depends on the mode of failure. This effect is not significant when the failure mode is by pull-out. On the contrary, fibers play an important positive role when there is splitting of concrete cover. The work by Harajli & Mabsout (2002), later than that by Harajli et al. (1995), comes to the same conclusion. In fact, this makes sense if one considers that fibers act once cracks have opened (sewing effect). When there is splitting, the effect of the fibers is clearly understandable: they act similarly to transverse reinforcement. By contrast, when the failure mode is pull-out, a network of microcracks appears around the rebar but the crack width is so small that fibers fail to bear tension and therefore do not contribute to bond capacity. In this sense, it seems appropriate to analyze those cases when there is splitting separately from those cases when failure mode is pull out, as is done in this thesis.

As a matter of fact, there is general consensus in literature regarding this point: the effect of fibers on bond is very significant when splitting occurs. Several studies (Reza & Rangan 1998, Cairns & Plizzari 2004, among others) have focused on analyzing the contribution of fibers to bond performance when concrete surrounding the rebar is cracked. Among them, one of the most interesting contributions is that reported by Cairns & Plizzari (2004), which considered the effect of fibers on bond in precracked or presplit specimens as shown in Figure 3.7. These studies concluded that fibers increase bond strength even when stirrups provide a good confinement (and these stirrups bear increasing loadings as the splitting cracks develop, see Giuriani et al. 1991).

So far we have been talking about the effect of fibers on bond of reinforcing bars to concrete in the following terms: what specific aspects of bond are affect by fibers, to what extent these effects are important, and on which concrete mixes these effects are more noticeable. Well, a different and complementary issue to the aforementioned aspects is trying to go beyond the local bond phenomena, i.e. how fibers affect bond at a structural level. Though these aspects fall out of the scope of

this thesis, it is worth mentioning works like that by Bischoff et al. (2004), because they provide a different point of view.

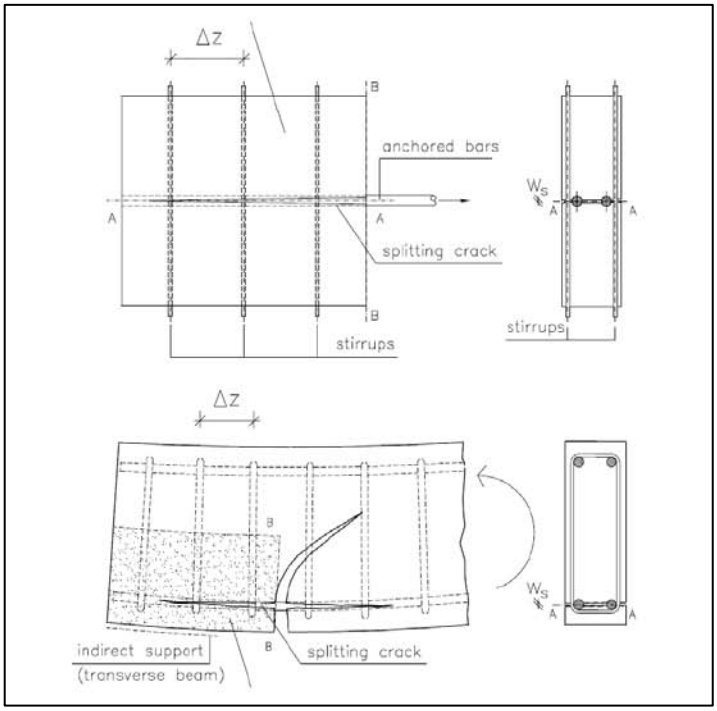

Figure 3.7. Presplit specimens (Plizzari et al. 2002).

Bischoff et al. (2004) point out that the load-bearing capacity of the cross-section of a SFRC member to resist a certain bending moment is higher than that of the same cross-section in a concrete member without fibers, because fibers in the cracked area of the cross-section contribute to residual strength by bearing part of the tensile stresses, as can be seen in Figure 3.8. Consequently, it can be argued that the presence of fibers slightly unloads the longitudinal reinforcement. Taking all this into account, they have studied the effect of fibers on bond by means of the spliced beam test, testing beams 3 meters long with transverse reinforcement in extreme sections to prevent shear failure. They have compared the results obtained for plain concretes to those obtained for fiber reinforced concrete (concrete compressive strength is approximately 80 MPa in both cases). The results show that bond strength when fibers are present is up to 18% higher. However, the aforementioned authors

conclude that, only 4% of this 18% increase is attributable to the direct effect of fibers: the remaining 14% increase derives from the fact that, for a certain bending moment, the tensile load that the longitudinal reinforcement has to bear is lower when fibers are used.

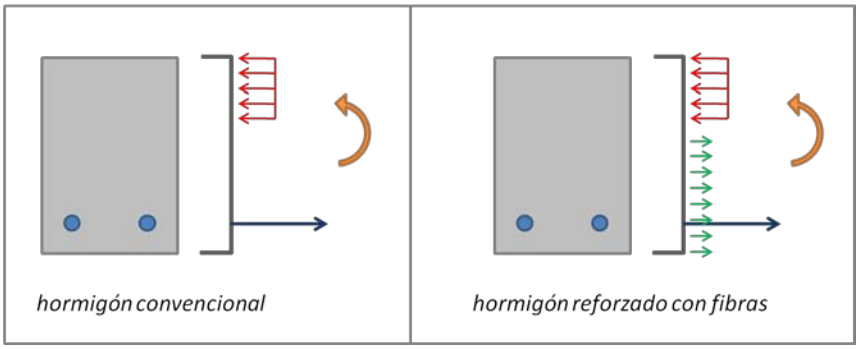

Figure 3.8. Compressive and tensile stresses distribution in the cross-section of a concrete member without and with fibers.

The conclusions that arrive Bischoff et al. (2004) show, therefore, a new light on the positions of Holschemacher and Weisse (2004), among others, since even assuming as true that the "direct" fiber to the maximum bond stress is of little importance (despite the reservations that follow from studies such as Hamad et al. 2001), this coupled with their contribution to adherence through a slight discharge of the main armor and would be significant enough to have it in account in the design of overlap and anchors.

In consequence, the conclusions drawn by Bischoff et al. (2004) provide a new frame for positions like that of Holschemacher & Weisse (2004), among others, regarding the utility of considering the fibers effect on bond or not when calculating development/splic lengths. Even if it is assumed that the "direct" effect of fibers on bond strength is negligible or unimportant (despite the reservations that follow from studies such as Hamad et al. 2001, as discussed in section 3.3), their contribution to bond performance by slightly unloading longitudinal reinforcing bars would be significant enough to account for it when designing a splice or anchorage.

3.5 Effect of Fibers on Bond Toughness

Fibers have a positive effect on the ductility of bond failure, and this is probably the least controversial aspect of fibers contribution to bond performance of all issues discussed in this chapter. However, the positive impact of fibers on bond toughness is usually examined by comparing different bond stress–slip curves only, in contrast with their influence on bond strength, which has received more attention in terms of quantification. Figure 3.9 shows several bond stress–slip curves where it can be observed that, for a certain value of rebar diameter, increasing fiber content implies increasing area under the curve (Harajli et al. 2002). It has been argued that the specific source of this ductility is that fibers restrain the propagation of longitudinal microcracks and therefore they allow a higher number of rebar ribs to take part in the stress transfer between rebar and surrounding concrete (Hamad et al. 2001).

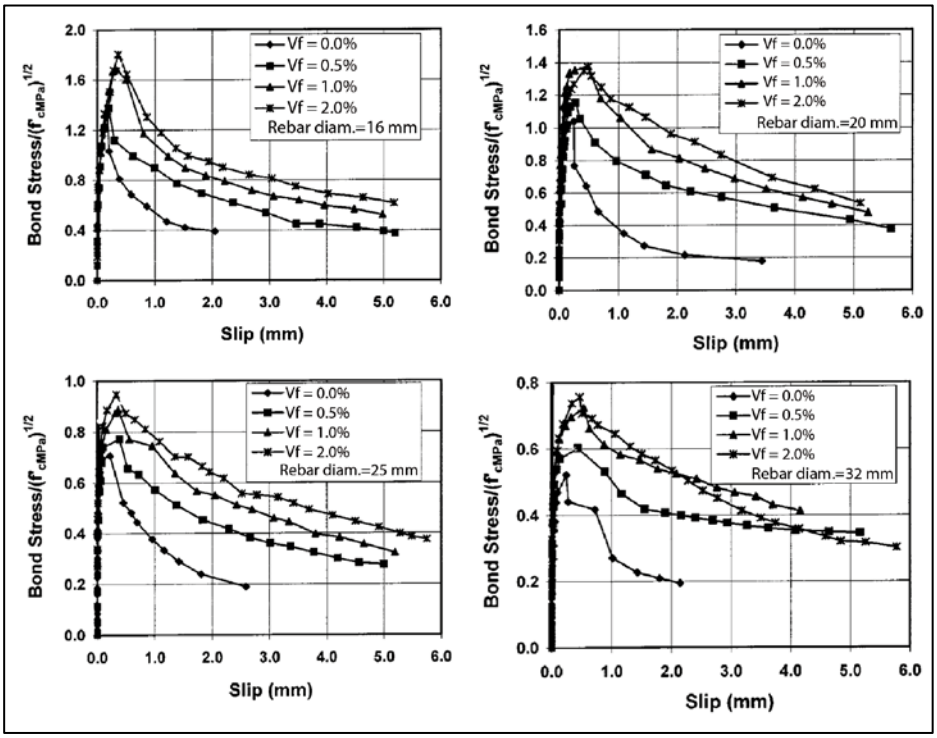

Figure 3.9. Bond toughness depending on fiber content and rebar diameter (adapted from Harajli et al. 2002).

Some authors have claimed that the effect of fiber contents on the ductility of bond failure is also dependent on concrete compressive strength. In some cases, areas under the bond stress–slip curve have been found to follow an almost linear tendency with respect to fiber content (García-Taengua et al. 2011), as shown in Figure 3.10. Dancygier & Katz (2012) have observed that this effect is more pronounced in the case of high-strength concrete, as shown in Figure 3.11.

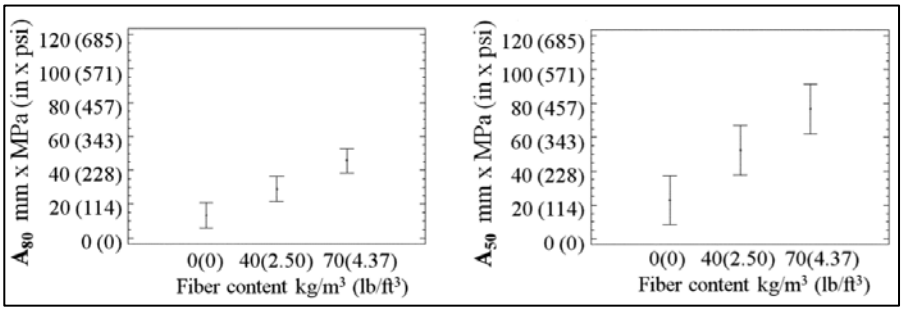

Figure 3.10. 95%-confidence intervals for areas under bond stress–slip curve vs fiber content (García-Taengua et al. 2011).

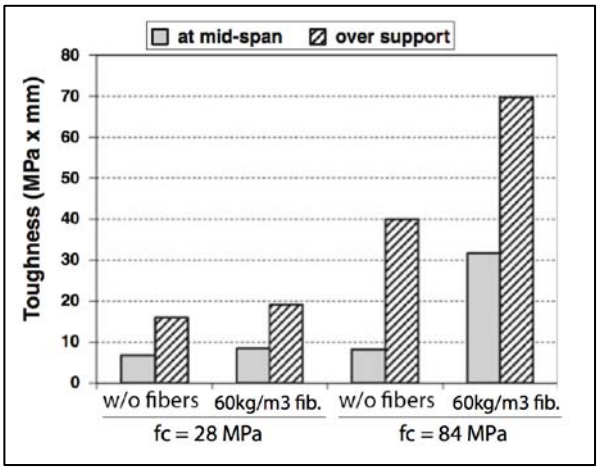

Figure 3.11. Area under bond stress–slip curve vs compressive strength and fiber content (Dancygier & Katz 2012).

The effect of fiber geometry on the ductility of bond failure is not clear. In some cases it has been argued that the impact of fiber slenderness and length on bond ductility is not significant, or at least not in the same degree as that of fiber content (García-Taengua et al. 2011).

4| Experimental Program

Part II: Experimental Program & Results

4| Experimental Program

PART II: EXPERIMENTAL PROGRAM & RESULTS

4.1 Factors and Levels

In the context of this research, the word 'factor' is used to refer to those variables which have been controlled and are supposed to have a potential effect on other variables or outcomes of the experiments: these are called 'response variables'.

A modified version of the Pull Out Test has been selected as the most appropriate test for the purposes of this research. Accordingly, response variables will be any parameters to be obtained from the bond stress–slip curves resulting of the pull out tests.

The selection of the factors to be considered and their levels, or values, has been performed on the basis of both economy and reliability: the number of factors and values per factor has been the minimum required to come to reliable conclusions. The point of departure has been Table 4.1, which summarizes the parameters that different codes take into account when estimating development lengths of reinforcing bars to concrete: the latest version of ACI 318 and Eurocode 2 as well as the Spanish Code for Structural Concrete (EHE-08).

Table 4.1. Factors considered for evaluating development length by different codes.

	ACI 318-11	EC-2	EHE-08
Concrete compressive strength	☑	☑	☑
Rebar diameter	☑	☑	☑
Steel yield strength	☑	☑	☑
Position of rebar during casting	☑	☑	☑
Lightweight concrete	☑	☑	☑
Epoxi coating of rebar	☑		
Additional concrete cover		☑	
Transverse reinforcement		☑	
Transverse pressure		☑	

The following aspects have been taken into account:

- ☐ There was no need to consider steel's yield strength because, although the Spanish code EHE-08 considers both 400 MPa and 500 MPa steel classes for reinforcing bars, the latter is much more widely used than the former. Therefore steel's yield strength has been 500 MPa in all cases.
- ☐ Lightweight concretes are out of the scope of this thesis, as well as the effect of epoxi coatings or that of transverse pressure. Therefore in all cases there is: normal-density concrete, uncoated rebars, and no pressures additionaly acting on the specimens tested.
- ☐ With respect to the rebar relative position in the cross-section during casting, and considering that bond performance is under study at a local level only, it has not been considered.

As a result of all aforementioned considerations, the experimental factors and their values have been as shown in Table 4.2:

Table 4.2. Factors and levels considered.

	Type I mixes	Type II mixes	Type III mixes
Rebar diameter, mm	8 16 20	8 12 16	8 12 16
Concrete cover	C1=30mm C2= (C1+C3)/2 C3=5 D	C1=2.5 D C2=3.5 D C3=5.0 D	C1=2.5 D C2=3.5 D C3=5.0 D
Fiber geometry (slenderness / length)	65/60 80/50	45/50 80/50 80/35	45/50 80/50 80/35
Fiber content, kg/m³	0 40 70	0 40 60	0 40 60

The values or levels considered for each one of the factors, as listed in Table 4.2, have been selected according to the following criteria:

- **CONCRETE COMPRESSIVE STRENGTH**. Three different reference mixes have been considered. Each one of them has led to a group of different mixes as a result of adding fibers. Since they have been produced and tested sequentially, they have been numbered accordingly: all type I mixes were produced and tested in a first stage, then all type II mixes, and finally all type III mixes. They differ in terms of water/cement ratio, maximum aggregate size, and cement content, and cover the range of compressive strength values between 30 MPa and 50 MPa. As a result, the research is focused on normal-strength concrete in agreement with the scope of the thesis.

- **REBAR DIAMETER**. Four different rebar diameters have been considered. 8mm rebars have been considered as representative of small rebars used in real applications (6mm and 8mm for building, 8mm and 10mm for civil engineering works). 16mm rebars have been selected because they are a commonplace in bond literature. At first (type I mixes) 20mm rebars were considered in addition to 8mm and 16mm diameters. However, after this first series, considering 8-12-16 mm diameters seemed more convenient than 8-16-20 mm. That is the reason why the values considered for rebar diameters are the same for type II and type III series but they differ from those for type I series (Table 2).

- **CONCRETE COVER**. Concrete cover values have been defined as a function of rebar diameter. C1 is the smallest concrete cover value: in the first stage (type I series) it was 30 mmn, which is the minimum value legally required according to Spanish code EHE-08. However, it was reset to 2.5 times the rebar diameter for type II and type III series, because this is usually the estimate of the frontier between splitting failures and pullout failures. C3 is 5 times the rebar diameter in all cases, because this is the situation that the Model Code (FIB 2010) defines as 'good confinement'. C2 was an intermediate value, C1<C2<C3: for type I series it was the average of C1 and C3, but for type II and type III series it was redefined as 3.5 times the rebar diameter.

- **DIMENSIONS OF STEEL FIBERS**. Four types of hooked-end fibers have been considered which are different in terms of slenderness and

length only: 45/50, 65/60, 80/35, and 80/50. They all are within the so-called macro-fibers and among the ones which are most widely used in precast industry.

- **FIBER CONTENT**. Fiber contents considered have been decided below 1% in volume fraction: in addition to unreinforced concrete (0 kg/m^3), fiber contents from 40 kg/m^3 (V_f=0.51%) to 60-70 kg/m^3 (V_f=0.76-0.89%) constitute the referential frame for most usual SFRC applications.

4.2 Materials

The three reference mix designs considered in this research are summarized in Table 4.3. Cement type CEM II/B-M 42.5 R was used in all cases. The aggregates used have been river sand, crushed limestone coarse aggregate, and limestone filler. The superplasticizer used has been a polycarboxylate ether. With respect to the steel fibers used, all of them are cold-drawn, hooked-end fibers made with low carbon steel (yield strength 1100 MPa minimum) and without any coating.

Table 4.3. Reference mix designs (kg/m^3).

	Type I	Type II	Type III
Water/Cement	0.60	0.45	0.55
Cement	325	440	325
Sand 0/4	1006	957	1050
Coarse aggr. 7/12	544	723	835
Coarse aggr. 12/20	362	-	-
Filler	-	72	37
Superplasticizer	1.40	10	1.40

Each one of these reference mix designs was initially tested and adjusted to admit a volume fraction of 0.5% of 65/60 fibers with slump values between 10 cm and 15 cm.

However, each one of these reference mix designs would be different in each particular case since fiber type and fiber content would differ

according to their having been defined as factors. Filler and admixture amounts were the only parameters adjusted in each case to keep slump values between 10 cm and 15 cm at the same time segregation was prevented.

4.3 Design of POT Specimens

Specimens for the Pull Out Test have been designed based on the RILEM recommendations (1970, 1983, 1996). The specimens used in this research, however, are not in total agreement with these recommendations: they are prismatic, not cubic specimens.

Furthermore, some preliminary calculations were made in order to avoid rebar yielding so that specimens failure could be related only to bond failure in all cases. These calculations concerning embedded length have followed the expressions given by Eurocode 2 (art. 8.4.2) and the Spanish code EHE-08 (art. 69.5.1.2) for determining average bond strength: f_{bd} (Eurocode) or τ_{bd} (Spanish code EHE-08).

Finally, specimens cross-section are defined as a function of rebar diameter and therefore varies depending on that parameter and on the concrete cover value considered in each particular case.

All these aspects are detailed in the following subsections.

4.3.1 LONGITUDINAL DIMENSIONS (RILEM)

As shown in Figure 4.1, RILEM recommendations for the Pull Out Test (1970, 1983, 1996) prescribes the following requirements:

- Total length of the specimen (L) is to be 10 times the rebar diameter, though never less than 200 mm.
- Embedded length (L') is to be 5 times the rebar diameter, where the absence of sleeve protection allows the generation of bond stresses between rebar and concrete.

These conditions have been observed in all POT specimens produced and tested.

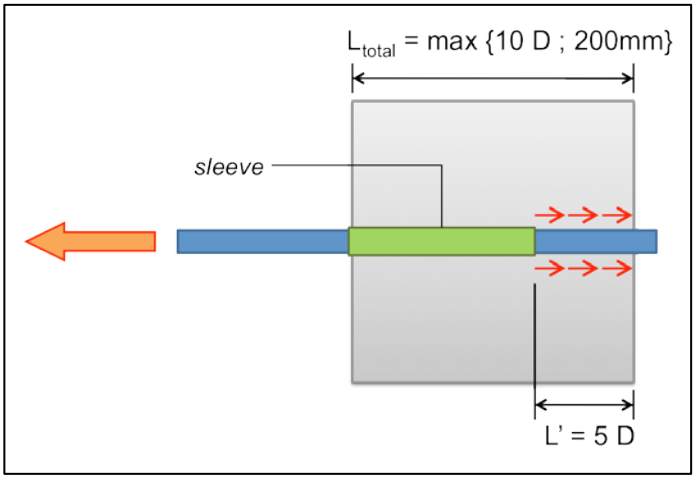

Figure 4.1. POT specimen according to RILEM recommendations

- ☐ Total length of the specimen (L_{total}) is to be 10 times the rebar diameter, though never less than 200 mm.
- ☐ Embedded length (L') is limited to 5 times rebar diameter by means of a sleeve, which is placed to prevent bonding contact between steel and concrete. This way, bond stresses are developed only along L', and not along the sleeve.

These conditions have been observed in all POT specimens produced and tested.

4.3.2 PREVENTING STEEL YIELDING

Eurocode 2 provides an expression to determine bond strength on the basis of a simplified, uniform distribution of bond stresses along embedded length (as shown in Figure 4.2). The same rationale is assumed by the Spanish code EHE-08. This is taken as reference to have a preliminary estimate of bond capacity of concrete.

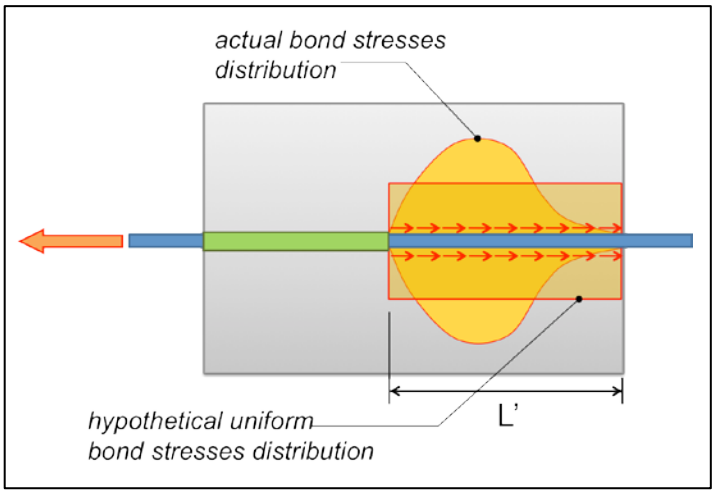

Figure 4.2. Real and simplified bond stresses distributions.

After that, the resulting force of all bond stresses is calculated and the condition of no rebar yielding is imposed. With that, one can estimate the embedded length value that would imply rebar yielding for each one of the rebar diameters considered. Embedded length values assumed for each of the rebar diameters considered have to be below these estimated limits.

The ultimate bond stress according to Eurocode 2 is:

$$f_{bd} = 2.25\eta_1\eta_2 f_{ctd} \tag{4.1}$$

where:

- f_{ctd} is the tensile strength of concrete. For the purpose of these preliminary calculations, it is estimated assuming a required compressive strength of 40 MPa. Therefore:

$$f_{ctd} = \frac{0.7 f_{ctm}}{1.5} = \frac{0.7 \times 0.3 \sqrt[3]{f_{ck}^2}}{1.5} = 1{,}6\ MPa \tag{4.2}$$

- η_1 is 0.7 or 1.0 depending on the position of rebar during the casting of concrete. It is assumed $\eta_1 = 1.0$.
- η_2 is 1.0 for rebar diameters not bigger than 32 mm.

With all that, ultimate bond stress is estimated as follows:

$$\tau = f_{bd} = 2{,}25\eta_1\eta_2 f_{ctd} = 2.25 \cdot 1.0 \cdot 1.0 \cdot 1.6 = 3.6\ MPa \tag{4.3}$$

If a simplified, uniform distribution is assumed for bond stress as shown in Figure 4.2, pull out force P_y corresponding to rebar yielding is as follows:

$$P_y(N) = \pi \cdot \phi(mm) \cdot L'_y(mm) \cdot \tau\left(\frac{N}{mm^2}\right) \tag{4.4}$$

Imposing no rebar yielding implies that rebar stress value is below steel's yield strength:

$$P(N) \leq P_y(N) = f_y(MPa) \cdot \frac{\pi \cdot \phi^2(mm^2)}{4} \tag{4.5}$$

Equations (4.4) and (4.5) together lead to the following:

$$\pi \cdot \phi(mm) \cdot L'(mm) \cdot \tau(MPa) \leq f_y(MPa) \cdot \frac{\pi \cdot \phi^2(mm^2)}{4} \tag{4.6}$$

And given that $\tau = 3.6\ MPa$ after (4.3) and steel's nominal yield strength is 500 MPa, it follows that the embedded length to prevent rebar yielding from occuring before bond failure has to verify the following condition:

$$L'(mm) \leq L'_y = 34.7 \cdot \phi(mm) \tag{4.7}$$

When this condition is applied to the rebar diameters considered in this research (Table 4.2), it is obtained that assuming RILEM recommendations concerning embedded length is appropriate in all cases, as shown in Table 4.4.

Table 4.4. Embedded length values: verification of no-rebar-yielding condition.

Rebar D (mm)	L' (mm)=5D	L'_y (mm)
8	40	278
12	60	416
16	80	555
20	100	694

4.3.3 LONGITUDINAL DIMENSIONS

Figure 4.3 summarizes longitudinal dimensions of the POT specimens used in this research depending on the rebar diameter considered in each case. Two aspects are particularly relevant:

- ☐ POT specimens used are not cubic (as required by RILEM recommendations) as a result of concrete cover being variable (Table 2).
- ☐ Rebar is not centered lengthwise because its position in the cross-section varies in each particular case, as concrete cover is one of the variables considered in this research. This is exemplified in Figure 4.3.

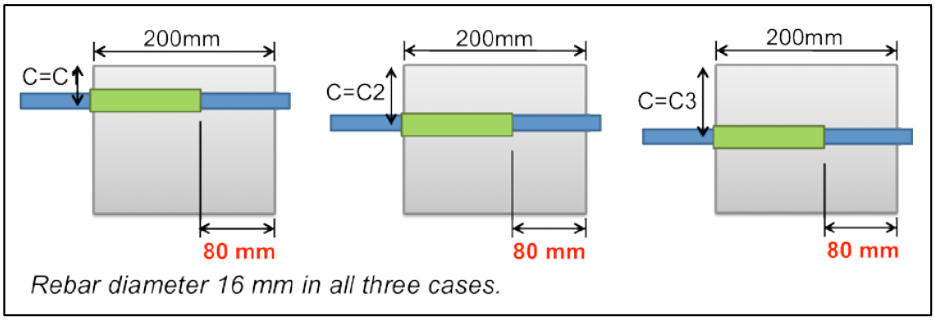

Figure 4.3. Longitudinal dimensions of POT specimens.

4.3.4 CROSS-SECTION

Cross-section of POT specimens is sketched in Figure 4.4 in terms of the diameter of the rebar (D), the side (S), and the factor 'concrete cover', variable (C). As shown in Figure 4, rebar is positioned excentrically so that the factor 'concrete cover' is restricted to two out of four semi-axes in the cross-section. With respect to the other two semi-axes, concrete cover had to be greater in order to have a good confinement. According to the Model Code (FIB 2010), it has a good confinement with concrete cover values bigger than 5 times the rebar diameter. It has been taken as reference a rebar diameter of 25 mm so that further research with bigger rebar diameters is compatible with all data obtained and reported herein. Accordingly, for the two semi-axes not considered as

variable within the cross-section, a minimum dimension of $5 \cdot 25 = 125$ mm was established.

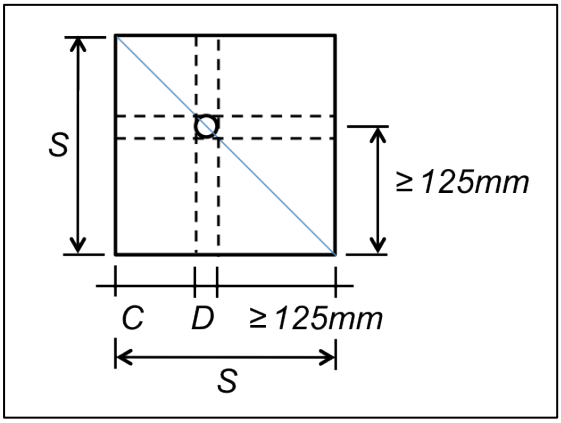

Figure 4.4. Cross-section of POT specimens.

4.4 Design of the Experiment

Usual approaches to study bond of rebars to concrete define a certain test and then analyze the effect that variations of some parameters have on experimental outputs. This is usually performed by varying only one parameter at a time, maintaining other parameters at their reference values. However, this strategy is not the most appropriate from a statistical point of view because it implicitly assumes that the effect of one parameter is independent of the values of the other parameters considered. This could be corrected by selecting a number of possible values for each parameter and then testing all possible combinations of all values considered for all parameters. But this leads to an amount of work which is not usually affordable. In order to solve these difficulties to come to statistically reliable conclusions without excessive costs in time and resources, the most convenient strategy is to rely on the principles of what is known as Design Of Experiments (DOE hereafter) to plan the testing campaign.

In this case, a total of 5 factors (compressive strength, fiber geometry, fiber content, rebar diameter, concrete cover) is under consideration,

each one of them at 3 different values. Testing all possible combinations would have meant $3^5 = 243$ combinations to be tested. In addition, if one intends to produce and test 3 POT specimens per combination, as it is usual in concrete research, this leads to a total of 729 POT specimens to be produced and tested. This would have been totally unaffordable.

What has been done is to apply DOE techniques to select a reduced number of combinations to be tested so that this reduction does not imply any bias or decrease in the reliability of the results to be drawn from the analysis of experimental results. This is possible by means of fractional factorial designs or test plans based on the so-called orthogonal arrays (Montgomery 2009). They make it possible to study the effects of a number of factors by testing only a few of all possible combinations.

The consideration given to concrete compressive strength as a factor is somewhat different with respect to how other factors have been handled when planning the experiment. This is justified as follows. Concrete compressive strength cannot be totally predetermined to a set of values as is the case with rebar diameter, fiber content, etc. Rather it scatters around the mean, or target value for each set of mixes coming from the same reference mix. Accordingly, concrete compressive strength is not a factor with three predetermined levels, but a continuous variable which takes a different value in each particular case. Since it could not be predetermined, it could not be treated in the same way as the other factors considered. Taking this into account, it was more convenient to organize the fractional factorial plan independently of concrete compressive strength, and then producing and testing all these combinations for Type I series first, then for Type II series, and then for Type III series. The result is a fractional factorial design organized in blocks, as summarized in Figure 4.5. Furthermore, the aforementioned way of considering concrete compressive strength makes it possible to approach the analysis of experimental results by conceptualizing it as a response surface.

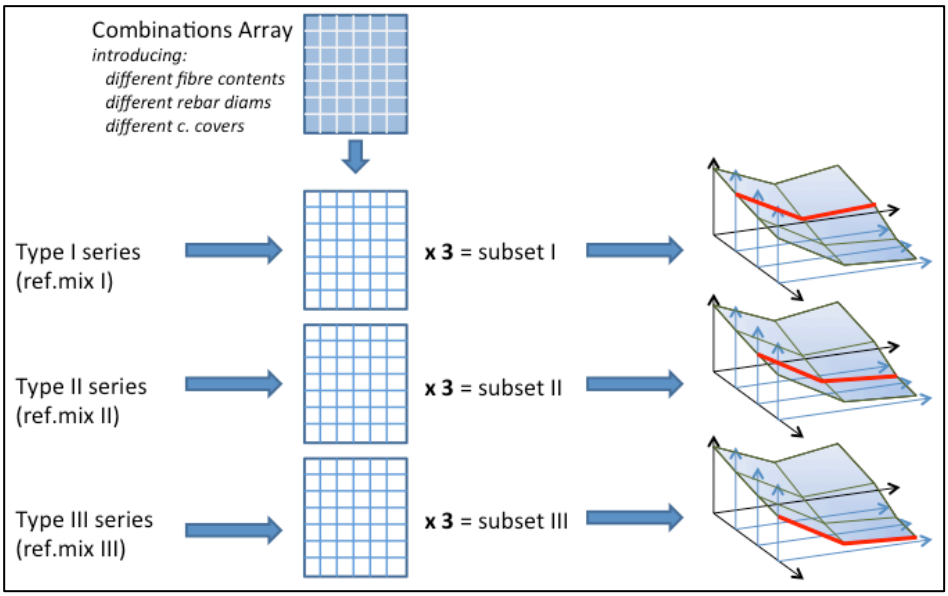

Figure 5. Structure of the experiment: fractional factorial plan organized in blocks.

The principles and rationale of DOE are summarized in Appendix 1. As a result of the application of this methodology to this research, the combinations to be tested for each series resulting from Type I, Type II, and Type III reference mixes are shown in Table 4.5, Table 4.6, and Table 4.7 respectively.

Table 5. Combinations tested (type I series).

	Fiber	F.Content	Diameter	C.Cover
I-1	65/60	40	16	C1
I-2	-	0	8	C2
I-3	65/60	70	20	C3
I-4	65/60	40	8	C3
I-5	-	0	20	C1
I-6	65/60	70	16	C2
I-7	80/50	40	20	C2
I-8	-	0	16	C3
I-9	80/50	70	8	C1

Each one of these combinations consisted of 3 POT specimens and 2 cylindrical specimens produced with concrete from the same batch.

As it can be seen in Table 5, having only two fiber types considered leads to an unbalanced number of combinations per fiber type after the orthogonal array L9 (Appendix 1, Montgomery 2009, Box et al. 2005) is adapted to this particular case. That is the reason why 3 fiber types instead of only 2 were considered for Type II and Type III series.

The number of POT specimens produced and tested is 9 x 3 = 27 for each series, and since there are 3 series, the total number of POT specimens in this research has been 27 x 3 = 81, far less than the 729 specimens that a complete experiment would have required.

Table 6. Combinations tested (type II series).

	Fiber	F.Content	Diameter	C.Cover
II-1	-	0	8	C1
II-2	80/35	60	8	C2
II-3	45/50	40	8	C3
II-4	45/50	60	12	C1
II-5	80/50	40	12	C2
II-6	-	0	12	C3
II-7	80/35	40	16	C1
II-8	-	0	16	C2
II-9	80/50	60	16	C3

Table 7. Combinations tested (type III series).

	Fiber	F.Content	Diameter	C.Cover
III-1	-	0	8	C1
III-2	80/50	40	12	C2
III-3	80/50	60	16	C3
III-4	-	0	12	C3
III-5	45/50	40	16	C1
III-6	45/50	60	8	C2
III-7	-	0	16	C2
III-8	80/35	40	8	C3
III-9	80/35	60	12	C1

4.5 Methodology and Procedures

4.5.1 PRODUCTION OF CONCRETE

All concrete mixes in this research have been produced by following the same process and sequence in all cases. The sequence of operations is summarized as follows:

- Pouring of coarse aggregate and sand, then premixing for 1 min.
- Pouring of cement, then premixing for 2 min.
- Pouring of water, then mixing for 2 min.
- Addition of the superplasticizer, then mixing for 2 min.
- Addition of fibers, gradually during 1 min.
- Mixing for 7 min.

The reason for adding the fibers after all other components is not in agreement with, for instance, recommendations by ACI 544 Committee with respect to the production of SFRC. However in this case, given the limitations of the mixer used (mixing energy and capacity) and the loss of workability when adding the fibers, it was necessary to add the superplasticizer before the fibers. This is also the reason why fibers were not added to the mixer quickly, but gradually. Figure 7 shows a detail of the mixer and the concrete being mixed.

Figure 7. Concrete mixing: a detail.

Right after mixing, concrete slump was measured according to the standard EN 12350-2:2006. The criterion established for fresh mixes was that slump values ranged between 10 cm and 15 cm. Then, the concrete used was poured back to the mixer, and after 1 more minute mixing, POT specimens and cylindrical specimens were cast.

4.5.2 MOULDS AND CASTING OF SPECIMENS

Cylindrical specimens were produced according to the standard EN 12390-2:2009. Right after casting, they were covered with plastic bags. 24 hours afterwards they were demoulded and moved to the climatic chamber, where they would remain until the 28th day after their production.

Specific moulds were prepared for POT specimens. They were prismatic but their dimensions were variable and the position of the embedded rebar was also variable depending on rebar diameter and concrete cover. That is why POT specimens could not produced by using preexisting moulds but moulds specifically designed for the purpose of moving some of their parts, as shown in Figures 4.8 and 4.9.

Walls of the mould corresponding to the bases of POT specimens were fabricated in veneered plywood, 20mm thick, and pierced with a hole of sufficient diameter for the passage therethrough of the rebar to be embedded. Figure 10 shows some of these movable parts of the moulds. At all times, special attention was given to the relative positioning of all mould walls so that they were parallel to each other, in order not to introduce errors in the specimens dimensions or the position of the rebar, which should be substantially parallel to all sides of the POT specimen.

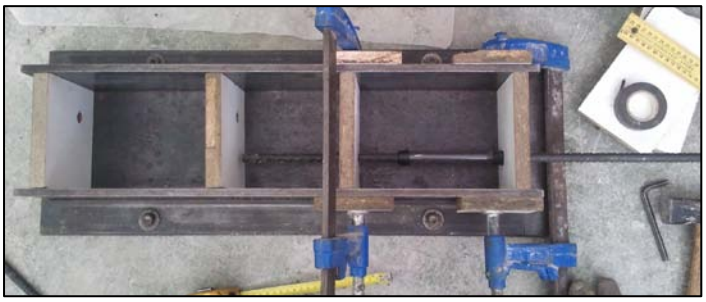

Figure 4.8. A view of a mould for POT specimens.

Figure 4.9. Detailed view of a mould for POT specimens.

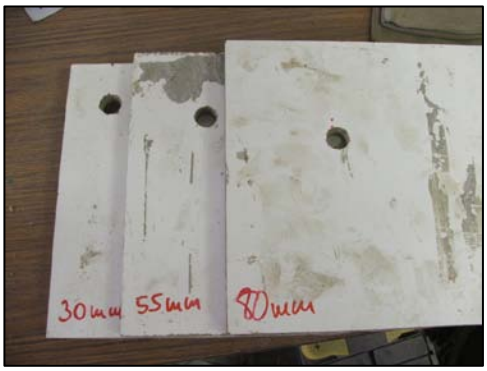

Figure 4.10. Movable parts of some moulds for POT specimens.

Rebars were passed through the holes, placing at the same time a plastic sleeve in order to limit the length where bond is to be mobilized between rebar and concrete, which is different in each case. Adhesive tape was used to fix the sleeve to the rebar in order to avoid that part of the cement paste entered between rebar and sleeve when casting the specimen.

Once the moulds were assemble with all walls properly positioned and rebars and sleeves were placed, moulds were cast. After concreting, the upper surface was finished with a trowel and the specimens were covered with a plastic sheet to minimize the loss of water.

24 hours thereafter specimens were demoulded (Figure 4.11) and moved to the climatic chamber, where they remained under standirdized conditions until their age was 28 days, when they would be tested.

Figure 4.11. Demoulding of a POT specimen.

4.5.3 TESTING

Each one of the batches of concrete produced was characterized by tesing under compression the two cylindrical specimens produced simultaneously with POT specimens. All cylindrical specimens were tested at the same age POT specimens were tested, i.e. 28 days. Test method to

determine compressive strength was carried out according to EN 12390-2:2001, as required by Spanish code EHE-08 (art. 86.3.2).

Pull out tests were carried out as shown in Figure 4.12. The specimen to be tested was supported by a rigid steel plate with a hole in its center to allow the rebar passing through. The lower end of the rebar was anchored by clamps. By operating a hydraulic system the supporting plate was pulled up and, as a result, the rebar was pulled out of the specimen.

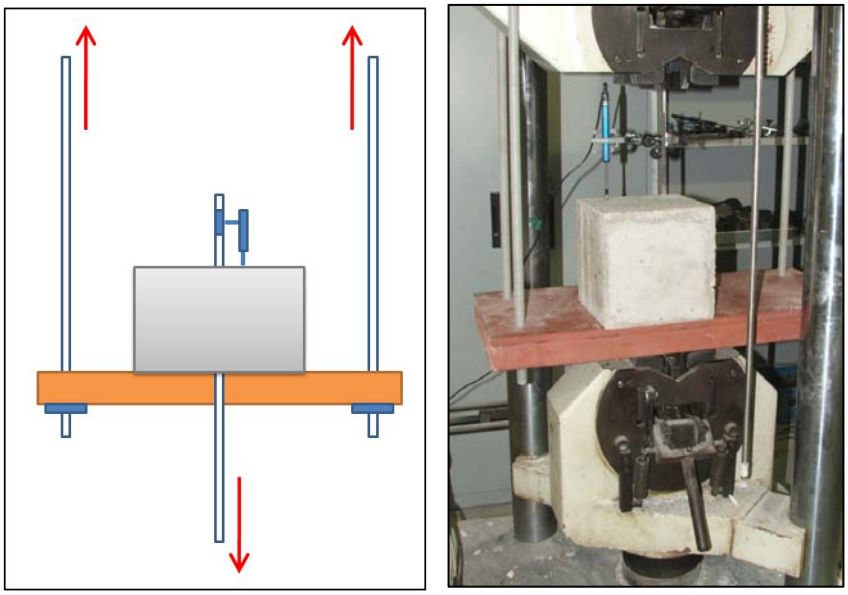

Figura 4.12. Force diagram (left) and a view of the pull out test as performed in this research (right).

The slip of the rebar was monitored on the surface opposite to that from which the rebar was being pulled out by means of a LVDT sensor. It was located on this surface in order to detect the load corresponding to the onset of bond stress along the entire embedded length.

Pull out tests were carried out by keeping the ratio of slip increase vs time approximately constant in all cases. The test ended once the load in the postpeak region decreased below 50% of the peak load, although in some occasions testing went on until total slip reached 10 mm.

5| Experimental Results

Part II: Experimental Program & Results

5| Experimental Results

PART II: EXPERIMENTAL PROGRAM & RESULTS

5.1 Concrete Compressive Strength

Regarding the values of compressive strength obtained, there is no point in talking of their being analyzed since concrete compressive strength is not an experimental outcome but a control parameter. As justified in Chapter 4, for each one of the 3 concretes considered in this study (Type I, Type II, and Type III), a total of 18 cylindrical specimens have been tested under compression. Table 5.1 shows for each concrete considered the 18 values obtained as well as their average, standard deviation and coefficient of variation (CoV).

The treatment that has been carried out on these results comprises the calculation of the average and standard deviation as well as the verification that they fit a normal or lognormal distribution. Outliers or anomalous data (which could be attributable to manufacturing errors) have been detected and discarded. The point in so doing is the following: if, among18 values, there is one that deviates significantly from the others, it must be discarded before estimating the mean and the standard deviation so that this estimated values are as accurate as possible.

Two different, and complementary, criteria or methods have been followed to the aforementioned purpose (see for instance Box et al. 2005):

- ☐ Determining the limits of the acceptance interval based on the interquartilic range.
- ☐ Agreement of data with the corresponding theoretical quantiles in a lognormal distribution by means of Q-Q plots.

Table 5.1. Concrete compressive strength results (MPa).

	Type I series	Type II series	Type III series
L1	34,4	30,5 (*)	41,3
	35,5	47,4	49,9
L2	33,3	39,9	46,3
	30	49,9	44,9
L3	31,1	42,2	44,4
	28,3	31,1 (*)	38,8
L4	35	47,1	40,5
	35	56,6	36
L5	32,2	49,9	40,5
	26,6	52,7	40,2
L6	33,2	51,6	43
	27,4	53,8	49,4
L7	32,4	57,7	44,4
	31,4	41,0	42,2
L8	28,7	44,8	46,9
	30,1	51,7	53
L9	32,1	42,2	53,5
	32,8	47,0	43,6
Average	32 MPa	48 MPa	44 MPa
Std. dev.	2.7 MPa	5.5 MPa	4.8 MPa
CoV (%)	8.5%	11%	10.8%

Limits based on the interquartilic range are determined as follows:

$$LL = Q_1 - 1.5 \cdot (Q_3 - Q_1) \tag{5.1}$$

$$UL = Q_3 + 1.5 \cdot (Q_3 - Q_1) \tag{5.2}$$

where LL is the lower limit, UL is the upper limit, Q1 is the first quantile or 25%-percentile, and Q3 is the third quantile or 75%-percentile.

After calculating these limits, if any value is outside the range they define, it is an outlier and therefore is discarded. Values marked with (*)

in Table 5.1 have been identified as outliers. The average and standard deviation have been calculated without these values.

Figures 5.1, 5.2, and 5.3 show the 18 compressive strength values obtained for Type I, Type II, and Type III concretes respectively. Horizontal lines correspond to the average (blue line) and the acceptance limits UL and LL (red lines).

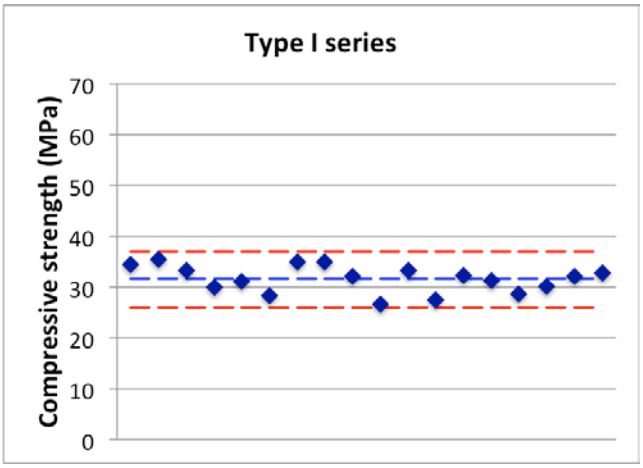

Figure 5.1. Type I series concrete compressive strength values.

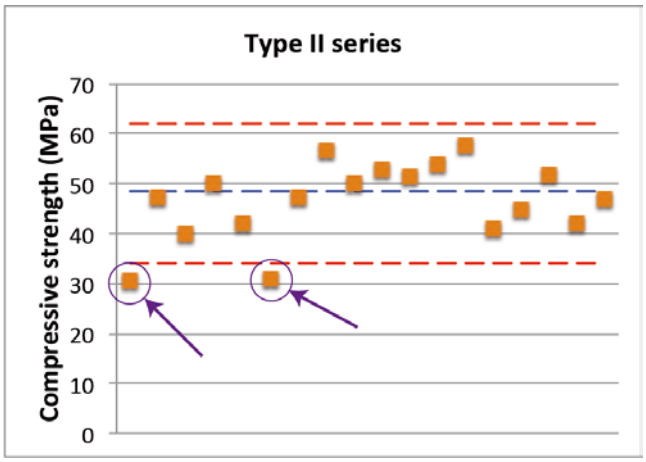

Figure 5.2. Type II series concrete compressive strength values (outliers marked with arrows).

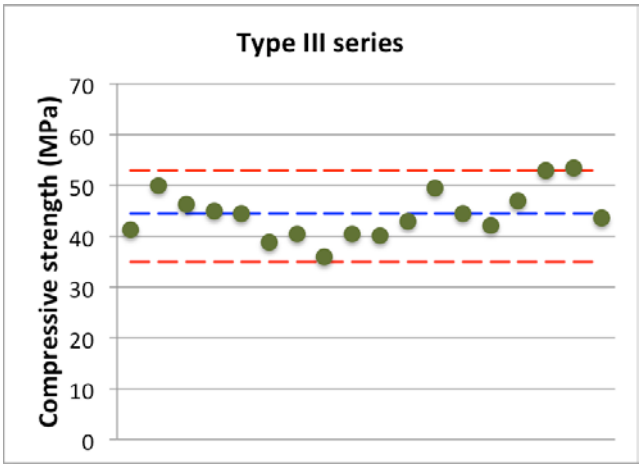

Figure 5.3. Type III series compressive strength values.

Figures 5.4, 5.5, and 5.6 show the Q-Q plots corresponding to compressive strength values for Type I, Type II, and Type III concretes respectively. These Q-Q compared observed vs predicted (or theoretical) quantiles based on the assumption of a lognormal distribution. The diagonal line corresponds exactly to the best fitting lognormal distribution.

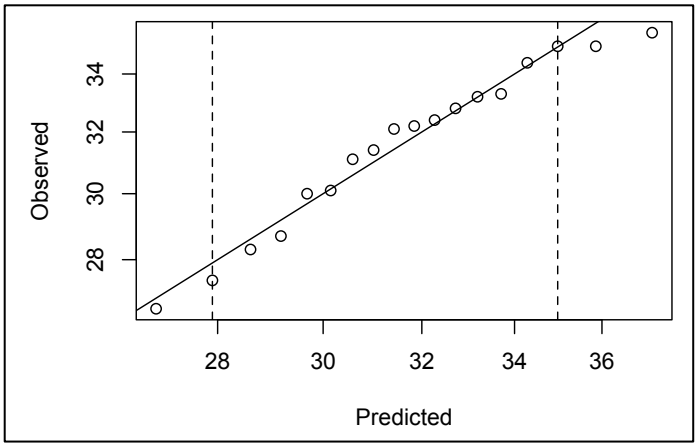

Figure 5.4. Q-Q plot (lognormal distribution) of Type I series concrete compressive strength values.

Points between dotted vertical lines are the ones that have been used to find the best fit lognormal distribution. Horizontal dotted lines indicate the limits out of which observations are outliers. It is very clear that only in the case of Type II series (Figure 5.5) there are outliers, while not in the other cases (Figures 5.4 and 5.6).

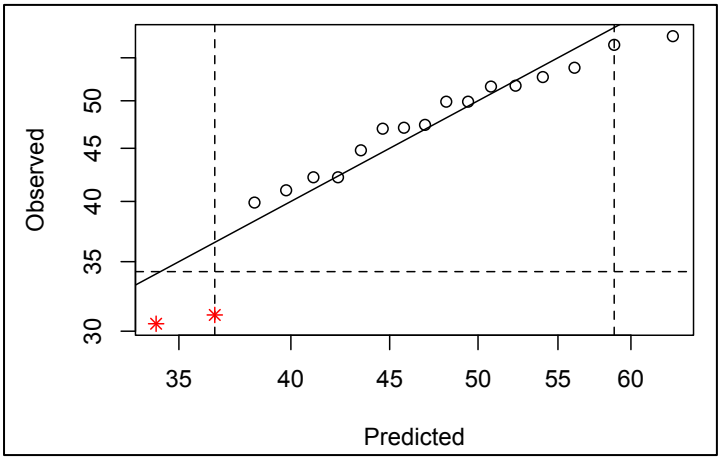

Figure 5.5. Q-Q plot (lognormal distribution) of Type II series concrete compressive strength values.

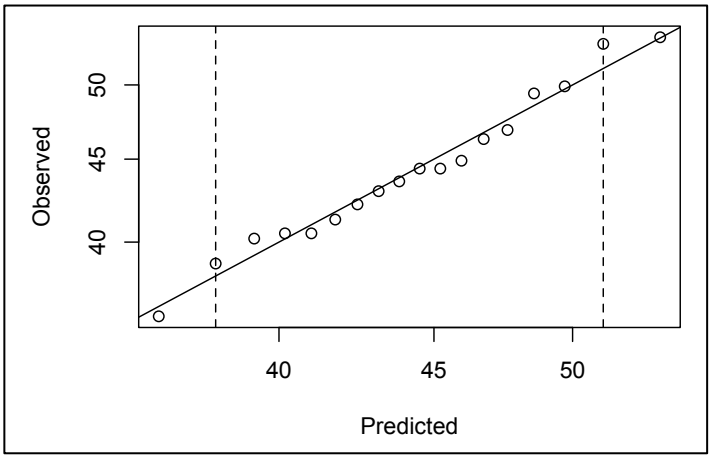

Figure 5.6. Q-Q plot (lognormal distribution) of Type III series concrete compressive strength values.

5.2 Pull Out Tests

After completion of the test, from each POT specimen it is obtained a curve which relates load values to the slip of the rebar. To transform this load-slip curves into bond stress–slip curves it is necessary to translate force values to stress values. In each specimen the embedment length has been perfectly defined, corresponding to the length along which bond stresses are developed. The total of this stress is balanced with the pullout load. Therefore, following the assumption of the hypothesis of uniformly distributed bond stresses, the average bond stress (or simply "bond stress" hereafter) can be obtained.

If L' is the embedment length, D is the rebar diameter, and P is the pulling load, it follows:

$$\tau\left(\frac{N}{mm^2}\right) \cdot \pi \cdot D(mm) \cdot L'(mm) = P(kN) \cdot 1000 \tag{5.3}$$

Therefore:

$$\tau(MPa) = \frac{P(kN) \cdot 1000}{\pi \cdot D(mm) \cdot L'(mm)} \tag{5.4}$$

PARAMETERS FOR UNIVARIATE ANALYSIS

The outcome of each Pull Out Test is a bond stress–slip curve, from which the following parameters have been defined as variables to be analyzed in this research:

- ☐ τ_{max}: bond strength, i.e. peak bond stress.
- ☐ A_{peak}: area under the curve up to the peak of the curve (Figure 5.7).
- ☐ A_{80}: area under the curve up to the a bond stress value equal to 80% of bond strength in the postpeak region of the curve (Figure 5.7).

- A_{50}: area under the curve up to the a bond stress value equal to 50% of bond strength in the postpeak region of the curve (see Figure 5.7).

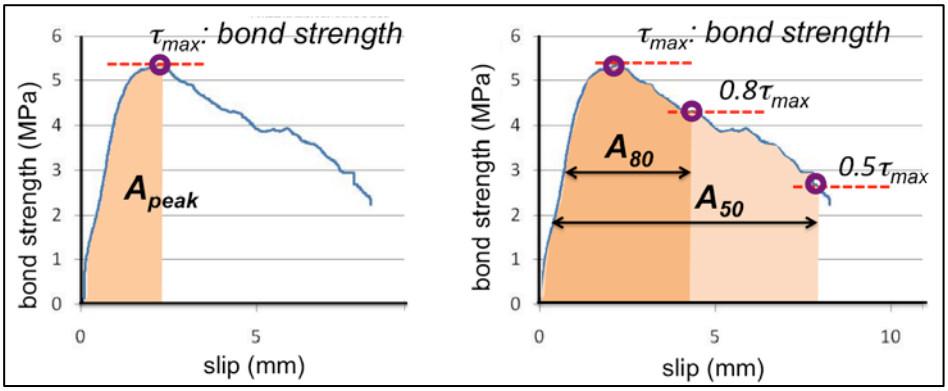

Figure 5.7. Definition of areas under the curve A_{peak} (left) A_{80}, and A_{50} (right).

Detailed numerical results for each of these parameters are given in Tables 5.2 to 5.4. The experimentally obtained bond stress–slip curves from which these values have been obtained can be found in Appendices A2, A3, and A4. Chapter 7 of this thesis is devoted to the in-depth analysis of these experimental results from a univariate perspective.

Table 5.2. Pull Out Tests results (Type I series).

	Bond strength (MPa)	Apeak (mmMPa)	A80 (mmMPa)	A50 (mmMPa)
I-1	4,74	3,97	9,58	21,9
	6,6	3,45	9,64	24,4
	7,38	12,3	20,5	29,8
I-2	9,45	8,27	26,3	43,7
	7,14	6,75	16,9	31,2
	8,5	4,24	17,6	44,4
I-3	19,9	22,9	97,7	191
	15,01	18,4	66,1	119
	20,4	34,3	97	167
I-4	7,77	7,12	17,8	31,6
	5,78	6,38	12,5	20,2
	9,78	16,6	30,5	54,1
I-5		*(splitting)*		
		(splitting)		
		(splitting)		
I-6	6,95	11,1	25,2	36,4
	6,73	11	23,6	33,1
	6,81	10,71	24,7	33,7
I-7	14	27,6	65,1	119
	11,22	19,8	44,4	76,8
	10,16	18,2	46,5	90
I-8	6,33	7,75	20,5	30,85
	4,8	5,72	12,9	20,3
	6,16	6,88	15,4	24,8
I-9	5,37	8,51	19,2	31,35
	6,5	10,73	22,3	32,5
	5	10,1	31,1	42,3

Table 5.3. Pull Out Tests results (Type II series).

	Bond strength (MPa)	Apeak (mmMPa)	A80 (mmMPa)	A50 (mmMPa)
II-1	13,79	6,82	13,00	25,85
	(splitting)			
	17,25	3,04	13,39	18,95
II-2	36,89	46,54	162,46	256,54
	25,36	15,09	30,06	150,22
	(failed)			
II-3	20,90	27,34	126,79	176,40
	20,16	29,55	115,01	157,34
	23,00	29,09	106,75	206,42
II-4	*(splitting)*			
	(splitting)			
	(splitting)			
II-5	*(splitting)*			
	(splitting)			
	23,90	8,97	26,52	47,62
II-6	27,75	23,50	72,90	148,98
	24,19	48,66	111,00	186,15
	23,92	25,32	86,30	179,85
II-7	*(splitting)*			
	(splitting)			
	(splitting)			
II-8	*(splitting)*			
	(splitting)			
	(splitting)			
II-9	*(splitting)*			
	(splitting)			
	(splitting)			

Table 5.4. Pull Out Tests results (Type III series).

	Bond strength (MPa)	Apeak (mmMPa)	A80 (mmMPa)	A50 (mmMPa)
III-1		*(splitting)*		
		(splitting)		
		(splitting)		
III-2	15,90	12,19	52,60	86,70
	12,84	12,23	38,50	66,50
	14,36	10,47	45,80	81,00
III-3	23,17	23,54	86,60	166,00
	25,08	25,58	120,00	249,00
	17,60	14,55	50,10	100,00
III-4	10,97	8,51	23,40	47,90
	13,14	15,58	34,00	55,60
	17,39	8,45	23,00	61,30
III-5		*(splitting)*		
		(splitting)		
		(splitting)		
III-6	21,85	14,15	40,60	77,70
	20,03	14,94	33,90	84,50
	24,11	12,84	28,40	66,10
III-7	21,22	19,49	65,90	117,00
		(splitting)		
	21,08	30,18	102,00	184,00
III-8	10,41	4,97	22,50	35,90
	10,99	5,27	18,40	29,40
	20,70	15,70	45,40	97,00
III-9	20,15	23,05	61,70	120,00
	21,66	26,46	60,90	123,00
	21,14	17,81	72,20	124,00

PARAMETERS FOR MULTIVARIATE ANALYSIS

A complementary way of analyzing bond stress–slip curves is by attempting to summarize the curve instead of considering only individual parameters as in univariate analysis. This can be achieved by means of multivariate techniques, as will be comprehensively explained in Chapter 8.

Each bond stress–slip curve has been discretized (Figure 5.8) and defined by bond stress values corresponding to the following slip values: 0.0mm, 0.1mm, 0.2mm, 0.4mm, 0.8mm, 1.2mm, 1.6mm, 2.0mm, 2.4mm, 2.8mm, 3.2mm, and 3.6mm. These values are taken as representative of bond stress–slip curves obtained from the pull out test in those cases where no splitting has occurred.

To cover the range of slips between 0.4mm and 3.6mm, the discretization of the curves has been made at intervals of 0.4mm. More data have been considered between 0.0mm and 0.4mm because describing the initial part of the curve needs more detail. Bond stress corresponding to the maximum pullout force achieved without slip (slip value of 0.0mm) has been taken as that corresponding to the onset of slips.

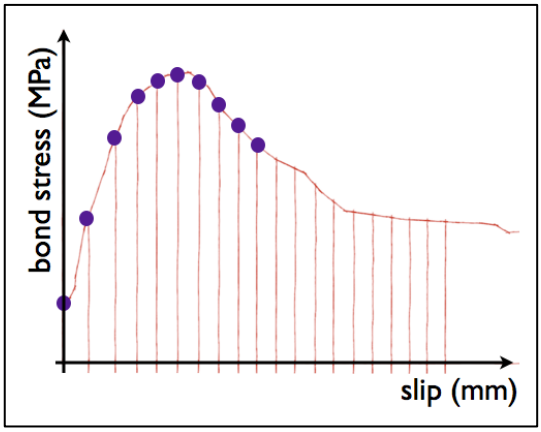

Figure 5.8. Illustration of the discretization of bond stress–slip curves to obtain variables for multivariate analysis.

Tables 5.5, 5.6, and 5.7 present the bond stress values considered for Type I, Type II, and Type III series respectively.

Table 5.5. Discretized POT curves (Type I series).

slip=	0.0	0.1	0.2	0.4	0.8	1.2	1.6	2.0	2.4	2.8	3.2	3.6
	1,9	2,3	3,4	4,5	4,7	4,4	4,1	3,8	3,6	3,3	3,1	1,9
I-1	3,9	4,5	5,7	6,6	6,1	5,4	5,0	4,6	4,3	4,1	4,0	3,9
	3,1	3,4	4,0	5,0	6,1	6,7	7,2	7,3	7,0	6,2	5,7	3,1
	4,4	5,6	7,0	8,9	9,4	9,2	8,7	8,3	7,9	7,6	7,3	4,4
I-2	1,8	2,6	4,3	6,1	7,1	7,0	6,8	6,3	5,8	5,3	4,9	1,8
	6,3	7,2	8,0	8,4	8,2	7,8	7,3	6,6	6,0	5,6	5,4	6,3
	5,9	8,7	12,5	17,3	19,3	19,8	19,7	19,5	19,1	18,7	18,2	5,9
I-3	5,9	8,2	11,0	13,9	14,9	14,9	14,8	14,6	14,4	14,2	13,9	5,9
	7,8	10,5	14,2	17,9	19,7	20,3	20,4	20,3	20,2	19,8	19,2	7,8
	2,5	3,8	5,7	7,3	7,7	7,4	7,4	6,9	5,9	5,5	5,2	2,5
I-4	0,2	0,6	2,5	4,0	5,4	5,7	5,5	5,1	4,7	4,2	3,9	0,2
	3,2	3,8	5,2	5,9	6,7	6,5	6,6	6,9	6,3	6,0	5,9	3,2
	4,7	5,7	7,1	8,3	9,0	9,4	9,8	9,6	8,8	8,5	7,8	4,7
I-6	3,9	4,4	5,4	6,3	6,6	6,7	6,6	6,5	6,1	5,9	5,7	3,9
	3,4	3,6	4,1	5,7	6,6	6,7	6,8	6,7	6,6	6,4	6,0	3,4
	2,4	2,8	3,7	6,6	10,6	12,7	13,6	13,9	14,0	13,9	13,5	2,4
I-7	2,4	2,6	3,3	5,6	8,1	9,6	10,5	11,1	11,2	10,6	10,3	2,4
	2,0	2,2	3,7	6,3	8,3	9,2	9,8	10,1	10,1	9,8	9,5	2,0
	1,8	2,1	2,6	4,4	5,7	6,3	6,3	6,0	5,8	5,6	5,4	1,8
I-8	2,2	2,6	3,6	4,5	4,7	4,7	4,6	4,4	4,1	3,8	3,5	2,2
	1,3	1,4	1,7	3,0	4,6	5,7	6,2	6,0	5,7	5,3	4,7	1,3
	1,2	1,6	2,1	3,9	4,9	5,2	5,3	5,2	5,0	4,8	4,5	1,2
I-9	0,9	2,5	4,1	5,7	6,1	6,3	6,5	6,4	6,3	6,0	5,6	0,9
	0,4	0,8	2,4	3,8	4,4	4,7	4,8	4,9	5,0	5,0	4,9	0,4

Table 5.6. Discretized POT curves (Type II series).

slip=	0.0	0.1	0.2	0.4	0.8	1.2	1.6	2.0	2.4	2.8	3.2	3.6
II-1	0,7	4,1	8,7	11,8	13,8	10,7	8,5	7,0	6,8	6,0	5,3	-
	1,5	12,1	16,8	16,7	15,5	12,2	7,1	5,6	4,4	-	-	-
II-2	5	18,9	25,0	32,5	35,9	36,6	36,6	36,0	34,5	33,6	32,7	32,1
	4	15,1	19,5	22,7	25,3	21,5	18,8	18,8	18,7	18,4	18,0	17,6
II-3	1,5	9,3	13,1	17,0	20,0	20,8	20,8	20,6	19,8	19,1	18,4	17,9
	1	9,8	13,8	16,7	19,0	19,8	20,2	19,7	19,2	18,8	18,2	17,8
	2	9,5	14,0	18,3	21,7	22,9	22,9	22,7	22,3	21,9	21,5	21,2
II-5	5,5	15,4	19,8	23,4	21,9	19,1	15,6	14,9	13,3	12,6	-	-
II-6	5	16,7	21,4	25,3	27,1	26,7	25,1	23,8	22,9	22,3	21,1	20,1
	3	10,1	14,5	19,0	22,0	23,1	23,4	23,7	23,6	23,1	22,5	21,9
	3,7	11,0	16,5	22,0	23,2	23,4	23,2	22,5	22,0	21,6	21,0	19,8

Table 5.7. Discretized POT curves (Type III series).

slip=	0.0	0.1	0.2	0.4	0.8	1.2	1.6	2.0	2.4	2.8	3.2	3.6
III-2	2,8	9,6	12,5	14,9	15,8	15,9	15,7	15,4	14,7	14,2	13,6	12,8
	2,0	7,7	9,4	11,0	12,7	12,8	12,6	12,1	11,7	11,0	10,5	10,1
	4,0	10,5	11,7	13,4	14,3	14,3	14,0	13,4	12,9	12,4	11,9	11,3
III-3	5,0	15,6	18,1	20,5	22,3	23,2	22,5	22,0	21,6	21,1	20,4	19,7
	4,5	19,1	21,3	23,5	24,8	25,1	24,9	24,5	23,9	23,5	22,9	22,4
	2,0	12,2	14,8	16,3	17,5	17,5	17,3	16,6	16,0	15,5	14,8	14,1
III-4	6,5	8,9	9,8	10,6	10,9	10,6	9,8	9,3	8,7	8,3	7,9	7,2
	1,8	5,8	8,2	10,3	12,3	13,0	13,0	12,5	11,9	10,9	10,0	9,2
	4,0	11,5	14,4	16,7	17,2	16,9	13,7	12,2	11,7	11,2	10,8	10,6
III-6	1,8	10,7	15,9	19,9	21,8	20,7	19,2	17,9	16,7	15,5	14,2	13,3
	0,2	5,7	12,2	17,3	19,6	19,8	18,2	16,0	14,8	14,1	13,4	12,6
	2,0	11,9	18,8	22,7	23,9	20,5	18,0	16,2	15,0	14,2	13,5	12,7
III-7	14,0	17,3	19,0	20,5	21,2	21,1	20,4	19,7	19,1	18,2	17,2	16,2
	3,0	13,5	17,4	19,7	20,7	20,9	21,1	20,8	20,4	20,1	19,6	19,3
III-8	1,8	6,3	9,6	10,3	10,3	10,1	9,7	9,1	8,3	7,8	7,3	6,5
	2,0	7,4	9,4	10,6	10,8	10,3	9,7	8,2	7,4	6,5	5,9	5,4
	2,0	9,9	15,2	19,1	20,5	20,5	19,6	18,5	17,2	15,7	14,9	14,2
III-9	2,5	8,3	12,7	16,2	18,8	19,8	20,1	19,6	19,0	17,9	16,8	15,7
	1,5	9,9	13,9	17,7	19,9	21,2	21,7	20,9	19,8	18,5	17,3	16,5
	2,0	12,6	16,8	19,6	21,0	21,1	20,6	20,1	19,4	18,5	17,8	17,2

6| Mode of Failure

Part III: Analysis of Results

6| Mode of Failure

PART III: ANALYSIS OF RESULTS

6.1 Logistic Binary Regression

LOGISTIC REGRESSION: OBJECTIVES AND DEFINITION

Logistic regression is a special form of regression to predict a binary, categorical variable, which classifies the analyzed items into two separate groups: those who fulfil a certain circumstance, and those who do not. The major goals of logistic binary regression are:

- ☐ To identify the variables that impact group membership or, in other words, that determine the probability that certain circumstance occurs or not.
- ☐ To establish a classification system based on the calculation of membership probabilities.

In this research the binary variable *y* is related to the mode of failure of a POT specimen. It is defined as follows: when the mode of failure is splitting, then $y=1$, and when the mode of failure is pullout, then $y=0$. Therefore, this chapter deals with the identification of variables that determine mode of bond failure, and the quantification of their effect on the tendency to splitting.

It is not possible to approach this problem by means of linear regression, i.e. to relate the values of *y* (0 or 1) to a number of factors, because the assumptions of linear regression would be violated as a consequence of the binary nature of the dependent variable. First, the error term of a discrete variable follows a binomial distribution instead of being normally distributed, and this invalidates all statistical testing based on the assumptions of normality. Second, the variance of a dichotomous

variable is not constant, creating instances of heteroscedasticity as well. And more importantly, neither violation can be remedied through transformation of the dependent or independent variables.

Logistic regression was developed to specifically deal with these issues. The approach it follows deals with the probability $p(y=1)=p$ instead of considering simply y. Since the binary dependent variable only takes the values of 0 and 1, the predicted probabilities must be bounded to fall within the same range. Logistic regression uses the S-shaped logistic curve to represent the relationship between the probability p and the dependent variables, which is defined as follows:

$$p = \frac{exp(x)}{1 + exp(x)} \tag{6.1}$$

where $p=p(y=1)$, and x is the independent variable, or factor on which such probability is dependent. When probability p is related to several factors, logistic curve is easily reformulated as follows:

$$p = \frac{exp(x_1 + \ldots + x_n)}{1 + exp(x_1 + \ldots + x_n)} \tag{6.2}$$

To estimate a logistic regression model, this curve of predicted probability values is fitted to actual data. Figure 6.1 shows two examples of fitting a logistic relationship to sample data. In the first case (Figure 6.1 left) the logistic curve cannot fit the data well, because a number of values of the independent variable have both outcomes (0 and 1). In this case the independent variable is not an apropriate factor to distinguish between the two outcomes, as shown by the high overlap of the two groups of dots. The second case (Figure 6.1 right) corresponds to a much more well-defined relationship, which can be satisfactorily based on the selected independent variable. When the two cases presented in Figure 6.1 are compared, one thing becomes clear: it is really important to identify which are the variables that significantly determine the values of y, so that an apropriate logistic model is developed.

Once the significant variables have been identified, the model is usually aimed at being used as a classification tool. For each observation, the output of the logistic model fitted by logistic regression is a probability

value between 0 and 1 which is based on the value(s) of the independent variable(s) and the estimated coefficients. If the predicted probability is greater than 0.5, then the prediction is assumed to be that the outcome is y=1 (event happens); otherwise, the outcome is predicted to be y=0 (event does not happen). This cutoff value is initially assumed to be 0.5 but it must be decided in each particular case so that the classification capacity of the model developed and fitted is maximized.

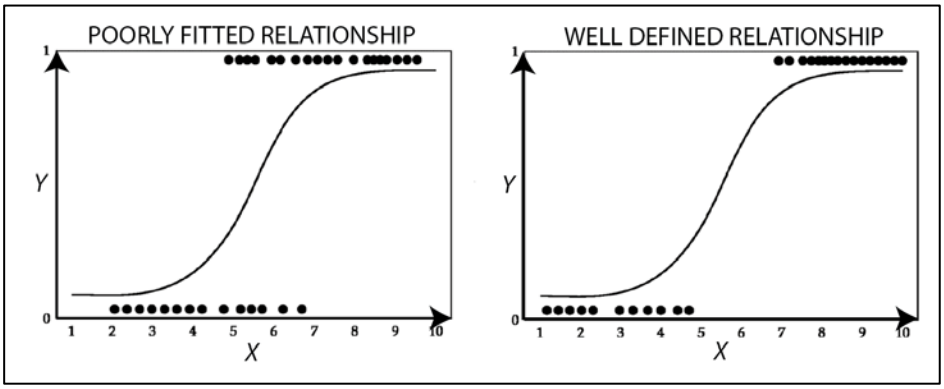

Figure 6.1. Examples of logistic curve fitting observed data (Hair et al. 2009).

DEVELOPING THE LOGISTIC MODEL

The previous subsection has presented logistic regression in terms of only one dependent variable x determining the values of y. This can be generalized. A logistic regression model where the probability p of an event (splitting failure in this case) is related to several variables is formulated as follows:

$$\frac{p}{1-p} = exp(b_0 + b_1x_1 + \ldots + b_nx_n) \qquad (6.3)$$

where p is the probability of the event, $x_1 \ldots x_n$ are independent variables, b_0 is the intercept or constant in the model, and $b_1 \ldots b_n$ are the coefficients weighing the effect of the variables involved on the odds-ratio. Coefficients b_0, $b_1 \ldots b_n$ are values to be estimated by fitting the model to

observed data, which is carried out by means of maximum likelihood estimation.

Once the coefficients have been estimated, statistical significance tests are carried out and a p-value is given to each one of the variables considered. The general criterion is that statistically significant variables present p-values not higher than 0.05. When one or more variables are identificad as non-significant, they are discarded and the model is simplified. This is sequentially carried out by means of the so-called stepwise backward regression, and p-values are recalculated until only variables which have a significant effect on the target probability are considered.

MEASURING THE ACCURACY OF THE LOGISTIC MODEL

Once a logistic model has been fitted there are three main groups of tools to assess how accurate it is in fitting the observed probabilities and as a classification tool:

- **ANALYSIS OF DEVIANCE**. With logistic regression, instead of R-squared as the statistic for overall fit of the model, we have deviance instead. The bigger the difference (or "deviance") of the observed values from the expected values, the poorer the fit of the model. So, we want a small deviance if possible. As we add more variables to the equation the deviance should get smaller, indicating an improvement in fit. Deviance is analogous to the sum of squares calculations in linear regression and is a measure of the lack of fit to the data in a logistic regression model. Deviance explained by a given model is compared to that explained by the saturated model, i.e. with a theoretically perfect fit, so that the percentage of explained deviance is obtained: the higher, the better. Furthermore, the corresponding statistical chi-square tests inform about the significance of the relationship modelled.

- **GOODNESS-OF-FIT STATISTICS**. Besides the explained deviance, two more statistics are used in this chapter. They are known as pseudo R-squared values because of their similitude to the classical R-

squared concept, and are based on the proportion of unexplained variance (deviance) that is reduced by incorporating variables to the model. These statistics are:

- Cox and Snell pseudo R-squared value. It is defined as follows:

$$R^2{}_{Cox-Snell} = 1 - \left(\frac{LL_{null}}{LL_{model}}\right)^{2/n} \quad (6.4)$$

where: LL_{null} stands for log-likelihood of the null model, which considers only a constant but no variables; LL_{model} is the log-likelihood corresponding to the model which is being assessed; and *n* is the number of observations. It is never equal to 1 because in the case that the model predicted the outcome perfectly, then $R^2 = 1 - (LL_{null})^{2/n}$.

- Nagelkerke pseudo R-squared value. It adjusts the pseudo R-squared value as defined by Cox and Snell so that the range of passible values extends to [0,1]. It is defined as follows:

$$R^2{}_{Nagelkerke} = \frac{R^2{}_{Cox-Snell}}{max\ R^2{}_{Cox-Snell}} = \frac{1 - \left(\frac{LL_{null}}{LL_{model}}\right)^{2/n}}{1 - (LL_{null})^{2/n}} \quad (6.5)$$

□ **PREDICTIVE ACCURACY: CLASSIFICATION TABLES AND PLOTS**. As it has been already mentioned, a certain probability has to be chosen as the threshold value to translate probabilities into *y*=1 and *y*=0 cases. The classification capacity of the fitted model varies depending on the cutoff probability value. Therefore it is necessary to find the cutoff probability value to maximize the predictive accuracy. Three tools for that purpose have been used in this chapter:

- Classification tables. Percentages of correctly assigned cases and incorrectly assigned cases are calculated separately for observed *y*=0 and *y*=1 situations. An overall percentage is also determined.
- Plots based on the Hosmer-Lemeshow discretization. They are offer the same information that the classification table

and allow clear visualization of uncorrectly assigned cases.

- Plots of correctly assigned cases vs cutoff probability. These plots present the percentages of correctly assigned cases (overall and separate y=0 and y=1 situations) vs the cutoff probability selected. They are a valuable tool when selecting the cutoff probability that maximizes the predictive accuracy of the fitted model.

6.2 Construction of a Semi-Empirical Model to Predict Splitting

FIRST STEP: ADDITIVE MODEL

An additive model for splitting probability of the POT specimens, i.e. a model which considers simple effects only, is taken as a point of departure. The probability of splitting failure, p, ranges between 0 and 1: p=0 means total certainty that the mode of failure is pullout, while p=1 means total certainty that splitting is to occur. This model is given by equation 6.6:

$$ln\left(\frac{p}{1-p}\right) = \nabla_0 + \nabla_c f_c + \nabla_d \mathrm{D} + \nabla_{cd}\frac{C}{D} + \nabla_f C_f + \nabla_{\lambda f}\lambda_f C_f + \nabla_{\ell f}\ell_f C_f \quad (6.6)$$

where p stands for the splitting probability, f_c is the average concrete compressive strength (MPa), D is rebar diameter (mm), C_f is fiber content (kg/m^3), λ_f is fiber slenderness, ℓ_f is fiber length (mm); and ∇_0, ∇_c, ∇_d, ∇_{cd}, ∇_f, $\nabla_{\lambda f}$, and $\nabla_{\ell f}$ are coefficients to be estimated.

In this model no interactions are considered: the contribution of each factor to the logarithm of the odds-ratio, $ln\left(\frac{p}{1-p}\right)$, is independent from the contributions of all other factors. That is the reason why this model is called 'additive': the effect of each factor is added to the effect of the other factors. The only exceptions are fiber slenderness and fiber length, which appear multiplying fiber content. The reason for their not being considered as standalone, simple effects is that they must not have any effect when fiber content is null: this way the products $\lambda_f C_f$ and $\ell_f C_f$ are forced to be null when fiber content, C_f is zero.

Coefficients are estimated by fitting the model to observed data, where frequency of splitting failures is taken as the observed probability, for instance: when 1 out of 3 POT specimens have undergone splitting, the observed splitting probability is $1/3$. Coefficients in equation 6.6 have

been calculated by means of maximum likelihood estimation. The results of estimations, together with the significance test associated to each factor, are shown in Table 6.1. The analysis of deviance corresponding to this model is shown in Table 6.2, and different goodness-of-fit measures of the estimated model are shown in Table 6.3.

Table 6.1. Estimation of coefficients and significance tests (additive model, eq.6.6).

		Coefficient	Std. error	p-value
(constant)	∇_0	–28.077	7.411	--
Compressive Strength	∇_c	0.636	0.166	0.0000
Cover/Diameter	∇_{cd}	–2.508	0.813	0.0000
Diameter	∇_d	0.623	0.181	0.0000
Fiber Content	∇_f	–0.213	0.166	0.1620
Fiber Slenderness, $\lambda_f C_f$	$\nabla_{\lambda f}$	0.000424	0.00124	0.7338
Fiber Length, $\ell_f C_f$	$\nabla_{\ell f}$	0.003597	0.00216	0.0565

Table 6.2. Analysis of Deviance (additive model, eq.6.6).

	Deviance	d.o.f.	p-value
Model	62.024	6	0.0000
Residuals	38.094	74	0.9998
Total (corr.)	100.12	80	--
Percentage of deviance explained by the model:			61.95%

Table 6.3. Goodness-of-Fit statistics (additive model, eq.6.6).

	Percentage
Explained Deviance	61.95%
Cox and Snell R-squared	53.5%
Nagelkerke R-squared	75.4%

As seen in Table 6.2, the p-value for the part of deviance explained by the model is less than 0.05, this indicating that there is indeed a statistically significant relationship to be explained by this model which is worth the search. Furthermore, the p-value for residual deviance is far bigger than 0.05, and this means that there is not a significant difference between the capacity of the fitted model and that of the hypothetical

best-fit model. In consequence, there is no reason to aim at much higher values for the explained deviance than that obtained in this case.

However, this model as given by equation 6.6 can be simplified according to Table 6.1, since not all p-values are less than 0.05: the product between fiber slenderness and fiber content does not represent a significant contribution to the logarithm of the odds-ratio. Therefore it must be discarded and the model is rewritten as given by equation 6.7:

$$ln\left(\frac{p}{1-p}\right) = \nabla_0 + \nabla_c f_c + \nabla_d \mathrm{D} + \nabla_{cd}\frac{C}{D} + \nabla_f C_f + \nabla_{\ell f}\ell_f C_f \qquad (6.7)$$

Then coefficients in the model are reestimated, and Tables 6.4, 6.5, and 6.6 are obtained.

Table 6.4. Estimation of coefficients and significance tests (additive model, eq.6.7).

		Coefficient	Std. error	p-value
(constant)	∇_0	–27.7776	7.29256	--
Compressive Strength	∇_c	0.623227	0.159617	0.0000
Cover/Diameter	∇_{cd}	–2.38935	0.701546	0.0000
Diameter	∇_d	0.618769	0.17703	0.0000
Fiber Content	∇_f	–0.166411	0.0902883	0.0249
Fiber Length, $\ell_f C_f$	$\nabla_{\ell f}$	0.00326078	0.00187441	0.0449

Table 6.5. Analysis of Deviance (additive model, eq.6.7).

	Deviance	d.o.f.	p-value
Model	61.9083	5	0.0000
Residuals	38.2092	75	0.9999
Total (corr.)	100.12	80	--
Percentage of deviance explained by the model:			61.84%

Table 6.6. Goodness-of-Fit statistics (additive model, eq.6.7).

	Percentage
Explained Deviance	61.84%
Cox and Snell R-squared	53.4%
Nagelkerke R-squared	75.3%

Since p-values are less than 0.05 for all factors considered in this model (Table 6.4), all of them have a significant effect on the odds-ratio and therefore there is no further simplification possible. Furthermore, the simplification of the additive model as given by equation 6.6 leading to equation 6.7 means no important reduction in the goodness of fit, as can be easily observed by comparing Tables 6.3 and 6.5. That is to say, the accuracy of both models is the same. In consequence, model as given by equation 6.7 is retained as the fitted additive model.

Once the model has been fitted, the outcome of any prediction is a probability. A predicted splitting probability has to be translated in terms of mode of failure to be compared with actual, real data. This is accomplished selecting a value for the so-called cutoff probability, which is initially established at 0.5. This is equivalent to the following assumption: predicted splitting probability values less than 0.5 imply pullout failure, while values bigger than 0.5 imply splitting failure. In consequence, the accuracy of the logistic model can be explored in a more intuitive, clear way by means of the so-called classification table. It compares the number of observed pullout cases to the number of predicted pullout cases, and the same for splitting cases. Percentages of correct sortings are then calculated, as shown in Table 6.7.

The classification table can be looked at in a graphical way if the range of predicted probabilities is divided into a number of intervals and then observed splitting cases vs pullout cases are plotted for each interval. This is the approach followed by the Hosmer-Lemeshow statistic, and is shown in Figure 6.2.

Table 6.7. Classification table, p*=0.5 (additive model, eq.6.7)

		Predicted		
Observed		pullout	splitting	**Percentage correct**
pullout	**56**	51	5	51/56= **91.1%**
splitting	**25**	6	19	19/25= **76.0%**
total	**81**		**overall**	(19+51)/81= **86.4%**

Of course these percentages will vary depending on the cutoff probability chosen. Therefore the second step after having fitted the

model is the search for the optimum cutoff probability for the model in order to maximize the percentage of correctly sorted cases. The selection of the most adequate cutoff probability value can be made on the basis of Figure 6.3.

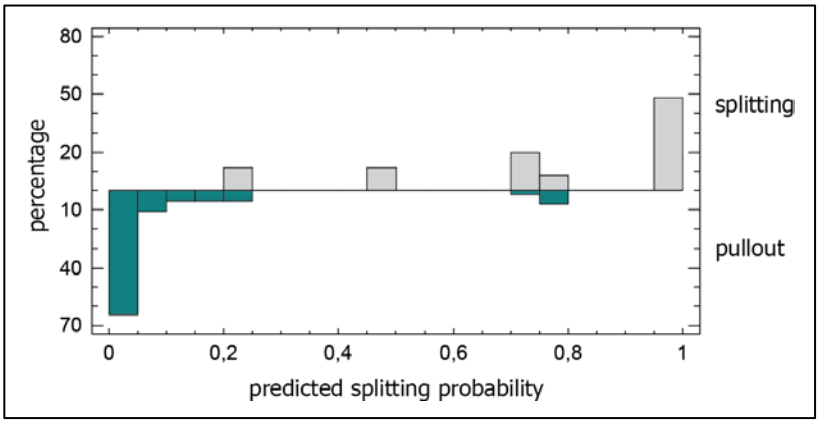

Figure 6.2. Hosmer-Lemeshow plot (additive model, eq.6.7).

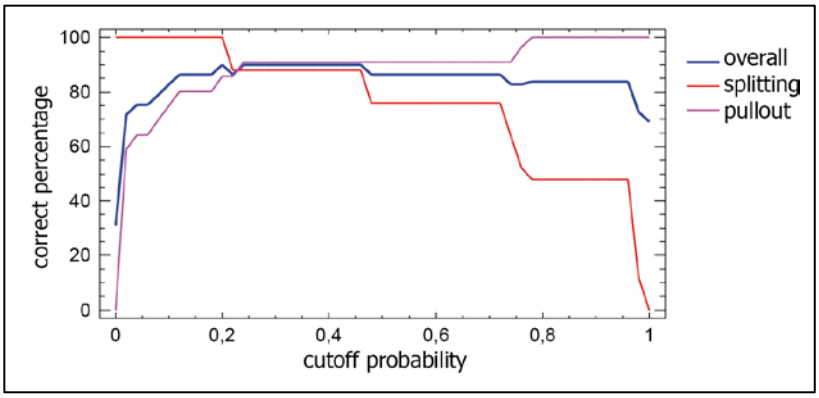

Figure 6.3. Percentage of correctly sorted cases vs the cutoff probability value (additive model, eq.6.7).

It is observed in Figure 6.3 that overall sorting efficiency is more or less the same for cutoff probability values between 0.2 and 0.5. However, the percentage of correctly sorted splitting cases is far better for a cutoff probability of 0.2, as shown in Table 6.8. The cost is, however, that the percentage of false positives (cases when splitting failure is predicted but does not occur) is increased.

Table 6.8. Classification table, p*=0.2 (additive model, eq.6.7)

Observed		Predicted: pullout	Predicted: splitting	Percentage correct
pullout	**56**	48	8	48/56= **85.7%**
splitting	**25**	0	25	25/25= **100.0%**
total	**81**		**overall**	(48+25)/81= **90.1%**

Finally, the model must be diagnosed. Figure 6.4 shows the normal probability plot of the standardized residuals, which compares their distribution to the normal distribution of mean zero and unit variance (theoretical quantiles). Since residuals are always expected to approximate the normal distribution (dotted line), this plot is a valuable tool to diagnose the fitted model and to detect influential, anomalous data through their unusually high residuals. In the case of this model, there are several observations that do not follow the normal distribution. Though this cannot be said to clearly compromise the performance of the model, it indicates that it is probably useful to reformulate the model and/or to include other effects that have not been taken into account so far. The following section is a step further in this direction.

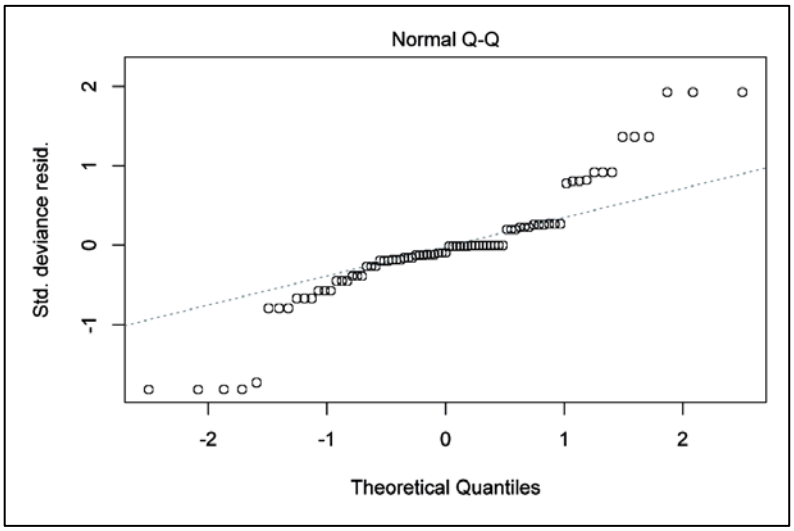

Figure 6.4. Normal probability plot of residuals.

SECOND STEP: CONSIDERING INTERACTIONS

The additive model given by equation 6.7 considered simple effects only and has proved three important aspects: a) there is a clear relation between the factors considered and the splitting probability which is worth the effort of modelling, as confirmed by the analysis of deviance; b) it is reasonable to aim at good levels of efficiency when predicting splitting failures; and c) there are no anomalous data that can compromise the estimation of parameters, as shown by Figure 6.4.

But the additive model is entirely empirical, since it does not embody a conceptual view on the phenomenon under study. It was a good point of departure, though, as it has been shown. This section deals with the embracement of interactions between the factors considered on the basis of previous knowledge on the mechanisms of bond. Therefore it is a step further to the semi-empirical modelling of splitting probability. This step is not motivated by the search for higher accuracy, because the analysis of deviance performed on the additive model has shown that the distance between the additive model and a hypothetical best-fit model is not statistically significant. Rather, this search is justified by the need of a model that, besides being accurate, helps with the conceptualization and understanding of the mechanisms of bond failure in relation to the effect of the factors considered and, particularly, of fibers.

Part I of this thesis has collected several evidence on the importance of confinement on bond failure modes. Concrete cover/diameter ratio is particularly significant. Therefore, it is reasonable to think that this ratio determines bond failure mode and its effect is modified by concrete properties. That is to say: instead of considering independent contributions of all factors, it is now assumed that all other factors (compressive strength, fibers) interact with, and therefore modify the effect of cover/diameter ratio. This model is given by equation 6.8:

$$ln\left(\frac{p}{1-p}\right) = \nabla_0 + \left(\nabla_{cd} + \nabla_c f_c + \nabla_{\mathcal{F}} C_f\right)\frac{C}{D} \qquad (6.8)$$

where ∇_0, ∇_{cd}, and ∇_c are coefficients to be estimated, and $\nabla_{\mathcal{F}}$ is a function of the geometry of fibers defined as follows:

$$\nabla_{\mathcal{F}} = \nabla_f + \nabla_{\lambda f}\lambda_f + \nabla_{\ell f}\ell_f \tag{6.9}$$

where ∇_f, $\nabla_{\lambda f}$, and $\nabla_{\ell f}$ are coefficients to be estimated.

The model thus formulated takes into account the nature of the phenomenon under study, and two aspects are particularly remarkable:

- The odds-ratio and therefore splitting probability are assumed to be mainly determined by concrete cover/diameter ratio (C/D), and the effect of this factor is modified by a function which depends on the properties of concrete, namely concrete compressive strength (f_c) and fiber content (C_f).
- The effect of fibers is assumed to be mainly dependent on fiber content (C_f), but the effect of fiber content is modified by means of a function which depends on fibers geometry, $\nabla_{\mathcal{F}}$.

The estimation of the coefficients in the model follows the procedure already described in the previous section.

Estimated coefficients, together with the corresponding significance tests, are shown in Table 6.9. The analysis of deviance corresponding to this model is shown in Table 6.10, and different measures of the goodness-of-fit of the estimated model are shown in Table 6.11.

Table 6.9. Estimation of coefficients and significance tests (semi-empirical model, eqs.6.8-9).

		Coefficient	Std. error	p-value
(constant)	∇_0	8.58577	2.25949	--
Cover/Diameter, C/D	∇_{cd}	-12.629	3.33076	0.0000
Compr. Strength, f_c C/D	∇_c	0.219206	0.059564	0.0000
Fiber Content, C_f C/D	∇_f	-0.105321	0.0366329	0.0004
Fiber Slenderness, $\lambda_f C_f$ C/D	$\nabla_{\lambda f}$	0.00032465	0.0002129	0.0799
Fiber Length, $\ell_f C_f$ C/D	$\nabla_{\ell f}$	0.0017429	0.0005959	0.0003

P-values are less than 0.05 for all factors considered in this model except the interaction $\lambda_f C_f$C/D, which is 0.0799 (Table 6.9). However, since

0.0799 is not much bigger than 0.05, it is preferred to retain this interaction in the model, thus considering all factors and interactions involved as having a significant effect on the odds-ratio.

Table 6.10. Analysis of Deviance (semi-empirical model, eqs.6.8-9).

	Deviance	d.o.f.	p-value
Model	54.4222	5	0.0000
Residuals	45.6954	75	0.9970
Total (corr.)	100.118	80	--
Percentage of deviance explained by the model:			54.36%

Table 6.11. Goodness-of-Fit statistics (semi-empirical model, eqs.6.8-9).

	Percentage
Explained Deviance	54.36%
Cox and Snell R-squared	48.9%
Nagelkerke R-squared	69.0%

Once the model has been fitted, the predicted splitting probabilities are translated in terms of mode of failure to be compared with actual, real data by initially assuming a cutoff probability of 0.5. The classification table obtained is shown in Table 6.12 and the corresponding Hosmer-Lemeshow plot is shown in Figure 6.5.

Table 6.12. Classification table, p*=0.5 (semi-empirical model, eqs.6.8-9).

		Predicted		
Observed		pullout	splitting	Percentage correct
pullout	**56**	53	3	53/56= **94.6%**
splitting	**25**	1	24	24/25= **96.0%**
total	**81**		**overall**	(24+53)/81= **95.1%**

As discussed in previous sections, these percentages vary depending on the cutoff probability selected. It is observed in Figure 6.6 that a cutoff probability value of 0.4 or 0.5 is the most adequate choice in terms of

overall sorting efficiency and particularly in terms of correct prediction of splitting failures. In consequence, there is no need of displacing the cutoff probability.

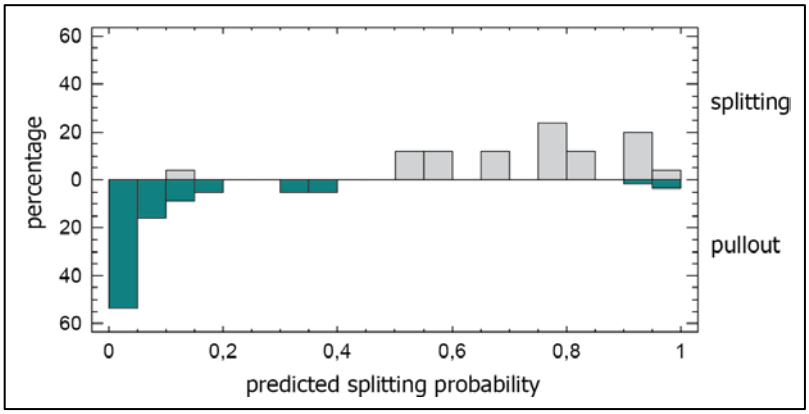

Figure 6.5. Hosmer-Lemeshow plot (semi-empirical model, eqs.6.8-9).

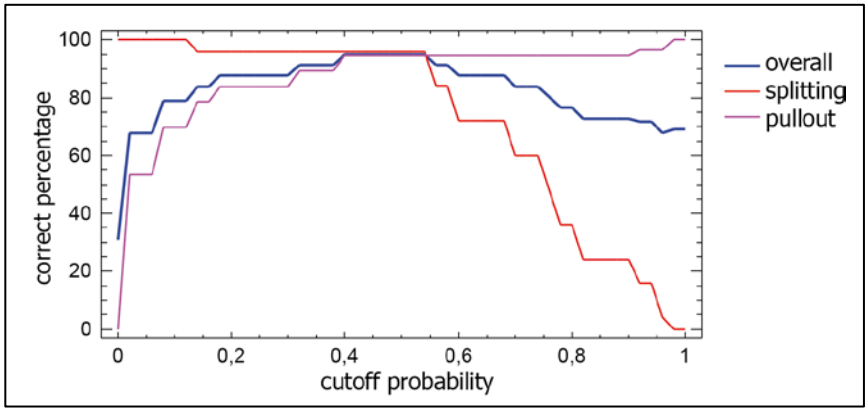

Figure 6.6. Percentage of correctly sorted cases vs the cutoff probability value (semi-empirical model, eqs.6.8-9).

Finally, Figure 6.7 shows the normal probability plot of the standardized residuals. This probability plot shows a better behavior of residuals than that observed in Figure 6.4, which is a sign that this model is better formulated than the additive model. There are only four observations which are slightly out of the trend of the normal distribution. These four observations are precisely the ones which are not correctly classified by

the model, as shown in Figure 6.8. It is worth mentioning that these four observations represent 4/81 = 4.9% of the data and, since the confidence interval assumed for all estimations is 95%, the fact that approximately 5% of observations are not correctly predicted by the fitted model is something to be expected.

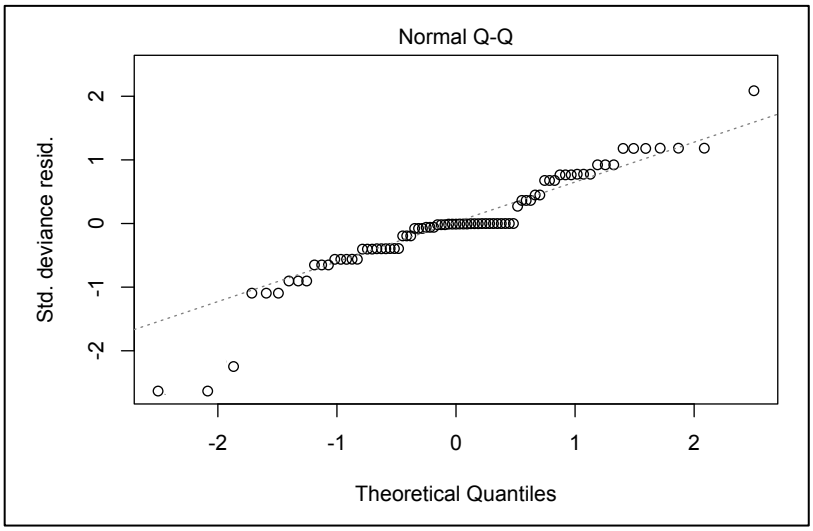

Figure 6.7. Normal probability plot of standardized residuals.

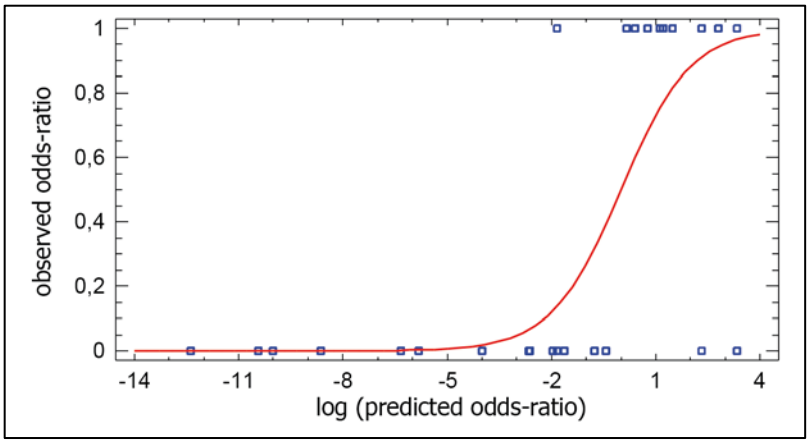

Figure 6.8. Observed vs predicted odds-ratios.

COMPARISON: ADDITIVE VS MODEL WITH INTERACTIONS

Two alternative models have been obtained to relate the splitting probability to the factors considered (concrete compressive strength, concrete cover/diameter ratio, fiber content, fiber slenderness, and fiber length). They are compared in Table 6.13 in terms of the values obtained for different Goodness-of-Fit statistics and their classification efficiency.

Table 6.13. Comparison between the two models obtained.

	Additive	w/ interactions
Explained Deviance	61.8%	54.4%
Nagelkerke R-squared	75.3%	69.0%
Classif. efficiency, overall	90.1%	95.1%
Classif. efficiency, splitting	100%	96.0%
Classif. efficiency, pullout	85.7%	94.6%

Both models are indeed alternatives since they are very similar in terms of the parameters compared in Table 6.13. However, the model with interactions, or semi-empirical model, is preferred for the following reasons. First, the studentized residuals are closer to being normally distributed in the case of the semi-empirical model (Figure 6.7) than in the case of the additive model (Figure 6.4). Second, the semi-empirical model is more efficient when classifying observed cases than the additive model (95.1% vs 90.1%). Third, the classification capacity is very much the same for both pullout and splitting failures in the case of the semi-empirical model, with a very low percentage of incorrectly classified pullout cases. And finally, and perhaps most importantly, the semi-empirical model brings about the possibility of approaching the study of the implications of the equation fitted on the grounds of a mechanical understanding of the phenomenon.

SEMI-EMPIRICAL MODEL OBTAINED

Equation 6.10 relates splitting probability to the factors considered in this research, and equation 6.11 presents the fiber function depending on fiber geometry which modifies the effect of fiber content.

$$ln\left(\frac{p}{1-p}\right) = 8.586 + \left(-12.63 + 0.219f_c + \nabla_{\mathcal{F}} C_f\right)\frac{C}{D} \quad (6.10)$$

$$\nabla_{\mathcal{F}} = -0.105 + 0.000325\lambda_f + 0.00174\ell_f \quad (6.11)$$

6.3 Interpretation

This section is devoted to closely looking at the semi-empirical model obtained to predict splitting failure of anchorages as given by equations 6.10 and 6.11. Such close reading of the model is necessary in order to attain a thorough understanding of the implications that these equations bring about.

CONCRETE COVER, FIBER CONTENT AND CONCRETE COMPRESSIVE STRENGTH

Figure 6.9 shows the values of splitting probability as predicted by the model versus the values of cover/diameter ratio and fiber content. This will be referred to as the splitting probability surface hereafter. Concrete is initially assumed to be 45-MPa and reinforced with 80/35 steel fibers, because no more than 3 dimensions can be plotted and concrete cover/diameter ratio and fiber content are the main variables of interest in this and the following figures.

The horizontal plane in Figure 6.9 represents the cutoff probability set at 0.5 for classification purposes, which distinguishes splitting failures from pullout failures. Accordingly, the intersection between this plane and the splitting probability surface leads to the minimum concrete cover/diameter values which are required to prevent splitting failures. This requirement varies with fiber content, as shown in Figure 6.10.

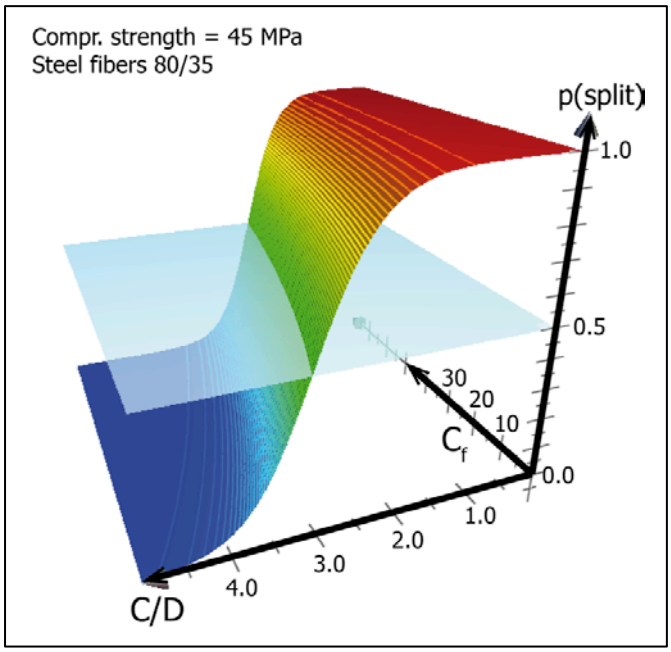

Figure 6.9. Splitting probability surface for 45-MPa concrete and 80/35 steel fibers.

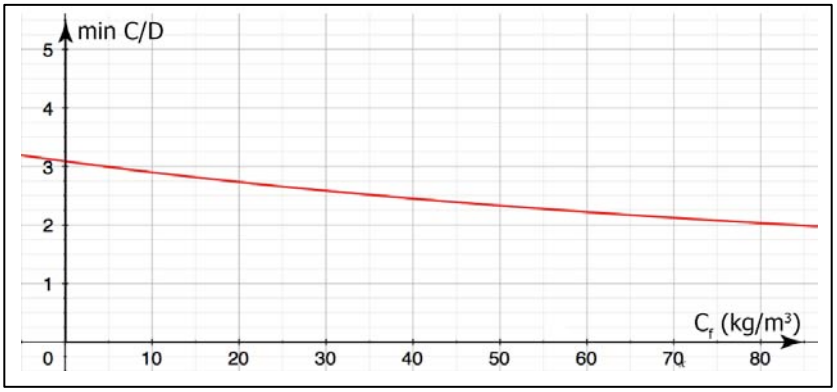

Figure 6.10. Minimum C/D values to avoid splitting failure of a 45-MPa concrete with 80/35 steel fibers.

For 45-MPa concrete without fibers, the minimum concrete cover/diameter ratio is 3. This means that for concrete cover/diameter ratios less than 3, splitting failure is expected. Figure 6.10 clearly shows that adding fibers to concrete prevents splitting failures. The minimum

required ratio is decreased to 2.5 when the fiber content is 40kg/m^3, and to 2 when the fiber content is 80kg/m^3.

Figure 6.11 shows the splitting probability surface evaluated for three different concrete compressive strength values. It can be observed that higher compressive strength values require higher concrete cover/diameter ratios for splitting failure to be prevented. When compressive strength of concrete increases, concrete tensile strength is increased and therefore hoop stresses developing around the rebar reach further away from it. In consequence, it is more likely that tensile stresses reach the surface of the specimen, this meaning a splitting failure. As a result, higher concrete cover values are required.

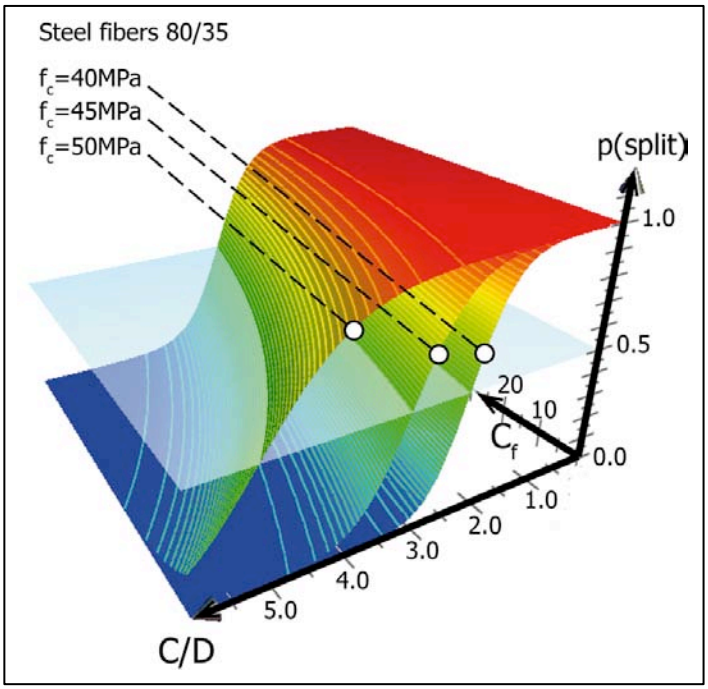

Figure 6.11. Splitting probability surfaces for concrete between 40MPa and 50MPa reinforced with 80/35 steel fibers.

The intersection by the horizontal plane corresponding to the cutoff probability offers a very interesting insight to the role that concrete cover, fiber content, and concrete compressive strength play when determining the mode of failure in bond.

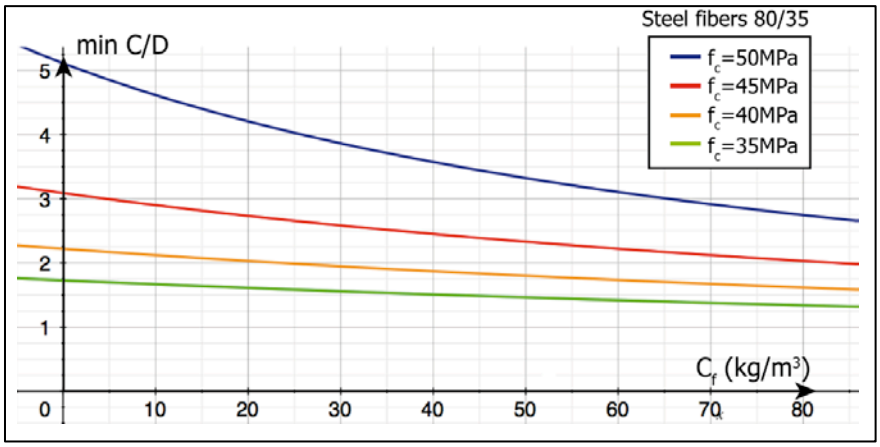

Figure 6.12. Minimum C/D values to avoid splitting failure of concrete reinforced with 80/35 steel fibers.

The favorable effect of fibers when preventing splitting failures has been revealed to be more important for higher compressive strength values. The reduction in the minimum cover/diameter ratio achieved when adding a certain fiber content to concrete is clearly bigger for 50-MPa concrete than for 35-MPa concrete, as can be seen in Figure 6.12.

There is another interesting remark to be made in relation to Figure 6.12. It is usually accepted that cover/diameter ratios bigger than 5 correspond to situations of good confinement of the rebar. However, Figure 6.12 seems to restrict the general validity of this assumption since, according to the model developed, a POT specimen made with 50-MPa concrete without fibers where concrete cover is 5 times the rebar diameter is likely to experience a splitting failure.

FIBER GEOMETRY

Figure 6.13 shows the splitting probability surface calculated for different values of fiber slenderness, under the assumptions of 45-MPa concrete and a fiber length of 50mm. The three splitting probability surfaces shown in Figure 6.13 are very close to each other. This points out that the effect of fiber slenderness on the mode of failure of an anchorage, though statistically significant, is not very important. The

intersection of these surfaces with the horizontal plane corresponding to the cutoff probability value of 0.5 leads to Figure 6.14, where minimum cover/diameter values are shown for different fiber contents and different values of fiber slenderness. It can be concluded that low fiber slenderness values are preferred to prevent splitting of concrete cover.

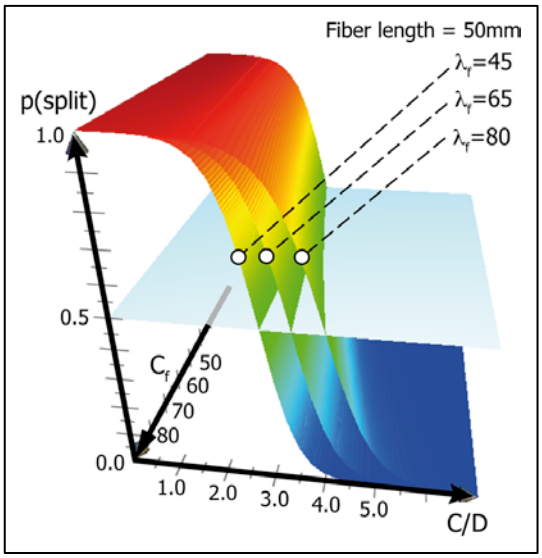

Figure 6.13. Splitting probability surfaces for 45-MPa concrete reinforced with 50-mm fibers.

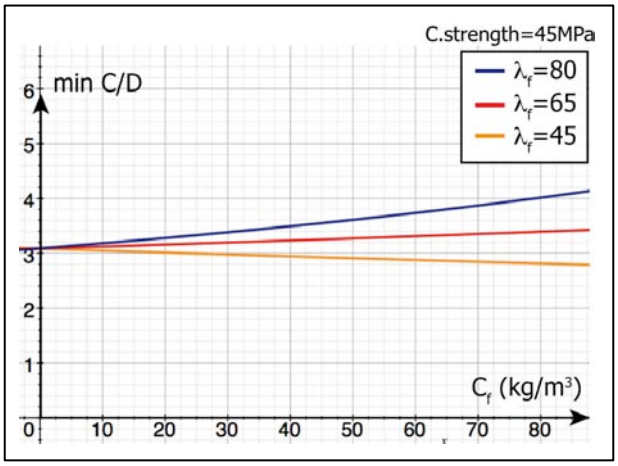

Figure 6.14. Minimum C/D values to avoid splitting failure of 45-MPa concrete reinforced with 50-mm fibers.

The case is far more surprising in relation to fiber length. Splitting probability surfaces for different fiber length values, assuming a 45-MPa concrete and a fiber slenderness of 65, are shown in Figure 6.15. Contrarily to what has been observed concerning fiber slenderness, splitting probability surfaces are clearly separated for different fiber length values, and this clearly indicates that the effect of fiber length on the mode of failure of anchorages, besides being statistically significant, is highly relevant.

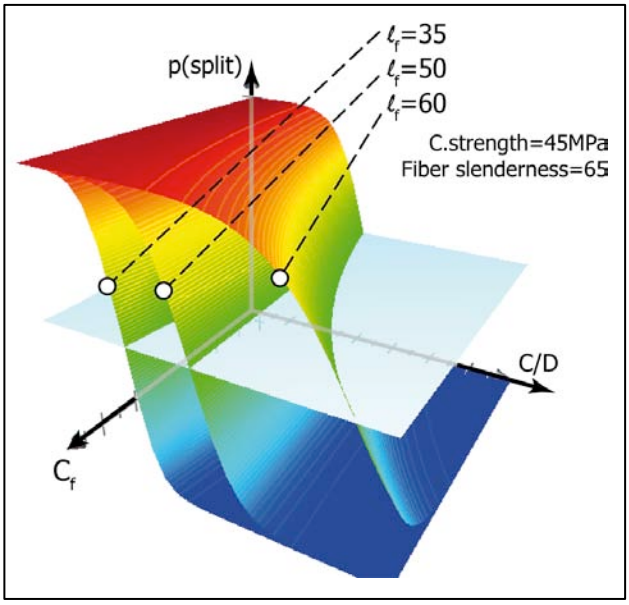

Figure 6.15. Splitting probability surfaces for 45-MPa concrete reinforced with fibers of slenderness 65.

Figure 6.16 shows the minimum cover/diameter values required to prevent splitting failures related to fiber content for different fiber slenderness values, obtained by means of intersecting the splitting probability surfaces by the plane corresponding to the cutoff probability.

It is observed that the favorable effect of increasing fiber contents is conditioned to fiber length. The use of long fibers can reverse the trends observed in Figure 6.12 and lead to the fact that increasing fiber contents would make the anchorage more prone to splitting and therefore would require higher concrete cover/diameter values to

prevent splitting failures. This would be the case of 60-mm length fibers, as observed in Figure 6.16.

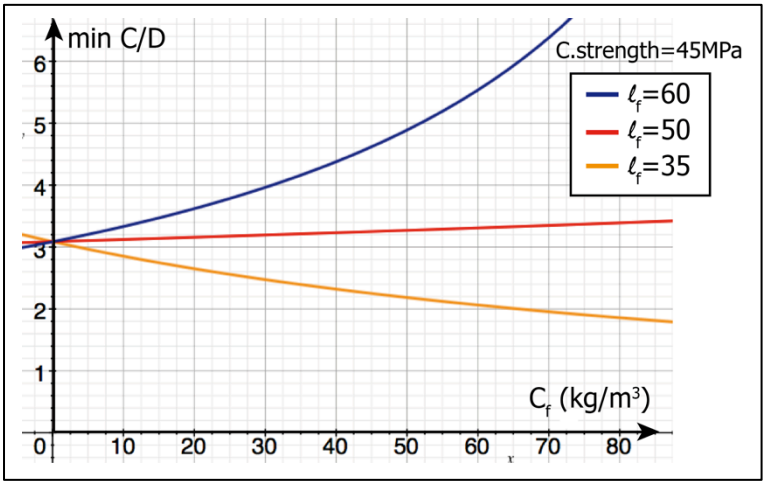

Figure 6.16. Minimum C/D values to avoid splitting failure of 45-MPa concrete reinforced with fibers of slenderness 65.

6.4 Potential of the model: charts to determine minimum C/D ratios

PRELIMINARIES

The generalization of a model that has been obtained by regression outside the range of data that have been used for its formulation often involves complications. The best practice to check if the model is valid outside the tested limits is to obtain new data to extend those limits and then to check and/or calibrate the model. This remark is applicable to simple linear regression, multiple linear regression, linear models obtained by other techniques, as well as logistic regression, which has been used in this chapter.

In the case of this research, Figure 6.17 shows the same curves as Figure 6.12 and also the curve corresponding to a compressive strength of 55 MPa, for which no data have been obtained in the experimental campaign. The shaded area defines the ranges tested: fiber content up to 60 kg/m3, cover/diameter ratios between 1.5 and 5.0, and concrete compressive strengths between 30 MPa and 50 MPa.

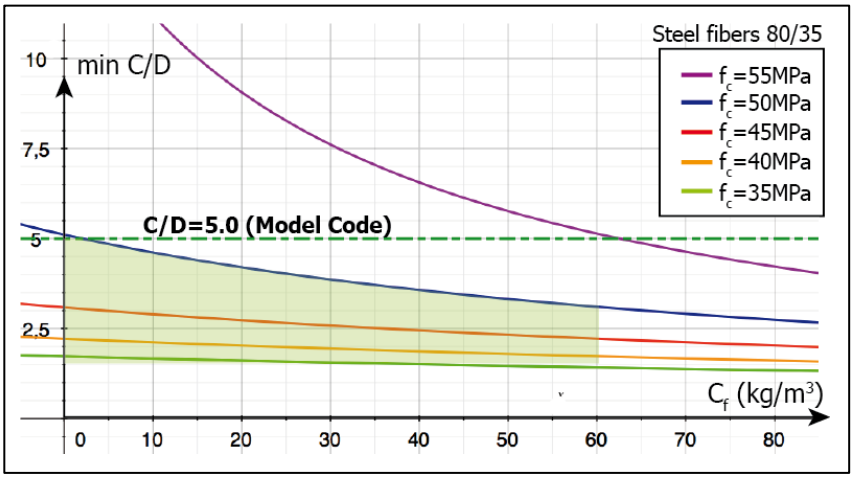

Figure 6.17. Generalizing the function relating min C/D to fiber content and concrete compressive strength.

Figure 6.17 shows that the extension of the model fails for a compressive strength value higher than the maximum tested value, since the values of cover/diameter ratio are unreasonably increased for low (or null) fiber contents. The reason for this behavior of the model is shown in Figure 6.18, where values of cover/diameter ratio are plotted vs concrete compressive strength. Again, the shaded area corresponds to the ranges tested. It is observed that this function, which is derived from the adjusted logistic model, presents an asymptotic discontinuity. This is because the cover/diameter ratio values are obtained from a logistic function which, by definition, has horizontal asymptotes.

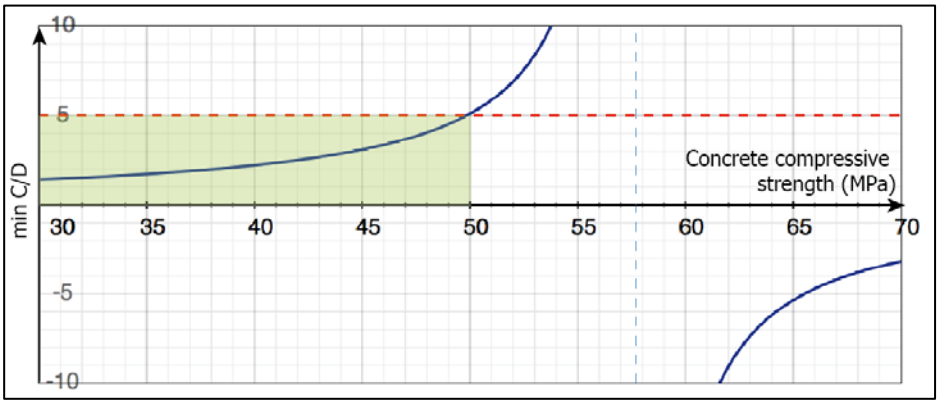

Figure 6.18. Min C/D vs concrete compressive strength derived from the fitted logistic function (concrete without fibers).

What has been detailed above, however, does not invalidate the fitted model and the conclusions obtained concerning the significance of the factors considered. It should be noted that the model obtained has been adjusted to values of frequency or probability of splitting failures, and not to minimum cover/diameter ratios. Given this, and in the absence of data out of the limits tested, an additional hypothesis is needed to come to a definition of the function for cover/diameter that is continuous and smooth.

ASSUMPTION OF MAXIMUM C/D RATIO ACCORDING TO MC

One hypothesis that can be assumed is the definition of good confinement provided by the Model Code (FIB 2010): values of cover/diameter ratio equal to or greater than 5 will not involve splitting failures. This scenario is shown in Figure 6.19 for concrete without fibers, imposed to the function which is derived from the logistic model experimentally fitted. A continuous, smooth function that best approximates the experimental curve and the hypothesis arising from the Model Code is shown in Figure 6.19 as "new equation".

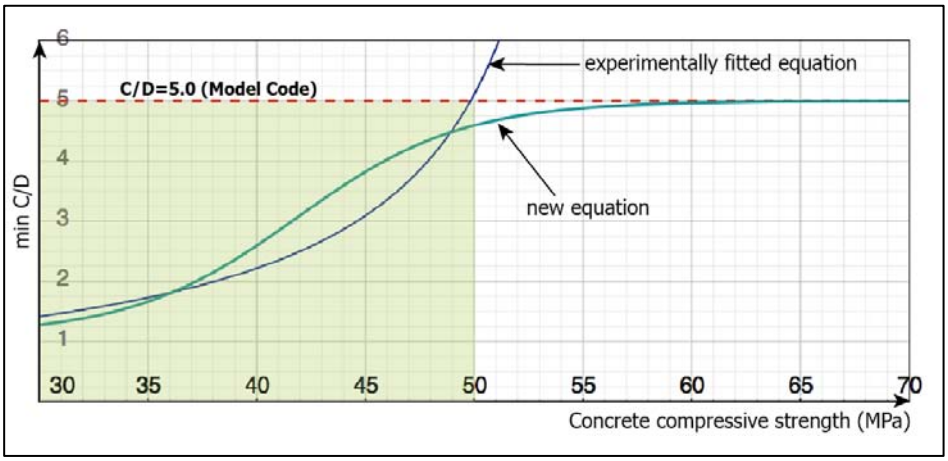

Figure 6.19. Function to relate min C/D to compressive strength (max C/D according to MC).

This new equation for concrete without fibers is as follows:

$$\frac{C}{D} = \frac{5 + exp\left(\frac{f_c - 30}{3.8}\right)}{4.5 + 0.2exp\left(\frac{f_c - 30}{3.8}\right)} \tag{6.12}$$

Figure 6.20 shows this function generalized for different fiber contents under the assumption concerning good confinement according to the Model Code. The three curves shown correspond to $\nabla_{\mathcal{F}} C_f$ values between –2.0 and 2.0 (tested values are between –2.5 and 2.5) in addition to unfibered concrete ($\nabla_{\mathcal{F}} C_f$=0). This generalized "new equation" is:

$$\frac{C}{D} = \frac{5 + exp\left(\frac{f_c + 5\nabla_F C_f - 30}{3.8}\right)}{4.5 + 0.2exp\left(\frac{f_c + 5\nabla_F C_f - 30}{3.8}\right)} \quad (6.13)$$

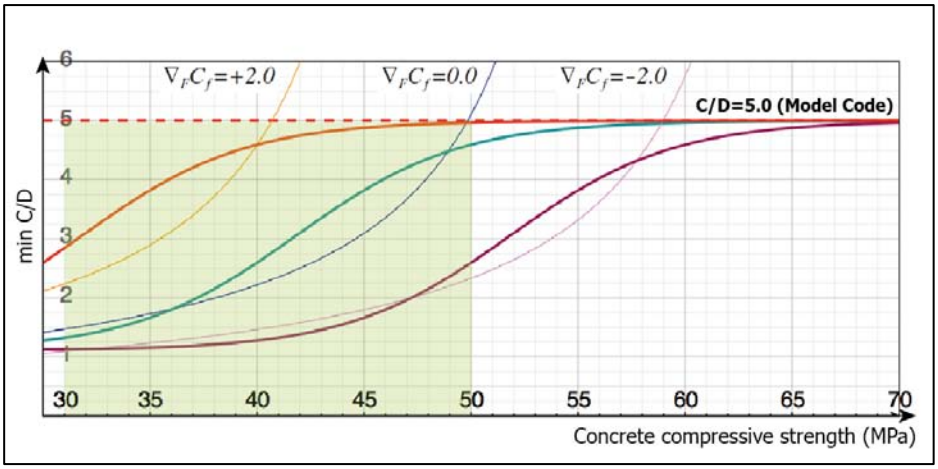

Figure 6.20. Generalized function to relate min C/D to compressive strength (max C/D according to MC).

However, it must be taken into account that the predictive capacity of the experimentally fitted model is 95%. Following Figures 6.19 and 6.20, the hypothesis that cover/diameter ratios of 5.0 (or higher) never correspond to splitting failures does not seem compatible with the experimental results. In these figures we see that the "new equation" forced by the assumed horizontal asymptote C/D = 5.0 is excessively diverging from the curve derived from the experimentally adjusted logistic model. This observation suggests that the hypothesis of good confinement as defined by the Model Code has to be checked. In the next subsection an alternative hypothesis is considered.

EXTENSION OF THE MODEL: PROPOSED CHARTS

An alternative hypothesis to that arising from the Model Code is that the value of cover/diameter ratio above which there is no splitting is higher than 5.0. This is equivalent to proposing a continuous, smooth function

which fits the curve derived experimentally from the combinations tested, and which has a horizontal asymptote above C / D = 5.0. The following function is proposed, and is shown in Figure 6.21:

$$\frac{C}{D} = 1.2 + \frac{(5.6 - 0.2\nabla_{\mathcal{F}} C_f) \cdot exp\left(\frac{f_c + 5\nabla_{\mathcal{F}} C_f - 50}{5}\right)}{0.6 + 0.9exp\left(\frac{f_c + 5\nabla_{\mathcal{F}} C_f - 50}{5}\right)} \qquad (6.14)$$

The tested combinations correspond to the shaded area in Figure 6.21. In the light of these new curves, it follows that the general limit that may be assumed for cover/diameter ratio as well confinement would not be 5.0 but around 7.5. However, this result needs to be confirmed in the future by performing new tests.

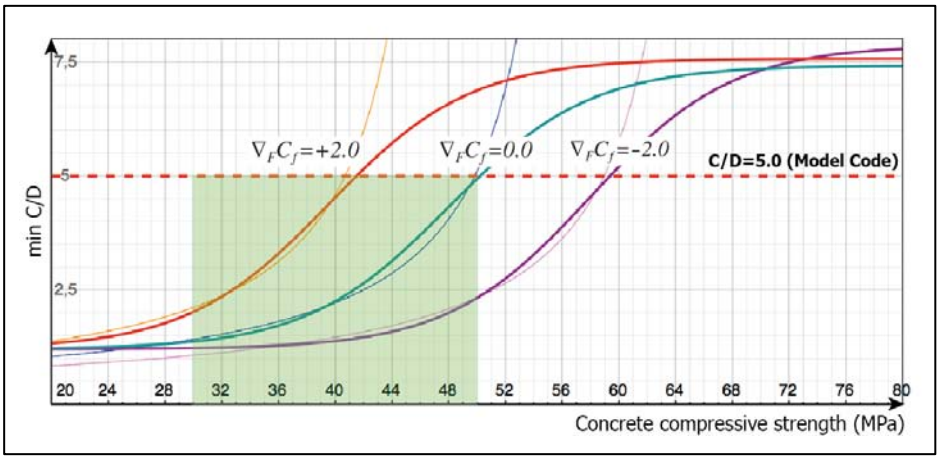

Figure 6.21. Generalized function to relate min C/D to compressive strength (MC definition not assumed).

From the new proposed function (equation 6.14) a chart is proposed to estimate the minimum cover/diameter ratio to prevent splitting from the values of concrete compressive strength, fiber content, and fiber length and slenderness. Figure 6.22 presents the chart to estimate the factor $\nabla_{\mathcal{F}}$ dependent on the geometry of the fiber. Figure 6.23 presents the chart to estimate the minimum cover/diameter ratio. Once again, the shaded area corresponds to the combinations tested in this research. Further tests are needed to confirm the rest of the chart outside the shaded area.

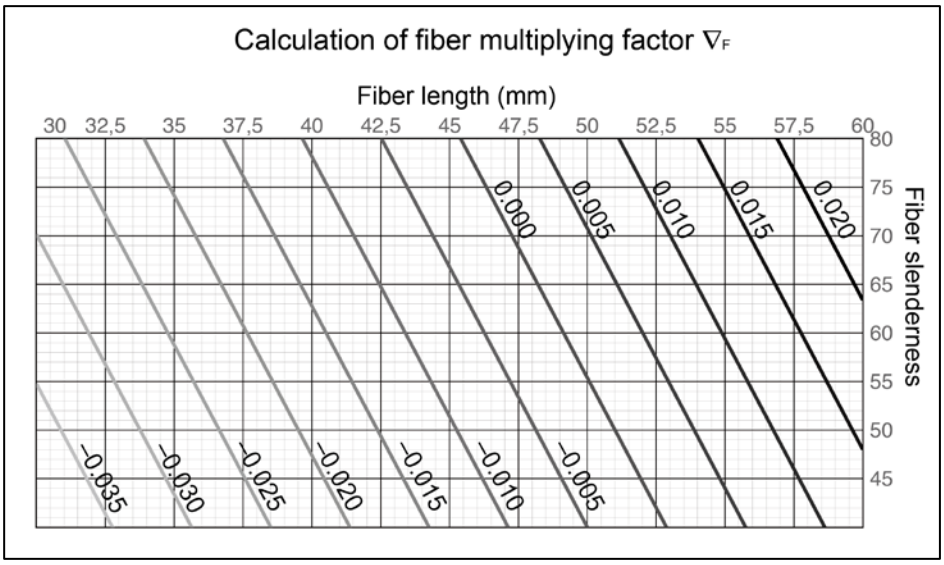

Figure 6.22. Chart to estimate the fiber multiplying factor dependent on fiber geometry.

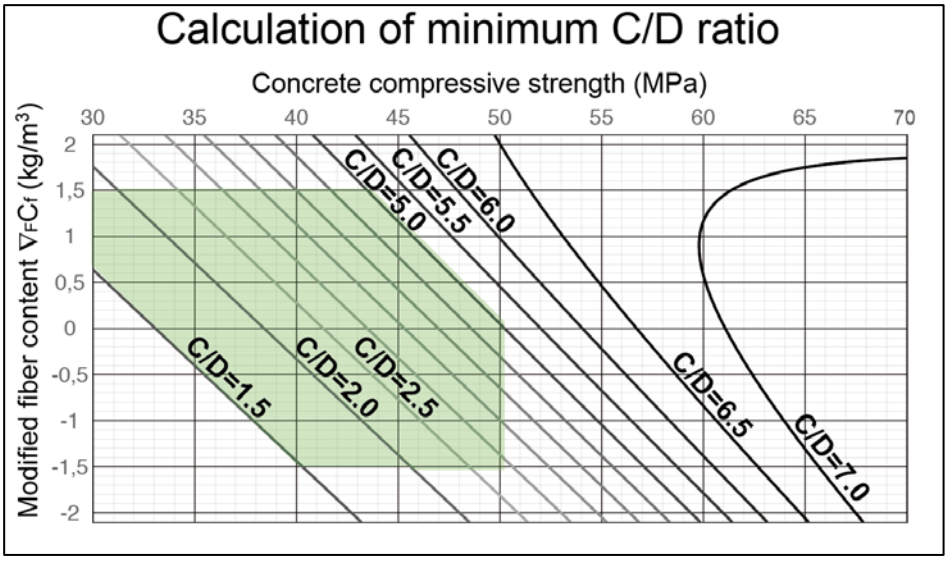

Figure 6.23. Proposed chart to estimate min C/D ratios to prevent splitting.

7| Univariate Analysis of Bond Parameters

Part III: Analysis of Results

7| Univariate Analysis of Bond Parameters

PART III: ANALYSIS OF RESULTS

7.1 Methodological Overview

The effects that the factors considered have on each one of the selected bond paramters (outputs of the bond stress–slip curves from the pull out test as defined in Chapter 5) have been assessed by means of multiple linear regression (MLR hereafter). Statistical inference regarding the relative importance of each factor has been carried out by means of significance tests on the coefficients estimated when fitting the MLR models relating each bond parameter to the factors considered.

To study separately the effect of each one of these factors on bond parameters, i.e. on the basis of one-to-one regression lines instead of applying MLR models would have been a defective approach. First, it would have offered no possibility of assessing their relative importance. And second, it would have implicitly assumed that the effect of each factor is the same regardless of the level of other factors.

The aim MLR modelling is not only to draw a set of descriptive equations for bond parameters, but also to identify which are the factors that have a really important, statistically significant effect. To do that successfully, the modelling process has followed an iterative construction and checking sequence at the same time the conceptual basis of the phenomenon under study is never forgotten.

Figure 7.1 summarizes the process that has been followed to model the relationships between the experimental results (bond parameters) and the factors considered. The same process has been followed for each bond parameter. It consists of the following steps:

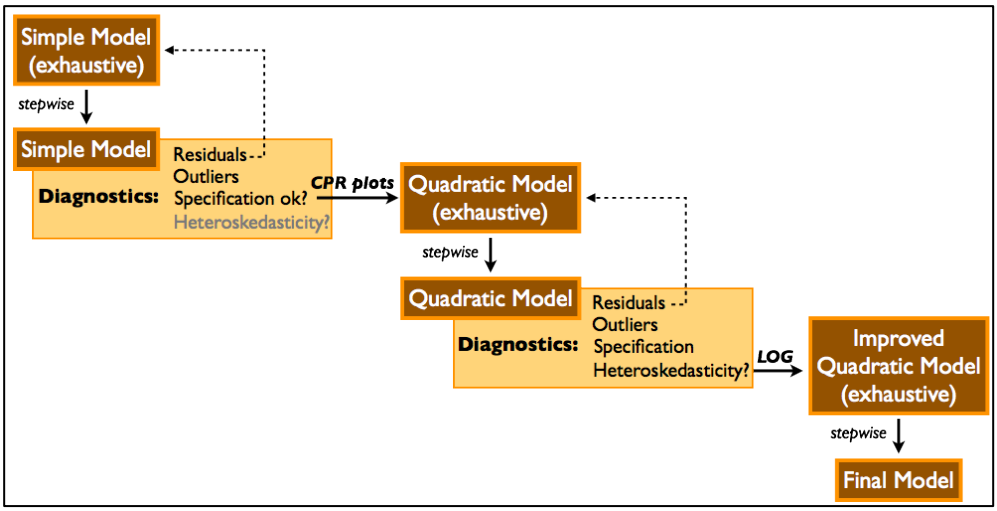

Figure 7.1. Overview of the modelling sequence.

- Construction and fitting of a simple, exhaustive model. This is a model that includes the simple effects of all factors considered. Considering only simple effects means that possible interactions are not taken into account. This model constitutes a first approximation.
- The simple model discussed in the previous section includes the simple effects of all factors (hence called exhaustive). However, not all factors are statistically significant. This means that the model can be simplified by disregarding insignificant factors without losing information. The procedure followed to obtain the simple model from the exhaustive simple model is stepwise regression in its backward mode. This is an iterative process which starts from the comprehensive model, and withdraws the least significant factor in each iteration, and recalculates the coefficients of the other factors at each step. Finally, the simple model obtained considers only statistically significant effects.
- The simple model obtained is then diagnosed:
    - Verification that residuals fit a normal distribution centered in zero. If this were not so, the initial model needs revision.

- Detection of outliers, or anomalous data: the convenience of their withdrawal is pondered and then the model is reestimated.
- Examination of the Component Plus Residual plots (CPR plots hereafter) to find if there is any quadratic trend that ha not been taken into account. If so, a quadratic model has to be developed to include them.

☐ Construction and fitting of an exhaustive quadratic model, i.e. considering anew simple effects and quadratic effects of all factors.

☐ Obtention of a quadratic model including only statistically significant effects (either simple or quadratic) by means of stepwise regression applied to the exhaustive quadratic model.

☐ The quadratic model is then diagnosed:

- Normal distribution of residuals.
- Detection and withdrawal of outliers, if any.
- Verifying that there is no heteroskedasticity in the model, i.e. that the scatter of residuals neither increases nor decreases with respect to the response variable values.

☐ In case heteroskedasticity is detected, this means that the scatter of response variable values increases or decreases with its mean value. This has to be taken into account in an improved quadratic model, which is developed for the logarithm of the response variable analyzed.

☐ The improved quadratic model is simplified by stepwise regression.

7.2 Bond Strength

SIMPLE MODEL

An additive, simple model for bond strength is taken as a point of departure. It explains bond strength as the result of adding the simple contributions of all factors considered. This model is given by equation 7.1:

$$\tau_{max} = \nabla_0 + \nabla_c f_c + \nabla_d \mathrm{D} + \nabla_{cd} \frac{C}{D} + \nabla_f C_f + \nabla_{\lambda f} \lambda_f C_f + \nabla_{\ell f} \ell_f C_f \qquad (7.1)$$

where τ_{max} stands for bond strength (MPa), f_c is average concrete compressive strength (MPa), D is rebar diameter (mm), C is concrete cover (mm), C_f is fiber content (kg/m^3), λ_f is fiber slenderness, ℓ_f is fiber length (mm); and ∇_0, ∇_c, ∇_d, ∇_{cd}, ∇_f, $\nabla_{\lambda f}$, and $\nabla_{\ell f}$ are coefficients to be estimated.

Neither interactions nor quadratic contributions have been considered so far. The only exceptions are fiber slenderness and fiber length, which appear multiplied by fiber content. The reason for their not being considered as standalone simple effects is that they must not have any effect on bond strength when fiber content is null. This way the products $\lambda_f C_f$ and $\ell_f C_f$ are forced to be null when fiber content C_f is zero.

Coefficients in equation 7.1 are estimated by fitting the model to observed data. Their estimates have been calculated by means of the least squares approach, i.e. minimizing the sum of squared residuals. The coefficients estimates and the corresponding significance tests are shown in Table 7.1. Since no p-value is bigger than 0.10, the model cannot be simplified by deleting any factor without significant loss of accuracy. The p-value obtained for the whole model is $4.236 \cdot 10^{-12} < 0.05$. This indicates a significant relationship between factors and response variable which is worth the modelling. The R-squared value is 72.94%.

Table 7.1. Estimation of coefficients and significance tests (simple model, eq.7.1)

		Coefficient	Std. error	p-value
(constant)	∇_0	–33.1449	5.58471	--
Compressive Strength	∇_c	0.87908	0.10935	0.0000
Cover/Diameter	∇_{cd}	0.99377	0.59258	0.1000
Diameter	∇_d	0.57903	0.16406	0.0009
Fiber Content	∇_f	0.45105	0.18267	0.0172
Fiber Slenderness, $\lambda_f C_f$	$\nabla_{\lambda f}$	–0.002434	0.001299	0.0671
Fiber Length, $\ell_f C_f$	$\nabla_{\ell f}$	–0.004306	0.002239	0.0604

Figure 7.1 shows the normal probability plot of the standardized residuals. It compares the residuals distribution to the expected normal distribution of mean zero and unit variance (theoretical quantiles). It can be observed that standardized residuals clearly follow the trend of a normal distribution with the exception of only one datum. However, calculations of leverage, Mahalanobis distances and Cook's statistic for all data (Box et al. 2005) have not detected any outliers or influential data. Therefore the case of this isolated datum is not problematic, and the model has been properly estimated.

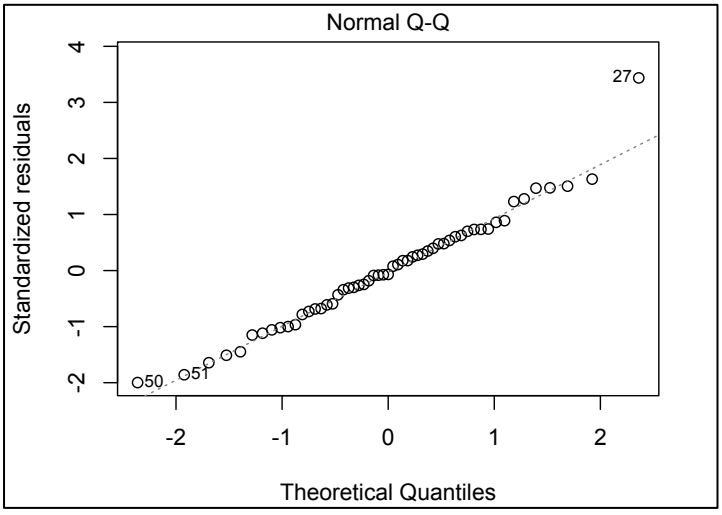

Figure 7.1. Normal probability plot of residuals (eq.7.1)

Finally, Figure 7.2 shows the so-called CPR (Component-Plus-Residual) plots. They are used to detect if there is any quadratic effect on bond strength that has been disregarded so far. The dotted red line corresponds to the fitted model (component line), while the green line is the one best fitting the residuals (residual line). It is clearly seen that rebar diameter has a quadratic effect on bond strength that must be incorporated to the model. This is carried out in the following section.

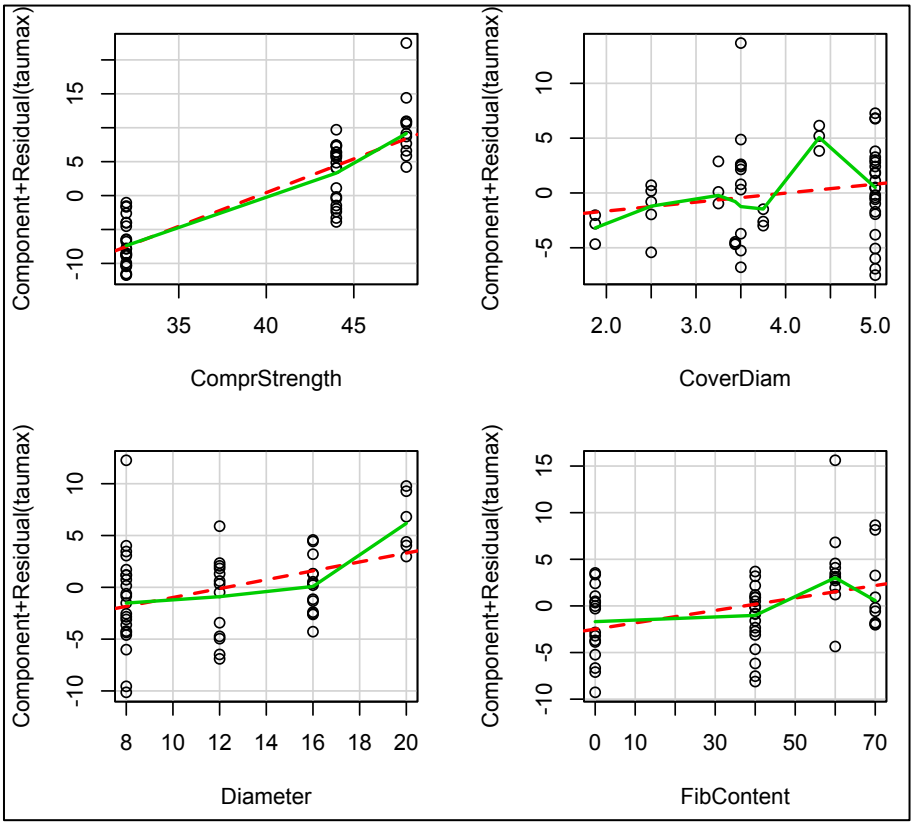

Figure 7.2. Component + Residual Plots

QUADRATIC MODEL

Since it has been detected that at least one of the factors considered may have a quadratic effect on bond strength which is statistically significant, the model is reframed as given by equation 7.2:

$$\tau_{max} = \nabla_0 + \nabla_c f_c + \nabla_{cc} {f_c}^2 + \nabla_d \mathrm{D} + \nabla_{dd} \mathrm{D}^2 + \nabla_{cd} \frac{C}{D} + \nabla_f C_f + \nabla_{ff} {C_f}^2 + \nabla_{\lambda f} \lambda_f C_f + \nabla_{\ell f} \ell_f C_f \quad (7.2)$$

Table 7.2 shows the coefficients estimates and the p-values obtained from the significance tests associated to these coefficients.

Table 7.2. Estimation of coefficients and significance tests (quadratic model, eq.7.2)

		Coefficient	Std. error	p-value
(constant)	∇_0	57.3648	41.5708	--
Compressive Strength	∇_c	–3.3038	2.3218	0.1617
	∇_{cc}	0.05433	0.02926	0.0699
Cover/Diameter	∇_{cd}	0.74687	0.5695	0.1963
Diameter	∇_d	–1.32185	1.2225	0.2853
	∇_{dd}	0.07456	0.0457	0.1098
Fiber Content	∇_f	0.33778	0.1934	0.0875
	∇_{ff}	0.00188	0.00105	0.0793
Fiber Slenderness, $\lambda_f C_f$	$\nabla_{\lambda f}$	–0.00212	0.00125	0.0976
Fiber Length, $\ell_f C_f$	$\nabla_{\ell f}$	–0.00500	0.00222	0.0289

Several p-values obtained are bigger than 0.10. Therefore the model can be simplified with no significant loss of accuracy by sequentially deleting these terms (stepwise regression). This leads to equation 7.3:

$$\tau_{max} = \nabla_0 + \nabla_c f_c + \nabla_{cc} {f_c}^2 + \nabla_{dd} \mathrm{D}^2 + \nabla_{cd} \frac{C}{D} + \nabla_f C_f + \nabla_{\lambda f} \lambda_f C_f + \nabla_{\ell f} \ell_f C_f \quad (7.3)$$

Table 7.3 shows the reestimated coefficients in the simplified quadratic model and the corresponding p-values. The R-squared value is 76.98%.

As Figure 7.3 shows, the distribution of the standardized residuals after the stepwise reduction of the quadratic model has suffered no important changes: they remain normally distributed.

Table 7.3. Estimation of coefficients and significance tests (quadratic model, eq.7.3)

		Coefficient	Std. error	p-value
(constant)	∇_0	70.0733	40.9249	--
Compressive Strength	∇_c	–4.4334	2.1557	0.0453
	∇_{cc}	0.06793	0.02739	0.0168
Cover/Diameter	∇_{cd}	1.0254	0.5512	0.0691
Diameter (quadratic)	∇_{dd}	0.02573	0.00585	0.0000
Fiber Content	∇_f	0.51084	0.1695	0.0042
Fiber Slenderness, $\lambda_f C_f$	$\nabla_{\lambda f}$	–0.00243	0.00119	0.0476
Fiber Length, $\ell_f C_f$	$\nabla_{\ell f}$	–0.00543	0.0021	0.0134

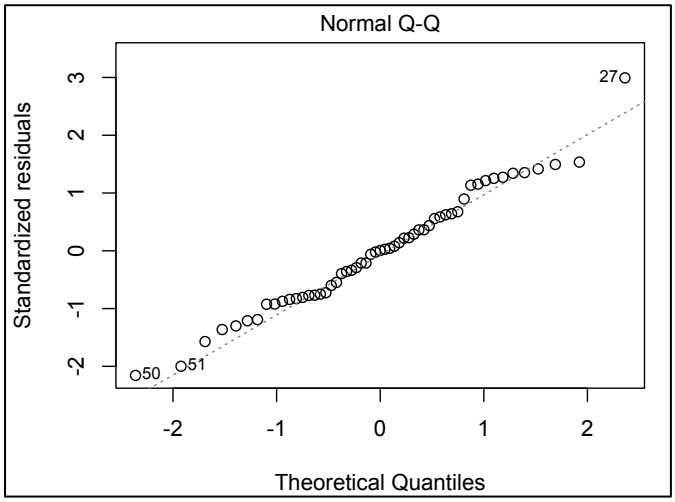

Figure 7.3. Normal probability plot of residuals (quadratic model, eq.7.3)

One last aspect must be checked. Figure 7.4 plots residuals vs fitted bond strength values. It can be seen that, with the exception of only one point, all residuals are scattered in a horizontal band. There is no sign indicating that their scatter varies with fitted values. This means that residuals variance is constant and does not depend on fitted values, therefore the model is homocedastic.

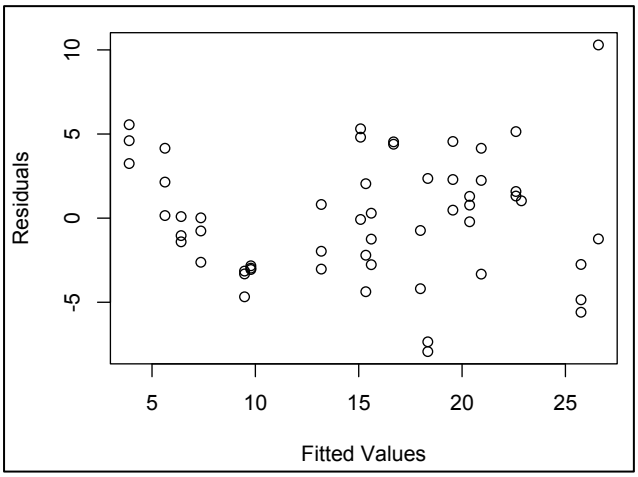

Figure 7.4. Plot of residuals vs fitted bond strength values (quadratic model, eq.7.3)

Since there are no outliers that require separate treatment, no specification errors left to be worked out, the standardized residuals are normally distributed, and the model proves homocedastic, this reduced, quadratic model for bond strength is adopted as final.

FINAL MODEL

Equation 7.4 presents the fitted model for bond strength, with an R-squared value of 76.98%:

$$\tau_{max} = 70.07 - 4.43f_c + 0.068{f_c}^2 + 0.026\mathrm{D}^2 + 1.03\frac{C}{D} + 0.51C_f - 0.0024\lambda_f C_f - 0.0054\ell_f C_f \qquad (7.4)$$

Figure 7.5 shows the predicted vs observed values of bond strength, together with the exact equivalence line and the limits of the 95%-confidence band. Figure 7.6 shows the effects plot corresponding to this model. Black lines are drawn according to mean values and red dashed lines limit the 95%-confidence band for predictions with this model. The analysis performed and reported herein has led to an expression which relates bond strength to statistically significant factors. However, although all of these factors have a statistically significant effect, it can be seen in Figure 7.6 that these effects are not of the same magnitude in all cases.

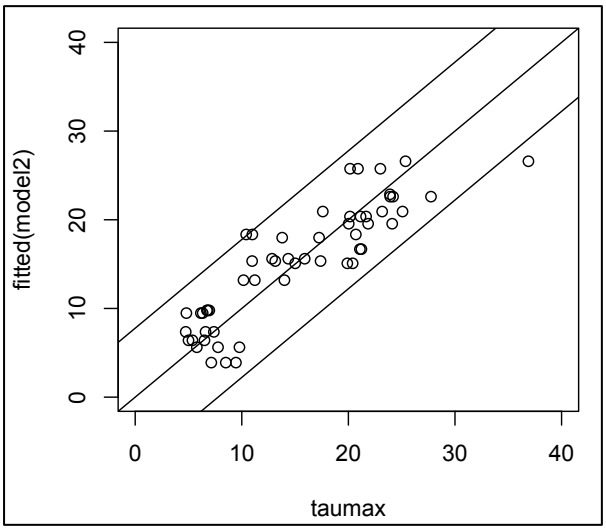

Figure 7.5. Predicted vs observed bond strength values.

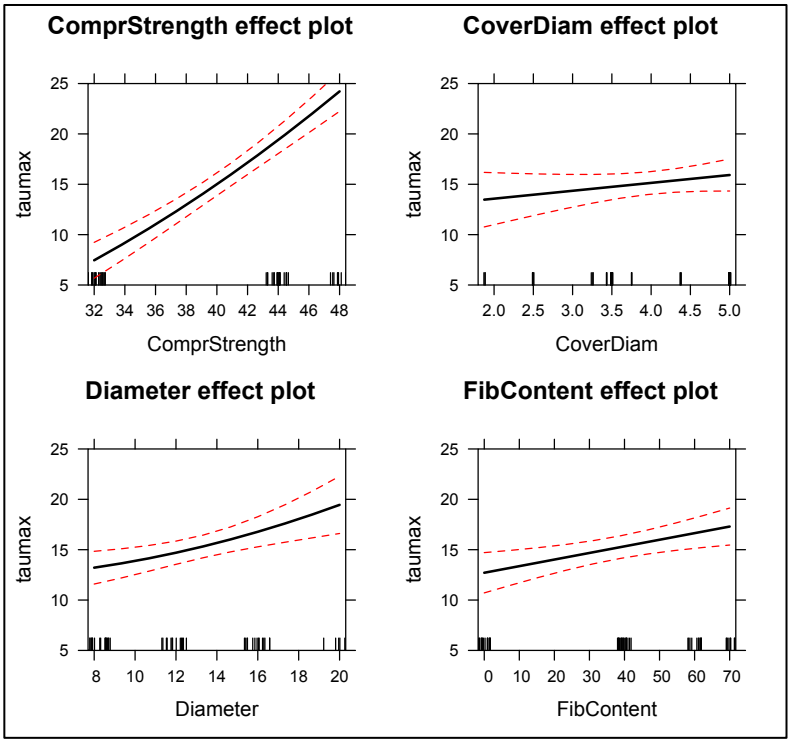

Figure 7.6. Effect plots for quadratic model (eq.7.3)

Effect plots in Figure 7.6 clearly show that concrete compressive strength is the most determining factor on bond strength. This is consistent with previous literature on the subject (see Chapter 2). The effect of passive confinement on bond strength, either cover/diameter ratio or fiber content, although statistically significant and positive, is less important than the effect of concrete compressive strength.

It should be noted that all cases which are being examined in this chapter correspond to pullout failures. Therefore, the most crucial process is the crushing of concrete wedges between ribs due to triaxial compression. Hence the most determining factor is naturally concrete compressive strength: the higher concrete compressive strength, the higher bond strength. In agreement with this, the effect of fibers on bond strength is mostly attributable to their effect on concrete mechanical properties and not to their confining effect.

Rebar diameter has a positive effect on bond strength as well, but for different reasons. The larger the diameter, the higher the bond stresses that are developed in the steel-concrete interface to balance the pullout, axial load applied to the rebar.

7.3 Toughness (I): A_{peak}

SIMPLE MODEL

A simple model for the area under the bond stress–slip curve up to the slip corresponding to peak bond stress, or bond strength (A_{peak} hereafter) is given by equation 7.5:

$$A_{peak} = \nabla_0 + \nabla_c f_c + \nabla_d \mathrm{D} + \nabla_{cd} \frac{C}{D} + \nabla_f C_f + \nabla_{\lambda f} \lambda_f C_f + \nabla_{\ell f} \ell_f C_f \qquad (7.5)$$

where A_{peak} stands for the aforementioned area (mmMPa), f_c is the average concrete compressive strength (MPa), D is rebar diameter (mm), C is concrete cover (mm), C_f is fiber content (kg/m^3), λ_f is fiber slenderness, ℓ_f is fiber length (mm); and ∇_0, ∇_c, ∇_d, ∇_{cd}, ∇_f, $\nabla_{\lambda f}$, and $\nabla_{\ell f}$ are coefficients to be estimated.

Estimates for the coefficients in equation 7.5 are shown in Table 7.4 together with the associated p-values. The p-value obtained for the model is $7.6 \cdot 10^{-4} < 0.05$ and the R-squared value is 37.1%.

Table 7.4. Estimation of coefficients and significance tests (simple model, eq.7.5)

		Coefficient	Std. error	p-value
(constant)	∇_0	–37.8616	11.5167	--
Compressive Strength	∇_c	0.6572	0.2255	0.0054
Cover/Diameter	∇_{cd}	2.515	1.222	0.0450
Diameter	∇_d	1.1591	0.3383	0.0013
Fiber Content	∇_f	0.6164	0.3767	0.1083
Fiber Slenderness, $\lambda_f C_f$	$\nabla_{\lambda f}$	–0.00301	0.00268	0.2677
Fiber Length, $\ell_f C_f$	$\nabla_{\ell f}$	–0.00629	0.00462	0.1794

Since p-values corresponding to fiber slenderness and length are bigger than 0.10, the model is simplified without significant loss of accuracy by

deleting these factors. Equation 7.6. is obtained. Table 7.5 shows the reestimated coefficients and p-values. The R-squared value is 34.45%.

$$A_{peak} = \nabla_0 + \nabla_c f_c + \nabla_d \mathrm{D} + \nabla_{cd} \frac{C}{D} + \nabla_f C_f \qquad (7.6)$$

Table 7.5. Estimation of coefficients and significance tests (simple model, eq.7.6)

		Coefficient	Std. error	p-value
(constant)	∇_0	–40.927	11.283	--
Compressive Strength	∇_c	0.8261	0.1874	0.0000
Cover/Diameter	∇_{cd}	2.2296	1.1929	0.0675
Diameter	∇_d	0.9494	0.3040	0.0029
Fiber Content	∇_f	0.0934	0.0459	0.0474

Figure 7.7 shows the normal probability plot of the standardized residuals, which prove to be normally distributed with the exception of two points. Since no outliers or influential data have been identified by means of other tests, it is reasonable to expect that this two points behave better after the model is refined in the following sections. Therefore, it is preferred not to remove them at this moment.

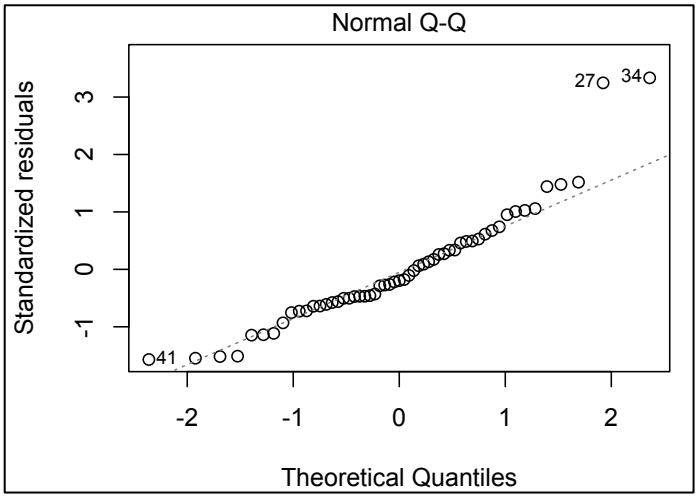

Figure 7.7. Normal probability plot.

Figure 7.8 shows the CPR plots. These plots reveal that both compressive strength and rebar diameter have a quadratic effect on A_{peak} that is disregarded in the model in its present form.

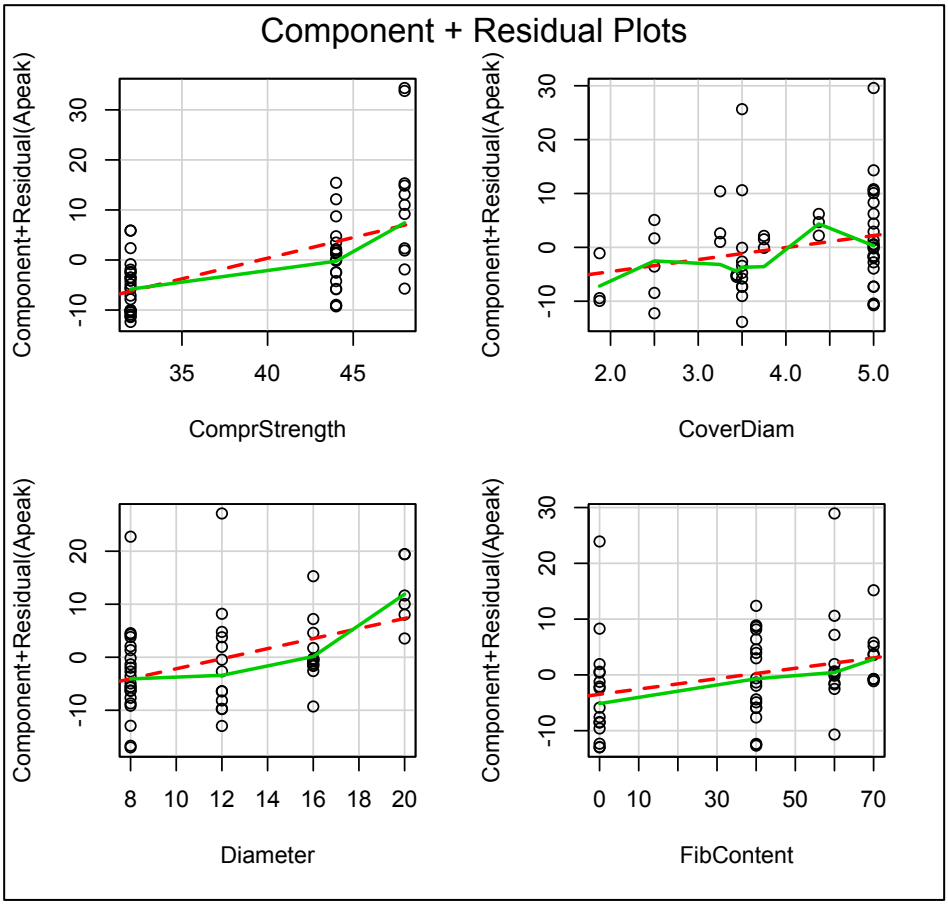

Figure 7.8. CPR plots.

QUADRATIC MODEL

The model for A_{peak} is reformulated as given by equation 7.7:

$$A_{peak} = \nabla_0 + \nabla_c f_c + \nabla_{cc} {f_c}^2 + \nabla_d \mathrm{D} + \nabla_{dd} \mathrm{D}^2 + \nabla_{cd} \frac{C}{D} + \nabla_f C_f + \nabla_{ff} {C_f}^2 + \nabla_{\lambda f} \lambda_f C_f + \nabla_{\ell f} \ell_f C_f \tag{7.7}$$

Table 7.6 shows the results of coefficients estimation and the p-values obtained from the significance tests associated to these coefficients. The R-squared is 49.97%.

Table 7.6. Estimation of coefficients and significance tests (quadratic model, eq.7.7)

		Coefficient	Std. error	p-value
(constant)	∇_0	222.408	86.389	--
Compressive Strength	∇_c	–12.746	4.825	0.0113
	∇_{cc}	0.1713	0.0608	0.0072
Cover/Diameter	∇_{cd}	2.5164	1.1834	0.0389
Diameter	∇_d	–0.07835	2.5405	0.9755
	∇_{dd}	0.0546	0.0949	0.5681
Fiber Content	∇_f	0.6853	0.4019	0.0951
	∇_{ff}	0.00162	0.00218	0.4629
Fiber Slenderness, $\lambda_f C_f$	$\nabla_{\lambda f}$	–0.003113	0.0026	0.2382
Fiber Length, $\ell_f C_f$	$\nabla_{\ell f}$	–0.00936	0.0046	0.0481

Several p-values obtained are bigger than 0.10. Therefore the model is simplified, and equation 7.8 is obtained:

$$A_{peak} = \nabla_0 + \nabla_c f_c + \nabla_{cc} {f_c}^2 + \nabla_{dd} \mathrm{D}^2 + \nabla_{cd} \frac{C}{D} + \nabla_f C_f + \nabla_{\ell f} \ell_f C_f \qquad (7.8)$$

Table 7.7 shows the reestimated coefficients in the simplified quadratic model and the corresponding p-values. The R-squared value is 47.68%.

As Figure 7.9 shows, the distribution of the standardized residuals after the stepwise reduction of the quadratic model has suffered no important changes: they remain normally distributed. No outliers or influential points have been detected either.

Finally, Figure 7.10 plots the residuals vs the fitted values of A_{peak}. The scatter of residuals increases with the fitted values of A_{peak}. This is a clear sign of the model's heteroscedasticity: variance of residuals is not constant. The model is improved in the following section to treat this problem.

Table 7.7. Estimation of coefficients and significance tests (quadratic model, eq.7.8)

		Coefficient	Std. error	p-value
(constant)	∇_0	218.282	82.442	--
Compressive Strength	∇_c	–12.649	4.344	0.0054
	∇_{cc}	0.17095	0.0552	0.0033
Cover/Diameter	∇_{cd}	2.5699	1.1113	0.0251
Diameter (quadratic)	∇_{dd}	0.04738	0.0112	0.0001
Fiber Content	∇_f	0.40328	0.1786	0.0286
Fiber Length, $\ell_f C_f$	$\nabla_{\ell f}$	–0.005946	0.00345	0.0916

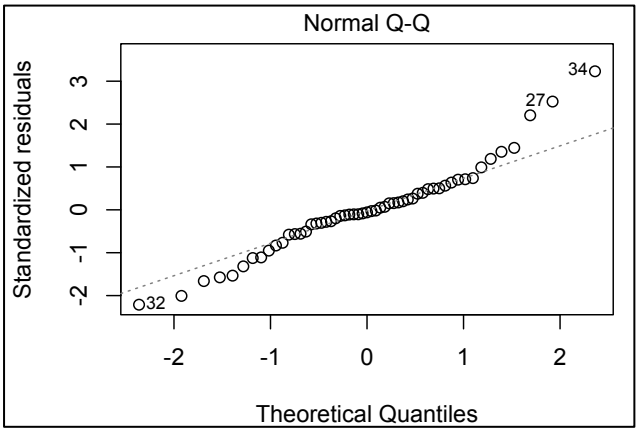

Figure 7.9. Normal probability plot.

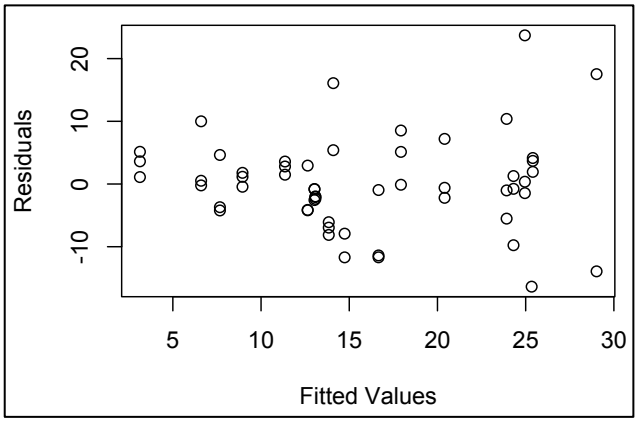

Figure 7.10. Residuals vs fitted A_{peak} values.

IMPROVED QUADRATIC MODEL

The model for A_{peak} is reformulated as given by equation 7.9:

$$log(A_{peak}) = \nabla_0 + \nabla_c f_c + \nabla_{cc} {f_c}^2 + \nabla_d \mathrm{D} + \nabla_{dd} \mathrm{D}^2 + \nabla_{cd} \frac{C}{D} + \nabla_f C_f + \nabla_{ff} {C_f}^2 + \nabla_{\lambda f} \lambda_f C_f + \nabla_{\ell f} \ell_f C_f \quad (7.9)$$

Table 7.8 shows the results of coefficients estimation and the p-values obtained from the significance tests associated to these coefficients. The R-squared is 51.4%.

Table 7.8. Estimation of coefficients and significance tests (quadratic model, eq.7.9)

		Coefficient	Std. error	p-value
(constant)	∇_0	9.2683	5.5026	--
Compressive Strength	∇_c	–0.4915	0.3073	0.1167
	∇_{cc}	0.00684	0.00387	0.0842
Cover/Diameter	∇_{cd}	0.1876	0.0754	0.0166
Diameter	∇_d	0.01434	0.1618	0.9298
	∇_{dd}	0.00289	0.0061	0.6351
Fiber Content	∇_f	0.045	0.0256	0.0854
	∇_{ff}	0.000114	0.000139	0.4168
Fiber Slenderness, $\lambda_f C_f$	$\nabla_{\lambda f}$	–0.000221	0.000166	0.1895
Fiber Length, $\ell_f C_f$	$\nabla_{\ell f}$	–0.000556	0.000293	0.0648

Several p-values obtained are bigger than 0.10. Therefore the model is simplified and equation 7.10 is obtained:

$$log(A_{peak}) = \nabla_0 + \nabla_{cc} {f_c}^2 + \nabla_{dd} \mathrm{D}^2 + \nabla_{cd} \frac{C}{D} + \nabla_f C_f \quad (7.10)$$

Table 7.9 shows the reestimated coefficients in the simplified quadratic model and the corresponding p-values. The R-squared value is 44.6%.

As Figure 7.11 shows, the distribution of the standardized residuals is now clearly normally distributed. Finally, Figure 7.12 plots the residuals vs the fitted values of A_{peak}: the model is now homocedastic.

Table 7.9. Estimation of coefficients and significance tests (quadratic model, eq.7.10)

		Coefficient	Std. error	p-value
(constant)	∇_0	–0.0762	0.455	--
Compr. Strength (quad.)	∇_{cc}	0.000734	0.000145	0.0000
Cover/Diameter	∇_{cd}	0.16713	0.0707	0.0220
Diameter (quadratic)	∇_{dd}	0.00275	0.000694	0.0002
Fiber Content	∇_f	0.00856	0.00273	0.0029

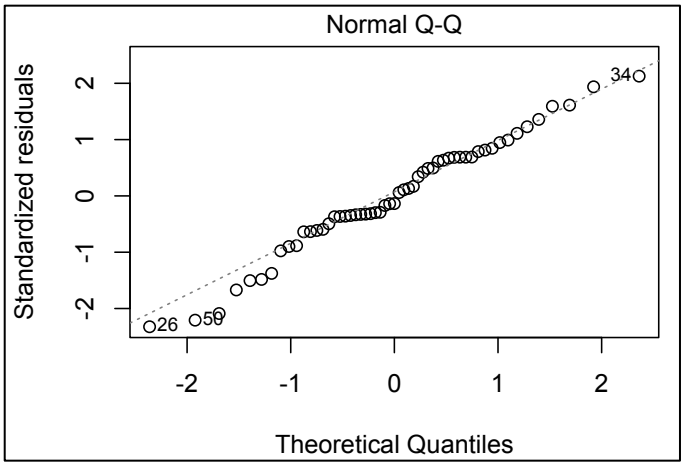

Figure 7.11. Normal probability plot of standardized residuals.

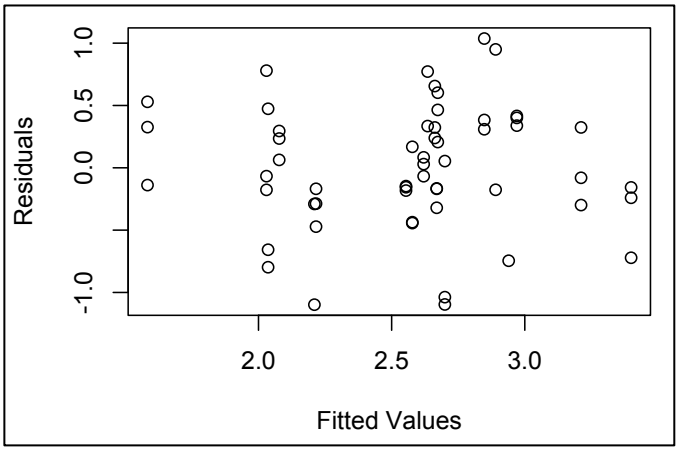

Figure 7.12. Plot of residuals vs fitted log(A_{peak}) values.

FINAL MODEL

Equation 7.11 presents the fitted model for A_{peak}, with an R-squared value of 44.6%:

$$log(A_{peak}) = -0.0762 + 0.000734{f_c}^2 + 0.00275\mathrm{D}^2 + 0.167\frac{C}{D} + 0.00856C_f \quad (7.11)$$

Figure 7.13 shows the predicted vs observed values of log(A_{peak}), together with the exact equivalence line and the limits of the 95%-confidence band.

Figure 7.14 shows the predicted vs observed values of untransformed A_{peak}. Together with the exact equivalence line, the 95%-confidence band is also shown as obtained from processing the limits in Figure 7.13.

Figure 7.15 shows the effects plot corresponding to this model. Black lines are drawn according to mean values and red dashed lines limit the 95%-confidence band for predictions with this model. It can be seen that the effect of all factors on bond strength is not of the same magnitude.

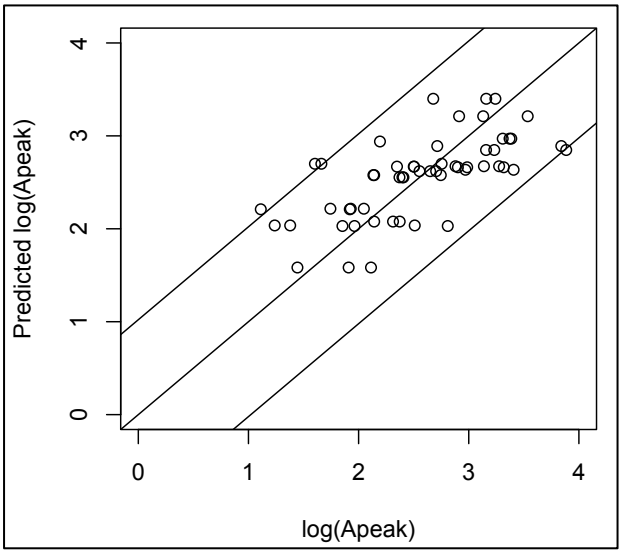

Figure 7.13. Predicted vs observed log(A_{peak}) values.

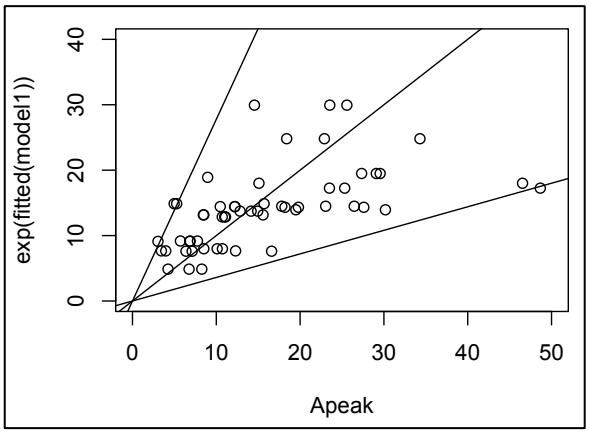

Figure 7.14. Predicted vs observed A_{peak} values.

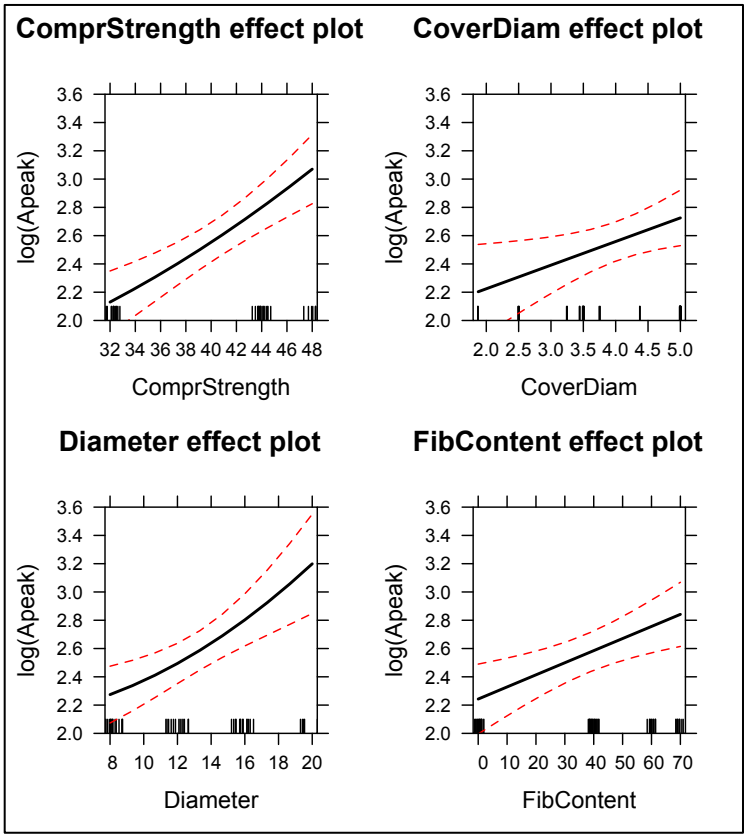

Figure 7.15. Effect plots for the improved quadratic model (eq.7.11).

7.4 Toughness (II): A_{50}

SIMPLE MODEL

A simple model for the area under the bond stress–slip curve up to the slip corresponding to 50% of bond strength (A_{50} hereafter) is given by equation 7.12:

$$A_{50} = \nabla_0 + \nabla_c f_c + \nabla_d \mathrm{D} + \nabla_{cd}\frac{C}{D} + \nabla_f C_f + \nabla_{\lambda f}\lambda_f C_f + \nabla_{\ell f}\ell_f C_f \qquad (7.12)$$

where A_{50} stands for the aforementioned area (mmMPa), f_c is the average concrete compressive strength (MPa), D is rebar diameter (mm), C is concrete cover (mm), C_f is fiber content (kg/m^3), λ_f is fiber slenderness, ℓ_f is fiber length (mm); and ∇_0, ∇_c, ∇_d, ∇_{cd}, ∇_f, $\nabla_{\lambda f}$, and $\nabla_{\ell f}$ are coefficients to be estimated.

Estimates of coefficients in equation 7.5 are shown in Table 7.10, together with the corresponding significance tests. The p-value obtained for the whole model is $8.81\cdot10^{-7}<0.05$, which means that there is a significant relationship between the variables and response variable worth the modelling. The R-squared value is 53.8%.

Table 7.10. Estimation of coefficients and significance tests (simple model, eq.7.12)

		Coefficient	Std. error	p-value
(constant)	∇_0	–329.9118	61.99	--
Compressive Strength	∇_c	5.4394	1.21	0.0000
Cover/Diameter	∇_{cd}	20.9603	6.58	0.0025
Diameter	∇_d	7.476	1.82	0.0002
Fiber Content	∇_f	3.4847	2.03	0.0921
Fiber Slenderness, $\lambda_f C_f$	$\nabla_{\lambda f}$	–0.0132	0.014	0.3639
Fiber Length, $\ell_f C_f$	$\nabla_{\ell f}$	–0.0364	0.025	0.1489

Since p-values corresponding to fiber slenderness and length are bigger than 0.10, the model is simplified without significant loss of accuracy by discarding these effects. This leads to equation 7.13. Table 7.11 shows the reestimated coefficients and the corresponding p-values. The R-squared value is 51.80%.

$$A_{50} = \nabla_0 + \nabla_c f_c + \nabla_d \mathrm{D} + \nabla_{cd} \frac{C}{D} + \nabla_f C_f \qquad (7.13)$$

Table 7.11. Estimation of coefficients and significance tests (simple model, eq.7.13)

		Coefficient	Std. error	p-value
(constant)	∇_0	–348.025	60.832	--
Compressive Strength	∇_c	6.428	1.010	0.0000
Cover/Diameter	∇_{cd}	19.088	6.432	0.0046
Diameter	∇_d	6.334	1.639	0.0003
Fiber Content	∇_f	0.746	0.248	0.0041

Figure 7.16 shows the normal probability plot of the standardized residuals, which prove normally distributed. Finally, Figure 7.17 shows the CPR plots. Both compressive strength and rebar diameter have quadratic effects on A_{50} that are disregarded in the model in its present form and must be considered.

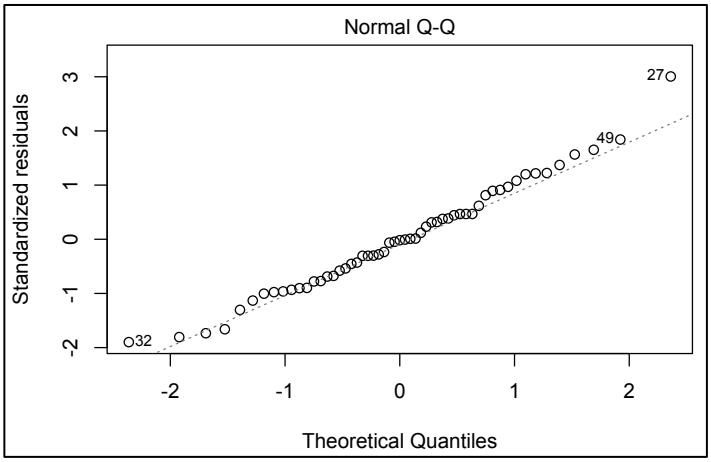

Figure 7.16. Normal probability plot.

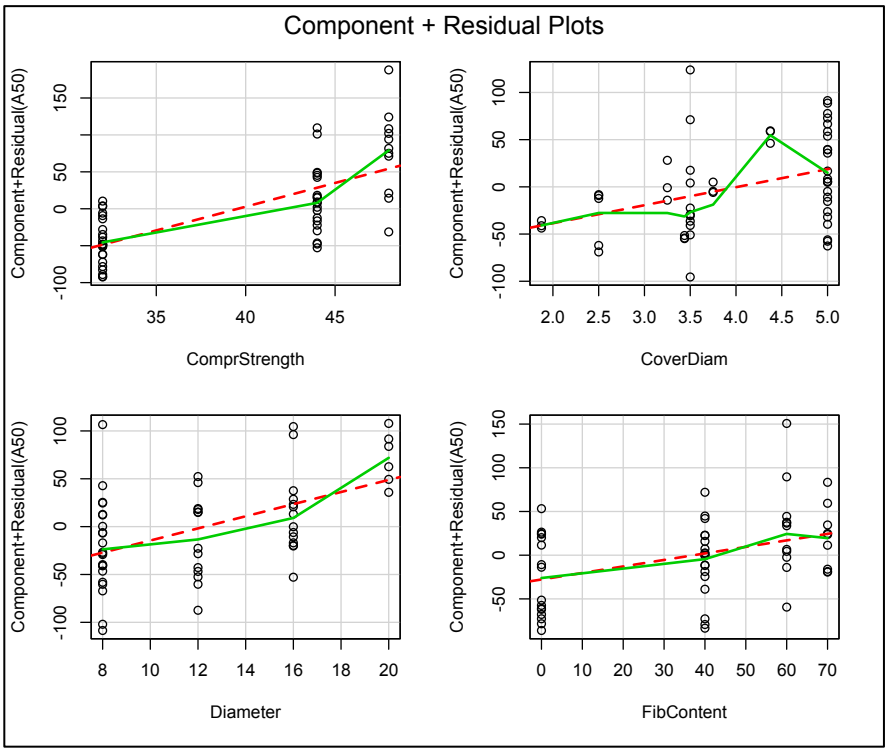

Figure 7.17. CPR plots.

QUADRATIC MODEL

The model for A_{50} is reformulated as given by equation 7.14:

$$A_{50} = \nabla_0 + \nabla_c f_c + \nabla_{cc} {f_c}^2 + \nabla_d \mathrm{D} + \nabla_{dd} \mathrm{D}^2 + \nabla_{cd} \frac{C}{D} + \nabla_f C_f + \nabla_{ff} {C_f}^2 + \nabla_{\lambda f} \lambda_f C_f + \nabla_{\ell f} \ell_f C_f \qquad (7.14)$$

Table 7.12 shows the estimates of coefficients in equation 7.14 and their corresponding p-values. The R-squared is 62.92%.

Table 7.12. Estimation of coefficients and significance tests (quadratic model, eq.7.14)

		Coefficient	Std. error	p-value
(constant)	∇_0	930.3612		--
Compressive Strength	∇_c	–57.3039	26.112	0.0334
	∇_{cc}	0.8058	0.3291	0.0183
Cover/Diameter	∇_{cd}	20.033	6.404	0.0031
Diameter	∇_d	–5.4871	13.7489	0.6917
	∇_{dd}	0.5287	0.5139	0.3091
Fiber Content	∇_f	3.3712	2.175	0.1282
	∇_{ff}	0.00979	0.0118	0.4116
Fiber Slenderness, $\lambda_f C_f$	$\nabla_{\lambda f}$	–0.0117	0.0141	0.4107
Fiber Length, $\ell_f C_f$	$\nabla_{\ell f}$	–0.0486	0.0249	0.0575

Several p-values obtained are bigger than 0.10. Therefore the model can be simplified with no significant loss of accuracy by sequentially discarding these terms. This stepwise, backward reduction leads to equation 7.15.

$$A_{50} = \nabla_0 + \nabla_c f_c + \nabla_{cc} {f_c}^2 + \nabla_{dd} \mathrm{D}^2 + \nabla_{cd} \frac{C}{D} + \nabla_f C_f + \nabla_{\ell f} \ell_f C_f \qquad (7.15)$$

Table 7.13 shows the reestimated coefficients in the simplified quadratic model and the corresponding p-values. The R-squared value is 61.51%.

Table 7.13. Estimation of coefficients and significance tests (quadratic model, eq.7.15)

		Coefficient	Std. error	p-value
(constant)	∇_0	961.0434	444.478	--
Compressive Strength	∇_c	–61.0522	23.422	0.0121
	∇_{cc}	0.8544	0.298	0.0006
Cover/Diameter	∇_{cd}	21.1024	5.992	0.0009
Diameter (quadratic)	∇_{dd}	0.30694	0.0605	0.0000
Fiber Content	∇_f	2.6301	0.963	0.0088
Fiber Length, $\ell_f C_f$	$\nabla_{\ell f}$	–0.0366	0.0186	0.0548

As Figure 7.18 shows, the distribution of the standardized residuals after the stepwise reduction of the quadratic model has suffered no important changes: they clearly remain normally distributed. No outliers or influential points have been detected either.

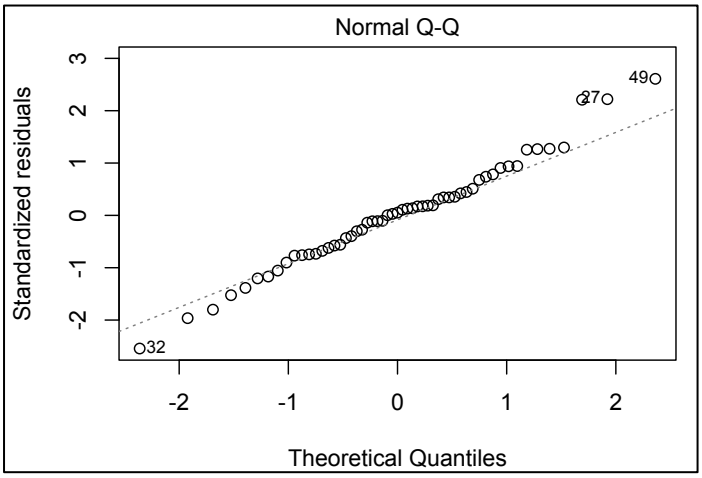

Figure 7.18. Normal probability plot.

Finally, Figure 7.19 plots residuals vs the fitted values of A_{50}. It is observed a clear tendency of the scatter of residuals: it increases when A_{50} values increase. This is a clear sign of heteroscedasticity: variance of residuals is not constant.

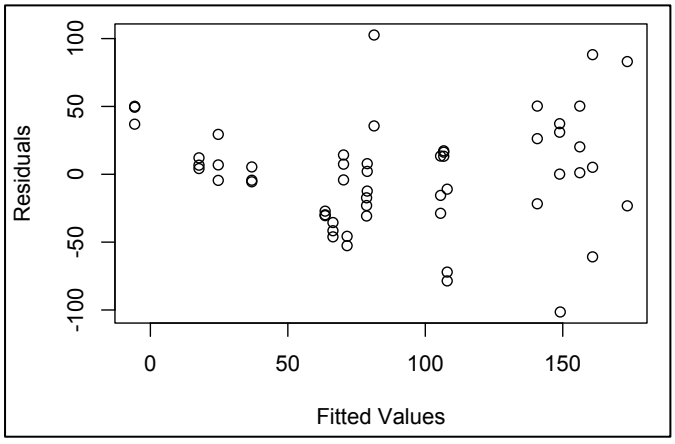

Figure 7.19. Plot of residuals vs fitted A_{50} values.

IMPROVED QUADRATIC MODEL

The model for A_{50} is reformulated as given by equation 7.16:

$$log(A_{50}) = \nabla_0 + \nabla_c f_c + \nabla_{cc} {f_c}^2 + \nabla_d \mathrm{D} + \nabla_{dd} \mathrm{D}^2 + \nabla_{cd} \frac{C}{D} + \nabla_f C_f + \nabla_{ff} {C_f}^2 + \nabla_{\lambda f} \lambda_f C_f + \nabla_{\ell f} \ell_f C_f \quad (7.16)$$

Table 7.14 shows the results of coefficients estimation and the p-values obtained from the significance tests associated to these coefficients. The R-squared is 64.48%.

Table 7.14. Estimation of coefficients and significance tests (quadratic model, eq.7.16)

		Coefficient	Std. error	p-value
(constant)	∇_0	5.963	5.447	--
Compressive Strength	∇_c	–0.2281	0.3042	0.4572
	∇_{cc}	0.003845	0.00383	0.3202
Cover/Diameter	∇_{cd}	0.2233	0.0746	0.0045
Diameter	∇_d	–0.133	0.1602	0.4108
	∇_{dd}	0.008944	0.00598	0.1423
Fiber Content	∇_f	0.04277	0.0253	0.0984
	∇_{ff}	0.0000957	0.000137	0.4904
Fiber Slenderness, $\lambda_f C_f$	$\nabla_{\lambda f}$	–0.000164	0.000164	0.3226
Fiber Length, $\ell_f C_f$	$\nabla_{\ell f}$	–0.000572	0.000291	0.0550

Several p-values obtained are bigger than 0.10. Therefore the model can be simplified with no significant loss of accuracy by sequentially discarding these terms. This leads to equation 7.17:

$$log(A_{50}) = \nabla_0 + \nabla_{cc} {f_c}^2 + \nabla_{dd} \mathrm{D}^2 + \nabla_{cd} \frac{C}{D} + \nabla_f C_f + \nabla_{\ell f} \ell_f C_f \quad (7.17)$$

Table 7.15 shows the reestimated coefficients in the simplified quadratic model and the corresponding p-values. The R-squared value is 61.22%.

Table 7.15. Estimation of coefficients and significance tests (quadratic model, eq.7.17)

		Coefficient	Std. error	p-value
(constant)	∇_0	0.76723	0.4463	--
Compr. Strength (quad.)	∇_{cc}	0.000953	0.00016	0.0000
Cover/Diameter	∇_{cd}	0.23776	0.0707	0.0015
Diameter (quadratic)	∇_{dd}	0.00359	0.00071	0.0000
Fiber Content	∇_f	0.027219	0.01088	0.0158
Fiber Length, $\ell_f C_f$	$\nabla_{\ell f}$	–0.00036	0.00021	0.0990

As Figure 7.20 shows, the distribution of the standardized residuals after the stepwise reduction of the quadratic model has suffered no important changes: they clearly remain normally distributed. No outliers or influential points have been detected either.

Finally, Figure 7.21 plots the residuals vs the fitted values of A_{50}. The scatter of residuals shows no tendency to increase or decrease with A_{50} values. Therefore the transformation of A50 to log(A_{50}) has achieved the model's homocedasticity: now variance of residuals is constant.

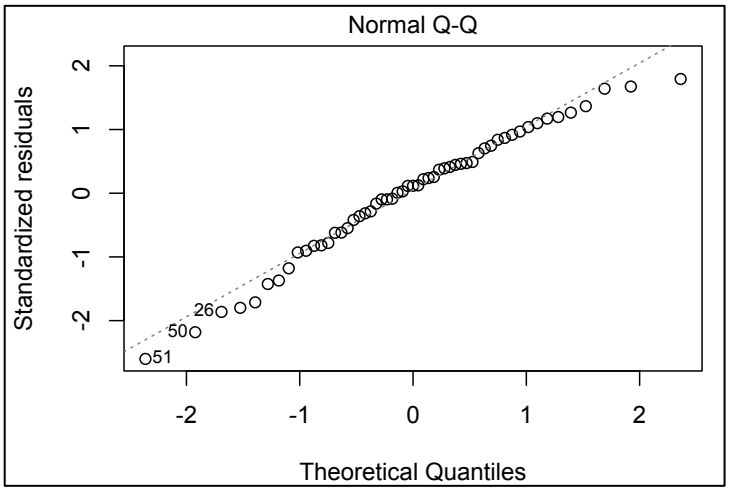

Figure 7.20. Normal probability plot of standardized residuals.

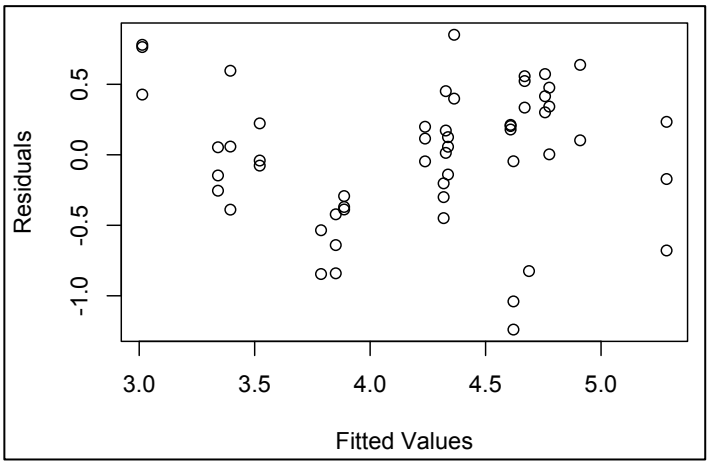

Figure 7.21. Plot of residuals vs fitted log(A_{50}) values.

FINAL MODEL

Equation 7.18 presents the fitted model for bond strength, with an R-squared value of 61.22%:

$$log(A_{50}) = 0.767 + 0.000953{f_c}^2 + 0.00359\mathrm{D}^2 + 0.238\frac{C}{D} + 0.0272C_f - 0.00036\ell_f C_f \qquad (7.18)$$

Figure 7.22 shows the predicted vs observed values of log(A_{50}), together with the exact equivalence line and the limits of the 95%-confidence band.

Figure 7.23 shows the predicted vs observed values of untransformed A_{50}. Together with the exact equivalence line, the 95%-confidence band is also shown as obtained from processing the limits in Figure 7.22.

Figure 7.24 shows the effects plot corresponding to this model. Black lines are drawn according to mean values and red dashed lines limit the 95%-confidence band for predictions with this model. It can be seen that the effect of all factors on bond strength is not of the same magnitude.

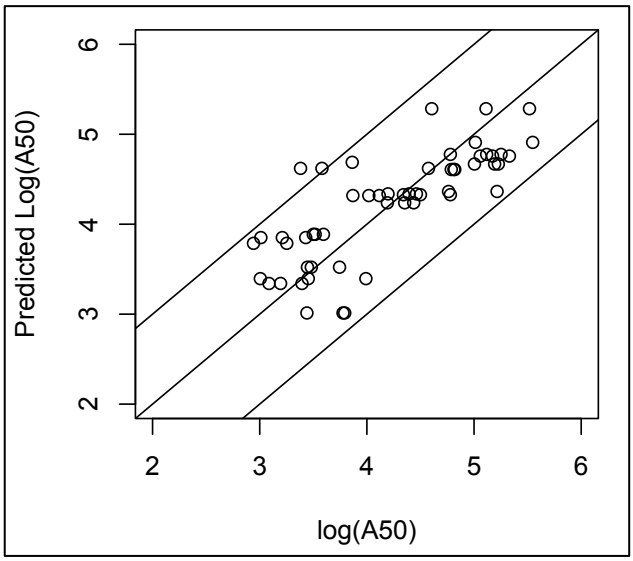

Figure 7.22. Predicted vs observed log(A_{50}) values.

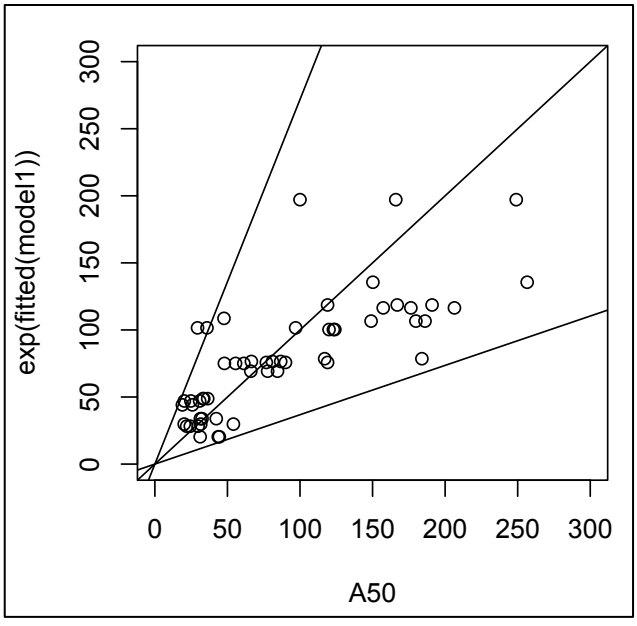

Figure 7.23. Predicted vs observed A_{50} values (untransformed).

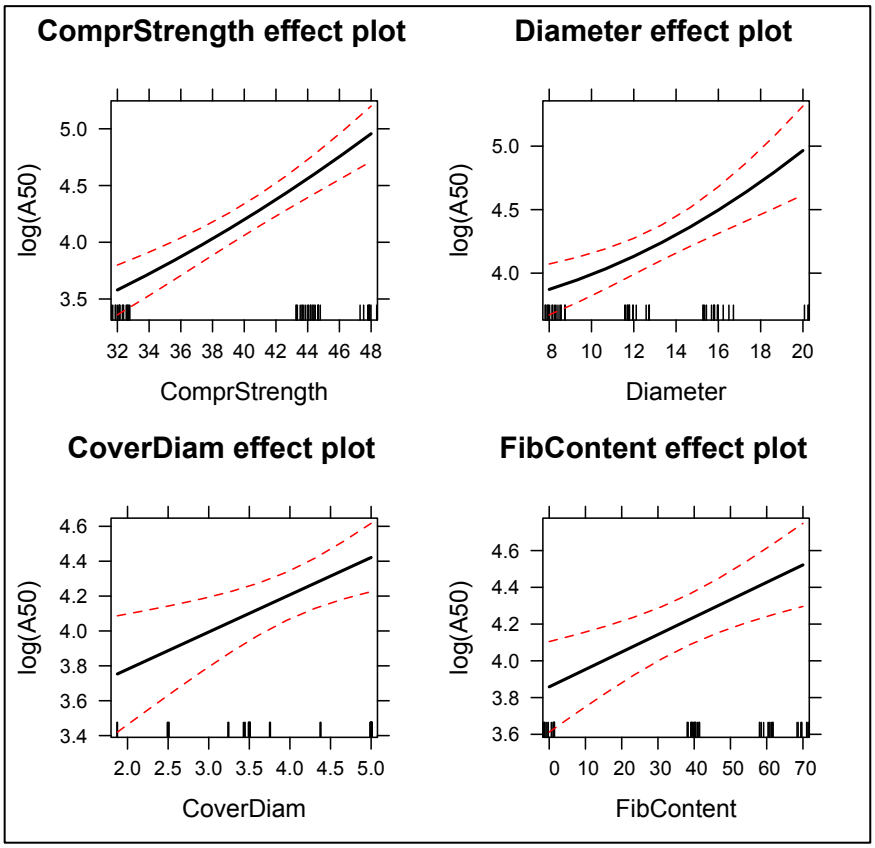

Figure 7.24. Effect plots for quadratic model (eq.7.18)

7.5 Toughness (III): A_{80}

SIMPLE MODEL

A simple model for the area under the bond stress–slip curve up to the slip corresponding to 80% of bond strength (A_{80} hereafter) is given by equation 7.19:

$$A_{80} = \nabla_0 + \nabla_c f_c + \nabla_d \mathrm{D} + \nabla_{cd} \frac{C}{D} + \nabla_f C_f + \nabla_{\lambda f} \lambda_f C_f + \nabla_{\ell f} \ell_f C_f \qquad (7.19)$$

where A_{80} stands for the aforementioned area (mmMPa), f_c is the average concrete compressive strength (MPa), D is rebar diameter (mm), C is concrete cover (mm), C_f is fiber content (kg/m^3), λ_f is fiber slenderness, ℓ_f is fiber length (mm); and ∇_0, ∇_c, ∇_d, ∇_{cd}, ∇_f, $\nabla_{\lambda f}$, and $\nabla_{\ell f}$ are coefficients to be estimated.

Estimates of coefficients in equation 7.19 and their corresponding p-values are shown in Table 7.16. The p-value obtained for the whole model is $2.83 \cdot 10^{-5} < 0.05$, which means that there is a significant relationship between the variables and response variable worth the modelling. The R-squared value is 46.02%.

Table 7.16. Estimation of coefficients and significance tests (simple model, eq.7.19)

		Coefficient	Std. error	p-value
(constant)	∇_0	–175.2	37.99	--
Compressive Strength	∇_c	2.925	0.744	0.0003
Cover/Diameter	∇_{cd}	11.56	4.03	0.0061
Diameter	∇_d	3.807	1.116	0.0013
Fiber Content	∇_f	1.709	1.243	0.1756
Fiber Slenderness, $\lambda_f C_f$	$\nabla_{\lambda f}$	–0.00826	0.0088	0.3546
Fiber Length, $\ell_f C_f$	$\nabla_{\ell f}$	–0.01469	0.0152	0.3398

Since p-values corresponding to fiber slenderness and length are bigger than 0.10, the model is simplified without significant loss of accuracy by discarding these effects. This leads to equation 7.20. Table 7.17 shows the reestimated coefficients in the simplified model and their corresponding p-values. The R-squared value is 44.76%.

$$A_{80} = \nabla_0 + \nabla_c f_c + \nabla_d \mathrm{D} + \nabla_{cd} \frac{C}{D} + \nabla_f C_f \qquad (7.20)$$

Table 7.17. Estimation of coefficients and significance tests (simple model, eq.7.20)

		Coefficient	Std. error	p-value
(constant)	∇_0	-182.276	36.896	--
Compressive Strength	∇_c	3.316	0.613	0.0000
Cover/Diameter	∇_{cd}	10.955	3.901	0.0071
Diameter	∇_d	3.296	0.994	0.0017
Fiber Content	∇_f	0.401	0.1503	0.0103

Figure 7.25 shows the normal probability plot of the standardized residuals. It is observed that standardized residuals are normally distributed.

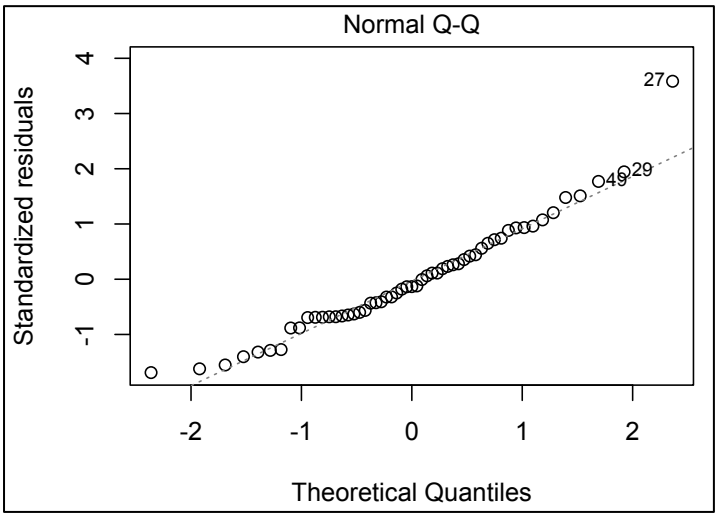

Figure 7.25. Normal probability plot.

Finally, Figure 7.26 shows the CPR (Component-Plus-Residual) plots. These plots reveal that both compressive strength and rebar diameter have quadratic effects on A_{80} that have been disregarded in the model in its present form. The next section deals with incorporating quadratic terms to model the relationship between A_{80} and the factors considered.

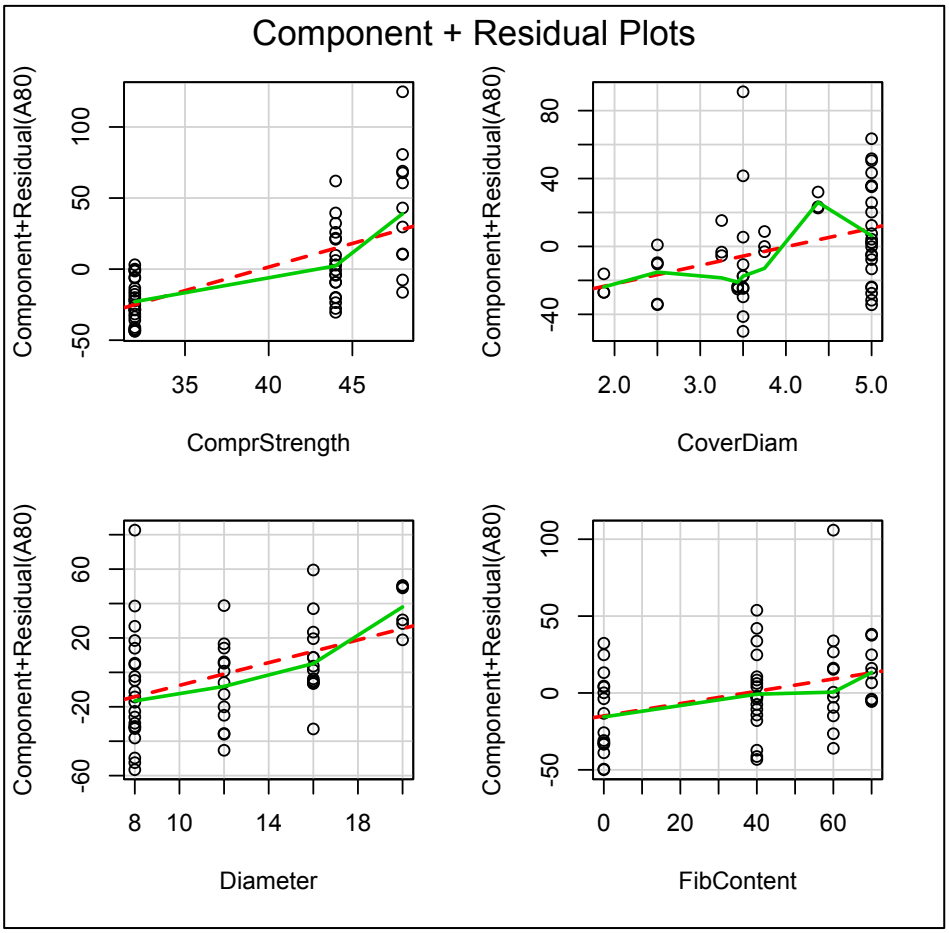

Figure 7.26. CPR plots.

QUADRATIC MODEL

The model for A_{80} is reformulated as given by equation 7.21:

$$A_{80} = \nabla_0 + \nabla_c f_c + \nabla_{cc} {f_c}^2 + \nabla_d \mathrm{D} + \nabla_{dd} \mathrm{D}^2 + \nabla_{cd} \frac{C}{D} + \nabla_f C_f + \nabla_{ff} {C_f}^2 + \nabla_{\lambda f} \lambda_f C_f + \nabla_{\ell f} \ell_f C_f \quad (7.21)$$

Table 7.18 shows the results of coefficients estimation and the p-values obtained from the significance tests associated to these coefficients. The R-squared is 55.61%.

Table 7.18. Estimation of coefficients and significance tests (quadratic model, eq.7.21)

		Coefficient	Std. error	p-value
(constant)	∇_0	614.5971	289.8605	--
Compressive Strength	∇_c	–37.2911	16.189	0.0259
	∇_{cc}	0.5148	0.2040	0.0152
Cover/Diameter	∇_{cd}	11.493	3.971	0.0058
Diameter	∇_d	–1.666	8.524	0.8459
	∇_{dd}	0.2315	0.3186	0.4714
Fiber Content	∇_f	1.9463	1.3486	0.1559
	∇_{ff}	0.00245	0.00733	0.7399
Fiber Slenderness, $\lambda_f C_f$	$\nabla_{\lambda f}$	–0.00783	0.00874	0.3748
Fiber Length, $\ell_f C_f$	$\nabla_{\ell f}$	–0.02267	0.01546	0.1494

Several p-values obtained are bigger than 0.10. Therefore the model can be simplified with no significant loss of accuracy by sequentially discarding these terms. This reduction leads to equation 7.8:

$$A_{80} = \nabla_0 + \nabla_c f_c + \nabla_{cc} {f_c}^2 + \nabla_{dd} \mathrm{D}^2 + \nabla_{cd} \frac{C}{D} + \nabla_f C_f \quad (7.22)$$

Table 7.19 shows the reestimated coefficients in the simplified quadratic model and their corresponding p-values. The R-squared value is 52.92%.

As Figure 7.27 shows, the distribution of the standardized residuals after the stepwise reduction of the quadratic model has suffered no important changes: they remain normally distributed. However, Figure 7.28 shows that the scatter of residuals is not constant. In consequence, the model must be improved in order to be homocedastic.

Table 7.27. Estimation of coefficients and significance tests (quadratic model, eq.7.22)

		Coefficient	Std. error	p-value
(constant)	∇_0	519.418	256.079	--
Compressive Strength	∇_c	–33.051	13.986	0.0221
	∇_{cc}	0.4674	0.1788	0.0118
Cover/Diameter	∇_{cd}	10.7212	3.6319	0.0048
Diameter (quadratic)	∇_{dd}	0.1428	0.0357	0.0002
Fiber Content	∇_f	0.4345	0.1419	0.0036

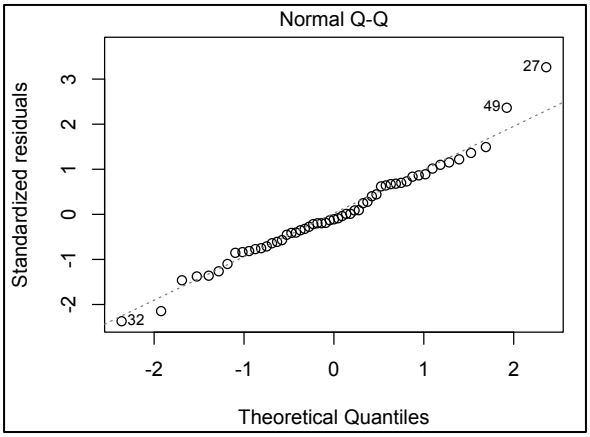

Figure 7.27. Normal probability plot.

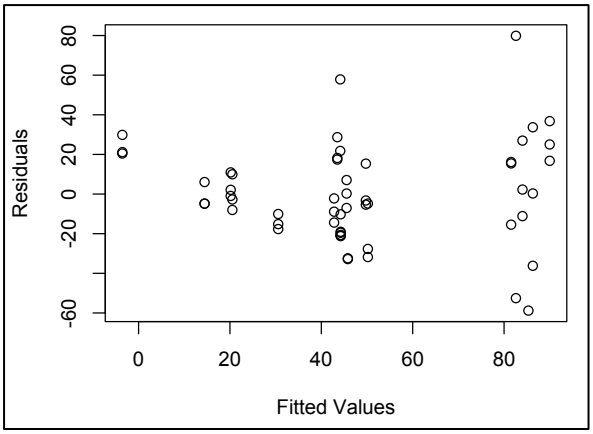

Figure 7.28. Plot of residuals vs fitted A50 values.

IMPROVED QUADRATIC MODEL

The model for A_{80} is reformulated as given by equation 7.23:

$$log(A_{80}) = \nabla_0 + \nabla_c f_c + \nabla_{cc} {f_c}^2 + \nabla_d \mathrm{D} + \nabla_{dd} \mathrm{D}^2 + \nabla_{cd} \frac{C}{D} + \nabla_f C_f + \nabla_{ff} {C_f}^2 + \nabla_{\lambda f} \lambda_f C_f + \nabla_{\ell f} \ell_f C_f \quad (7.23)$$

Table 7.28 shows the results of coefficients estimation and the p-values obtained from the significance tests associated to these coefficients. The R-squared is 60.14%.

Several p-values obtained are bigger than 0.10. Therefore the model can be simplified with no significant loss of accuracy by sequentially discarding these terms until all effects in the model are only those statistically significant. This stepwise, backward reduction leads to equation 7.24:

$$log(A_{80}) = \nabla_0 + \nabla_{cc} {f_c}^2 + \nabla_{dd} \mathrm{D}^2 + \nabla_{cd} \frac{C}{D} + \nabla_f C_f \quad (7.24)$$

Table 7.29 shows the reestimated coefficients in the simplified quadratic model and the corresponding p-values. The R-squared value is 56.45%.

Table 7.28. Estimation of coefficients and significance tests (quadratic model, eq.7.23)

		Coefficient	Std. error	p-value
(constant)	∇_0	6.484	5.609	--
Compressive Strength	∇_c	–0.2988	0.313	0.3453
	∇_{cc}	0.00469	0.00395	0.2410
Cover/Diameter	∇_{cd}	0.2422	0.0768	0.0029
Diameter	∇_d	–0.0883	0.165	0.5952
	∇_{dd}	0.00701	0.00616	0.2614
Fiber Content	∇_f	0.0329	0.0261	0.2130
	∇_{ff}	0.000088	0.000142	0.5383
Fiber Slenderness, $\lambda_f C_f$	$\nabla_{\lambda f}$	–0.000116	0.000169	0.4976
Fiber Length, $\ell_f C_f$	$\nabla_{\ell f}$	–0.000423	0.000299	0.1645

Table 7.29. Estimation of coefficients and significance tests (quadratic model, eq.7.24)

		Coefficient	Std. error	p-value
(constant)	∇_0	0.20404	0.454	--
Compr. Strength (quad.)	∇_{cc}	0.000975	0.000145	0.0000
Cover/Diameter	∇_{cd}	0.23456	0.0706	0.0017
Diameter (quadratic)	∇_{dd}	0.003176	0.000693	0.0000
Fiber Content	∇_f	0.00962	0.00273	0.0009

As Figure 7.29 shows, the distribution of the standardized residuals after the stepwise reduction of the quadratic model has suffered no important changes: they clearly remain normally distributed. No outliers or influential points have been detected either.

Finally, Figure 7.30 plots the residuals vs the fitted values of A_{50}. The scatter of residuals shows no clear tendency to increase or decrease with the fitted values of A_{80}. Therefore the transformation of A_{80} to $\log(A_{80})$ has proved an apropriate tool to achieve the model's homocedasticity: now variance of residuals is constant.

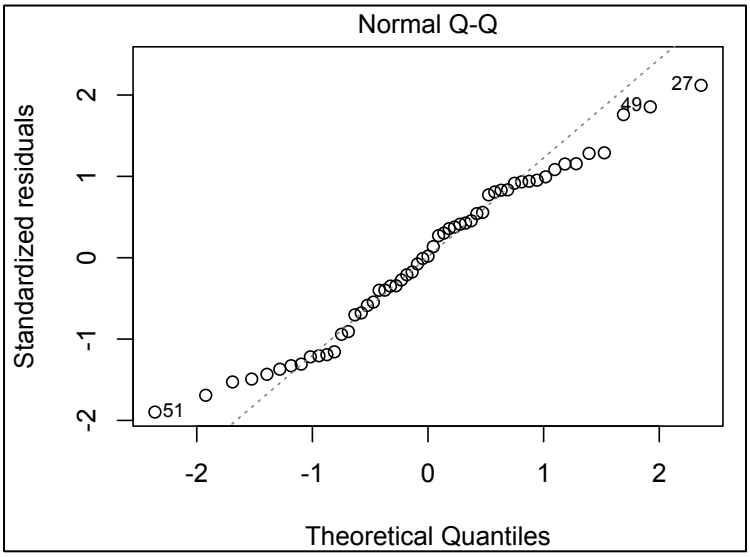

Figure 7.29. Normal probability plot of standardized residuals.

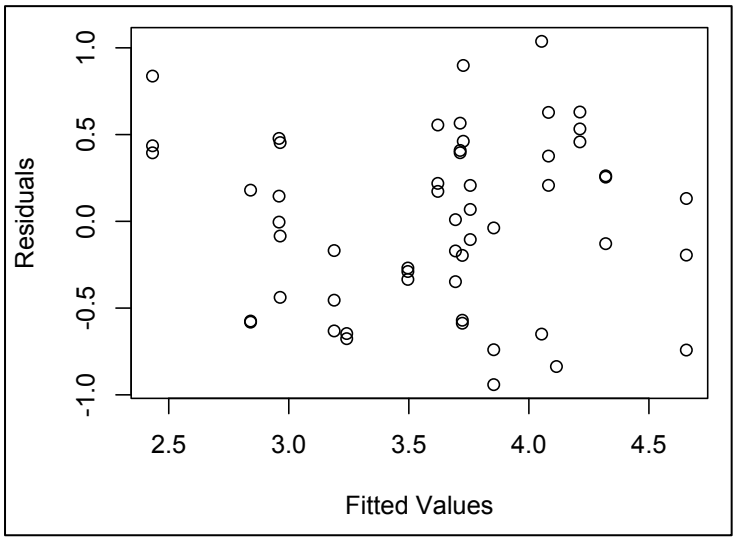

Figure 7.30. Plot of residuals vs fitted log(A_{80}) values.

FINAL MODEL

Equation 7.25 presents the fitted model for bond strength, with an R-squared value of 56.45%:

$$log(A_{80}) = 0.204 + 0.000975{f_c}^2 + 0.00318\mathrm{D}^2 + 0.235\frac{C}{D} + 0.00962C_f \qquad (7.25)$$

Figure 7.31 shows the predicted vs observed values of log(A_{80}), together with the exact equivalence line and the limits of the 95%-confidence band.

Figure 7.32 shows the predicted vs observed values of untransformed A_{80}. Together with the exact equivalence line, the 95%-confidence band is also shown as obtained from processing the limits in Figure 7.31.

Figure 7.33 shows the effects plot corresponding to this model. Black lines are drawn according to mean values and red dashed lines limit the 95%-confidence band for predictions with this model. It can be seen that the effect of all factors on bond strength is not of the same magnitude.

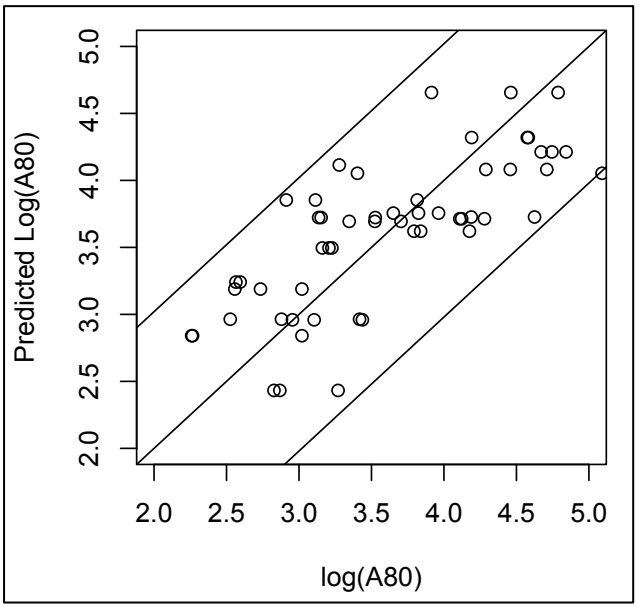

Figure 7.31. Predicted vs observed log(A_{80}) values.

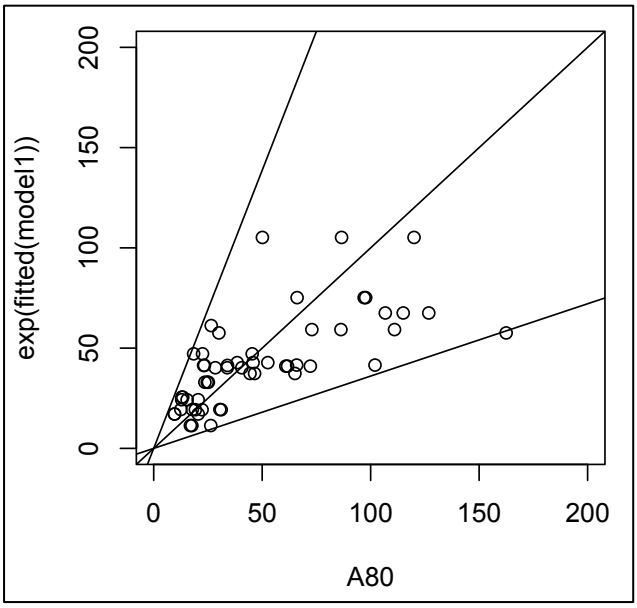

Figure 7.32. Predicted vs observed A_{80} values (untransformed).

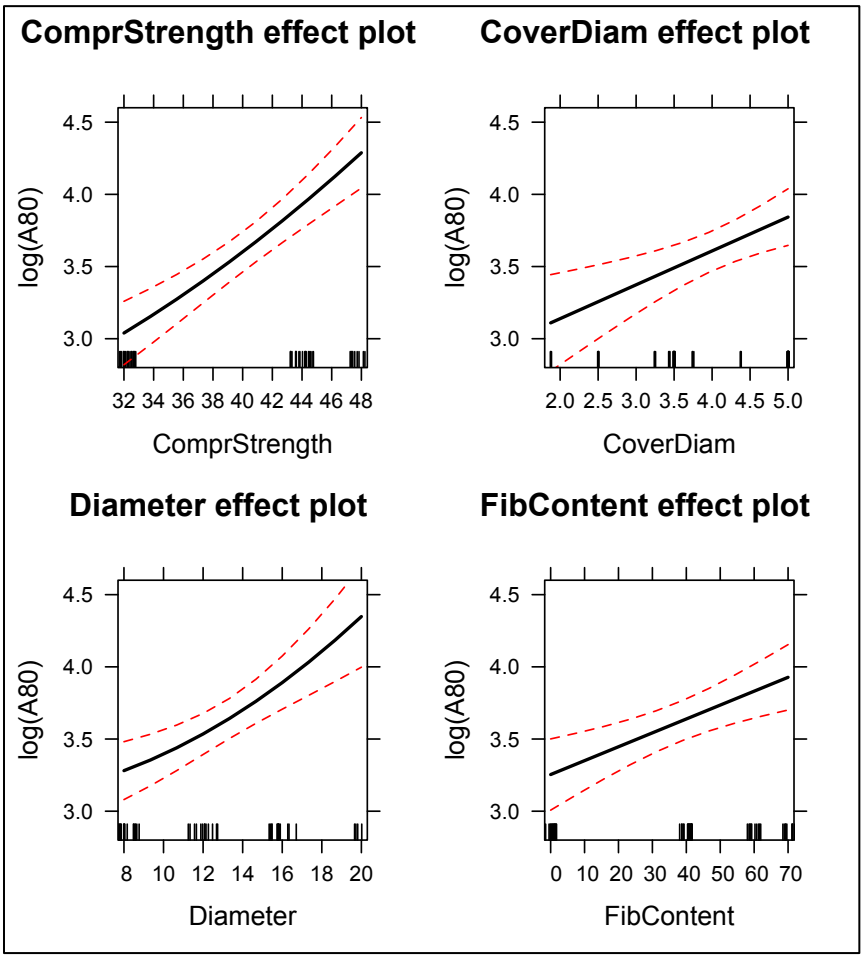

Figure 7.33. Effect plots for quadratic model (eq.7.25)

8| Multivariate Analysis of Bond Stress–Slip Curves

Part III: Analysis of Results

8| Multivariate Analysis of Bond Stress–Slip Curves

PART III: ANALYSIS OF RESULTS

8.1 Introduction and Methodology

The objectives of this first section are: a) description of the motivation for a new analysis of the experimental results, which complements the views discussed in chapter 7; b) brief introduction to Principal Component Analysis; and c) description of the methodology of analysis reported in the different sections of this chapter.

PRELIMINARIES AND OBJECTIVES

In chapter 7, several parameters obtained from the bond stress–slip curves (τ_{max}, A_{peak}, A_{50}, and A_{80}) were analyzed in a univariate way. This means that the effect of the variables considered (compressive strength, diameter, cover/diameter, fiber geometry and content) on each one of these parameters was studied separately.

In this chapter the effect of the aforementioned variables on the whole bond stress–slip curve is analyzed. To do so, each curve has been discretized and defined by a number of parameters –bond stress values corresponding to the following slip values: 0.0mm, 0.1mm, 0.2mm, 0.4mm, 0.8mm, 1.2mm, 1.6mm, 2.0mm, 2.4mm, 2.8mm, 3.2mm, and 3.6mm.

To cover the range of slips between 0.4mm and 3.6mm, the discretization of the curves has been made at intervals of 0.4mm. More data have been considered between 0.0mm and 0.4mm because describing the initial part of the curve needs more detail. Bond stress corresponding to the maximum pullout force achieved without slip (slip value of 0.0mm) has been taken as that corresponding to the onset of slips.

This makes a total of 12 variables taken as representative of bond stress–slip curves obtained from the pull out test in those cases where no splitting has occurred. This means that each experimental curve is assigned a 12-dimension vector.

In consequence, the experimental output from the pull out test is a 12-dimension vector corresponding to each one of the combinations tested, when no splitting occured. The objective of this chapter is to analyze the effect that concrete compressive strength, rebar diameter, concrete cover, fiber geometry, and fiber content have on this vector, which represents the bond stress–slip curve up to a slip of 3.6 mm.

PRINCIPAL COMPONENTS ANALYSIS (PCA)

Principal Component Analysis (hereafter PCA) is a simple, non-parametric method of extracting relevant information from datasets consisting of a considerable number of variables which represent some phenomenon. Its primary purpose is to take advantage of the correlation structure existing among those variable to eventually summarize the information they contain.

In the case of this research, the dataset to be summarized is a matrix **X** with 12 columns, each one of them containing the bond stress value corresponding to a certain slip value. Each row in this matrix is the 12-dimension vector which defines the bond stress–slip curve obtained from testing some specimen.

PCA is a procedure based on linear transformation of the initial matrix, or dataset, into a new coordinate system. The aim is to reduce dimensionality of this dataset with the condition of losing as little information as possible. Information is directed to variance. This linear transformation is based on the following decomposition of the original matrix:

$$\mathbf{X} = \mathbf{U}\,\mathbf{D}\,\mathbf{V}^T + \mathbf{E} \tag{8.1}$$

where: **X** is the original matrix, **D** is a diagonal matrix, **U** and **V** are orthogonal, rotation matrices, and **E** is an error matrix.

This can be understood in the following terms. Test results are data in a 12-dimension space originally expressed in a set of coordinates which is not orthogonal, since the 12 bond stress variables are expected to be highly correlated. If such matrix is decomposed according to equation 1, all these data are rewritten in terms of a set of orthogonal, uncorrelated coordinates. In addition, if the decomposition is exhaustive, then **E** would be a null matrix. But, since the objective is to simplify the information, only the highest singular values are retained, and then the error matrix **E** contains the remaining part of the original information.

These operations are illustrated in Figure 8.1 for the case of 3 dimensions instead of 12 in order to make graphical representation possible. First, experimental data are plotted as-obtained, since the original variables (measurements) are $\{y_1, y_2, y_3\}$. However, it is observed that the preferential or main direction followed by data does not correspond to any of the original axes. If axes are rotated, then the rotated set of variables $\{y'_1, y'_2, y'_3\}$ is obtained. Each one of these new variables is a linear combination of the original ones. The advantage is that, once rotated, data can be described in terms of only one of the rotated variables (in this case, y'_1) with a minimal loss of the information. In this way, scatter of data as projected onto new axes y'_2 and y'_3 is assigned to residual matrix **E**.

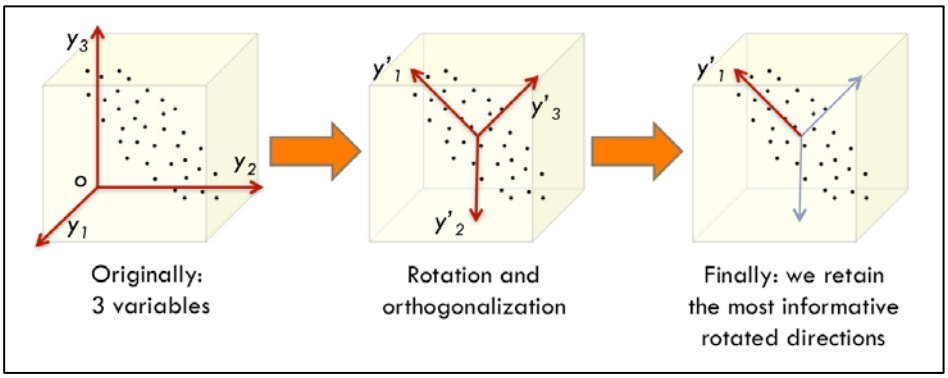

Figure 8.1. Illustration of PCA operations.

The fact that the first of the rotated axes is aligned with the most important principal direction in the data is equivalent to say that the

direction with maximum variance defines the direction of the first principal component, i.e. the first dimension of the new coordinate system. The second principal component is extracted so that it is orthogonal (=uncorrelated) to the first and explains most of the remaining variance has to be found. Following this approach we get an orthogonal basis of the vector space of the dataset.

From the preceding paragraph it is clear that PCA is intimately related to the mathematical technique of singular value decomposition. As will be justified in the following subsection, the aimed linear transformation of matrix **X** is based on the Singular Value Decomposition (SVD) of its covariance (or correlation) matrix.

Covariance measures the degree of the linear relationship between two variables. By definition, covariance matrix is a square, symmetric matrix: diagonal terms are the variance of variables and off-diagonal terms stand for covariances between different variables.

MATHEMATICAL FRAMEWORK

Let **X** be the original dataset, where each row corresponds to a bond stress–slip curve, and the columns correspond to bond stress values. If n is the number of curves, and m is the number of bond stress values retained to define each curve, then **X** is an nxm matrix.

In cases like this, i.e. several variables related to the same phenomenon and/or defined in a similar way, initial variables are highly correlated to one another. Let τ_i, τ_j be two of these variables. Then, correlation between them is defined as follows:

$$r(\tau_i, \tau_j) = \frac{cov(\tau_i, \tau_j)}{s(\tau_i)\, s(\tau_j)} = \frac{\sum_{k=1}^{n} (\tau_i(k) - \overline{\tau_i})(\tau_j(k) - \overline{\tau_j})}{(n-1)\, s(\tau_i)\, s(\tau_j)} \qquad (8.2)$$

It is customary to standardize all variables prior to PCA: they are centered and scaled to unit variance. This is done to simplify expression 8.2: then $\overline{\tau_i} = \overline{\tau_j} = 0$ and $s(\tau_i) = s(\tau_j) = 1$, and expression 8.2 is simplified as follows:

$$r(x_i, x_j) = \frac{\sum_{k=1}^{n} x_i(k)\, x_j(k)}{(n-1)} \tag{8.3}$$

In this case, correlations and covariances are directly obtained from one another, and PCA is said to be based on the correlation matrix.

Expression 8.3 can be written in matrix form to include all correlations between variables:

$$r(x_i, x_j) = [r_{ij}]_{\substack{i=1\dots n \\ j=1\dots n}} = \frac{1}{(n-1)}\, \mathbf{X}\,\mathbf{X}^T \tag{8.4}$$

$\mathbf{XX}^T$ is the covariance matrix. From 8.4 it follows that, as long as all variables are centered and scaled to unit variance, it is equivalent to work with the correlation matrix or the covariance matrix.

The goal of PCA is to find a new set of variables which are uncorrelated to one another. This can be expressed as the search of a transformation matrix **R** which rotates the original matrix **X** leading to a new matrix, **Y**:

$$\mathbf{Y} = \mathbf{R}\,\mathbf{X} \tag{8.5}$$

The condition that the new variables are uncorrelated implies that the correlation between any two of these new variables is:

$$r(y_i, y_j) = \frac{\sum_{k=1}^{n} y_i(k)\, y_j(k)}{(n-1)} = \begin{cases} 0, & i \neq j \\ 1, & i = j \end{cases} \tag{8.6}$$

Accordingly, the new, the covariance or correlation matrix of the rotated dataset **Y**, i.e. $\mathbf{YY}^T$ has to be diagonal.

Bearing in mind how this new matrix **Y** has been defined (equation 8.5), the new covariance or correlation matrix can be calculated as follows:

$$\mathbf{Y}\,\mathbf{Y}^T = \mathbf{R}\,\mathbf{X}\,(\mathbf{R}\,\mathbf{X})^T = \mathbf{R}\,\mathbf{X}\,\mathbf{X}^T\,\mathbf{R}^T \tag{8.7}$$

On the other hand, since the correlation matrix of original data $\mathbf{XX}^T$ is real, symmetric, and squared, it can be diagonalized:

$$\mathbf{X}\,\mathbf{X}^T = \mathbf{P}\,\mathbf{D}\,\mathbf{P}^T \tag{8.8}$$

If equations 8.7 and 8.8 are brought together, it follows:

$$\mathbf{Y}\,\mathbf{Y}^T = \mathbf{R}\,\mathbf{X}\,\mathbf{X}^T\,\mathbf{R}^T = \mathbf{R}\,\mathbf{P}\,\mathbf{D}\,\mathbf{P}^T\mathbf{R}^T \tag{8.9}$$

It turns out that if the rotation matrix is selected to be $\mathbf{R} = \mathbf{P}^T$ then $\mathbf{Y}\mathbf{Y}^T$ is automatically diagonal:

$$\left.\begin{array}{c}\mathbf{Y}\,\mathbf{Y}^T = \mathbf{R}\,\mathbf{X}\,\mathbf{X}^T\,\mathbf{R}^T = \mathbf{R}\,\mathbf{P}\,\mathbf{D}\,\mathbf{P}^T\mathbf{R}^T \\ \mathbf{R} = \mathbf{P}^T\end{array}\right\} \rightarrow \mathbf{Y}\,\mathbf{Y}^T = \mathbf{P}^T\,\mathbf{P}\,\mathbf{D}\,\mathbf{P}^T\mathbf{P} = \mathbf{D} \tag{8.10}$$

Therefore:

- ☐ The key to obtain the new set of variables is to diagonalize the correlation matrix of original dataset $\mathbf{X}\mathbf{X}^T$.
- ☐ The rotation matrix to be applied to the original dataset **X** so that it is transfromed into the rotated, uncorrelated dataset **Y** consists of the eigenvectors of the correlation matrix of the original dataset $\mathbf{X}\mathbf{X}^T$. This way the objective of obtaining a new, uncorrelated set of variables has been achieved.
- ☐ The new set of variables in which rotated dataset **Y** is associated to the eigenvalues of the correlation matrix of the original dataset $\mathbf{X}\mathbf{X}^T$. This means that the projected inertia, i.e. the scatter of data when projected onto the first new variable, is maximized. The projected inertia onto the second new variable will be less than that onto the first one. This is so because the terms in the diagonal matrix **D** are eigenvalues: they are ordered. In consequence, a subset of these new variables can be selected so that the loss of information is minimal. This way the objective of reducing the dimension of the dataset can be achieved.

METHODOLOGICAL OVERVIEW

As it has been already stated, the objective of this chapter is to analyze the effects that concrete compressive strength, rebar diameter, concrete cover, fiber geometry, and fiber content have on the whole bond stress–slip curve, discretized and defined by 12 bond stress values. To achieve this objective, the analysis is organized as follows:

- Principal Component Analysis is applied to the pull out tests data matrix, which consists of 12 columns (each row in this matrix is the 12-dimension vector which defines the bond stress–slip curve obtained from testing a specimen) to reduce the number of parameters with no significant loss of information. This is dealt with in section 8.2, according to the following procedure:
    - A first analysis is carried out and then the results of this first PCA are diagnosed in order to detect outliers or anomalous data.
    - After removal of anomalous data, a second analysis is carried out. Definite principal dimensions are obtained.
    - Experimental POT curves (each one of them is a 12-dimension vector) are projected to the obtained principal dimensions. These projected results are the latent variables T_1 and T_2.
- Multiple linear regression is applied to analyze the effects that concrete compressive strength, rebar diameter, concrete cover, fiber geometry, and fiber content have on the first latent variable T_1 (section 8.3).
- Multiple linear regression is applied to analyze the effects that concrete compressive strength, rebar diameter, concrete cover, fiber geometry, and fiber content have on the first latent variable T_2 (section 8.4).

8.2 Principal Components Analysis

PRELIMINARIES

A total of 12 variables has been taken as representative of bond stress–slip curves obtained from the pull out test in those cases where no splitting has occurred. There was no possibility of either further discretizing the curves or covering a large range of slip values. This is because there have to be more cases than variables in any dataset to be explored by means of multivariate techniques such as PCA. The usual recommendation in literature is that the ratio between no.cases/no.variables is not less than 5. In this research, 51 specimens experienced a pullout failure. In consequence, the aforementioned ratio is $51/12 = 4.25 \sim 5$. Nevertheless the discretization of bond stress–slip curves proposed here is reasonable.

Prior to PCA, some statistical tests on the original dataset have to be performed. These tests are aimed at detect whether the degree of correlation between variables is significant or not. The need of performing these tests is justified by key aspect PCA is based upon. The search for principal components assumes that principal directions exist in the 12-dimension space defined by experimental data. These preliminary tests, namely Bartlett's sphericity test and KMO test (named after Kaiser, Meyer, and Olkin), fulfil this preliminary examination of the original dataset. The Bartlett's sphericity test leads to a p-value of $0.0000<0.05$. The KMO test shows an overall measure of sampling adequacy is 0.85. Since Bartlett's p-value is less than 0.05 and KMO measure is higher than 0.5, factor analyses and PCA are appropriate.

FIRST ANALYSIS AND DIAGNOSIS

Table 8.1 shows the eigenvalues obtained by diagonalization of the correlation matrix as well as the percentage of total variance explained by each of the principal directions, i.e. principal components, associated to these eigenvalues.

Table 8.1. Eigenvalues and percentage of variance explained by each principal component.

	Eigenvalue	Variance explained (%)	Cumulative variance (%)
PC1	10.54	87.85	87.85
PC2	1.00	8.33	96.18
PC3	0.387	3.22	99.41
PC4	0.052	0.43	99.84
PC5	0.011	0.09	99.94
PC6	0.004	0.03	99.97
PC7	0.002	0.01	99.98
PC8	0.001	0.01	99.99
PC9	0.001	<0.01	99.99
PC10	<0.001	<0.01	99.99
PC11	<0.001	<0.01	99.99
PC12	<0.001	<0.01	100.00

Figure 8.2 shows the screeplot corresponding to this analysis, where eigenvalues (Table 8.1) are plotted for the principal components obtained. The red horizontal line corresponds to an eigenvalue of 1 and constitutes the Kaiser's criterion to decide the number of principal components which are worth retaining.

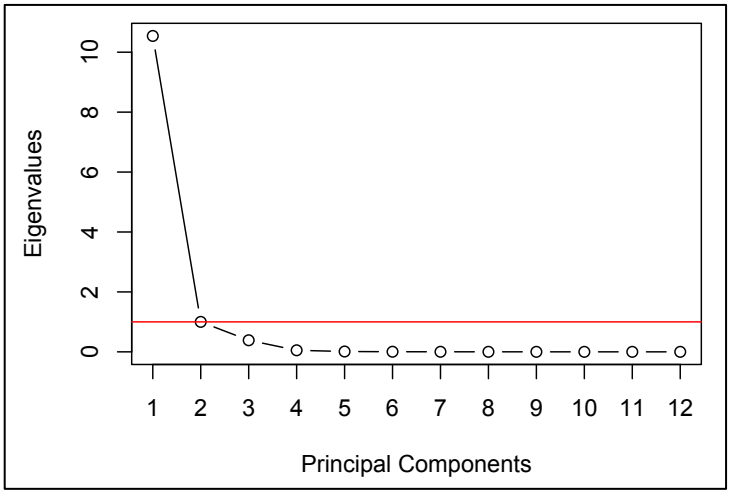

Figure 8.2. Screeplot corresponding to the first PCA.

This criterion is based on the fact that any component with an eigenvalue less than 1.00 is less informative than any of the original variables. Since the aim of PCA is to find new uncorrelated, highly informative directions to reduce the dimension of the original dataset, only components corresponding to eigenvalues higher than 1.00 are worth retaining for further analysis. Figure 8.3 plots the percentage of variance explained by each one of the principal components.

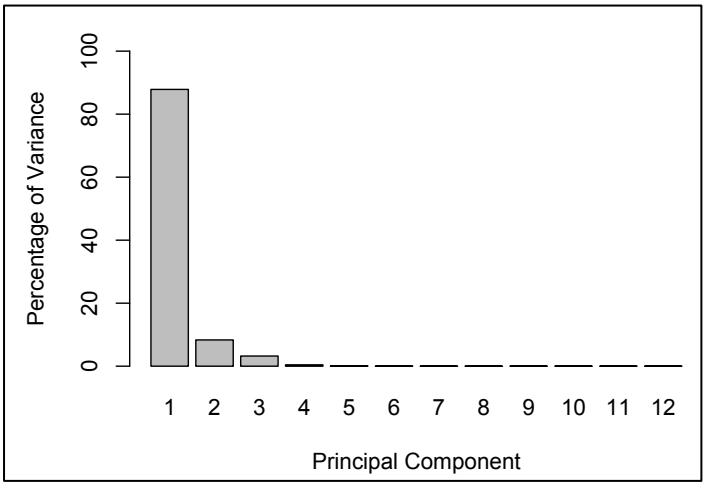

Figure 8.3. Percentage of variance explained by each principal component.

With all that, taking into account Kaiser's criterion and the fact that the first two principal components stand for 96.18% of variance in the original dataset, they are the only ones selected. This way, the original 12-dimension space has been reduced to a 2-dimension space with no significant loss of information.

Table 8.2 shows the loadings of all original variables on the two principal components retained. Each loading is the correlation between one of the original variables and the corresponding principal component. They provide the key for interpreting the principal components selected. To that purpose, higher loadings are highlighted in bold.

Concerning PC1, bond stress values corresponding to all slips except that of initiation are weighted by loadings which are approximately 0.3 in all cases. This indicates that PC1 stands for the sum of all bond stress values except that corresponding to the onset of slips. Then, PC1 represents the area under the bond stress–slip curve.

Concerning PC2, it is related to the onset of slips, since all loadings are neglectable when compared to those corresponding to the onset of slips.

Table 8.2. Loadings of original variables on the principal components selected.

	PC1	PC2
tau00	0.1293	**0.8664**
tau01	**0.2824**	**0.3096**
tau02	**0.2922**	0.1678
tau04	**0.2974**	0.0715
tau08	**0.302**	-0.0021
tau12	**0.3058**	-0.0623
tau16	**0.305**	-0.1115
tau20	**0.3035**	-0.1301
tau24	**0.302**	-0.1375
tau28	**0.3005**	-0.1443
tau32	**0.2993**	-0.1494
tau36	**0.298**	-0.1577

A very important aspect must be remarked at this point. Given the mathematical basis of PCA, the two principal components, PC1 and PC2, are orthogonal. This means: they are totally uncorrelated to one another. Taking into account the interpretation found for PC1 and PC2 on the basis of loadings values, the following conclusion is drawn: the onset of slips has nothing to do with the rest of the curve, namely ductility: both aspects of bond behaviour prove to be disconnected.

A complementary way of interpreting PC1 and PC2 is considering contributions of initial variables to these components. If x_i is one of the original variables, and $t_{i,k}$ is its loading on the k-th principal component, then its contribution to that component is determined as follows:

$$contribution_k(x_i) = t_{i,k}^2 \tag{8.11}$$

Table 8.3 shows the contributions of all original variables to the selected principal components PC1 and PC2, in percentage. Contribution values as well as the biplot shown in Figure 8.4 are really helpful to clarify the interpretations given for the selected components. It is observed that most of the original variables are mainly projected onto the direction defined by PC1, while bond stress corresponding to the onset of slips has little weight on this direction but determines the orthogonal direction, PC2.

Table 8.3. Contributions of original variables to principal components.

	PC1	PC2
tau00	1.67 %	75.07 %
tau01	7.98 %	9.59 %
tau02	8.54 %	2.82 %
tau04	8.85 %	0.51 %
tau08	9.12 %	0.00 %
tau12	9.35 %	0.39 %
tau16	9.31 %	1.24 %
tau20	9.21 %	1.69 %
tau24	9.12 %	1.89 %
tau28	9.03 %	2.08 %
tau32	8.96 %	2.23 %
tau36	8.88 %	2.49 %

Finally, Figure 8.5 shows the projection of experimental bond stress–slip curves onto the reduced two-dimension space defined by principal components PC1 and PC2.

After PCA has been performed and experimental results, initially expressed as 12-dimension vectors, have been projected onto a 2-dimension space, the PC1 axis is indeed the direction along which points are naturally distributed: it explains most of the variance, or inertia, of experimental data. PC2 axis is orthogonal to PC1 and explains most part of the remaining variance. Both axes intercept each other at the center of gravity of these points.

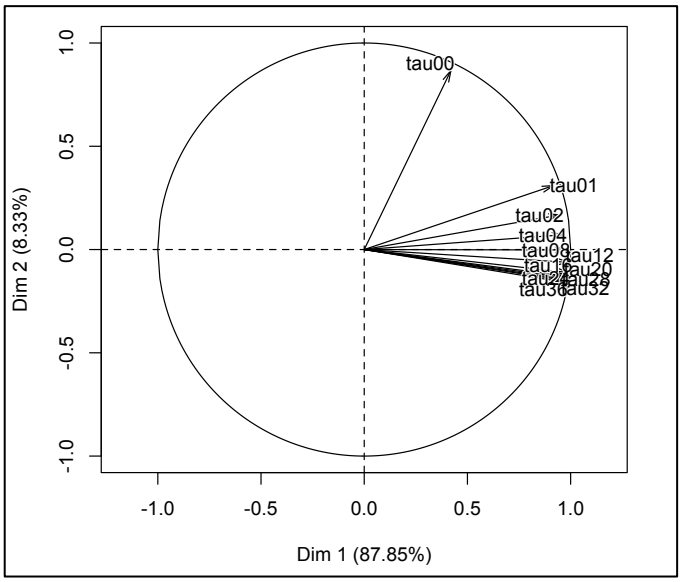

Figure 8.4. Biplot of principal components PC1 and PC2.

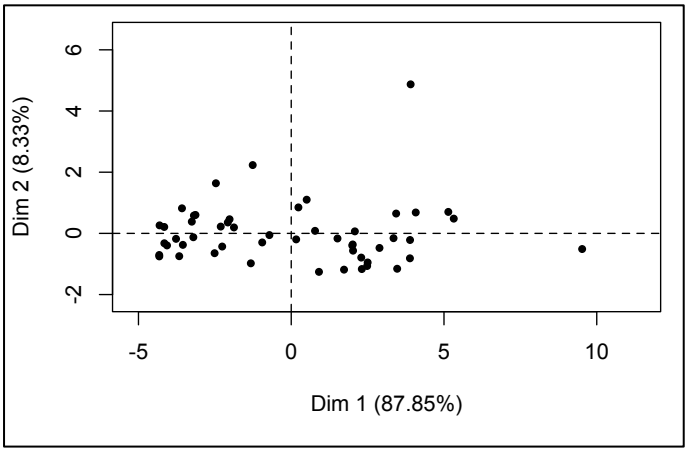

Figure 8.5. Experimental curves represented in the new coordinates.

However, in Figure 8.5 there are two points (representing two bond stress–slip curves) which seem excessively displaced from the other. The inspection of contributions of each datum to PC1 and PC2 makes it possible to find out whether they have to be considered as outliers. When the contribution of a certain datum to a principal component is

excessively high, the leverage of such datum might be conditioning the directions of the new axes.

The contribution of each datum to one principal dimension is the ratio between the inertia of its projection and the inertia of the whole scatterplot projection onto that dimension. Contributions of experimental data to PC1 and PC2 directions are shown in Figures 8.6 and 8.7 respectively. Horizontal lines show the average contribution plus three times the standard deviation, and are taken as threshold to detect excessively large contributions.

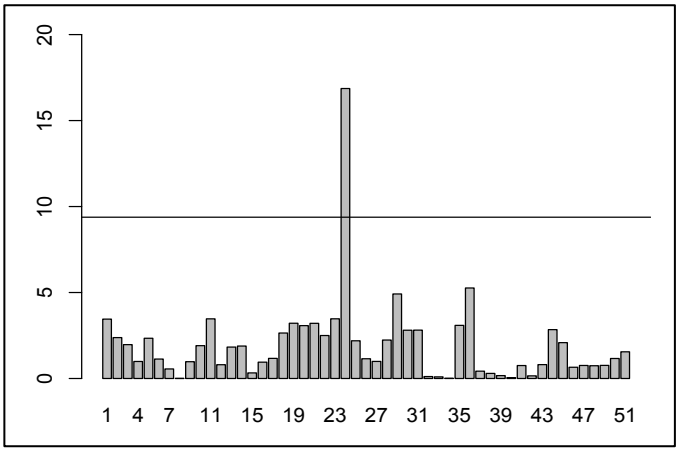

Figure 8.6. Contributions to PC1.

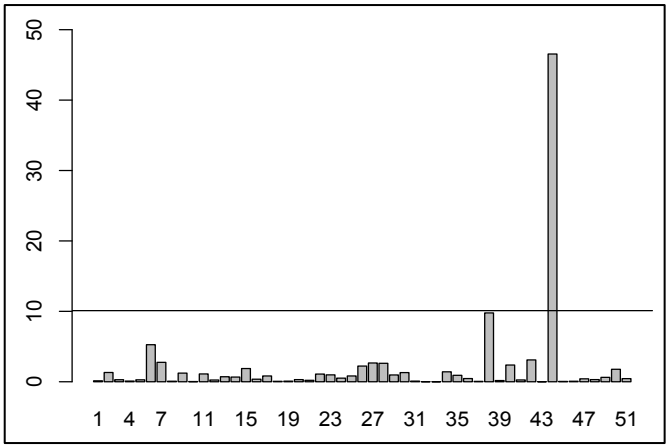

Figure 8.7. Contributions to PC2.

There are clearly two data that might be conditioning directions PC1 and PC2. It is convenient to discard them and reperform the PCA. This is carried out in the following subsection.

SECOND ANALYSIS

Table 8.4 shows the eigenvalues and the percentage of total variance explained by the principal components associated to these eigenvalues. When compared to Table 8.1, no relevant changes can be observed. No relevant changes are observed in the screeplot either as shown in Figure 8.8, which relates eigenvalues vs principal components together with the threshold line according to Kaiser's criterion.

This way, the first two principal components are selected, which represent 95.73% of variance in the original dataset. Table 8.5 shows recalculated loadings of all original variables on the two principal components retained. No relevant changes are detected if these loadings are compared to those in Table 8.2. Therefore the interpretation of principal components PC1 and PC2 stays the same as in the previous subsection.

Table 8.4. Eigenvalues and percentage of variance explained by each principal component.

	Eigenvalue	Variance explained (%)	Cumulative variance (%)
PC1	10.45	87.04	87.04
PC2	1.04	8.69	95.73
PC3	0.435	3.63	99.36
PC4	0.055	0.46	99.81
PC5	0.014	0.11	99.93
PC6	0.004	0.04	99.97
PC7	0.002	0.02	99.98
PC8	0.001	0.01	99.99
PC9	0.001	<0.01	99.99
PC10	<0.001	<0.01	99.99
PC11	<0.001	<0.01	99.99
PC12	<0.001	<0.01	100.00

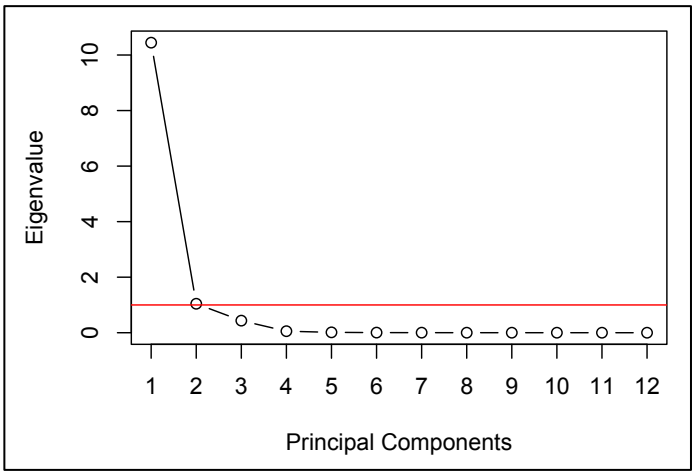

Figure 8.8. Screeplot corresponding to the second PCA.

Table 8.5. Loadings of original variables on the principal components selected.

	PC1	PC2
tau00	0.1235	**0.8446**
tau01	**0.2819**	**0.3223**
tau02	**0.2919**	0.188
tau04	**0.2967**	0.1006
tau08	**0.3022**	0.0216
tau12	**0.3069**	-0.0564
tau16	**0.3061**	-0.1219
tau20	**0.3042**	-0.1449
tau24	**0.3024**	-0.153
tau28	**0.3007**	-0.1567
tau32	**0.2994**	-0.1559
tau36	**0.298**	-0.1599

Table 8.6 shows the recalculated contributions of original variables to the selected principal components PC1 and PC2, in percentage. These contributions have suffered no significant changes after the two outliers detected have been discarded. The biplot shown in Figure 8.9 shows no relevant changes either.

Table 8.6. Contributions of original variables to principal components.

	PC1	PC2
tau00	1.53 %	71.33 %
tau01	7.95 %	10.39 %
tau02	8.52 %	3.54 %
tau04	8.81 %	1.02 %
tau08	9.13 %	0.05 %
tau12	9.42 %	0.32 %
tau16	9.37 %	1.49 %
tau20	9.26 %	2.10 %
tau24	9.15 %	2.34 %
tau28	9.04 %	2.45 %
tau32	8.96 %	2.43 %
tau36	8.88 %	2.56 %

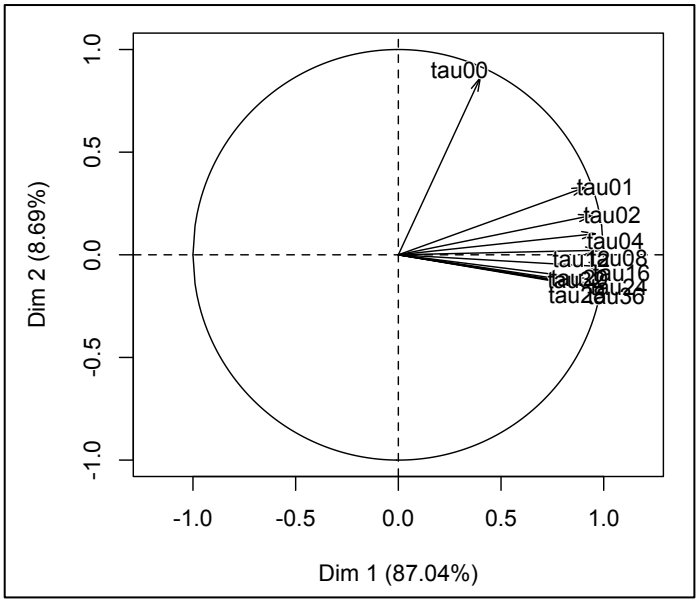

Figure 8.9. Biplot of principal components PC1 and PC2.

Finally, Figure 8.10 shows the projection of experimental bond stress–slip curves onto the reduced two-dimension space defined by principal

components PC1 and PC2. In this case, no point seems to be excessively distant from all others.

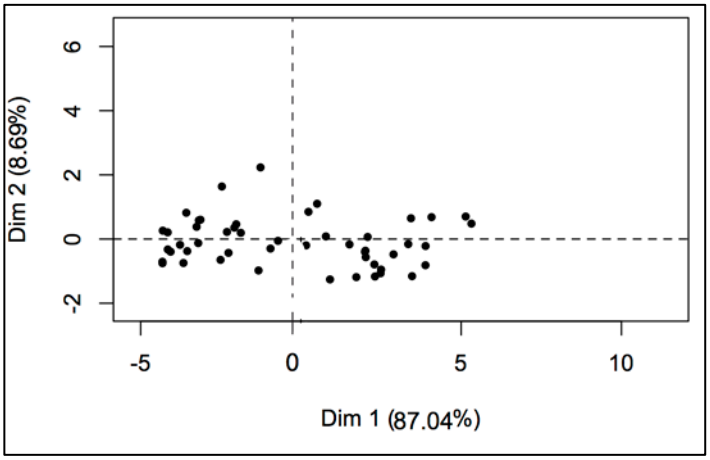

Figure 8.10. Experimental curves represented in the new coordinates.

The new contribution plots are shown in Figures 8.11 and 8.12, together with the horizontal lines which stand for the average contribution plus three times the standard deviation. It can be observed that the situation has significantly improved with respect to that in Figures 8.6 and 8.7.

No excessive contributions are now detected concerning PC1 (Figure 8.11), which is the most important since it corresponds to the higgest eigenvalue and represents 87.04% of the information. With respect to PC2, there is only one datum whose contribution is excessive. However, since PC2 direction is forced to be orthogonal to PC1 direction and no incongruencies are found in Figure 8.10, discarding this only datum would not produce any changes on the principal dimensions selected. Therefore, the PCA leading to these dimensions PC1 and PC2 can now be considered as final as it has been conveniently diagnosed.

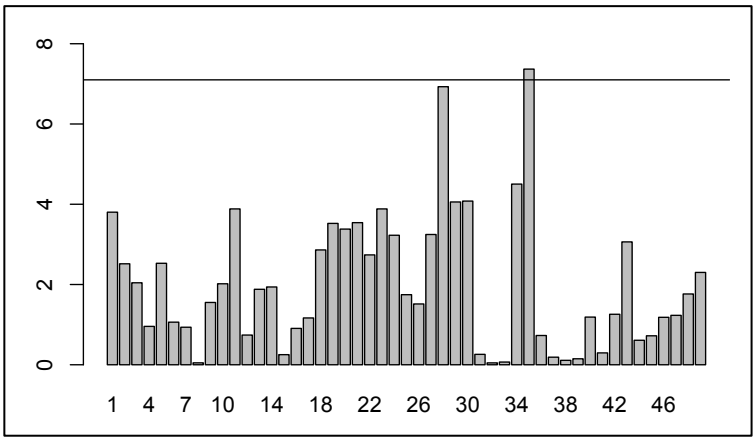

Figure 8.11. Contributions to PC1.

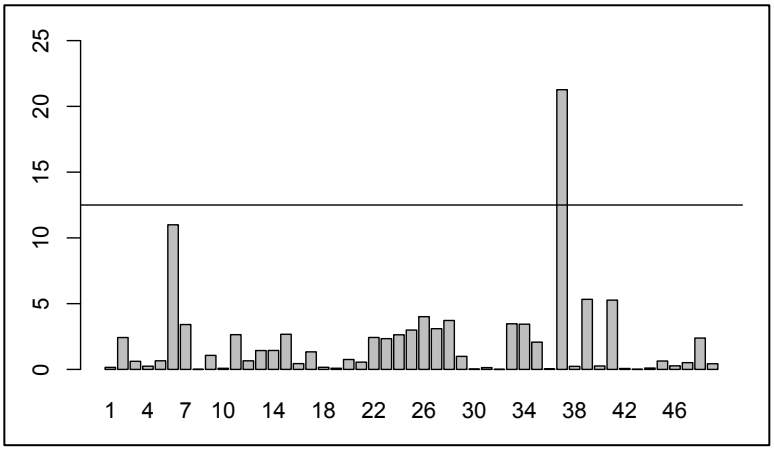

Figure 8.12. Contributions to PC2.

PROJECTION OF EXPERIMENTAL CURVES TO PRINCIPAL DIMENSIONS

Table 8.7 shows experimental results from pull out tests with no splitting, where T_1 and T_2 are the two new parameters describing bond stress–slip curves after projection to the principal dimensions defined by PC1 and PC2. Therefore parameters T_1 and T_2 constitute the experimental output for each combination of variables tested.

Table 8.7. Experimental results after PCA reduction.

	fc	D	C/D	λ_f/l_f	C_f	T_1	T_2
1	32	16	1.875	65/60	40	-4.4114	0.2823
2	32	16	1.875	65/60	40	-3.5886	1.113
3	32	16	1.875	65/60	40	-3.2336	0.5608
4	32	8	4.375	65/60	0	-2.2125	0.3529
5	32	8	4.375	65/60	0	-3.5975	-0.5789
6	32	8	4.375	65/60	0	-2.331	2.3705
7	32	20	5	65/60	70	2.1881	-1.3205
8	32	20	5	65/60	70	0.4973	-0.0341
9	32	20	5	65/60	70	2.8189	-0.7384
10	32	8	5	65/60	40	-3.2139	-0.2077
11	32	8	5	65/60	40	-4.4584	-1.162
12	32	8	5	65/60	40	-1.9466	0.5785
13	32	16	3.4375	65/60	70	-3.1024	0.8562
14	32	16	3.4375	65/60	70	-3.1499	0.858
15	32	20	3.25	80/50	40	-1.1355	-1.1683
16	32	20	3.25	80/50	40	-2.1536	-0.475
17	32	20	3.25	80/50	40	-2.4436	-0.8262
18	32	16	5	80/50	0	-3.827	-0.2872
19	32	16	5	80/50	0	-4.246	0.2129
20	32	16	5	80/50	0	-4.1598	-0.6208
21	32	8	3.75	80/50	70	-4.2572	-0.5318
22	32	8	3.75	80/50	70	-3.7433	-1.1141
23	32	8	3.75	80/50	70	-4.4583	-1.0934
24	-	-	-	-	-	-	-
25	48	8	3.5	80/35	60	4.0641	1.16
26	48	8	5	45/50	40	2.9894	-1.2367
27	48	8	5	45/50	40	2.7848	-1.4317
28	48	8	5	45/50	40	4.0761	-1.2578
29	48	12	5	80/35	0	5.955	1.379
30	48	12	5	80/35	0	4.5566	-0.7118
31	48	12	5	80/35	0	4.569	0.1028
32	44	12	3.5	80/50	40	1.1528	0.2653
33	44	12	3.5	80/50	40	-0.4925	-0.026
34	44	12	3.5	80/50	40	0.5881	1.3314

Table 8.7(cont.). Experimental results after PCA reduction.

	fc	D	C/D	λ_f/l_f	C_f	T_1	T_2
35	44	16	5	80/50	60	4.8002	1.3258
36	44	16	5	80/50	60	6.1406	1.0292
37	44	16	5	80/50	60	1.932	-0.131
38	44	12	5	80/35	0	-0.9834	3.2966
39	44	12	5	80/35	0	-0.7515	-0.3447
40	44	12	5	80/35	0	0.8739	1.6502
41	44	8	3.5	45/50	60	2.4659	-0.3658
42	44	8	3.5	45/50	60	1.2307	-1.6407
43	44	8	3.5	45/50	60	2.5377	0.1891
44	-	-	-	-	-	-	-
45	44	16	3.5	80/50	0	3.9587	0.0483
46	44	8	5	80/35	40	-1.7676	0.2293
47	44	8	5	80/35	40	-1.9221	0.5714
48	44	8	5	80/35	40	2.4601	-0.3734
49	44	12	2.5	80/35	60	2.5106	-0.5121
50	44	12	2.5	80/35	60	3.0048	-1.104
51	44	12	2.5	80/35	60	3.4317	-0.4694

8.3 Effects on latent variable T_1

SIMPLE MODEL

A simple model for T_1 is given by equation 8.12:

$$T_1 = \nabla_0 + \nabla_c f_c + \nabla_d \mathrm{D} + \nabla_{cd}\frac{C}{D} + \nabla_f C_f + \nabla_{\lambda f}\lambda_f C_f + \nabla_{\ell f}\ell_f C_f \qquad (8.12)$$

where T_1 stands for the projection of experimental bond stress–slip curves onto the first principal component PC1 (dimensionless), f_c is the average concrete compressive strength (MPa), D is rebar diameter (mm), C is concrete cover (mm), C_f is fiber content (kg/m^3), λ_f is fiber slenderness, ℓ_f is fiber length (mm); and ∇_0, ∇_c, ∇_d, ∇_{cd}, ∇_f, $\nabla_{\lambda f}$, and $\nabla_{\ell f}$ are coefficients to be estimated.

Estimates for the coefficients in equation 8.12 are shown in Table 8.8 together with the associated p-values. The p-value obtained for the model is $1.026{\cdot}10^{-11}<0.05$ and the R-squared value is 76.4%.

Table 8.8. Estimation of coefficients and significance tests (simple model, eq.8.12).

		Coefficient	Std. error	p-value
(constant)	∇_0	–22.91	2.311	--
Compressive Strength	∇_c	0.4278	0.051	0.0000
Cover/Diameter	∇_{cd}	0.492	0.286	0.0922
Diameter	∇_d	0.264	0.071	0.0006
Fiber Content	∇_f	0.078	0.085	0.3656
Fiber Slenderness, $\lambda_f C_f$	$\nabla_{\lambda f}$	–0.00054	0.00056	0.3412
Fiber Length, $\ell_f C_f$	$\nabla_{\ell f}$	–0.00031	0.0011	0.7716

Since several p-values are higher than 0.10, the model is simplified without significant loss of accuracy by sequentially deleting factors until only statistically significant effects remain. Equation 8.13 is obtained.

$$T_1 = \nabla_0 + \nabla_c f_c + \nabla_d \mathrm{D} + \nabla_{cd} \frac{C}{D} + \nabla_f C_f \qquad (8.13)$$

Table 8.9 shows the reestimated coefficients and p-values. The R-squared value is 75.78%.

Table 8.9. Estimation of coefficients and significance tests (simple model, eq.8.13).

		Coefficient	Std. error	p-value
(constant)	∇_0	–23.029	2.26	--
Compressive Strength	∇_c	0.4383	0.0389	0.0000
Cover/Diameter	∇_{cd}	0.4794	0.259	0.0719
Diameter	∇_d	0.2449	0.061	0.0002
Fiber Content	∇_f	0.0247	0.0099	0.0171

Figure 8.13 shows the normal probability plot of the standardized residuals, which prove to be normally distributed. No outliers or influential data have been identified.

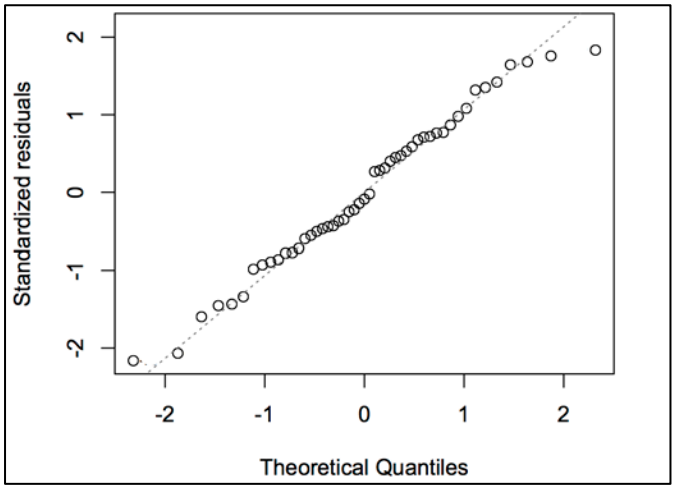

Figure 8.13. Normal probability plot of standardized residuals.

Figure 8.14 shows the CPR plots. These plots reveal that rebar diameter has a quadratic effect on T_1 that is disregarded in the model in its present form.

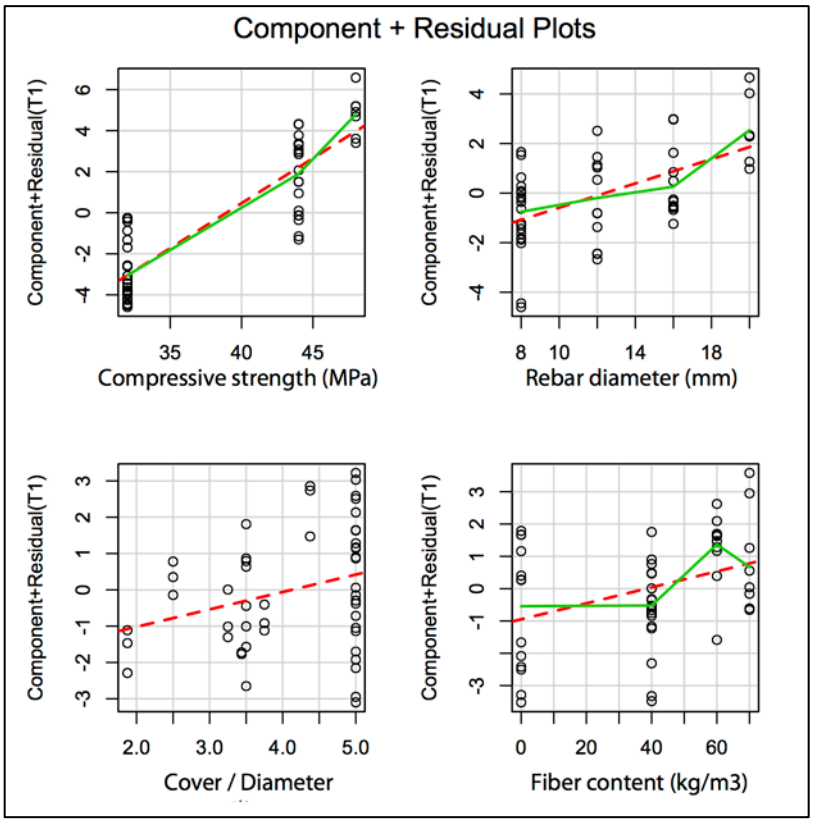

Figure 8.14. CPR plots.

QUADRATIC MODEL

The model for T_1 is reformulated as given by equation 8.14:

$$T_1 = \nabla_0 + \nabla_c f_c + \nabla_{cc} {f_c}^2 + \nabla_d \mathrm{D} + \nabla_{dd} \mathrm{D}^2 + \nabla_{cd} \frac{C}{D} + \nabla_f C_f + \nabla_{ff} {C_f}^2 + \nabla_{\lambda f} \lambda_f C_f + \nabla_{\ell f} \ell_f C_f \quad (8.14)$$

Table 8.10 shows the results of coefficients estimation and the p-values obtained from the significance tests associated to these coefficients. The R-squared is 81.36%.

Table 8.10. Estimation of coefficients and significance tests (quadratic model, eq.8.14).

	Coefficient	Std. error	p-value
(constant)	5.607	19.19	--
Compressive Strength	–0.6183	1.064	0.5645
(quadratic)	0.01458	0.0135	0.2851
Cover/Diameter	–0.01734	0.329	0.9582
Diameter	–0.981	0.654	0.1418
(quadratic)	0.046	0.0241	0.0633
Fiber Content	–0.08563	0.105	0.4178
(quadratic)	0.00118	0.000484	0.0192
Fiber Slenderness, $\lambda_f C_f$	0.000024	0.00059	0.9673
Fiber Length, $\ell_f C_f$	0.0004	0.0011	0.7210

Several p-values obtained are bigger than 0.10. Therefore the model is simplified by stepwise regression, and equation 8.15 is obtained:

$$T_1 = \nabla_0 + \nabla_c f_c + \nabla_{cc} {f_c}^2 + \nabla_{dd} \mathrm{D}^2 + \nabla_{cd} \frac{C}{D} + \nabla_f C_f + \nabla_{\ell f} \ell_f C_f \qquad (8.15)$$

Table 8.11 shows the reestimated coefficients in the simplified quadratic model and the corresponding p-values. The R-squared value is 77.23%.

Table 8.11. Estimation of coefficients and significance tests (quadratic model, eq.8.15).

		Coefficient	Std. error	p-value
(constant)	∇_0	–13.33	1.524	--
Compr. Str. (quadratic)	∇_{cc}	0.00582	0.00049	0.0000
Cover/Diameter	∇_{cd}	0.412	0.251	0.109
Diameter (quadratic)	∇_{dd}	0.00978	0.00226	0.0000
Fiber Content	∇_f	0.02284	0.0097	0.023

As Figure 8.15 shows, the distribution of the standardized residuals after the stepwise reduction of the quadratic model has suffered no important changes: they remain normally distributed. No outliers or influential points have been detected either.

Finally, Figure 8.16 plots the residuals vs the fitted values of T_1. No signs of heteroskedasticity are found, and therefore the fitted model is considered as final.

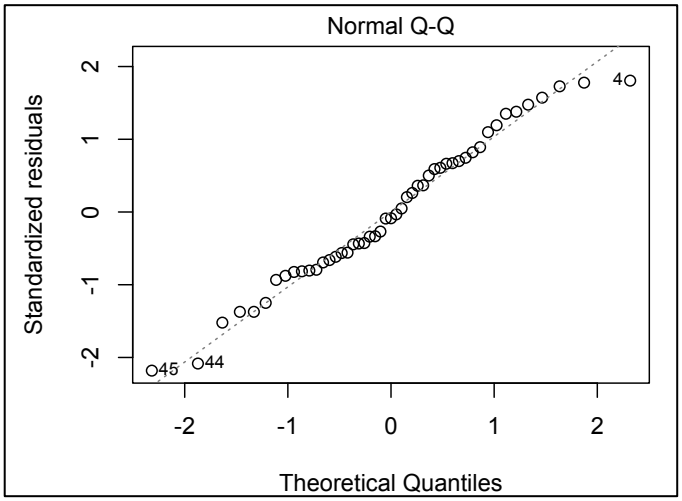

Figure 8.15. Normal probability plot of standardized residuals.

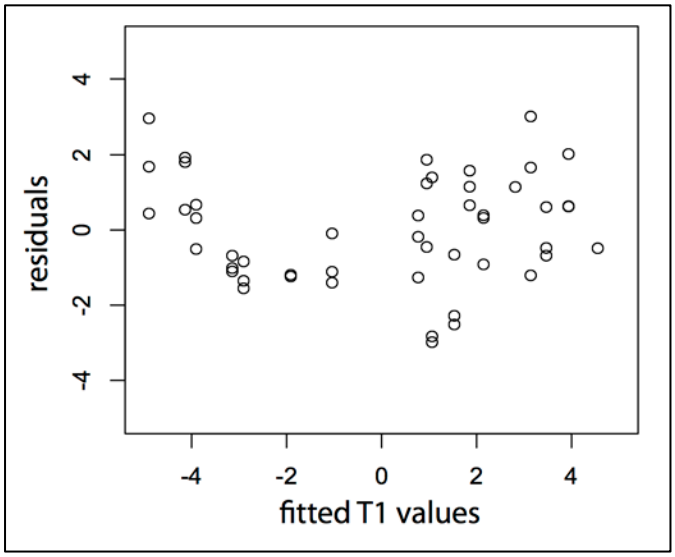

Figure 8.16. Residuals vs fitted T_1 values.

FINAL MODEL

Equation 8.16 presents the fitted model for T_1, with an R-squared value of 77.2%:

$$T_1 = -13.33 + 0.00582{f_c}^2 + 0.00978\mathrm{D}^2 + 0.412\frac{C}{D} + 0.0228C_f \qquad (8.16)$$

Figure 8.17 shows the predicted vs observed values of T_1, together with the exact equivalence line and the limits of the 95%-confidence band.

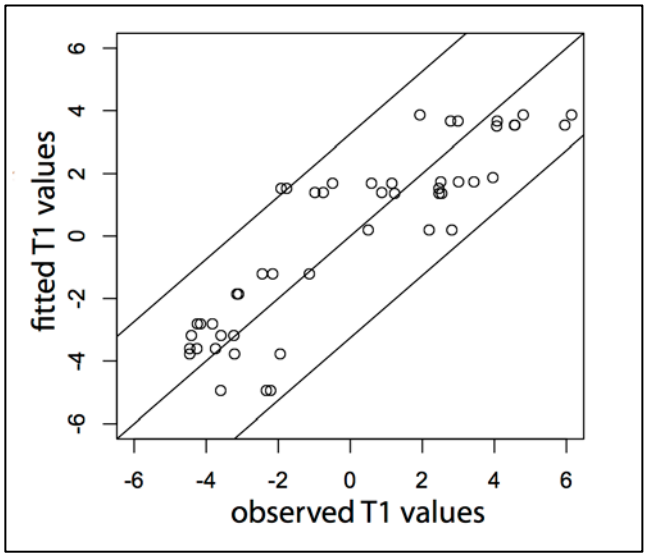

Figure 8.17. Predicted vs observed T_1 values.

Figure 8.18 shows the effects corresponding to this model. Black lines are drawn according to mean values and red dashed lines limit the 95%-confidence band for predictions with this model. It can be seen that the effect of all factors on bond strength is not of the same magnitude. Concrete compressive strength is revealed as the determining factor in opposition to cover/diameter ratio, which has the least important effect on T_1. This can be concluded as well by using expression 8.16 to compare different scenarios, considering that each factor has a different range of variation. If concrete compressive strength is increased from 32 MPa to 48 MPa, then T_1 is increased in 7.5 units. On the contrary, if cover/diameter ratio is increased from 2.0 to 5.0, then T_1 is increased in

1.3 units. If the effects of all factors on T_1 within their range of variation (as considered in this research) are referred to that of cover/diameter ratio, it can be said that the effect of fiber content, rebar diameter, and concrete compressive strength on T_1 are 20%, 150%, and 480% higher than the effect of cover/diameter, respectively.

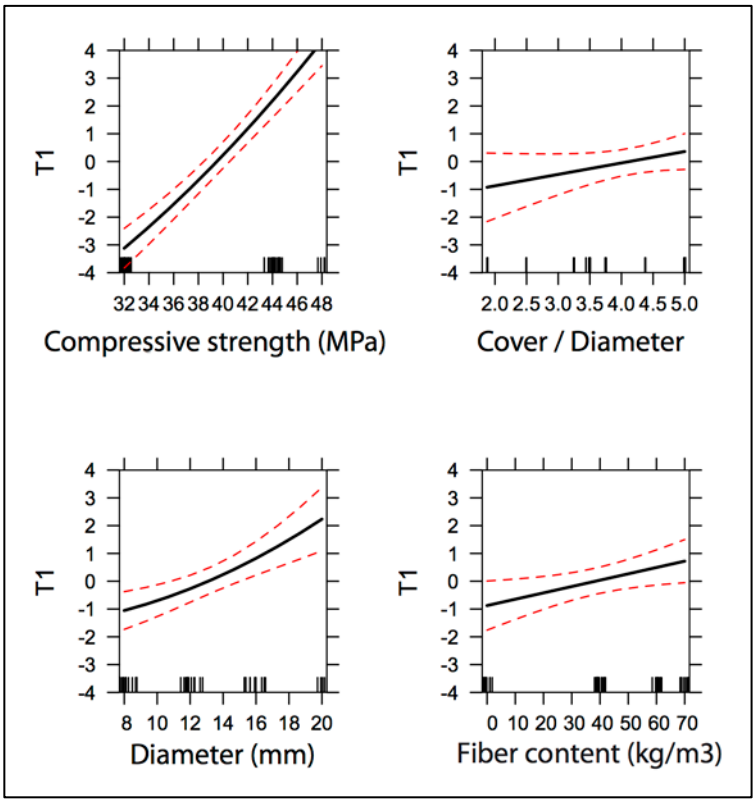

Figure 8.18. Main effects plots for T_1.

All of these factors have a positive effect on T_1 and therefore have a positive impact on the ductility of bond failure. However, it is important to remember the conclusions obtained in chapter 6 regarding the mode of failure. Increasing all these factors means that T_1 increases as long as splitting does not occur. Because modifying these factors varies the probability of splitting as well. Taking into account the model obtained in chapter 6, increasing concrete compressive strength and/or fiber content implies an increase in the probability of splitting. Accordingly, an

adequate confinement has to be provided to increase T_1 and therefore bond failure ductility by means of increasing concrete compressive strength and/or fiber content. This can be understood in the following terms as well: the only means to improve bond failure ductility without increasing the risk of splitting are:

- ☐ Increasing concrete cover/diameter ratio.
- ☐ Increasing rebar diameter without decreasing cover/diameter ratio, i.e. increasing concrete cover proportionally.

8.4 Effects on latent variable T_2

SIMPLE MODEL

A simple model for T_2 is given by equation 8.17:

$$T_2 = \nabla_0 + \nabla_c f_c + \nabla_d \mathrm{D} + \nabla_{cd} \frac{C}{D} + \nabla_f C_f + \nabla_{\lambda f} \lambda_f C_f + \nabla_{\ell f} \ell_f C_f \qquad (8.17)$$

where T_2 stands for the projection of experimental bond stress–slip curves onto the first principal component PC2 (dimensionless), f_c is the average concrete compressive strength (MPa), D is rebar diameter (mm), C is concrete cover (mm), C_f is fiber content (kg/m^3), λ_f is fiber slenderness, ℓ_f is fiber length (mm); and ∇_0, ∇_c, ∇_d, ∇_{cd}, ∇_f, $\nabla_{\lambda f}$, and $\nabla_{\ell f}$ are coefficients to be estimated.

Estimates for the coefficients in equation 8.17 are shown in Table 8.12 together with the associated p-values. The R-squared value is 22.8%.

Table 8.12. Estimation of coefficients and significance tests (simple model, eq.8.17).

		Coefficient	Std. error	p-value
(constant)	∇_0	–0.4058	1.32	--
Compressive Strength	∇_c	0.0572	0.0292	0.0563
Cover/Diameter	∇_{cd}	–0.2135	0.163	0.1978
Diameter	∇_d	–0.032	0.041	0.4339
Fiber Content	∇_f	–0.1378	0.0487	0.0072
Fiber Slenderness, $\lambda_f C_f$	$\nabla_{\lambda f}$	0.000785	0.00032	0.0187
Fiber Length, $\ell_f C_f$	$\nabla_{\ell f}$	0.00137	0.0006	0.0283

Since several p-values are higher than 0.10, the model is simplified without significant loss of accuracy by sequentially deleting factors until only statistically significant effects remain. Equation 8.18 is obtained. Table 8.13 shows the reestimated coefficients and p-values. The R-squared value is 19.3%.

$$T_2 = \nabla_0 + \nabla_c f_c + \nabla_d \mathrm{D} + \nabla_{cd} \frac{C}{D} + \nabla_f C_f \qquad (8.18)$$

Table 8.13. Estimation of coefficients and significance tests (simple model, eq.8.18).

		Coefficient	Std. error	p-value
(constant)	∇_0	–1.3002	1.117	--
Compressive Strength	∇_c	0.045	0.0276	0.1100
Fiber Content	∇_f	–0.105	0.041	0.0135
Fiber Slenderness, $\lambda_f C_f$	$\nabla_{\lambda f}$	0.000648	0.00029	0.0318
Fiber Length, $\ell_f C_f$	$\nabla_{\ell f}$	0.000955	0.0005	0.0647

Figure 8.19 shows the normal probability plot of the standardized residuals, which prove to be normally distributed. There is no evidence of outliers or influential data.

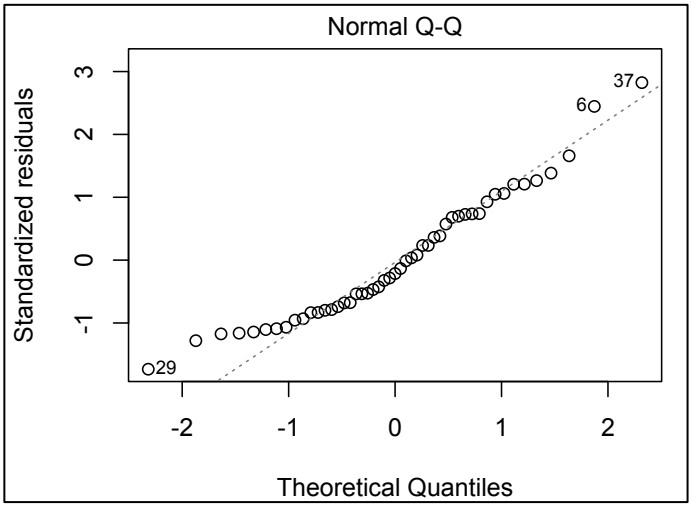

Figure 8.19. Normal probability plot.

In order to detect quadratic effects which should be considered in the model, scatterplots are more apropriate than CPR plots in the case of this model. Figure 8.20 shows the scatterplots of T_2 vs each of the variables. Green lines represent a merely linear fitting. Red segments link group average values and therefore provide an insight to quadratic effects,

whenever present. Red dotted lines correspond to 95%-confidence limits for each of these average values. It is observed a quadratic effect of rebar diameter and concrete compressive strength on T_2 which has to be considered.

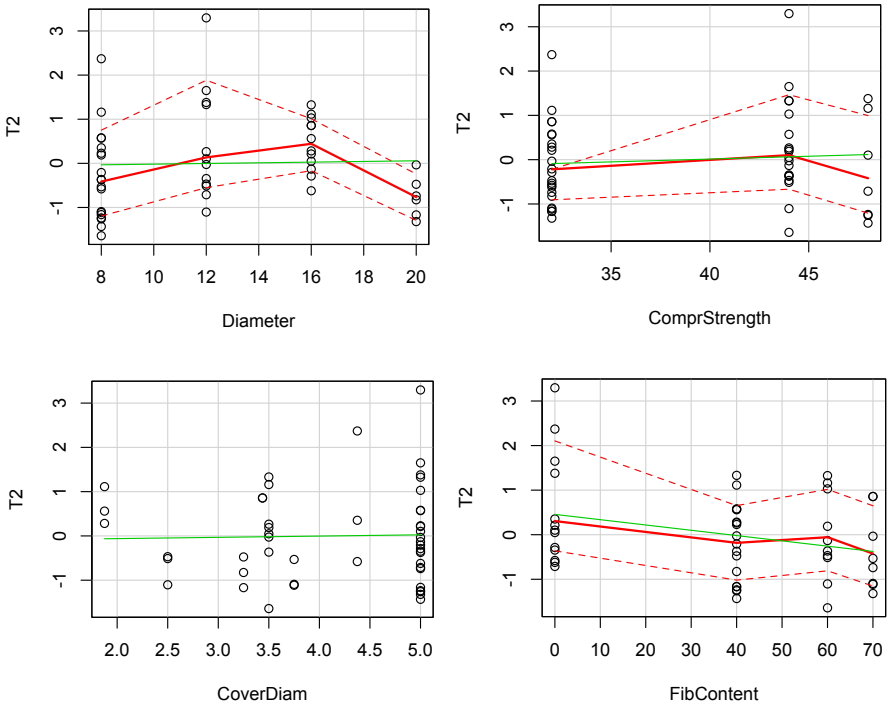

Figure 8.20. Scatterplots and regression lines linking group average values.

QUADRATIC MODEL

The model for T_2 is reformulated as given by equation 8.19:

$$T_2 = \nabla_0 + \nabla_c f_c + \nabla_{cc} {f_c}^2 + \nabla_d \mathrm{D} + \nabla_{dd} \mathrm{D}^2 + \nabla_{cd} \frac{C}{D} + \nabla_f C_f + \nabla_{ff} {C_f}^2 + \nabla_{\lambda f} \lambda_f C_f + \nabla_{\ell f} \ell_f C_f \quad (8.19)$$

Table 8.14 shows the results of coefficients estimation and the p-values obtained from the significance tests associated to these coefficients. The R-squared is 30.8%.

Table 8.14. Estimation of coefficients and significance tests (quadratic model, eq.8.19).

	Coefficient	Std. error	p-value
(constant)	–20.34	11.69	--
Compressive Strength	1.025	0.648	0.1215
	–0.0126	0.0082	0.1317
Cover/Diameter	–0.135	0.2	0.5049
Diameter	0.241	0.398	0.5485
	–0.0105	0.015	0.4805
Fiber Content	–0.1285	0.064	0.0505
	0.000135	0.00029	0.6481
Fiber Slenderness, $\lambda_f C_f$	0.000606	0.00036	0.0993
Fiber Length, $\ell_f C_f$	0.00128	0.00067	0.0654

Several p-values obtained are bigger than 0.10. Therefore the model is simplified by stepwise regression, and equation 8.20 is obtained:

$$T_2 = \nabla_0 + \nabla_c f_c + \nabla_{cc} {f_c}^2 + \nabla_f C_f + \nabla_{\lambda f} \lambda_f C_f + \nabla_{\ell f} \ell_f C_f \qquad (8.20)$$

Table 8.15 shows the reestimated coefficients in the simplified quadratic model and the corresponding p-values. The R-squared value is 25.6%.

Table 8.15. Estimation of coefficients and significance tests (quadratic model, eq.8.19).

		Coefficient	Std. error	p-value
(constant)	∇_0	–22.81	11.3	--
Compressive Strength	∇_c	1.183	0.596	0.0535
Compr. Str. (quadratic)	∇_{cc}	–0.0146	0.0076	0.0626
Fiber Content	∇_f	–0.109	0.0397	0.0085
Fiber Slenderness, $\lambda_f C_f$	$\nabla_{\lambda f}$	0.00059	0.00029	0.0467
Fiber Length, $\ell_f C_f$	$\nabla_{\ell f}$	0.00109	0.00049	0.0324

Figure 8.21 shows the normal probability plot of standardized residuals, which remain normally distributed with the exception of some values. Figure 8.22 confirms that one of them is an outlier according to the Cook's distance criterion. This is probably the reason why the quadratic effect of diameter, detected in Figure 8.20, has not been identified as significant when simplifying equation 8.19 by stepwise regression.

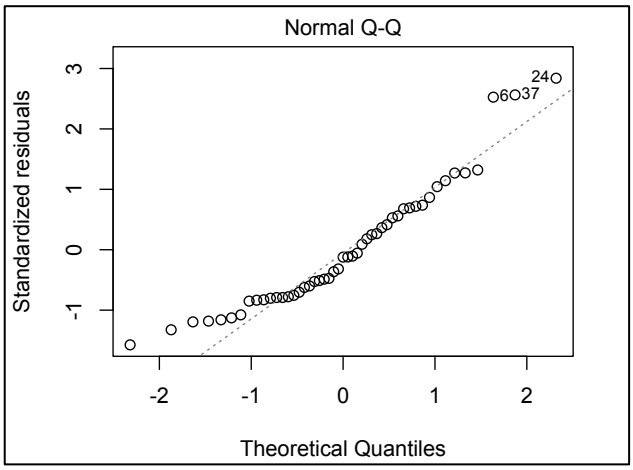

Figure 8.21. Normal probability plot.

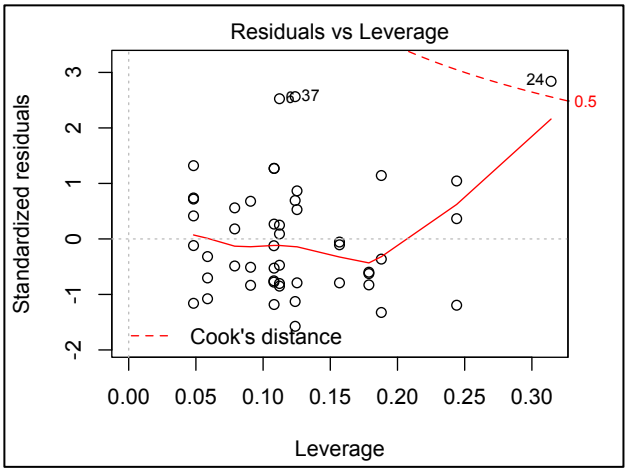

Figure 8.22. Residuals vs leverage plot.

Once this datum has been discarded, the model is recalculated and simplified by stepwise regression. Equation 8.21 is obtained:

$$T_2 = \nabla_0 + \nabla_c f_c + \nabla_{cc} {f_c}^2 + \nabla_d \mathrm{D} + \nabla_{dd} \mathrm{D}^2 + \nabla_f C_f + \nabla_{\ell f} \ell_f C_f \qquad (8.21)$$

Table 8.16 shows the reestimated coefficients in the simplified quadratic model and the corresponding p-values. The R-squared value is 40.1%.

Table 8.16. Estimation of coefficients and significance tests (quadratic model, eq.8.21)

		Coefficient	Std. error	p-value
(constant)	∇_0	–36.47	11.53	--
Compressive Strength	∇_c	1.761	0.627	0.0076
Compr. Str. (quadratic)	∇_{cc}	–0.0226	0.008	0.0073
Diameter		0.605	0.265	0.0276
Diameter (quadratic)		–0.0233	0.01	0.0259
Fiber Content	∇_f	–0.0661	0.023	0.0068
Fiber Length, $\ell_f C_f$	$\nabla_{\ell f}$	0.00105	0.00043	0.0194

Figure 8.23 shows the normal probability plot of standardized residuals, which remain normally distributed. No outliers have been found after the previously detected one has been discarded. Figure 8.24 shows that scatter of residuals is not related to T_2 values. As a result, the model can now be considered as final.

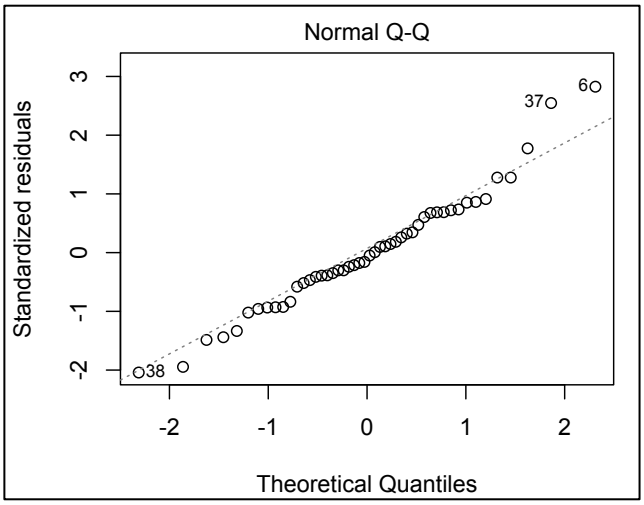

Figure 8.23. Normal probability plot.

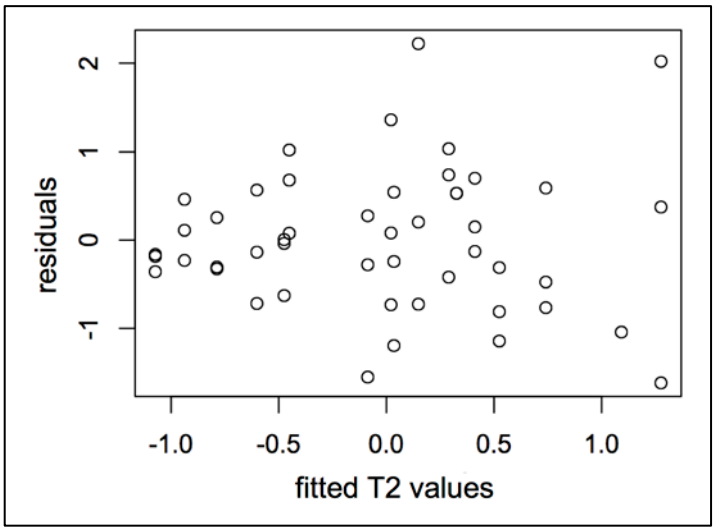

Figure 8.24. Residuals vs predicted T_2 values.

FINAL MODEL

Equation 8.22 presents the fitted model for T_2, with an R-squared value of 40.1%:

$$T_2 = -36.47 + 1.761 f_c - 0.0226 {f_c}^2 + 0.605\mathrm{D} - 0.0233\mathrm{D}^2 - 0.0661 C_f + 0.00105 \ell_f C_f \quad (8.22)$$

Figure 8.25 shows the predicted vs observed values of T_2, together with the exact equivalence line and the limits of the 95%-confidence band. It is observed that the scatter of T_2 values is higher than that of T_1 values. Furthermore the R-squared value obtained for T_2 is 40.1%, much less than that obtained for T_1. These two facts mean that T_2, and therefore the bond stress corresponding to the onset of slippage, is a less stable parameter than T_1 or the area under the bond stress–slip curve.

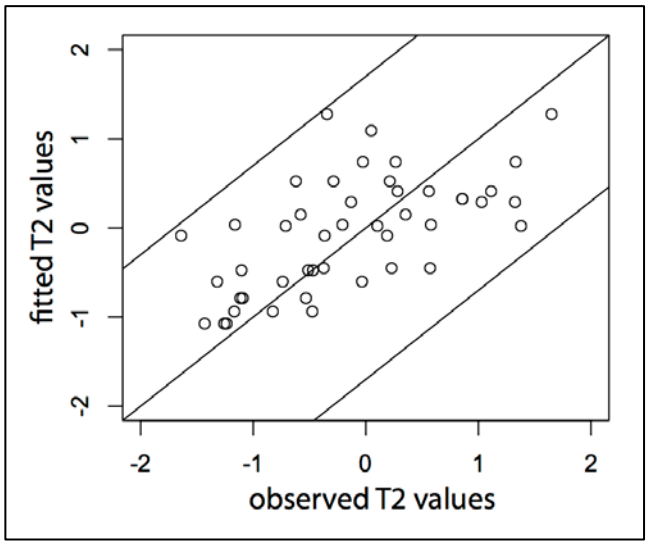

Figure 8.25. Predicted vs observed T_2 values.

Figure 8.26 shows the effects plot corresponding to this model. Black lines are drawn according to mean values and red dashed lines limit the 95%-confidence band for predictions with this model.

Concrete compressive strength and fiber content have a positive effect on T_2. The interpretation can be that these factors improve the quality of concrete matrix around the rebar, namely tensile strength. Therefore the loss of strain compatibility between rebar and concrete is delayed when concrete compressive strength and/or fiber content are increased. The effect of fiber content on T_2 is modified by fiber length.

Rebar diameter has a positive effect on T2 as well, but the interpretation of this finding is different from that concerning concrete compressive strength or fiber content. This is possibly due to the fact that embedment length directly depends on rebar diameter (see chapter 4). Since slips have been monitored at the free end of the rebar, the onset of slips corresponds to the moment when bond stresses are activated along all the embedment length. When a higher rebar diameter is considered, there is a higher embedment length, and therefore it takes higher energy to activate bond stresses along this length.

This analysis has proved as well that concrete cover/diameter ratio has no influence on the onset of slips. This is an important finding because it proves that concrete cover/diameter ratio has no effect on bond of rebars to concrete until the phenomenon reaches the structural scale.

This confirms the interpretation given to the effect of fibers on T2 as a consequence of their improving the matrix quality: passive confinement is not activated before slippage begins. Therefore the effect of fibers on T2 is the result of their contribution to the properties of the material, while their effect on T1 was a result of their structural function. Finally, it is worth mentioning that this two-phase role of fibers on bond of rebars to concrete is coherent with the distinction between the role of fibers at the scale of the material and at a structural scale (see chapter 1, and Rossi 1995).

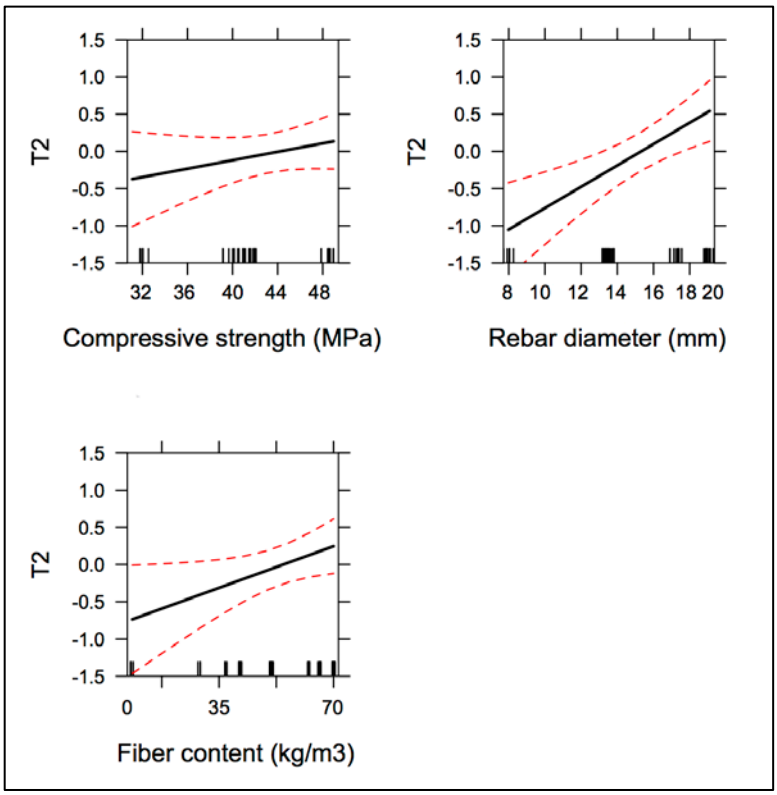

Figure 8.26. Main effects plots for T_2.

9| Conclusions and Future Research

Part IV: Conclusions

9| Conclusions and Future Research

PART IV: CONCLUSIONS

9.1 Conclusions

STATE OF THE ART

- ☐ The study of previous literature has revealed important points of ongoing discussion regarding different issues, especially the following: a) whether the effect of fibers on bond strength is negligible or not, b) whether the effect of fibers on bond strength is dependent on any other factors such as concrete compressive strength or concrete cover, c) quantifying the effect of fibers on the ductility of bond failure (bond toughness).

- ☐ It has been observed in previous experimental studies on this issue the tendency to treat bond strength values all together, regardless of the mode of failure. Therefore it has been identified the need to study separately the effect of fibers on bond when there is cover splitting and when there is not.

MODES OF BOND FAILURE

- ☐ An accurate model for predicting the mode of bond failure has been developed. It relates splitting probability to the values of concrete compressive strength, rebar diameter, concrete cover, fiber content, fiber length, and fiber slenderness. It has been verified that the margin of error is less than 5% when fitting the experimental results.

- ☐ Higher compressive strength values require higher concrete cover/diameter ratios for splitting failure to be prevented. When compressive strength of concrete increases, concrete tensile strength is

increased and therefore hoop stresses developing around the rebar reach further away from it.

- ☐ It has been proved that increasing fiber content restrains the risk of splitting failure. The favorable effect of fibers when preventing splitting failures has been revealed to be more important for higher concrete compressive strength values.

- ☐ Fiber slenderness and fiber length modify the effect of fiber content on splitting probability and therefore on minimum cover/diameter ratios required to prevent splitting failures. Higher fiber slenderness and/or fiber length values imply an increase in bond capacity of concrete and therefore require higher concrete cover values to prevent splitting when developing higher bond stresses.

- ☐ The favorable effect of increasing fiber contents is conditioned to fiber length. The use of long fibers can even lead to the fact that increasing fiber contents would make the anchorage more prone to splitting.

- ☐ Two charts have been developed for estimating the minimum cover/ diameter ratio required to prevent splitting as a function of fiber content, fiber geometry, and concrete compressive strength. It appears that the definition of the good confinement situations corresponding to cover/diameter = 5.0, as established by the Model Code, is possibly insufficient for SFRCs when concrete compressive strength higher than 50 MPa.

BOND PERFORMANCE

- ☐ Predictive equations have been obtained for estimating bond strength and areas under the bond stress–slip curve as a function of concrete compressive strength, rebar diameter, concrete cover, fiber content, fiber slenderness and fiber length, when no splitting occurs.

- ☐ The values of the ductility parameters considered in this thesis, namely areas under the bond stress–slip curve, are more scattered when their average value increases. This is not the case for bond strength.

- Increasing fiber content has a slightly positive impact on bond strength, which is mainly determined by concrete compressive strength. On the contrary, fibers have a very important effect on the ductility of bond failure, just as well as concrete cover, as long as no splitting occurs.

MULTIVARIATE ANALYSIS

- Multivariate analysis has proved that bond stress corresponding to the onset of slippage behaves independently from the rest of the bond stress–slip curve. The effect of fibers and concrete compressive strength on bond stress values corresponding to the onset of slips is mainly attributable to their influence on the material mechanical properties. On the contrary, the effect of fibers and concrete cover on the rest of the bond stress–slip curve is due to their structural role.

9.2 Future Research

The experimental study on which the conclusions drawn in this thesis are based includes concretes compressive strengths between 30 MPa and 50 MPa, steel fiber contents (macrofibers) not greater than 70 kg/m^3, rebar diameters between 8 mm and 20 mm, and concrete cover values not higher than 5 times the rebar diameter. Therefore, the validity of these conclusions can be accepted without reservation only within these ranges. No extrapolation beyond the values tested for these factors can be considered as definite. It is also important to remark that these experimental results have been obtained by means of the Pull Out Test: variations in the observed behaviors are likely if bond is analyzed by means of different test setups or methodologies.

The generalization of any model outside the range of data that have been used for its formulation often involves complications. This remark is applicable to multiple linear regression as well as logistic regression, which have been used to develop the models and charts obtained in this thesis. Further tests are needed to confirm to check if these models and charts hold outside the tested limits in order to obtain new data to extend those limits and then to check and/or calibrate the model.

The analysis of modes of bond failure (Chapter 6) has brought up the need to extend the experimental campaign to concretes with compressive strength above 50 MPa and also to cover/diameter ratios higher than 5.0. In the future it is convenient to determine whether the charts provided at the end of Chapter 6 for estimating the minimum concrete cover/diameter ratio to prevent splitting failures must be modified.

The conclusions of this thesis are limited to steel, hooked-end macrofibers. In the future it will be investigated whether the behavior of macrofibers in terms of bond is comparable, and to what extent, to that of equivalent contents of steel microfibers, since the mechanisms of microfibers and macrofibers on the material and structural levels are not coincident.

The impact of the quality of concrete matrix on bond performance has been considered only through concrete compressive strength. However, future studies are needed to clarify whether other factors directly related

to concrete matrix have significant effects on bond strength and toughness. Future research must address issues such as aggregates size distribution, maximum aggregate size, water/cement ratio, and cement content and their influence on bond performance, since the effect of all these factors on bond of reinforcement to concrete may have other components than that related to concrete compressive strength.

Finally, there is the issue of the validity of these conclusions if bond is not studied locally (Pull Out Test) but by means of a rather structural test, such as beam end tests or spliced beam tests. It will be necessary to replicate the experimental program using one of these tests to assess if the results and conclusions are different or not, and to what extent.

References

Aarup, B. & Jensen, B.C., 1998. Bond Properties of High-Strength Fiber Reinforced Concrete. ACI Special Publication, 180, pp.459–472.

Abrishami, H.H. & Mitchell, D., 1996. Analysis of Bond Stress Distributions in Pullout Specimens. Journal of Structural Engineering, 122(3), pp.255–261. ACI Committee 408, 2003. ACI408R-03: Bond and Development of Straight Reinforcing Bars in Tension, American Concrete Institute.

Abrishami, H.H. & Mitchell, D., 1997. Influence of Steel Fibers on Tension Stiffening. ACI Structural Journal, 94(6), pp.769–776.

ACHE – Spanish Society for Structural Concrete (Asociación Científico-Técnica del Hormigón Estructural), 2000. Manual de tecnología del hormigón reforzado con fibras de acero, Madrid, Spain, 125 pp.

ACI Committee 318, 2011. ACI 318-11: Building Code Requirements for Structural Concrete and Commentary. Ed. by American Concrete Institute (ACI), Farmington Hills, Michigan, United States, 503 pp.

ACI Committee 408, 2003. Report ACI 408R-03: Bond and Development of Straight Reinforcing Bars in Tension. Ed. by American Concrete Institute (ACI), Farmington Hills, Michigan, United States, 49 pp.

ACI Committee 544, 1996 (reapproved 2009). Report ACI 544.1R-96: Report on Fiber Reinforced Concrete. Ed. by American Concrete Institute (ACI), Farmington Hills, Michigan, United States, 66 pp.

ACI Committee 544, 1988 (reapproved 2009). Report ACI 544.4R-88: Design Considerations for Steel Fiber Reinforced Concrete. Ed. by American Concrete Institute (ACI), Farmington Hills, Michigan, United States, 18 pp.

Arango, S., García-Taengua, E., et al., 2012a. A Comprehensive Study on the Effect of Fibers and Loading on Flexural Creep of SFRC. In 8th RILEM International Symposium on Fibre Reinforced Concrete BEFIB 2012. 8th RILEM International Symposium on Fibre Reinforced Concrete BEFIB 2012. Guimaraes, Portugal, pp. 173–174.

Arango, S.E., Serna, P., et al., 2012b. A Test Method to Characterize Flexural Creep Behaviour of Pre-cracked FRC Specimens. Experimental Mechanics, 52(8), pp.1067–1078.

Arel, H.S. & Yazici, S., 2012. Concrete-reinforcement bond in different concrete classes. Construction and Building Materials, 36, pp.78–83.

Auer, M. & Stempniewski, L., 2012. The influence of the damage state of the surrounding concrete on the bond stress-slip relationship. In Bond in Concrete 2012. Bond in Concrete 2012. Brescia, Italy, pp. 47–54.

Azizinamini, A., Stark, M., Roller, J.J., & Ghosh, S.K., 1993. Bond Performance of Reinforcing Bars Embedded in High-Strength Concrete. ACI Structural Journal, 90(5), pp.554–561.

Baena, M. et al., 2012. Modelling of bond and tension stiffening in FRP RC tensile members. In Bond in Concrete 2012. Bond in Concrete 2012. Brescia, Italy.

Balaguru, P., Gambarova, P.G., Rosati, G., & Schuman, C.E., 1995. Bond of reinforcing bars and prestressing tendons in HPFRCC matrices. 2nd International Workshop, High performance fiber reinforced cement composites, vol. 2, A.E.Naaman & H.W.Reinhard eds., University of Michigan, Ann Arbor, pp.325–363.

Bamonte, P. & Valente, M., 2012. Application of a closed-form solution for simulating bond between concrete and steel in service conditions. In Bond in Concrete 2012. Bond in Concrete 2012. Brescia, Italy, pp. 153–160.

Bamonte, P.F. & Gambarova, P.G., 2007. High-Bond Bars in NSC and HPC: Study on Size Effect and on the Local Bond Stress-Slip Law. Journal of Structural Engineering, 133(2), p.225.

Banholzer, B., Brameshuber, W. & Jung, W., 2005. Analytical simulation of pull-out tests—the direct problem. Cement and Concrete Composites, 27(1), pp.93–101.

Banthia, N. & Nandakumar, N., Crack growth resistance of hybrid fiber reinforced cement composites. Cement and Concrete Composites, 25(1), pp.3–9.

Baran, E., Akis, T. & Yesilmen, S., 2012. Pull-out behavior of prestressing strands in steel fiber reinforced concrete. Construction and Building Materials, 28(1), pp.362–371.

Barragán, B.E. & Zerbino, R., 2008. Creep behaviour of cracked steel fibre reinforced concrete beams. In 7th RILEM Symposium on Fibre Reinforced Concrete BEFIB2008. 7th RILEM Symposium on Fibre Reinforced Concrete BEFIB2008. Chennai, India, pp. 577–586.

Bayasi, Z. & Soroushian, P., 1990. Local bond behaviour of deformed bars in steel fibre reinforced concrete joints. Magazine of Concrete Research, 42(151), pp.91–95.

Bazant, Z.P. & Sener, S., 1988. Size Effect in Pullout Tests. ACI Materials Journal, 85(5), pp.347–351.

Bazant, Z.P., Li, Z. & Thoma, M., 1995. Identification of stress-slip law for bar or fiber pullout by size effect tests. Journal of Engineering Mechanics, 121(5), pp.620–625.

Bernardi, P., Cerioni, R. & Michelini, E., 2012. Numerical modelling of bond in cracked reinforced concrete elements. In Bond in Concrete 2012. Bond in Concrete 2012. Brescia, Italy, pp. 177–184.

Bischoff, P., Bérubé, F. & Lawrence, G., 2004. Use of steel fibres to enhance bond and development of reinforcing bars in high-strength reinforced concrete beams. In 6th RILEM Symp. on Fibre-Reinforced Concretes (FRC) BEFIB2004. 6th RILEM Symp. on Fibre-Reinforced Concretes (FRC) BEFIB2004. Varenna, Italy.

Bony, J.C., Claude, G. & Soretz, S., 1973. Comparaison des essais d'adhérence par flexion (beam test) et par traction (pull-out test). Materials and Structures, 6(5), pp.395–401.

Bossio, M.E. et al., 2012. Pull out behaviour of macro synthetic fibres: effects of fibre type, matrix strength and microcracking. In Bond in Concrete 2012. Bond in Concrete 2012. Brescia, Italy, pp. 901–906.

Box, G.E.P., Hunter, J.S., & Hunter, W.G., 2005. Statistics for Experimenters (2nd ed.). Ed. by Wiley-Blackwell, New Jersey, United States, 664 pp.

Buratti, N. & Mazzotti, C., 2012. Effects of different types and dosages of fibres on the long-term behaviour of fibre-reinforced self-compacting concrete. In 8th RILEM International Symposium on Fibre Reinforced Concrete BEFIB 2012. 8th RILEM International Symposium on Fibre Reinforced Concrete BEFIB 2012. Guimaraes, Portugal, pp. 177–178.

Cairns, J. & Abdullah, R., 1995. An evaluation of bond pullout tests and their relevance to structural performance. Structural Engineer, 73(11), pp.179–185.

Cairns, J. & Jones, K., 1996. An Evaluation of the Bond-Splitting Action of Ribbed Bars. ACI Materials Journal, 93(1), pp.10–19.

Cairns, J. & Jones, K., 1995. The splitting forces generated by bond. Magazine of Concrete Research, 47(171), pp.153–165.

Cairns, J. & Plizzari, G.A., 2003. Towards a harmonised European bond test. Materials and Structures, 36(8), pp.498–506.

Cairns, J. & Plizzari, G.A., 2004. Bond behaviour of conventional reinforcement in fibre reinforced concrete. In 6th RILEM Symp. on Fibre-Reinforced Concretes (FRC) BEFIB2004. 6th RILEM Symp. on Fibre-Reinforced Concretes (FRC) BEFIB2004. Varenna, Italy.

Campione, G., 2008. Simplified Flexural Response of Steel Fiber-Reinforced Concrete Beams. Journal of Materials in Civil Engineering, 20(4), p.283.

Campione, G., Cucchiara, C. & La Mendola, L., 2005. Steel–concrete bond in lightweight fiber reinforced concrete under monotonic and cyclic actions. Engineering structures, 27(6), pp.881–890.

Casanova, A., Jason, L. & Davenne, L., 2012. Bond slip model for the simulation of reinforced concrete structures. Engineering structures, 39, pp.66–78.

Cattaneo, S. & Rosati, G., 2000. Bond and splitting in high performance fiber reinforced concrete. In 5th RILEM Symp. on Fibre Reinforced Concrete (FRC). 5th RILEM Symp. on Fibre Reinforced Concrete (FRC). Lyon, France, pp. 567–576.

Centonze, G., Leone, M. & Aiello, M.A., 2012. Experimental Bond Analysis of FRC element reinforced with steel bars. In Bond in Concrete 2012. Bond in Concrete 2012. Brescia, Italy, pp. 809–816.

Chao, S., Naaman, A. & Parra-Montesinos, A., 2009. Bond Behavior of Reinforcing Bars in Tensile Strain-Hardening Fiber-Reinforced Cement Composites. ACI Structural Journal, 106(6), pp.897–906.

Chapman, R.A. & Shah, S.P., 1987. Early-age Bond Strength in Reinforced Concrete. ACI Materials Journal, 84(6), pp.501–510.

Cheung, A.K.F. & Leung, C.K.Y., 2008. Experimental study of the bond between steel reinforcement and self-compacting high strength fiber reinforced cementitious composites. In 7th RILEM Symposium on Fibre Reinforced Concrete BEFIB2008. 7th RILEM Symposium on Fibre Reinforced Concrete BEFIB2008. Chennai, India, pp. 667–678.

Chung, D.D.L., 2005. Dispersion of Short Fibers in Cement. Journal of Materials in Civil Engineering, 17(4), pp.379–383.

Dancygier, A., Katz, A. & Wexler, U., 2006. Bond-Slip Behavior of Reinforcement in NSC and HSC with and without Steel Fibers. In M. S. KONSTA-GDOUTOS, ed. Measuring, Monitoring and Modeling Concrete Properties. Dordrecht: Springer Netherlands, pp. 145–150.

Dancygier, A.N. & Katz, A., 2012. Bond over direct support of deformed rebars in normal and high strength concrete with and without fibers. Materials and Structures, 45(1-2), pp.265–275.

Dancygier, A.N., Katz, A. & Wexler, U., 2010. Bond between deformed reinforcement and normal and high-strength concrete with and without fibers. Materials and Structures, 43(6), pp.839–856.

Daoud, A. & Lorrain, M., 2003. Influence de la position des armatures sur l'adhérence des bétons autoplaçants: interprétation par analyse d'image. Materials and Structures, 36(4), pp.231–237.

Darwin, D., McCabe, S. L., Idun, E. K., & Schoenekase, S. P., 1992. Development Length Criteria: Bars Not Confined by Transverse Reinforcement. ACI Structural Journal, 89(6), pp. 709–720.

Darwin, D. & Zuo, J., 1996. Development Length Criteria for Conventional and High Relative Rib Area Reinforcing Bars. ACI Structural Journal, 93(3), pp.347–359.

De Larrard, F., Shaller, I. & Fuchs, J., 1993. Effect of the Bar Diameter on the Bond Strength of Passive Reinforcement in High-Performance Concrete. ACI Materials Journal, 90(4), pp.333–339.

De Larrard, F., 1999. Concrete Mixture Proportioning. A Scientific Approach, ed. by E&FN Spoon, London.

Dinh, H.H., Parra-Montesinos, G. & Wight, J.K., 2008. On the shear behavior of steel fiber reinforced concrete beams. In 7th RILEM Symposium on Fibre Reinforced Concrete BEFIB2008. 7th RILEM Symposium on Fibre Reinforced Concrete BEFIB2008. Chennai, India, pp. 399–408.

Di Prisco, M., Plizzari, G. & Vandewalle, L., 2009. Fibre reinforced concrete: new design perspectives. Materials and Structures, 42(9), pp.1261–1281.

Draper, N., & Smith, H., 1998. Applied Regression Analysis (3rd ed.). Ed. by Wiley-Blackwell, New York, United States, 736 pp.

Dupont, D., Vandewalle, L. & De Bonte, F., 2002. Influence of steel fibres on local bond behaviour. In Bond in Concrete 2002. Bond in Concrete 2002. Budapest, Hungary, pp. 783–790.

Dupray, F., Malecot, Y. & Daudeville, L., 2009. Experimental behaviour of high-performance concrete in confined tension. Materials and Structures, 43(5), pp.699–707.

Eligehausen, R., 1979. Bond in Tensile Lapped Splices of Ribbed Bars with Straight Anchorages [Ubergreifungsstösse zugbeanspruchter Rippenstäbe mit geradem Stabenden]. Publication no. 301, German Institute for Reinforced Concrete [Deutscher Ausschuss für Stahlbeton], Berlin, 118 pp.

Eligehausen, R., Popov, E., & Bertero, V., 1983. Local bond stress-slip relationship of ribbed bars under generalized excitations. Report UCB/EERC83-23, Earthquake Engineering Research Center, Dept. of Civil Engineering, University of California, Berkeley.

EN 1992-1-1, 2004. Eurocode 2: Design of Concrete Structures – Part 1-1: General Rules and Rules for Buildings. Ed. by European Committee for Standardization, Brussels, Belgium, 225 pp.

Ertzibengoa, D., Matthys, S. & Taerwe, L., 2013. Bond characteristics of carbon and stainless steel flat rebars with an alternate rib pattern. Materials and Structures, 46(7), pp.1107–1121.

Ezeldin, A. & Balaguru, P., 1989. Bond Behavior of Normal and High-Strength Fiber Reinforced Concrete. ACI Materials Journal, 86(5), pp.515–524.

Fantilli, A.P. & Vallini, P., 2004. Tension Stiffening Range in FRC Elements. In 6th RILEM Symp. on Fibre Reinforced Concretes (FRC) BEFIB 2004. 6th RILEM Symp. on Fibre Reinforced Concretes (FRC) BEFIB 2004. Varenna, Italy, pp. 847–856.

Fantilli, A.P., Mihashi, H. & Vallini, P., 2005. Strain compatibility between HPFRCC and steel reinforcement. Materials and Structures, 38(4), pp.495–503.

Fantilli, A.P. & Vallini, P., 2007. A Cohesive Interface Model for the Pullout of Inclined Steel Fibers in Cementitious Matrixes. Journal of Advanced Concrete Technology, 5(2), pp.247–258.

Fantilli, A.P., Mihashi, H. & Vallini, P., 2008. Effect of Bond-Slip on the Crack Bridging Capacity of Steel Fibers in Cement-Based Composites. Journal of Materials in Civil Engineering, 20(9), pp.588–598.

Feldman, L.R. & Bartlett, F.M., 2008. Bond in Flexural Members with Plain Steel Reinforcement. ACI Structural Journal, 105(5), pp.552–560.

Ferrara, L., Park, Y.-D. & Shah, S.P., 2008. Correlation among Fresh State Behavior, Fiber Dispersion, and Toughness Properties of SFRCs. ASCE Journal of Materials in Civil Engineering, 20(7), pp.493–501.

FIB–The International Federation for Structural Concrete, 2000. FIB Bulletin No. 10: Bond of reinforcement in concrete. Lausanne, Switzerland, 434 pp.

FIB–The International Federation for Structural Concrete, 2012. FIB Bulletin No. 65: Model Code 2010 - Final draft, Volume 1. Lausanne, Switzerland, 350 pp.

FIB–The International Federation for Structural Concrete, 2012. FIB Bulletin No. 66: Model Code 2010 - Final draft, Volume 2. Lausanne, Switzerland, 370 pp.

Fu, X. & Chung, D.D.L., 1998. Decrease of the Bond Strength between Steel Rebar and Concrete with Increasing Curing Age. Cement and Concrete Research, 28(2), pp.167–169.

Fu, X. & Chung, D.D.L., 1997. Improving the bond strength between steel rebar and concrete by increasing the water/cement ratio. Cement and Concrete Research, 27(12), pp.1805–1809.

Gambarova, P.G., 2012. Bond in reinforced concrete: where do we stand today? In Bond in Concrete 2012. Bond in Concrete 2012. Brescia, Italy, pp. 1–13.

Gambarova, P.G. & Rosati, G., 1996. Bond and splitting in reinforced concrete: test results on bar pull-out. Materials and Structures, 29(5), pp.267–276.

Gambarova, P.G. & Rosati, G.P., 1997. Bond and Splitting in Bar Pull-Out: Behavioural Laws and Concrete Cover Role. Magazine of Concrete Research, 49(179), pp.99–110.

Gambarova, P.G., Rosati, G.P. & Zasso, B., 1989a. Steel-to-concrete bond after concrete splitting: constitutive laws and interface deterioration. Materials and Structures, 22(5), pp.347–356.

Gambarova, P.G., Rosati, G.P. & Zasso, B., 1989b. Steel-to-concrete bond after concrete splitting: test results. Materials and Structures, 22(1), pp.35–47.

García-Taengua, E. et al., 2012. New Views on the Study of Variables Affecting Bond of Reinforcing Bars to Steel Fiber Reinforced Concrete. In 8th RILEM International Symposium on Fibre Reinforced Concrete BEFIB 2012. 8th RILEM International Symposium on Fibre Reinforced Concrete BEFIB 2012. Guimaraes, Portugal, pp. 93–94.

García-Taengua, E., Martí-Vargas, J.R. & Serna-Ros, P., 2011. Statistical Approach to Effect of Factors Involved in Bond Performance of Steel Fiber-Reinforced Concrete. ACI Structural Journal, 108(4), pp.461–468.

Gilbert, R.I., Mazumder, M. & Chang, Z.T., 2012. Bond, slip and cracking within the anchorage length of deformed reinforcing bars in tension. In Bond in Concrete 2012. Bond in Concrete 2012. Brescia, Italy, pp. 331–338.

Gjorv, O.E., Monteiro, P.J.M. & Mehta, P.K., 1990. Effect of Condensed Silica Fume on the Steel-Concrete Bond. ACI Materials Journal, 87(6), pp.573–580.

Güneyisi, E., Gesoglu, M. & Ipek, S., 2013. Effect of steel fiber addition and aspect ratio on bond strength of cold-bonded fly ash lightweight aggregate concretes. Construction and Building Materials, 47, pp.358–365.

Haddad, R.H. & Abendeh, R.M., 2004. Effect of thermal cycling on bond between reinforcement and fiber reinforced concrete. Cement and Concrete Composites, 26(6), pp.743–752.

Haddad, R.H., Al-Saleh, R.J. & Al-Akhras, N.M., Effect of elevated temperature on bond between steel reinforcement and fiber reinforced concrete. Fire Safety Journal, 43(5), pp.334–343.

Hair, J.F., Black, W.C., Babin, B.J., & Anderson, R.E., 2009. Multivariate Data Analysis (7th ed.). Ed. by Prentice Hall, New Jersey, United States, 816 pp.

Hamad, B.S., 1995. Bond Strength Improvement of Reinforcing Bars with Specially Designed Rib Geometries. ACI Structural Journal, 92(1), pp.3–13.

Hamad, B.S. & Itani, M.S., 1998. Bond Strength of Reinforcement in High Performance Concrete: Role of Silica Fume, Casting Position, and Superplasticizer Dosage. ACI Materials Journal, 95(5), pp.499–511.

Hamad, B.S. & Machaka, M.F., 1999. Effect of transverse reinforcement on bond strength of reinforcing bars in silica fume concrete. Materials and Structures, 32(6), pp.468–476.

Hamad, B.S., Harajli, M.H. & Jumaa, G., 2001. Effect of Fiber Reinforcement on Bond Strength of Tension Lap Splices in High-Strength Concrete. ACI Structural Journal, 98(5), pp.638–647.

Hamad, B.S. & Rteil, A.A., 2006. Comparison of Roles of FRP Sheets, Stirrups, and Steel Fibers in Confining Bond Critical Regions. Journal of Composites for Construction, 10(4), pp.330–336.

Harajli, M.H., 1994. Development/Splice Strength of Reinforcing Bars Embedded in Plain and Fiber Reinforced Concrete. ACI Structural Journal, 91(5), pp.511–520.

Harajli, M.H., Hout, M. & Jalkh, W., 1995. Local Bond Stress-Slip Behavior of Reinforcing Bars Embedded in Plain and Fiber Concrete. ACI Materials Journal, 92(4), pp.343–354.

Harajli, M.H. & Salloukh, K.A., 1997. Effect of Fibers on Development/Splice Strength of Reinforcing Bars in Tension. ACI Materials Journal, 94(4), pp.317–324.

Harajli, M., Hamad, B. & Karam, K., 2002. Bond-slip Response of Reinforcing Bars Embedded in Plain and Fiber Concrete. Journal of Materials in Civil Engineering, 14(6), pp.503–511.

Harajli, M.H. & Mabsout, M.E., 2002. Evaluation of Bond Strength of Steel Reinforcing Bars in Plain and Fiber-Reinforced Concrete. ACI Structural Journal, 99(4), pp.509–517.

Harajli, M.H., Hamad, B.S. & Rteil, A.A., 2004. Effect of Confinement on Bond Strength between Steel Bars and Concrete. ACI Structural Journal, 101(5), pp.595–603.

Harajli, M., 2004. Comparison of Bond Strength of Steel Bars in Normal- and High-Strength Concrete. ASCE Journal of Materials in Civil Engineering, 16(4), pp.365–374.

Harajli, M.H., 2007. Numerical Bond Analysis Using Experimentally Derived Local Bond Laws: A Powerful Method for Evaluating the Bond Strength of Steel Bars. Journal of Structural Engineering, 133(5), pp.695–705.

Harajli, M.H. & Gharzeddine, O., 2007. Effect of Steel Fibers on Bond Performance of Steel Bars in NSC and HSC under Load Reversals. Journal of Materials in Civil Engineering, 19(10), pp.864–873.

Holschemacher, K. & Weisse, D., 2004. Bond of reinforcement in fibre reinforced concrete. In 6th RILEM Symp. on Fibre-Reinforced Concretes (FRC) BEFIB2004. 6th RILEM Symp. on Fibre-Reinforced Concretes (FRC) BEFIB2004. Varenna, Italy.

Hosny, A. et al., 2012. Development Length of Unconfined Conventional and High-Strength Steel Reinforcing Bars. ACI Structural Journal, 109(5), pp.655–664.

Hughes, B.P. & Videla, C., 1992. Design criteria for early-age bond strength in reinforced concrete. Materials and Structures, 25(8), pp.445–463.

Hwang, S.J., Lee, Y.Y. & Lee, C.S., 1994. Effect of Silica Fume on the Splice Strength of Deformed Bars of High-Performance Concrete. ACI Structural Journal, 91(3), pp.294–302.

Ichinose, T. et al., 2004. Size effect on bond strength of deformed bars. Construction and Building Materials, 18(7), pp.549–558.

Jansson, A., Löfgren, I., Lundgren, K. & Gylltoft, K., 2012a. Bond between reinforcement and self-compacting steel-fibre-reinforced concrete. In Bond in Concrete 2012. Bond in Concrete 2012. Brescia, Italy, pp. 323–329.

Jansson, A., Löfgren, I., Lundgren, K. & Gylltoft, K., 2012b. Bond of reinforcement in self-compacting steel-fibre-reinforced concrete. Magazine of Concrete Research, 64(7), pp.617–630.

Jiang, D.H., Shah, S.P. & Andonian, A.T., 1984. Study of the Transfer of Tensile Forces by Bond. ACI Journal Proceedings, 81(3), pp.251–259.

Kaklauskas, G. et al., 2012. Experimental validation of different approaches in modeling tension-stiffening of bending members reinforced with steel and GFRP bars. In Bond in Concrete 2012. Bond in Concrete 2012. Brescia, Italy, pp. 835–842.

Kayali, O., 2004. Effect of high volume fly ash on mechanical properties of fiber reinforced concrete. Materials and Structures, 37(5), pp.318–327.

Kleinbaum, D.G., & Klein, M., 2010. Logistic Regression: A Self-Learning Text (3rd ed.). Ed. by Springer, New Jersey, United States, 701 pp.

Köksal, F. et al., 2013. Fracture energy-based optimisation of steel fibre reinforced concretes. Engineering Fracture Mechanics, 107, pp.29–37.

König, G. & Kützing, L., 1999. Modelling the Increase of Ductility of HPC under Compressive Forces - A Fracture Mechanics Approach. Proceedings of the 3rd RILEM International Workshop on High Performance Fiber Reinforced Cement Composites (HPFRCC3), Mainz (Germany), pp.251–259.

Kützing, L. & König, G., 1999. Design Principals for Steel Fibre Reinforced Concrete - A Fracture Mechanics Approach. Leipzig Annual Civil Engineering Report (LACER4).

Kwan, A.K.H. & Ng, I.Y.T., 2007. Adding steel fibres to improve shock vibration resistance of concrete. Magazine of Concrete Research, 59(8), pp.587–597.

Larusson, L.H. & Fischer, G., 2012. Bond slip and crack development in FRC and regular concrete specimens longitudinally reinforced with FRP or steel under tension loading. In Bond in Concrete 2012. Bond in Concrete 2012. Brescia, Italy, pp. 847–854.

Lawler, J.S., Zampini, D. & Shah, S.P., 2005. Microfiber and Macrofiber Hybrid Fiber-Reinforced Concrete. Journal of Materials in Civil Engineering, 17(5), pp.595–604.

Lin, Y., Lin, Y.-F. & Hsiao, C., 2009. Evaluation of bond quality at the interface between steel bar and concrete using the small-dimension break-off test. Materials and Structures, 43(5), pp.583–595.

Lundgren, K., 2005. Bond between ribbed bars and concrete. Part 1: Modified model. Magazine of Concrete Research, 57(7), pp.371–382.

Lundgren, K. & Gylltoft, K., 2000. A Model for the Bond between Concrete and Reinforcement. Magazine of Concrete Research, 52(1), pp.53–63.

Makni, M. et al., 2012. Bond strength prediction using artificial neural network technique. In Bond in Concrete 2012. Bond in Concrete 2012. Brescia, Italy, pp. 55–62.

Malvar, L.J., Cox, J.V. & Cochran, K.B., 2003. Bond between Carbon Fiber Reinforced Polymer Bars and Concrete. I: Experimental Study. Journal of Composites for Construction, 7(2), pp.154–163.

Mathey, R.G. & Watstein, D., 1961. Investigation of Bond in Beam and Pull-Out Specimens with High-Yield-Strength Deformed Bars. ACI Journal Proceedings, 57(3), pp.1071–1090.

Mazaheripour, H. et al., 2012. Experimental and theoretical study on bond behavior of GFRP bars in steel fiber reinforced self compacting concrete. In Bond in Concrete 2012. Bond in Concrete 2012. Brescia, Italy, pp. 817–824.

Mazzarolo, E. et al., 2012. Long anchorage bond–slip formulation for modeling of r.c. elements and joints. Engineering structures, 34, pp.330–341.

Ministerio de Fomento, 2008. Instrucción Española de Hormigón Estructural EHE-08, Madrid, Spain, 304 pp.

Montgomery, D.C., 2009. Design and Analysis of Experiments (7th ed). Ed. by John Wiley & Sons, New Jersey, United States, 680 pp.

Morley, P.D. & Royles, R., 1983. Response of the Bond in Reinforced Concrete to High Temperatures. Magazine of Concrete Research, 35(123), pp.67–74.

Muttoni, A. & Fernández Ruiz, M., 2012. Influence of geometric, strain and size effects on bond in structural concrete. In Bond in Concrete 2012. Bond in Concrete 2012. Brescia, Italy, pp. 15–21.

Naaman, A.E., 2008. Development and evolution of tensile strain-hardening FRC composites. In 7th RILEM Symposium on Fibre Reinforced Concrete BEFIB2008. 7th RILEM Symposium on Fibre Reinforced Concrete BEFIB2008. Chennai, India, pp. 1–28.

Nammur, G. & Naaman, A.E., 1989. Bond Stress Model for Fiber Reinforced Concrete Based on Bond Stress-Slip Relationship. ACI Materials Journal, 86(1), pp.45–57.

Narayanan, R. & Darwish, I.Y.S., 1988. Fiber Concrete Deep Beams in Shear. ACI Structural Journal, 85(2), pp.141–149.

Nataraja, M.C., Dhang, N. & Gupta, A.P., 2000. Toughness characterization of steel fiber-reinforced concrete by JSCE approach. Cement and Concrete Research, 30(4), pp.593–597.

Nejadi, S. & Aslani, F., 2012. Bond of deformed reinforcing steel bars embedded in steel fiber reinforced self-compacting concrete. In Bond in Concrete 2012. Bond in Concrete 2012. Brescia, Italy, pp. 757–764.

Okelo, R. & Yuan, R.L., 2005. Bond Strength of Fiber Reinforced Polymer Rebars in Normal Strength Concrete. Journal of Composites for Construction, 9(3), pp.203–213.

Pajak, M. & Ponikiewski, T., 2013. Flexural behavior of self-compacting concrete reinforced with different types of steel fibers. Construction and Building Materials, 47, pp.397–408.

Parmentier, B., Vandewalle, L. & Van Rickstal, F., 2008. Evaluation of the scatter of the postpeak behaviour of fibre reinforced concrete in bending: A step towards reliability. 7th RILEM Symposium on Fibre Reinforced Concrete BEFIB2008 (Chennai, India), pp. 133–143.

Pereira, E.N.B., Barros, J.A.O. & Camões, A., 2008. Steel Fiber-Reinforced Self-Compacting Concrete: Experimental Research and Numerical Simulation. Journal of Structural Engineering, 134(8), pp.1310–1321.

Prisco, M., Plizzari, G. & Vandewalle, L., 2009. Fibre reinforced concrete: new design perspectives. Materials and Structures, 42(9), pp.1261–1281.

RILEM-CEB-FIP, 1970. Bond test for reinforcing steel: 2. Pull-Out Test. Materials and Structures, 3(3), pp.175–178.

RILEM, 1983 (1994), RC6–Bond test for reinforcement steel. 2. Pull-out test. RILEM Recommendations for the Testing and Use of Constructions Materials, pp. 218-220, ed. by E & FN SPON.

Robins, P.J. & Standish, I.G., 1984. The influence of lateral pressure upon anchorage bond. Magazine of Concrete Research, 36(129), pp.195–202.

Rossi, P., 1995. Les bétons de fibres métalliques. Presses de l'École des Ponts et Chaussées, Paris, France, 312 pp.

Russo, G. & Pauletta, M., 2006. A simple method for evaluating the maximum slip of anchorages. Materials and Structures, 39(5), pp.533–546.

Russo, G., Pauletta, M. & Mitri, D., 2009. Solution for bond distribution in asymmetric R.C. structural members. Engineering structures, 31(3), pp.633–641.

Russo, G., Zingone, G. & Romano, F., 1990. Analytical Solution for Bond-Slip of Reinforcing Bars in R.C. Joints. Journal of Structural Engineering, 116(2), pp.336–355.

Samen Ezeldin, A. & Balaguru, P.N., 1989. Bond Behavior of Normal and High-Strength Fiber Reinforced Concrete. ACI Materials Journal, 86(5).

Schumacher, P. et al., 2004. Bond of reinforcing bars in steel fiber reinforced concrete. In 5th International PhD Symposium in Civil Engineering. 5th International PhD Symposium in Civil Engineering. pp. 1205–1212.

Serna, P. & Arango, S.E., 2008. Evolution of the Flexural Behaviour of Precracked SFRC in Marine Environment. In 7th RILEM Symposium on Fibre Reinforced Concrete BEFIB2008. 7th RILEM Symposium on Fibre Reinforced Concrete BEFIB2008. Chennai, India, pp. 595–605.

Serna, P. et al., 2009. Structural cast-in-place SFRC: technology, control criteria and recent applications in spain. Materials and Structures, 42(9), pp.1233–1246.

Shah, A.A. & Ribakov, Y., 2011. Recent trends in steel fibered high-strength concrete. Materials & Design, 32(8-9), pp.4122–4151.

Shah, S.P. & Ferrara, L., 2008. Self Consolidating Fiber Reinforced Concrete. In 7th RILEM Symposium on Fibre Reinforced Concrete BEFIB2008. 7th RILEM Symposium on Fibre Reinforced Concrete BEFIB2008. Chennai, India, pp. 641–659.

Silva Filho, L.C.P. et al., 2012. Analysis of the influence of rebar geometry variations on bonding strength in the pull-out test. In Bond in Concrete 2012. Bond in Concrete 2012. Brescia, Italy, pp. 63–68.

Sivakumar, A. & Santhanam, M., 2007. Mechanical properties of high strength concrete reinforced with metallic and non-metallic fibres. Cement and Concrete Composites, 29(8), pp.603–608.

Song, P. & Hwang, S., 2004. Mechanical properties of high-strength steel fiber-reinforced concrete. Construction and Building Materials, 18(9), pp.669–673.

Soretz, S., 1972. A comparison of beam tests and pull-out tests. Materials and Structures, 5(4), pp.261–264.

Soretz, S. & Hölzenbein, H., 1979. Influence of Rib Dimensions of Reinforcing Bars on Bond and Bendability. ACI Journal, 76(1), pp.111–125.

Soroushian, P., Mirza, F. & Alhozaimy, A., 1994. Bonding of Confined Steel Fiber Reinforced Concrete to Deformed Bars. ACI Materials Journal, 91(2), pp.141–149.

Sustersic, J. et al., 2008. Behavior of concrete with very high fiber content. In 7th RILEM Symposium on Fibre Reinforced Concrete BEFIB2008. 7th RILEM Symposium on Fibre Reinforced Concrete BEFIB2008. Chennai, India, pp. 183–190.

Suwannakarm, S., Naaman, A.E. & El-Tawil, S., 2008. Stress versus crack opening displacement response of FRC composites with different fibers. 7th RILEM Symposium on Fibre Reinforced Concrete BEFIB2008 (Chennai, India), pp. 1039–1054.

Tanikella, P.N.D. & Gettu, R., 2008. On the distribution of fibers in self compacting concrete. 7th RILEM Symposium on Fibre Reinforced Concrete BEFIB2008 (Chennai, India), pp. 1147–1153.

Tastani, S.P. & Pantazopoulou, S.J., 2006. Bond of GFRP Bars in Concrete: Experimental Study and Analytical Interpretation. Journal of Composites for Construction, 10(5), p.381.

Tastani, S.P. & Pantazopoulou, S.J., 2010. Direct Tension Pullout Bond Test: Experimental Results. Journal of Structural Engineering, 136(6), pp.731–743.

Tastani, S.P. & Pantazopoulou, S.J., 2012. Modelling reinforcement-to-concrete bond. In Bond in Concrete 2012. Bond in Concrete 2012. Brescia, Italy, pp. 137–144.

Tavares, A.J. et al., 2012. Bond between steel-concrete: numerical analysis of the influence of geometrical parameters and the anchorage length. In Bond in Concrete 2012. Bond in Concrete 2012. Brescia, Italy, pp. 145–152.

Tepfers, R., 1973. A theory of bond applied to overlapped tensile reinforcement splices for deformed bars. PhD Thesis, Chalmers Univ. of Tech. (Göteborg, Sweden), Publication 73(2), 328 pp.

Tepfers, R., 1979. Cracking of Concrete Cover Along Anchored Deformed Reinforcing Bars. Magazine of Concrete Research, 31(106), pp.3–12.

Torrijos, M.C. et al., 2008. Orientation and distribution of steel fibres in self-compacting concrete. In 7th RILEM Symposium on Fibre Reinforced Concrete BEFIB2008. 7th RILEM Symposium on Fibre Reinforced Concrete BEFIB2008. Chennai, India, pp. 729–738.

Torrijos, M.C., Barragán, B.E. & Zerbino, R.L., 2010. Placing conditions, mesostructural characteristics and post-cracking response of fibre reinforced self-compacting concretes. Construction and Building Materials, 24(6), pp.1078–1085.

Turk, K., Caliskan, S. & Sukru Yildirim, M., 2003. Influence of loading condition and reinforcement size on the concrete/reinforcement bond strength. Structural Engineering and Mechanics, 19(3), pp.337–346.

Uygunoğlu, T., 2008. Investigation of microstructure and flexural behavior of steel-fiber reinforced concrete. Materials and Structures, 41(8), pp.1441–1449.

Vandewalle, L., Heirman, G. & Van Rickstal, F., 2008. Fibre orientation in self-compacting fibre reinforced concrete. In 7th RILEM Symposium on Fibre Reinforced Concrete BEFIB2008. 7th RILEM Symposium on Fibre Reinforced Concrete BEFIB2008. Chennai, India, pp. 719–728.

Walker, P.R., Batayneh, M.K. & Regan, P.E., 1997. Bond strength tests on deformed reinforcement in normal weight concrete. Materials and Structures, 30(7), pp.424–429.

Xiao, J. & Falkner, H., 2007. Bond behaviour between recycled aggregate concrete and steel rebars. Construction and Building Materials, 21(2), pp.395–401.

Xu, F. et al., 2012. Experimental Study on the Bond Behavior of Reinforcing Bars Embedded in Concrete Subjected to Lateral Pressure. ASCE Journal of Materials in Civil Engineering, 24(1), pp.125–133.

Yalciner, H., Eren, O. & Sensoy, S., 2012. An experimental study on the bond strength between reinforcement bars and concrete as a function of concrete cover, strength and corrosion level. Cement and Concrete Research, 42(5), pp.643–655.

Yao, W., Li, J. & Wu, K., 2003. Mechanical properties of hybrid fiber-reinforced concrete at low fiber volume fraction. Cement and Concrete Research, 33(1), pp.27–30.

Yazici, S. & Sahan Arel, H., 2013. The effect of steel fiber on the bond between concrete and deformed steel bar in SFRCs. Construction and Building Materials, 40, pp.299–305.

Yerex, L., Wenzel, T.H., & Davies, R., 1985. Bond Strength of Mild Steel in Polypropylene Fiber Reinforced Concrete. ACI Journal Proceedings, 82(1), pp.40–45.

Yun, H.D., Yang, I.S., Kim, S.W., Jeon, E., Choi, C.S., & Fukuyama, H., 2007. Mechanical properties of high-performance hybrid-fibre-reinforced cementitious composites. Magazine of Concrete Research, 59(4), pp.257–2715.

A1 | Fundamentals of Statistical Design of Experiments (DOE)

Appendices

A1 | Fundamentals of Statistical Design of Experiments

A2 | Bond Stress – Slip Curves (Type I Series)

A3 | Bond Stress – Slip Curves (Type II Series)

A4 | Bond Stress – Slip Curves (Type III Series)

Líneas básicas del diseño y análisis de experimentos

Serna, P., Taengua, E.G.
Dpto. de Ing. de la Construcción y Proyectos de Ing. Civil
Universitat Politècnica de València

1. Objetivo del texto

En el presente escrito se pretende exponer el procedimiento general del Diseño de Experimentos, desarrollado a partir de los trabajos de Taguchi [1].

2. Introducción

Frecuentemente, cuando se plantea una investigación experimental, se pretende analizar de qué factores depende una propiedad determinada (diseño factorial) y, en su caso, obtener una función que relacione el valor de dicha propiedad con los de los valores que pueden tomar los factores[1].
Ante un problema como éste, el procedimiento a seguir es el siguiente:

1. Definición de la/s característica/s a estudiar, que serán las variables respuesta.
2. Selección de los factores a considerar en el experimento y decisión de los niveles de variación a estudiar para cada factor.
   Debe seleccionarse el número de factores y los niveles a estudiar con criterio económico: reducirlos a un número mínimo pero intentando controlar el máximo de efectos. Reducir en exceso los factores o niveles puede conducir a la pérdida del sentido del estudio y con ello a resultados incorrectos.
3. Decisión del número de pruebas a realizar y definición de las mismas.

Así, si se desea conocer de qué depende el módulo de elasticidad de un hormigón fabricado con áridos reciclados, se puede pensar en un conjunto de factores y niveles de los mismos como la que se presenta en la tabla 1.

[1] Puede haber experimentos que, por naturaleza, no puedan organizarse según un diseño factorial, como los de carácter sociológico (v.g. encuestas), aunque en ciencia e ingeniería la mayoría de experimentos se pueden someter a un diseño factorial. Es por ello que en adelante cuando hablemos de diseño de un experimento nos estaremos refiriendo a diseños factoriales.

FACTORES	NIVELES DE VARIACIÓN
Calidad del hormigón de origen de los áridos recibidos (f_c)	f_c = 25 ; 35
Contenido en desclasificados (%)	6% ; 10 %
Calidad del hormigón objetivo ($f_{c,obj}$)	$f_{c,obj}$ = 20 ; 40
Sustitución del árido grueso por árido reciclado (%)	20% ; 100 %
Criterio de sustitución	2 niveles: mg (-10% ; +10%)

Tabla 1. Ejemplo de planteamiento de factores y niveles para un experimento.

En la decisión de qué factores considerar en el experimento juega un papel importante tanto el conocimiento empírico o teórico que se tenga del fenómeno estudiado como la intuición de lo que pueda ser o no influyente. El acierto en la elección de los niveles también es importante: un factor puede aparecer como significativo simplemente porque la diferencia entre los niveles del mismo sea grande.

El número de pruebas de que conste el experimento deberá surgir de un compromiso entre: el nivel de resolución o fiabilidad que se quiere tener de las conclusiones (tanto mayor cuantas más pruebas se hagan) y la minimización del tiempo invertido en el experimento. En este sentido, recurrir al uso de fracciones factoriales será de gran ayuda.

Un estudio completo de esta programación exigiría realizar un plan de ensayos que contemplaría 2 x 2 x 2 x 2 x 3 = 48 combinaciones distintas.

Para reducir el número de ensayos es frecuente optar por plantear un ensayo tipo y sobre él analizar el efecto de las variaciones de cada factor por separado. En el ejemplo propuesto anteriormente, el caso tipo podría ser: un hormigón base de 25 MPa, del que se fabrican áridos reciclados con un porcentaje de desclasificados del 6%, se utilizará para fabricar un H40 sustituyendo el 20% del árido grueso manteniendo la granulometría. El efecto del contenido en desclasificados se analizaría añadiendo 1 ensayo que coincidiría con el ensayo base en todo, salvo en el factor que se estudia, que tomaría el valor del 10%. Los otros factores se analizarían del mismo modo actuando siempre alrededor del ensayo base. De este modo, el estudio se realizaría con solo 6 ensayos.

Sin embargo, este modo de proceder no es estadísticamente el más adecuado. Para compaginar la economía en esfuerzo experimental pero manteniendo el rigor científico en el diseño del programa de ensayos, nos apoyaremos en principios estadísticos.

3. Consideraciones para el diseño de experimentos

Cuando se plantea diseñar un programa de ensayos, se deben tener en cuenta aspectos como:

- Los objetivos de experimentos con un número considerable de factores pueden no conseguirse con diseños que intenten esclarecer uno a uno el efecto de los distintos factores. Es incorrecto presuponer que el valor óptimo de la variable respuesta es el óptimo de los óptimos parciales conseguidos variando solamente un factor cada vez y dejando el resto fijos.
- Principios erróneos como el mencionado pueden conducir a pérdidas de tiempo y recursos o a resultados no concluyentes.
- Factores no controlados comprometen las conclusiones del experimento.
- La no observancia de un mismo procedimiento y condiciones en todas las pruebas que constituyen el experimento puede enmascarar el efecto de los distintos factores.

Un uso efectivo de los principios estadísticos en el diseño de experimentos permite un diseño económico y eficiente de los mismos, que permite evaluar los efectos individuales y sus interacciones [2].

Aquí plantearemos un procedimiento para el diseño de experimentos, cuyo soporte estadístico es el análisis de la varianza o ANOVA.

El procedimiento que se propone consiste en seleccionar un número reducido de pruebas, de manera que del estudio de sus resultados sea posible extraer suficientes información para garantizar un análisis de la influencia de los distintos factores con garantías.

4. Terminología

- **Factor.** Variable controlable experimentalmente que se supone puede tener un efecto sobre la llamada variable respuesta.
- **Variable respuesta.** Resultado de un experimento.
- **Prueba.** Combinación de los factores, cada uno a un nivel de variación determinado, a la cual va asociada una observación experimental de la variable respuesta.
- **Niveles.** Valores prefijados que puede tomar un factor.

- **Diseño o experimento.** Especificación de un conjunto de pruebas experimentales, obtenidas asignando diferentes valores a los factores y pudiendo haber replicaciones.
- **Replicación.** Repetición de una prueba (o de un conjunto de ellas) dos o más veces.
- **Efecto.** Cambio en la variable respuesta que se produce entre 2 condiciones experimentales. En concreto, el efecto que produce un factor sobre la variable respuesta es la variación del valor de la misma al variar el factor.
- **Interacción entre 2 o más factores.** Existe si el efecto de uno de ellos depende de los niveles de los otros factores implicados en la interacción.
- **Orden de una interacción.** Número de factores implicados en la misma. Los efectos de las interacciones de orden mayor que 2 suelen ser inexistentes, [2].

5. Procedimiento para el diseño del experimento

Se plantearán diseños de tipo fracción factorial, en los que el número de pruebas se ve reducido en relación al diseño factorial completo de acuerdo con criterios que son válidos desde un punto de vista estadístico.

Los planes factoriales altamente fraccionados, más conocidos como **orthogonal arrays**, nacieron de los trabajos de Taguchi [1], orientados a generalizar y facilitar la aplicación del Diseño de Experimentos en círculos industriales, y por extensión a los investigadores en general, sin precisar de grandes conocimientos estadísticos. Con ellos se consigue [2] estudiar el efecto de un número elevado de factores con pocas pruebas, a cambio de desestimar el efecto de las interacciones de orden elevado (de más de 2 efectos, cuya importancia sería de todas formas despreciable).

La elección del orthogonal array que conviene utilizar en cada caso depende del número de factores a estudiar y los niveles de variación de cada uno. Los más comunes se muestran en el anejo “Catálogo de orthogonal arrays”. La denominación que se les da es del tipo *Lx*, donde x es el número de pruebas de que consta el array.

Por ejemplo, si se pretende diseñar un experimento que permita el estudio de hasta 7 factores a 2 niveles sobre una variable respuesta dada, se puede recurrir al orthogonal array L8, mostrado en la tabla 2.

En ella cada columna *j* corresponde a un factor, mientras que cada fila *i* corresponde a una prueba de las que conforman el experimento. Así pues, el elemento *ij* indicará el nivel al que se debe fijar el factor *j* en la prueba *i*.

Prueba	1	2	3	4	5	6	7
1	1	1	1	1	1	1	1
2	1	1	1	2	2	2	2
3	1	2	2	1	1	2	2
4	1	2	2	2	2	1	1
5	2	1	2	1	2	1	2
6	2	1	2	2	1	2	1
7	2	2	1	1	2	2	1
8	2	2	1	2	1	1	2

Tabla 2. Orthogonal array L8.

Una buena fracción factorial no confunde nunca efectos simples entre sí. Sin embargo, debido al tan reducido número de pruebas con que se trabaja, es habitual que los efectos de las interacciones se confundan con los efectos simples de los factores estudiados. Por ello cada orthogonal array se acompaña de una tabla de doble entrada que recibe el nombre de tabla de interacciones. En la mayoría de casos en que se recurre a un orthogonal array para diseñar un experimento no se utilizan todas las columnas del mismo, puesto que el número de factores considerados normalmente es menor al número de factores que permite estudiar el orthogonal array. En esos casos conviene elegir las columnas a utilizar intentando no tomar aquéllas en las que se confunden interacciones de otras columnas también escogidas, y para eso se utiliza la tabla de interacciones. En la tabla 3 se muestra como ejemplo la tabla de interacciones del orthogonal array L8.

1	2	3	4	5	6	7
1	3	2	5	4	7	6
	2	1	6	7	4	5
		3	7	6	5	4
			4	1	2	3
				5	3	2
					6	1

Tabla 3. Tabla de interacciones del orthogonal array L8.

Elegidas dos columnas cualesquiera del orthogonal array, por ejemplo la 2 y la 4, en la tabla de interacciones se observa que la interacción de los efectos simples de estas columnas se recoge en la columna 6. Si tomásemos también esta columna del

orthogonal array para otro factor, al estudiar su efecto estaríamos confundiendo el efecto simple de cada factor con los efectos simples de los otros dos.

Si por exigencias del propio experimento el número de factores es tal que obliga a emplear columnas del orthogonal array que incluyan interacciones, cuando posteriormente se analicen los resultados del experimento habrá que tener en cuenta que los efectos simples de los factores incluirán también parte del efecto de determinadas interacciones. Puesto que a la vista de la tabla de interacciones se puede saber cuáles son las que inerfieren cada efecto simple, o bien se pueden plantear experimentos adicionales destinados a clarificarlo, o bien se puede tener de antemano conocimiento de la importancia o no de las interacciones en cuestión.

Por último, es bastante común que se quieran considerar en un experimento un número de factores y/o niveles que no coincidan exactamente con ningún orthogonal array de los que se manejan usualmente. En ese caso, Romero y Zúnica [3], proponen unos "trucos" para la adaptación de un orthogonal array al número deseado de factores y/o niveles, y que son totalmente válidos porque no alteran las propiedades fundamentales del orthogonal array[2]. Son los siguientes:

1. En una columna de un factor a 3 niveles es posible acomodar un factor a 2 niveles haciendo equivalentes 2 de los 3 niveles primitivos. Se tiene un ejemplo en la tabla 4.
2. En cualquier diseño con factores a 2 niveles es posible acomodar un factor a 4 niveles usando 2 columnas cualesquiera y la correspondiente a su interacción. Se tiene un ejemplo en la tabla 5.
3. En un diseño con factores a 2 niveles es posible acomodar un factor a 3 niveles usando el truco 2 y luego haciendo equivalentes 2 de los nuevos 4 niveles.

Nº prueba	FACTOR A
1	1
2	2
3	3
4	1
5	2
6	3
7	1
8	2
9	3

Nº prueba	FACTOR A
1	1
2	2
3	1
4	1
5	2
6	1
7	1
8	2
9	1

Tabla 4. Ejemplo del truco 1.

Nº prueba	FACTOR A	FACTOR B
1	1	1
2	1	2
3	1	1
4	1	2
5	2	1
6	2	2
7	2	1
8	2	2

	A * B
1 * 1 →	1
1 * 2 →	2
1 * 1 →	1
1 * 2 →	2
2 * 1 →	3
2 * 2 →	4
2 * 1 →	3
2 * 2 →	4

Tabla 5. Ejemplo del truco 2.

[2] Propiedades fundamentales de los orthogonal arrays, que son intrínsecas a la construcción de los mismos. No han sido descritas en el presente escrito por excederse del alcance del mismo.

6. Indicaciones para el desarrollo del experimento

Lo más aconsejable es que la secuencia de realización de las pruebas no siga ningún orden, ya que una secuenciación excesiva de las pruebas podría introducir interferencias anómalas en el experimento, como errores por distracción del experimentador en las últimas pruebas.

Si se incluyen ***replicaciones*** o repeticiones de las pruebas, ha de actuarse, siempre que sea posible, de forma equilibrada: se hablará de ***diseño balanceado o equilibrado*** cuando todas las pruebas se repitan un mismo número de veces. Esto permitirá analizar el error experimental (ya que una misma prueba no proporciona 2 veces el mismo resultado exactamente). Además, las replicaciones aumentan los grados de libertad del experimento, teniéndose un análisis más robusto.

7. Análisis de los resultados: ANOVA

Una vez realizado el experimento y obtenidos los resultados, la variabilidad en los valores que ha tomado la variable respuesta se debe a:

1. A la variación de los factores estudiados según sus niveles.
2. A factores no considerados y al *ruido* experimental, que es el propio error inherente a cualquier experimento.

La variabilidad de la variable respuesta se recoge en lo que se llama la suma de cuadrados del experimento, que conceptualmente se asimila a la suma de errores al cuadrado:

$$SC_{TOTAL} = \sum_{i} \left(x_i - \bar{x}\right)^2$$

Siguiendo la idea de que la variabilidad total del experimento es la suma de una variabilidad debida a los factores y de una variabilidad no controlada o *residual*, se tiene:

$$SC_{TOTAL} = \sum SC_{FACTORES} + SC_{RESIDUAL}$$

Resulta obvio que la influencia de un factor determinado sobre la variabilidad de la variable respuesta será tanto más importante cuanto mayor sea la suma de cuadrados

asociada a éste, o dicho de otro modo: a mayor suma de cuadrados de un factor, más influyente es.

No obstante, la afirmación anterior se tiene que matizar, porque no es lo mismo un factor con 2 niveles de variación que uno con 4 niveles. En este sentido, es fácil entender que un factor para el que se han considerado muchos niveles de variación producirá mayor variabilidad en la respuesta que un factor considerado a pocos niveles.

Para relativizar la influencia de cada factor en la variabilidad de la variable respuesta en función del número de niveles considerado para cada uno, se introduce el concepto de *grados de libertad* tanto del experimento como de los factores, y a continuación el concepto de *cuadrado medio*, que es el cociente entre la suma de cuadrados y los grados de libertad del factor (la relativización de la suma de cuadrados según el número de niveles del factor).

Si el experimento consta en total de un número N de pruebas, entonces se dice que el experimento tiene N-1 grados de libertad totales.

Un factor F_i para el que se consideran N_{fi} niveles, tendrá N_{fi}-1 grados de libertad.

La diferencia entre los grados de libertad totales y la suma de los grados de libertad de todos los factores es igual a los grados de libertad del *residuo*. En este sentido, se habla de residuo como un factor más, y es el que agruparía toda la parte de variación que no queda explicada por los factores.

En resumen, se tiene:

Grados de libertad totales: $glt = N - 1.$

Grados de libertad de los factores: $glf = \sum_i (N_{fi} - 1).$

Grados de libertad residuales: $glr = glt - glf.$

En general se recomienda que $glr \geq 4$ para que un ANOVA se pueda considerar robusto, esto es, para que las conclusiones que de él se derivan se puedan considerar como tales. Hay diversas formas de aumentar los grados de libertad residuales en fase de diseño del experimento:

- Aumentar el número de pruebas.
- Reducir el número de factores considerados.
- Replicar el diseño (realizar todas las pruebas 2 veces).

El análisis de la varianza se suele hacer con la ayuda de paquetes informáticos, por lo que interesa comentar cómo se deben interpretar los resultados de los mismos, tanto en forma de tablas como salidas gráficas.

8. Análisis de la varianza (ANOVA) con Statgraphics*

Este epígrafe no pretende ser un manual del software Statgraphics, sino una iniciación a la interpretación de las tablas de anova y los gráficos del análisis de la varianza necesarios para poder pretender realizar un buen diseño del experimento.

Tras introducir los datos y resultados del experimento en el programa y solicitar el análisis de la varianza, el programa realiza contrastes de hipótesis y se obtiene una tabla de anova, que tiene el siguiente aspecto:

Analysis of Variance for DIAMETER - Type III Sums of Squares

Source	Sum of Squares	Df	Mean Square	F-Ratio	P-Value
MAIN EFFECTS					
A:ADMIXTURE	21896,8	2	10948,4	3,55	0,0397
B:CEMENT	11193,6	2	5596,82	1,82	0,1781
C:FILLER	23011,3	3	7670,43	2,49	0,0769
D:GRAVEL	6543,29	2	3271,64	1,06	0,3571
E:SAND	15466,4	3	5155,48	1,67	0,1912
F:WATER	10467,2	2	5233,59	1,70	0,1982
RESIDUAL	104776,0	34	3081,66		
TOTAL (CORRECTED)	191167,0	48			

All F-ratios are based on the residual mean square error.

Cada fila de la tabla corresponde a uno de los factores considerados. En la columna **Df** se indican los grados de libertad de los factores y los que quedan para el residuo.

Antes de comenzar a sacar conclusiones debemos comprobar que el número de grados de libertad residuales es superior a 4.

Observando los p-valores mostrados en la columna **P-Value**, aquellos factores con p-valor *igual o inferior a 0,05* serán considerados estadísticamente significativos: tienen un efecto considerable sobre la variable respuesta. El valor límite de p-valor igual a 0,05 resulta de admitir una confianza del 95%.

Los factores con p-valores muy grandes son claramente no significativos. La forma lógica de proceder con ellos es eliminarlos y repetir el análisis sin tomarlos en consideración. Se procede así porque, ya que se conoce que un factor no es influyente,

* Statgraphics Plus 5.1, © 1994 – 2001 Statistical Graphics Corp.

al no considerarlo se están ganando grados de libertad para el residuo, y con ello se clarifica más la consideración de significancia o no de los efectos de los otros factores.
En el caso de la tabla anterior, el factor ADMIXTURE aparece con un p-valor = 0,0397, por lo que su efecto sobre DIAMETER es estadísticamente significativo. Para FILLER se tiene un p-valor = 0,0769, próximo a 0,05 aunque superior. El factor GRAVEL, con un p-valor = 0,3571 es claramente no influyente. No considerándolo se obtiene:

Analysis of Variance for DIAMETER - Type III Sums of Squares

Source	Sum of Squares	Df	Mean Square	F-Ratio	P-Value
MAIN EFFECTS					
A:ADMIXTURE	22554,8	2	11277,4	3,65	0,0361
B:CEMENT	9618,87	2	4809,44	1,56	0,2250
C:FILLER	24604,4	3	8201,46	2,65	0,0633
D:SAND	16382,1	3	5460,7	1,77	0,1711
E:WATER	10868,1	2	5434,04	1,76	0,1870
RESIDUAL	111320,0	36	3092,22		
TOTAL (CORRECTED)	191167,0	48			

All F-ratios are based on the residual mean square error.

En esta segunda tabla de anova se tiene el factor FILLER con un p-valor = 0,0633, se ha visto disminuido respecto del valor que tenía en la tabla anterior y queda aún más cercano a 0,05. Por ello, en este caso se podría concluir que dicho factor también es influyente, aunque esta afirmación ya no cuenta con un nivel de confianza del 95%, sino del 100 – 6,33 = 93,67%. Por lo tanto, sólo ADMIXTURE y FILLER tienen un efecto estadísticamente significativo sobre la variable respuesta DIAMETER; el resto, no.
Existe también una forma gráfica para deducir las conclusiones anteriores, referentes a qué factores son influyentes y cuáles no: son los **gráficos de intervalos LSD** (siglas de *Least Significative Difference*). En ellos se representa un segmento para cada nivel del factor seleccionado. En el caso de factores de tipo cualitativo[3], cuando los segmentos se solapan entre sí, la influencia del factor no es estadísticamente influyente; cuando los segmentos claramente no se solapan, el factor es influyente. En la figura 1 se muestra un ejemplo de cada caso. En el caso de factores de tipo cuantitativo no se puede concluir que un factor sea significativo o no a partir de un gráfico de intervalos

[3] Un factor de tipo cualitativo es aquél que no es continuo. Por ejemplo, el hecho de usar cohesionante o no en la fabricación del hormigón, tendríamos el factor COHESIONANTE con dos niveles: sí y no, que normalmente se denotan por 1 y 0.

LSD, éste simplemente aportaría información de la tendencia (crecimiento, decrecimiento, forma cuadrática, etc) en la variable respuesta producida por la variación del factor.

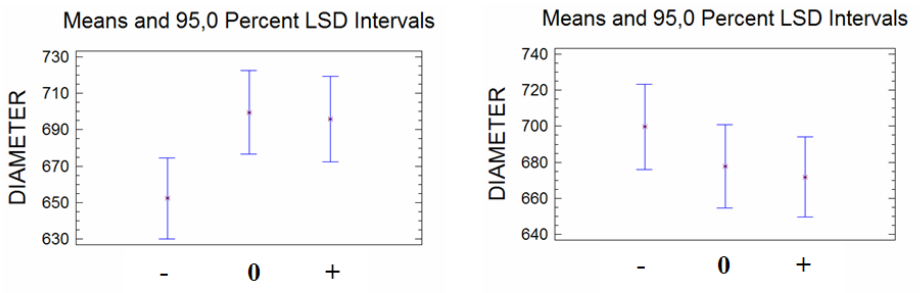

Fig. 1. Comparación del gráfico LSD de un factor cualitativo influyente con otro no influyente.

9. Estudios de regresión con Statgraphics

Tras determinar con el análisis de la varianza los factores que tienen un efecto estadísticamente significativo sobre una variable respuesta, el objetivo último de un estudio de regresión es llegar a obtener una expresión matemática que estime los valores de una variable aleatoria Y a partir de los valores de una o más variables (aleatorias o no) de las que la primera depende, X_i, que ecuación que constituirá la formulación matemática de un modelo.

Las consideraciones teóricas y cálculos que se realizan en un estudio de regresión no se tratarán en el presente texto porque los estudios de regresión en la práctica se llevan a cabo con la ayuda de un paquete informático. Aquí se seguirá utilizando el Statgraphics.

En una primera aproximación, se considerarán sólo aquellos factores cuyo efecto ha resultado ser estadísticamente significativo en el análisis de la varianza. Tras ello, se obtiene una tabla como la siguiente:

Multiple Regression Analysis

Dependent variable: DIAMETER

Parameter	Estimate	Standard Error	T Statistic	P-Value
CONSTANT	-1243,88	8601,97	-0,144604	0,8857
ADMIXTURE	3375,4	2230,37	1,51338	0,1375
FILLER	-119,846	73,6768	-1,62665	0,1111
ADMIXTURE^2	-274,921	185,952	-1,47845	0,1466
FILLER^2	0,397021	0,245933	1,61435	0,1138
WATER/CEMENT	1099,53	403,822	2,7228	0,0093

Analysis of Variance

Source	Sum of Squares	Df	Mean Square	F-Ratio	P-Value
Model	57841,7	5	11568,3	3,73	0,0068
Residual	133326,0	43	3100,6		
Total (Corr.)	191167,0	48			

R-squared = 30,2571 percent
R-squared (adjusted for d.f.) = 22,1474 percent
Standard Error of Est. = 55,688
Mean absolute error = 40,0141
Durbin-Watson statistic = 2,84462 (P=0,0008)
Lag 1 residual autocorrelation = -0,423571

Para interpretar los resultados, la atención debe centrarse especialmente en lo que ha sido recuadrado en rojo: las columnas **Parameter**, **P-Value** y los valores de **R-squared**.

En la columna **Parameter** encontraremos, además de los factores que han sido considerados en el estudio de regresión, un factor llamado CONSTANT que el programa considera por defecte y que se correspondería con la constante aditiva de la ecuación, lo que en una recta sería la ordenada en el origen.

El **P-Valor** de nuevo indica la significancia de la introducción del factor en cuestión en el modelo. Así, los que aparezcan con un p-valor > 0,05 son aquéllos cuya consideración o no consideración en el modelo no afecta especialmente al nivel de ajuste obtenido. Dichos factores deben ser excluídos del modelo porque no contribuyen demasiado al buen ajuste del modelo y sin embargo sí que complican la ecuación obtenida añadiendo términos innecesarios.

Una vez eliminados, se repite el análisis con sólo los factores con p-valores < 0,05. Diremos que un ajuste o estudio de regresión es "bueno" cuando los valores que proporciona la ecuación encontrada en función de los factores se aproximan considerablemente a los valores realmente observados. El parámetro **R-squared** o R^2 es una medida de este ajuste: un R^2 próximo al 100% indica que la ecuación que se ha

encontrado con la regresión es prácticamente la "exacta", mientras que un R^2 bajo indica que no se ha conseguido un buen ajuste. El programa también proporciona un valor **R-squared (adjusted for d.f.)**, que no es más que el valor de R^2 "relativizado" al tamaño del experimento, y sólo sirve para comparar la calidad de las regresiones conseguidas en experimentos con distinto número de pruebas.

Se tiene que llegar a un compromiso entre la exactitud (maximizar el R^2 del ajuste) y la simplicidad de la ecuación. Para aumentar el valor del R^2 se procederá a ir modificando los factores considerados, interacciones e incluso funciones de los factores (exponencial, elevado al cuadrado, etc), retirando los que presenten p-valores > 0,05. Es importante destacar que la ecuación que se encuentre debe revestir un cierto significado físico, y en la mayoría de casos no tendrá sentido considerar funciones extrañas.

El mismo programa proporcionará el valor de la ecuación correspondiente al ajuste, y en este punto hay que recordar que no siempre se podrá llegar hasta esta situación: puede que la variable que se trata de relacionar con los factores presente demasiada variabilidad no controlada, que no se hayan considerado los factores adecuados, o que simplemente el experimento esté mal concebido.

Por último, cualquier paquete informático ofrece salidas gráficas interesantes también a nivel de los estudios de regresión. Por ejemplo, el Statgraphics ofrece la posibilidad de representar, una vez hecha la regresión, los valores observados frente a los calculados de la variable respuesta, de forma que cuanto más centrada esté la nube de puntos en torno a la recta bisectriz, mayor será la precisión de la ecuación obtenida. En la figura 2 se compara la gráfica de observados-calculados en un regresión con buen ajuste con la obtenida en una regresión con mal ajuste.

Fig.2. Comparación de un buen ajuste (izquierda) con un mal ajuste (dcha.).

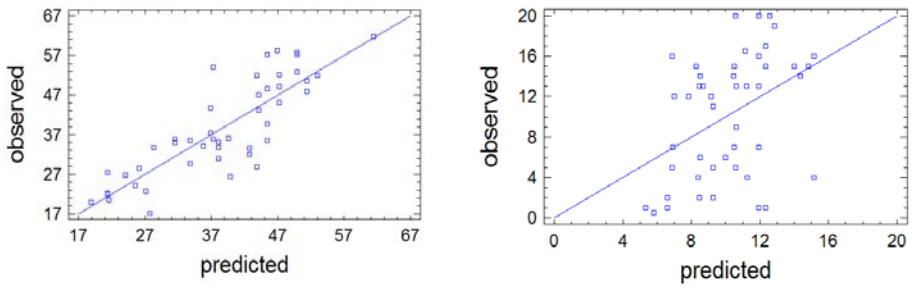

Anejo: Catálogo de orthogonal arrays [4]

L8

Permite estudiar hasta 7 factores (todos a 2 niveles) en 8 pruebas.

Orthogonal array

Prueba	F1	F2	F3	F4	F5	F6	F7
1	1	1	1	1	1	1	1
2	1	1	1	2	2	2	2
3	1	2	2	1	1	2	2
4	1	2	2	2	2	1	1
5	2	1	2	1	2	1	2
6	2	1	2	2	1	2	1
7	2	2	1	1	2	2	1
8	2	2	1	2	1	1	2

Tabla de interacciones

1	2	3	4	5	6	7
1	3	2	5	4	7	6
	2	1	6	7	4	5
		3	7	6	5	4
			4	1	2	3
				5	3	2
					6	1

[4] Tomados de Romero y Zúnica, [3].

L16

Permite estudiar hasta 15 factores (todos a 2 niveles) en 16 pruebas.

Orthogonal array

Prueba	F1	F2	F3	F4	F5	F6	F7	F8	F9	F10	F11	F12	F13	F14	F15
1	1	1	1	1	1	1	1	1	1	1	1	1	1	1	1
2	1	1	1	1	1	1	1	2	2	2	2	2	2	2	2
3	1	1	1	2	2	2	2	1	1	1	1	2	2	2	2
4	1	1	1	2	2	2	2	2	2	2	2	1	1	1	1
5	1	2	2	1	1	2	2	1	1	2	2	1	1	2	2
6	1	2	2	1	1	2	2	2	2	1	1	2	2	1	1
7	1	2	2	2	2	1	1	1	1	2	2	2	2	1	1
8	1	2	2	2	2	1	1	2	2	1	1	1	1	2	2
9	2	1	2	1	2	1	2	1	2	1	2	1	2	1	2
10	2	1	2	1	2	1	2	2	1	2	1	2	1	2	1
11	2	1	2	2	1	2	1	1	2	1	2	2	1	2	1
12	2	1	2	2	1	2	1	2	1	2	1	1	2	1	2
13	2	2	1	1	2	2	1	1	2	2	1	1	2	2	1
14	2	2	1	1	2	2	1	2	1	1	2	2	1	1	2
15	2	2	1	2	1	1	2	1	2	2	1	2	1	1	2
16	2	2	1	2	1	1	2	2	1	1	2	1	2	2	1

Tabla de interacciones

1	2	3	4	5	6	7	8	9	10	11	12	13	14	15
1	3	2	5	4	7	6	9	8	11	10	13	12	15	14
	2	1	6	7	4	5	10	11	8	9	14	15	12	13
		3	7	6	5	4	11	10	9	8	15	14	13	12
			4	1	2	3	12	13	14	15	8	9	10	11
				5	3	2	13	12	15	14	9	8	11	10
					6	1	14	15	12	13	10	11	8	9
						7	15	14	13	12	11	10	9	8
							8	1	2	3	4	5	6	7
								9	3	2	5	4	7	6
									10	1	6	7	4	5
										11	7	6	5	4
											12	1	2	3
												13	3	2
													14	1

L9

Permite estudiar hasta 4 factores a 3 niveles en 9 pruebas.

Orthogonal array

Prueba	F1	F2	F3	F4
1	1	1	1	1
2	1	2	2	2
3	1	3	3	3
4	2	1	2	3
5	2	2	3	1
6	2	3	1	2
7	3	1	3	2
8	3	2	1	3
9	3	3	2	1

No se acompaña tabla de interacciones porque cada interacción doble se “reparte” entre los efectos simples de los otros factores.

L18

Permite estudiar 1 factor a 2 niveles y hasta 7 factores a 3 niveles en 18 pruebas.

Orthogonal array

Prueba	F1	F2	F3	F4	F5	F6	F7	F8
1	1	1	1	1	1	1	1	1
2	1	1	2	2	2	2	2	2
3	1	1	3	3	3	3	3	3
4	1	2	1	1	2	2	3	3
5	1	2	2	2	3	3	1	1
6	1	2	3	3	1	1	2	2
7	1	3	1	2	1	3	2	3
8	1	3	2	3	2	1	3	1
9	1	3	3	1	3	2	1	2
10	2	1	1	3	3	2	2	1
11	2	1	2	1	1	3	3	2
12	2	1	3	2	2	1	1	3
13	2	2	1	2	3	1	3	2
14	2	2	2	3	1	2	1	3
15	2	2	3	1	2	3	2	1
16	2	3	1	3	2	3	1	2
17	2	3	2	1	3	1	2	3
18	2	3	3	2	1	2	3	1

Tampoco se acompaña tabla de interacciones porque sucede lo mismo que en el L9.

L27

Permite estudiar hasta 13 factores a 3 niveles en 27 pruebas.

Orthogonal array

Prueba	F1	F2	F3	F4	F5	F6	F7	F8	F9	F10	F11	F12	F13
1	1	1	1	1	1	1	1	1	1	1	1	1	1
2	1	1	1	1	2	2	2	2	2	2	2	2	2
3	1	1	1	1	3	3	3	3	3	3	3	3	3
4	1	2	2	2	1	1	1	2	2	2	3	3	3
5	1	2	2	2	2	2	2	3	3	3	1	1	1
6	1	2	2	2	3	3	3	1	1	1	2	2	2
7	1	3	3	3	1	1	1	3	3	3	2	2	2
8	1	3	3	3	2	2	2	1	1	1	3	3	3
9	1	3	3	3	3	3	3	2	2	2	1	1	1
10	2	1	2	3	1	2	3	1	2	3	1	2	3
11	2	1	2	3	2	3	1	2	3	1	2	3	1
12	2	1	2	3	3	1	2	3	1	2	3	1	2
13	2	2	3	1	1	2	3	2	3	1	3	1	2
14	2	2	3	1	2	3	1	3	1	2	1	2	3
15	2	2	3	1	3	1	2	1	2	3	2	3	1
16	2	3	1	2	1	2	3	3	1	2	2	3	1
17	2	3	1	2	2	3	1	1	2	3	3	1	2
18	2	3	1	2	3	1	2	2	3	1	1	2	3
19	3	1	3	2	1	3	2	1	3	2	1	3	2
20	3	1	3	2	2	1	3	2	1	3	2	1	3
21	3	1	3	2	3	2	1	3	2	1	3	2	1
22	3	2	1	3	1	3	2	2	1	3	3	2	1
23	3	2	1	3	2	1	3	3	2	1	1	3	2
24	3	2	1	3	3	2	1	1	3	2	2	1	3
25	3	3	2	1	1	3	2	3	2	1	2	1	3
26	3	3	2	1	2	1	3	1	3	2	3	2	1
27	3	3	2	1	3	2	1	2	1	3	1	3	2

Tabla de interacciones

1	2	3	4	5	6	7	8	9	10	11	12	13
1	3	2	2	6	5	5	9	8	8	12	11	11
	4	4	3	7	7	6	10	10	9	13	13	12
	2	1	1	8	9	10	5	6	7	5	6	7
		4	3	11	12	13	11	12	13	8	9	10
		3	1	9	10	8	7	5	6	6	7	5
			2	13	11	12	12	13	11	10	8	9
			4	10	8	9	6	7	5	7	5	6
				12	13	11	13	11	12	9	10	8
				5	1	1	2	3	4	2	4	8
					7	6	11	13	12	8	10	9
					6	1	4	2	3	8	2	4
						5	13	12	11	10	9	8
						7	3	4	2	4	3	2
							12	11	13	9	8	10
							8	1	1	2	3	4
								10	9	5	7	6
								9	1	4	2	3
									8	7	6	5
									10	3	4	2
										6	7	7
										11	1	1
											13	12
											12	1
												11

Bibliografía (Appendix A1)

1. Taguchi, G., *System of experimental Design: Engineering Methods to optimize Quality and minimize Costs*. Ed. Unipub, New York, Estados Unidos, 1988.
2. Mason et al., *Statistical Design and Analysis of Experiments*. Ed. John Wiley and Sons, Estados Unidos, 2003.
3. *R. Romero y L. Zúnica*, Estadística: diseño de experimentos, modelos de regresión. *Editado por el Servicio de Publicaciones de la Univ. Politécnica de Valencia*, Valencia, 1993.

A2| Bond Stress – Slip Curves (Type I Series)

Appendices

A1| Fundamentals of Statistical Design of Experiments

A2| Bond Stress – Slip Curves (Type I Series)

A3| Bond Stress – Slip Curves (Type II Series)

A4| Bond Stress – Slip Curves (Type III Series)

Specimen I L1 1

Descriptors		
Rebar diameter =	16	mm
Cover/Diameter =	1,875	
Fiber content =	40	kg/m3
Fiber type =	65_60	

Bond Parameters		
Bond strength =	4,75	MPa
Area A_peak =	3,97	mmMPa
Area A_80 =	9,58	mmMPa
Area A_50 =	21,90	mmMPa

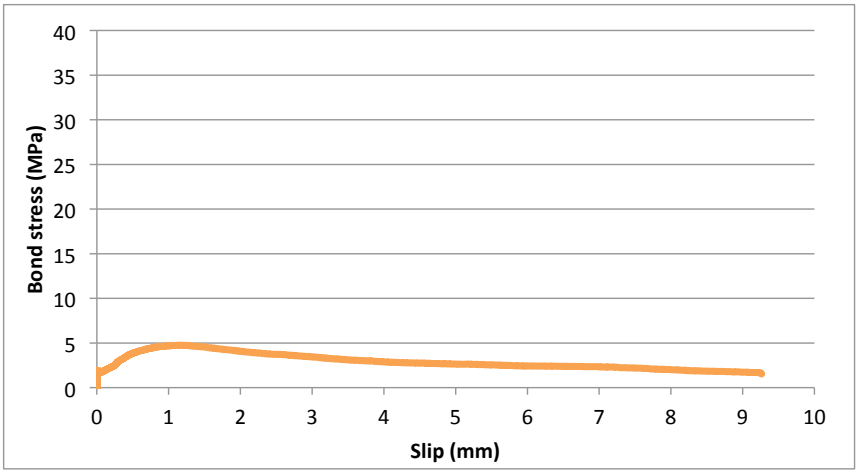

Specimen I L1 2

Descriptors		
Rebar diameter =	16	mm
Cover/Diameter =	1,875	
Fiber content =	40	kg/m3
Fiber type =	65_60	

Bond Parameters		
Bond strength =	6,61	MPa
Area A_peak =	3,45	mmMPa
Area A_80 =	9,64	mmMPa
Area A_50 =	24,40	mmMPa

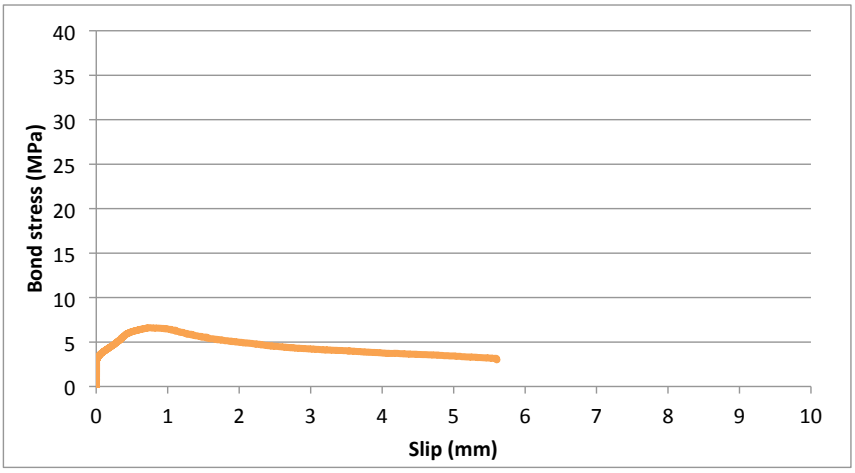

Specimen I L1 3

Descriptors		
Rebar diameter =	16	mm
Cover/Diameter =	1,875	
Fiber content =	40	kg/m3
Fiber type =	65_60	

Bond Parameters		
Bond strength =	7,38	MPa
Area A_peak =	12,30	mmMPa
Area A_80 =	20,50	mmMPa
Area A_50 =	29,80	mmMPa

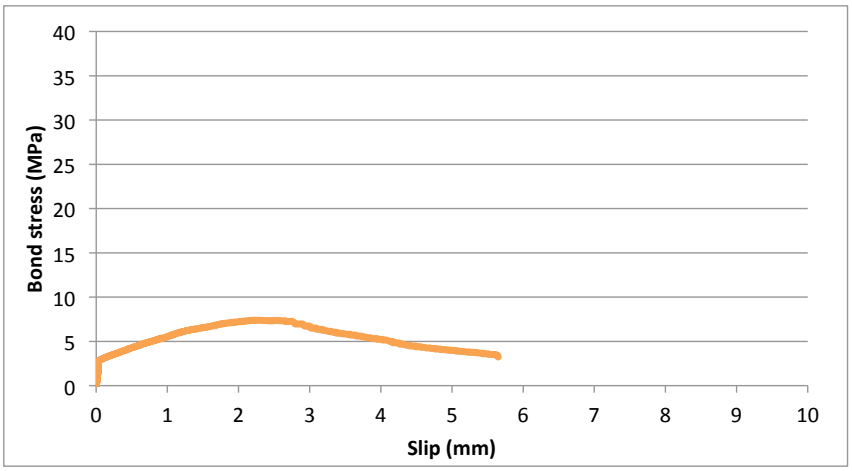

Specimen I L2 1

Descriptors		
Rebar diameter =	8	mm
Cover/Diameter =	4,375	
Fiber content =	0	kg/m3
Fiber type =		

Bond Parameters		
Bond strength =	9,45	MPa
Area A_peak =	8,27	mmMPa
Area A_80 =	26,30	mmMPa
Area A_50 =	43,70	mmMPa

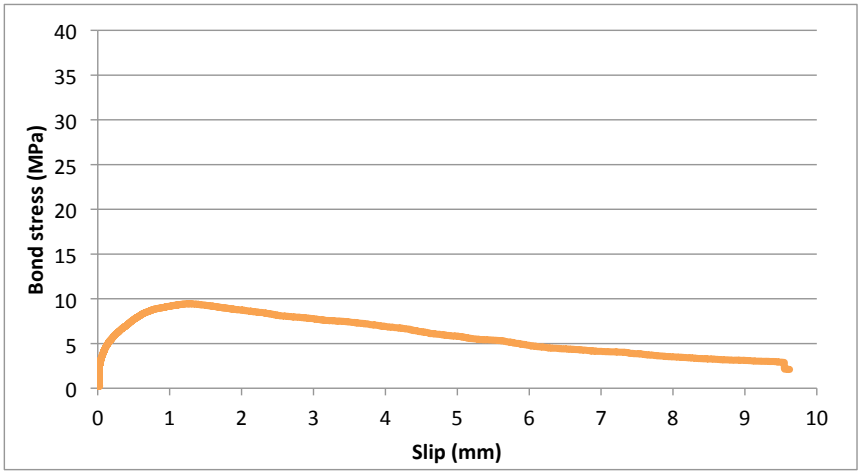

Specimen I L2 2

Descriptors		
Rebar diameter =	8	mm
Cover/Diameter =	4,375	
Fiber content =	0	kg/m3
Fiber type =		

Bond Parameters		
Bond strength =	7,15	MPa
Area A_peak =	6,75	mmMPa
Area A_80 =	16,90	mmMPa
Area A_50 =	31,20	mmMPa

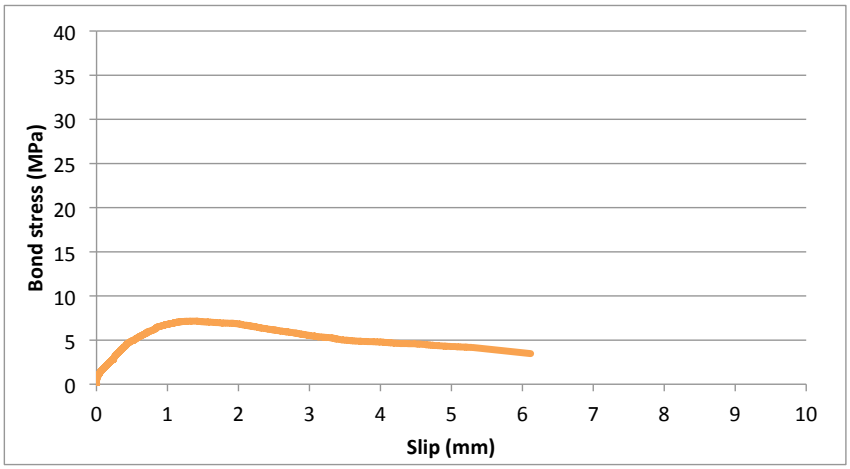

Specimen I L2 3

Descriptors		
Rebar diameter =	8	mm
Cover/Diameter =	4,375	
Fiber content =	0	kg/m3
Fiber type =		

Bond Parameters		
Bond strength =	8,50	MPa
Area A_peak =	4,24	mmMPa
Area A_80 =	17,60	mmMPa
Area A_50 =	44,40	mmMPa

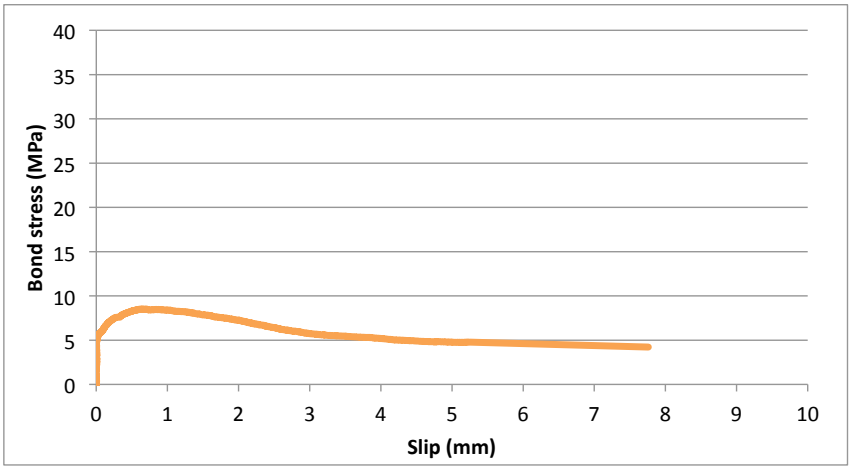

Specimen I L3 1

Descriptors		
Rebar diameter =	20	mm
Cover/Diameter =	5	
Fiber content =	70	kg/m3
Fiber type =	65_60	

Bond Parameters		
Bond strength =	19,90	MPa
Area A_peak =	22,90	mmMPa
Area A_80 =	97,70	mmMPa
Area A_50 =	191,00	mmMPa

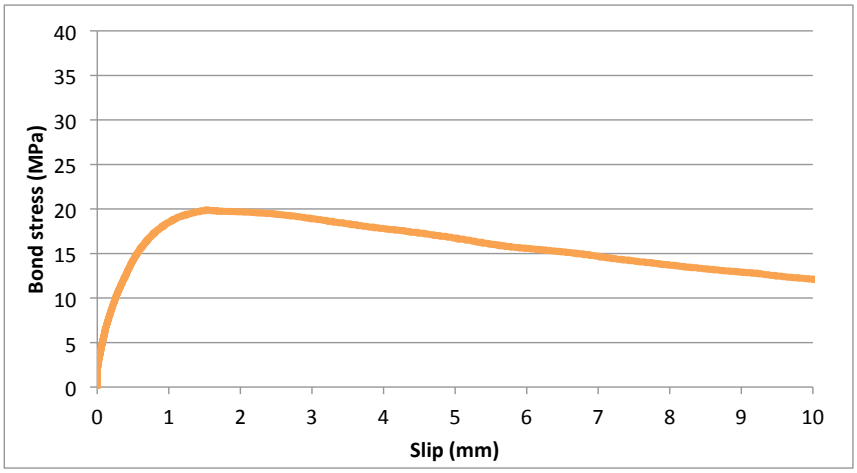

Specimen I L3 2

Descriptors		
Rebar diameter =	20	mm
Cover/Diameter =	5	
Fiber content =	70	kg/m3
Fiber type =	65_60	

Bond Parameters		
Bond strength =	15,01	MPa
Area A_peak =	18,40	mmMPa
Area A_80 =	66,10	mmMPa
Area A_50 =	119,00	mmMPa

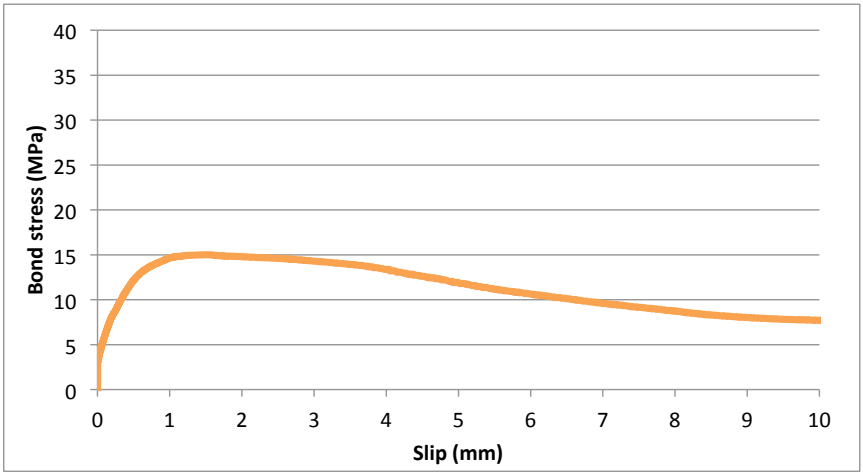

Specimen I L3 3

Descriptors		
Rebar diameter =	20	mm
Cover/Diameter =	5	
Fiber content =	70	kg/m3
Fiber type =	65_60	

Bond Parameters		
Bond strength =	20,40	MPa
Area A_peak =	34,30	mmMPa
Area A_80 =	97,00	mmMPa
Area A_50 =	167,00	mmMPa

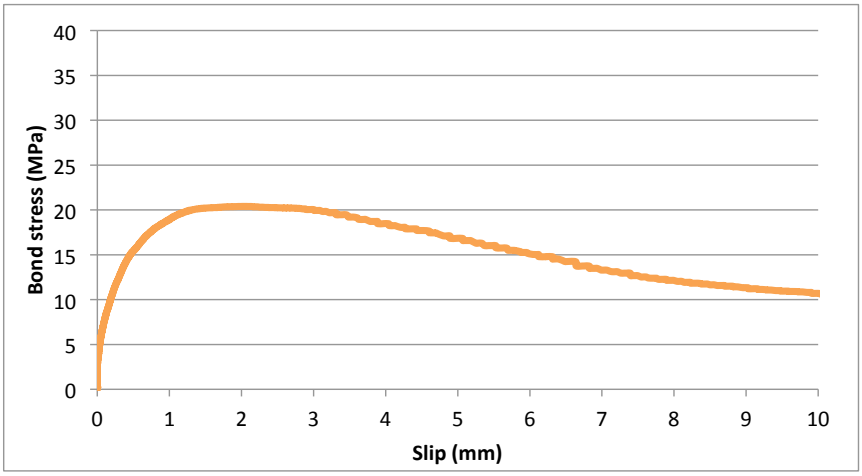

Specimen I L4 1

Descriptors		
Rebar diameter =	8	mm
Cover/Diameter =	5	
Fiber content =	40	kg/m3
Fiber type =	65_60	

Bond Parameters		
Bond strength =	7,78	MPa
Area A_peak =	7,12	mmMPa
Area A_80 =	17,80	mmMPa
Area A_50 =	31,60	mmMPa

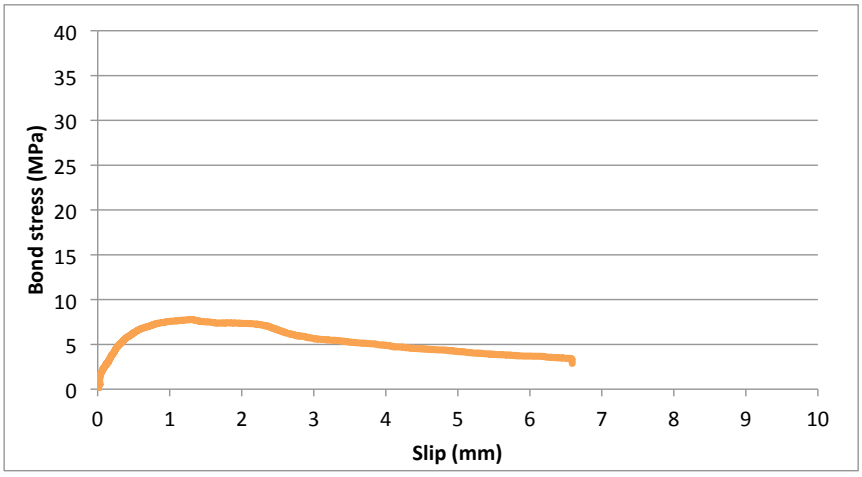

Specimen I L4 2

Descriptors		
Rebar diameter =	8	mm
Cover/Diameter =	5	
Fiber content =	40	kg/m3
Fiber type =	65_60	

Bond Parameters		
Bond strength =	5,77	MPa
Area A_peak =	6,38	mmMPa
Area A_80 =	12,50	mmMPa
Area A_50 =	20,20	mmMPa

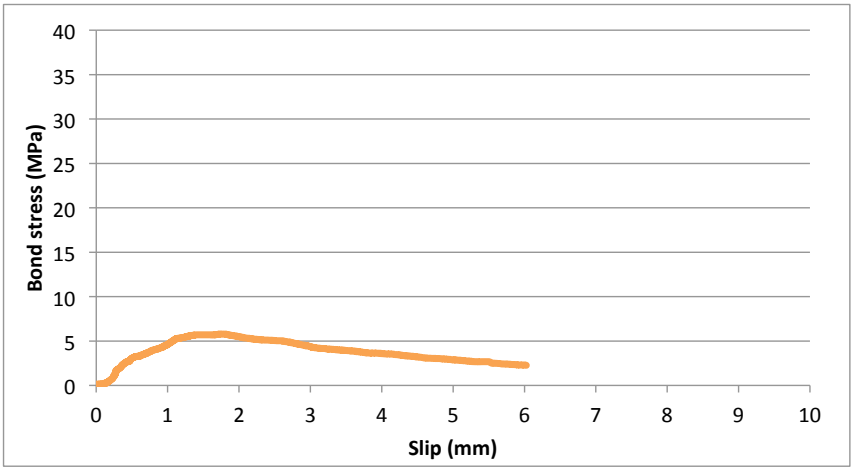

Specimen I L4 3

Descriptors		
Rebar diameter =	8	mm
Cover/Diameter =	5	
Fiber content =	40	kg/m3
Fiber type =	65_60	

Bond Parameters		
Bond strength =	9,78	MPa
Area A_peak =	16,60	mmMPa
Area A_80 =	30,50	mmMPa
Area A_50 =	54,10	mmMPa

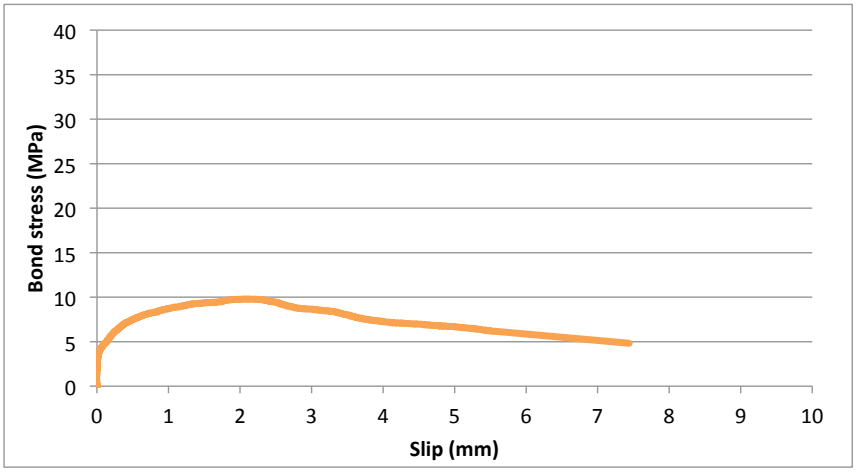

Specimen I L5 1

Descriptors		
Rebar diameter =	20	mm
Cover/Diameter =	1,5	
Fiber content =	0	kg/m3
Fiber type =		

Bond Parameters		
Bond strength =	11,97	MPa
Area A_peak =		mmMPa
Area A_80 =		mmMPa
Area A_50 =		mmMPa

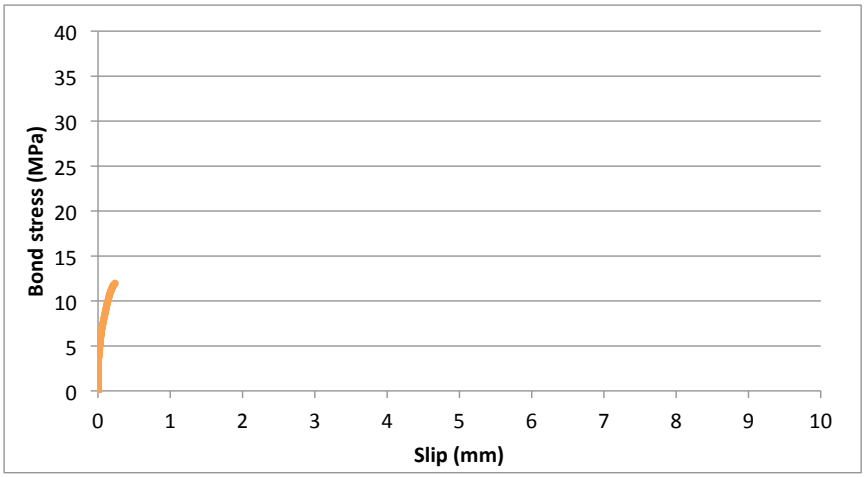

Specimen I L5 2

Descriptors		
Rebar diameter =	20	mm
Cover/Diameter =	1,5	
Fiber content =	0	kg/m3
Fiber type =		

Bond Parameters		
Bond strength =	11,89	MPa
Area A_peak =		mmMPa
Area A_80 =		mmMPa
Area A_50 =		mmMPa

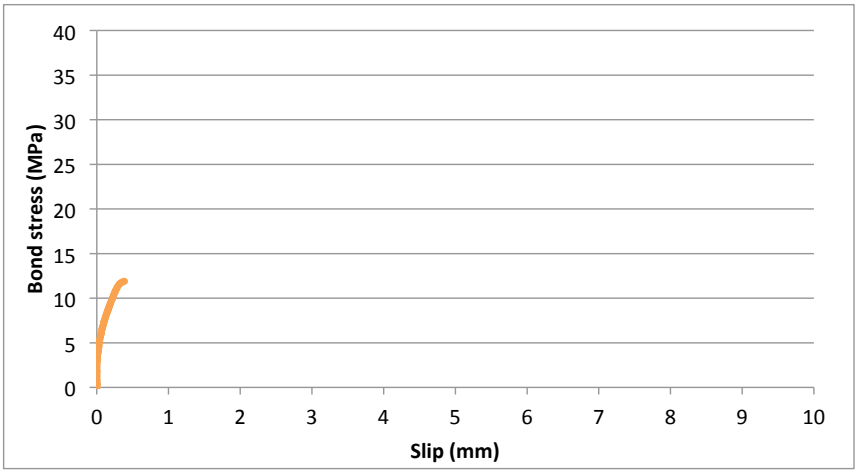

Specimen I L5 3

Descriptors		
Rebar diameter =	20	mm
Cover/Diameter =	1,5	
Fiber content =	0	kg/m3
Fiber type =		

Bond Parameters		
Bond strength =	6,66	MPa
Area A_peak =		mmMPa
Area A_80 =		mmMPa
Area A_50 =		mmMPa

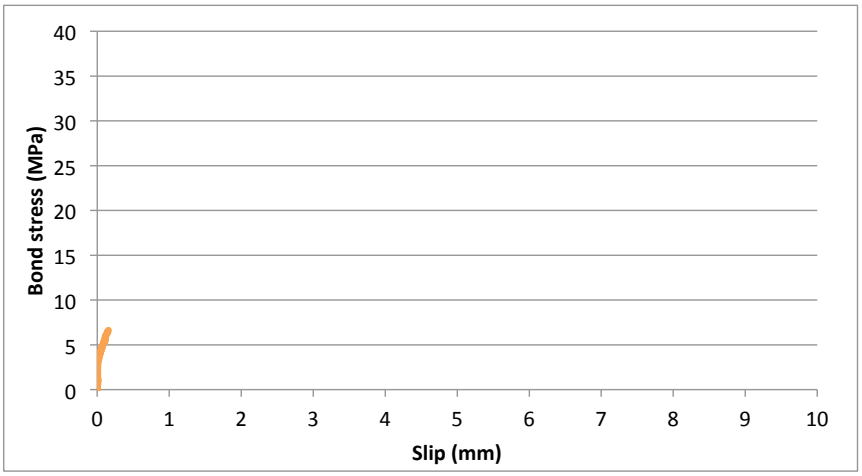

Specimen I L6 1

Descriptors		
Rebar diameter =	16	mm
Cover/Diameter =	3,44	
Fiber content =	70	kg/m3
Fiber type =	65_60	

Bond Parameters		
Bond strength =	6,73	MPa
Area A_peak =	11,10	mmMPa
Area A_80 =	25,20	mmMPa
Area A_50 =	36,40	mmMPa

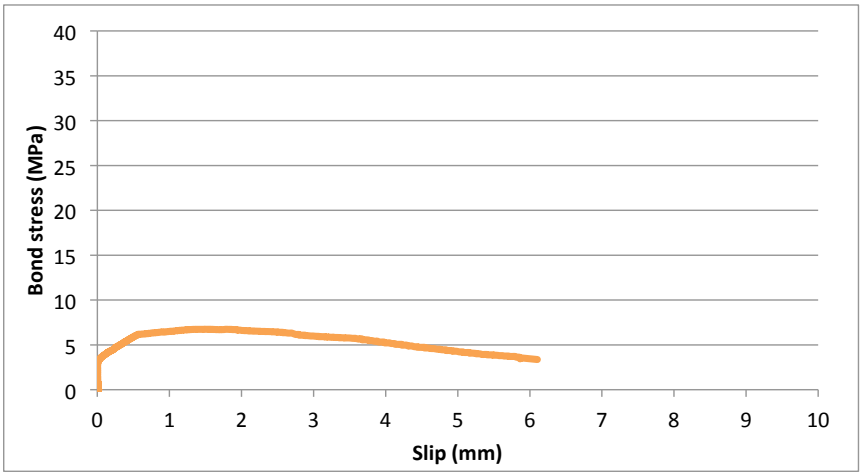

Specimen I L6 2

Descriptors		
Rebar diameter =	16	mm
Cover/Diameter =	3,44	
Fiber content =	70	kg/m3
Fiber type =	65_60	

Bond Parameters		
Bond strength =	6,81	MPa
Area A_peak =	11,00	mmMPa
Area A_80 =	23,60	mmMPa
Area A_50 =	33,10	mmMPa

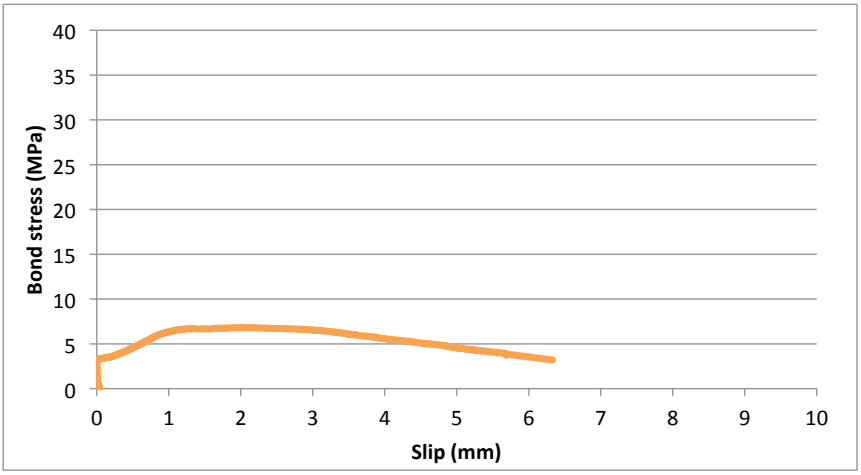

Specimen I L6 3

Descriptors		
Rebar diameter =	16	mm
Cover/Diameter =	3,44	
Fiber content =	70	kg/m3
Fiber type =	65_60	

Bond Parameters		
Bond strength =	6,73	MPa
Area A_peak =	10,71	mmMPa
Area A_80 =	24,70	mmMPa
Area A_50 =	33,70	mmMPa

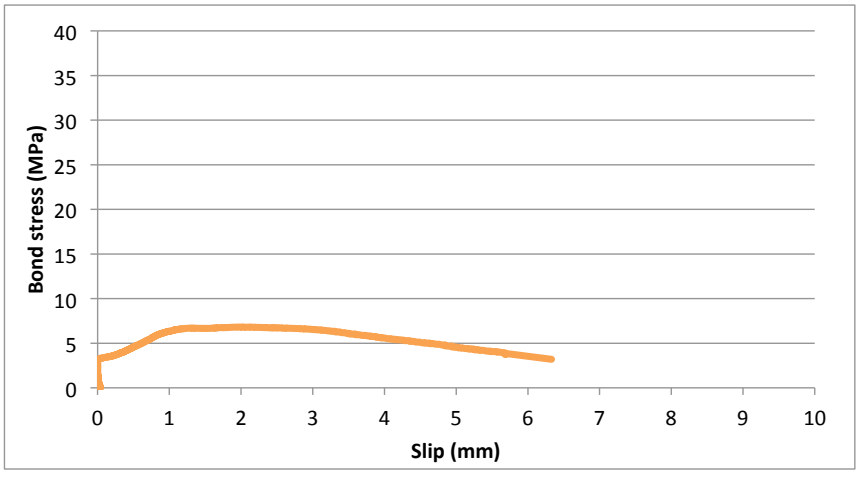

Specimen I L7 1

Descriptors		
Rebar diameter =	20	mm
Cover/Diameter =	3,25	
Fiber content =	40	kg/m3
Fiber type =	80_50	

Bond Parameters		
Bond strength =	14,00	MPa
Area A_peak =	27,60	mmMPa
Area A_80 =	65,10	mmMPa
Area A_50 =	119,00	mmMPa

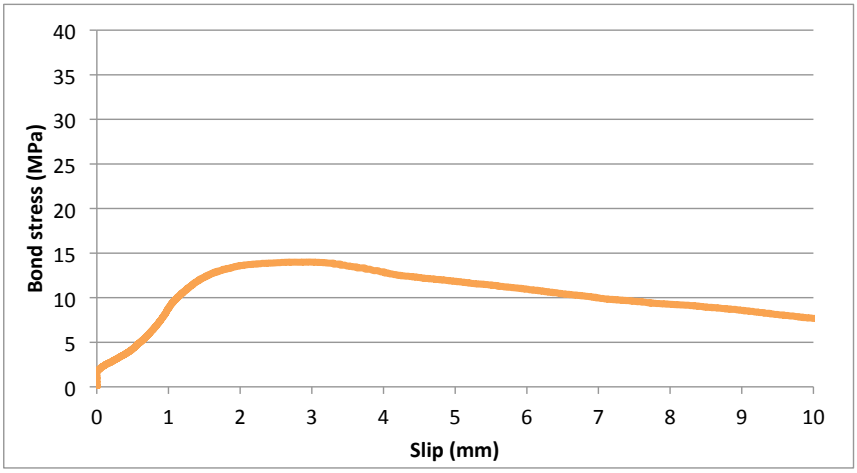

Specimen I L7 2

Descriptors		
Rebar diameter =	20	mm
Cover/Diameter =	3,25	
Fiber content =	40	kg/m3
Fiber type =	80_50	

Bond Parameters		
Bond strength =	11,22	MPa
Area A_peak =	19,80	mmMPa
Area A_80 =	44,40	mmMPa
Area A_50 =	76,80	mmMPa

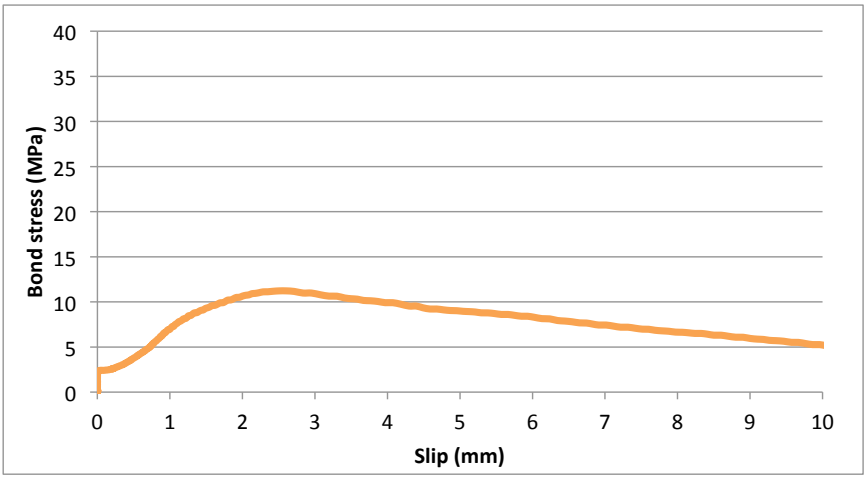

Specimen I L7 3

Descriptors		
Rebar diameter =	20	mm
Cover/Diameter =	3,25	
Fiber content =	40	kg/m3
Fiber type =	80_50	

Bond Parameters		
Bond strength =	10,16	MPa
Area A_peak =	18,20	mmMPa
Area A_80 =	46,50	mmMPa
Area A_50 =	90,00	mmMPa

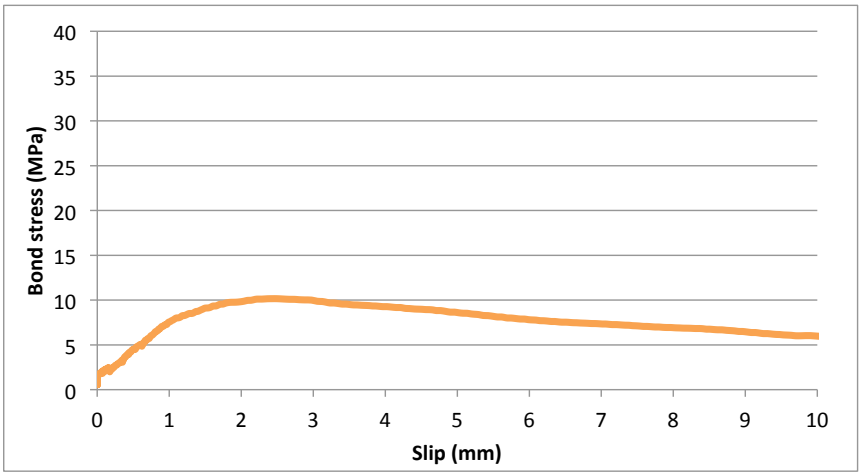

Specimen I L8 1

Descriptors		
Rebar diameter =	16	mm
Cover/Diameter =	5	
Fiber content =	0	kg/m3
Fiber type =		

Bond Parameters		
Bond strength =	6,33	MPa
Area A_peak =	7,75	mmMPa
Area A_80 =	20,50	mmMPa
Area A_50 =	30,85	mmMPa

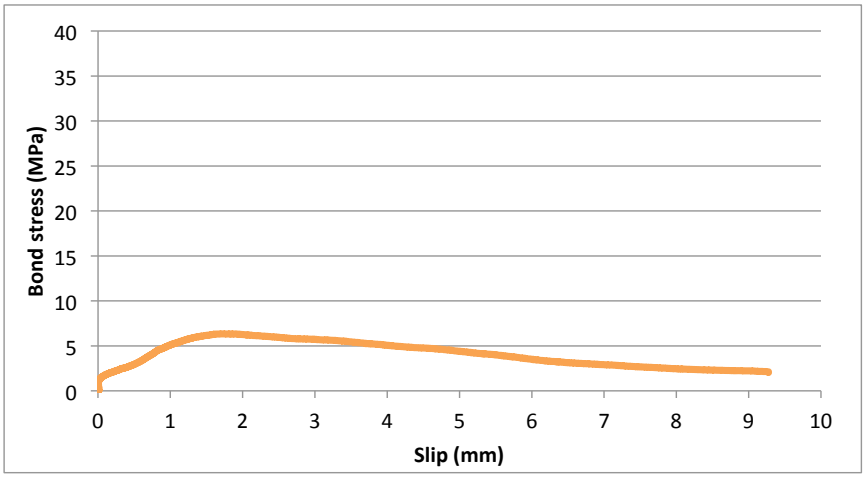

Specimen I L8 2

Descriptors		
Rebar diameter =	16	mm
Cover/Diameter =	5	
Fiber content =	0	kg/m3
Fiber type =		

Bond Parameters		
Bond strength =	4,80	MPa
Area A_peak =	5,72	mmMPa
Area A_80 =	12,90	mmMPa
Area A_50 =	20,30	mmMPa

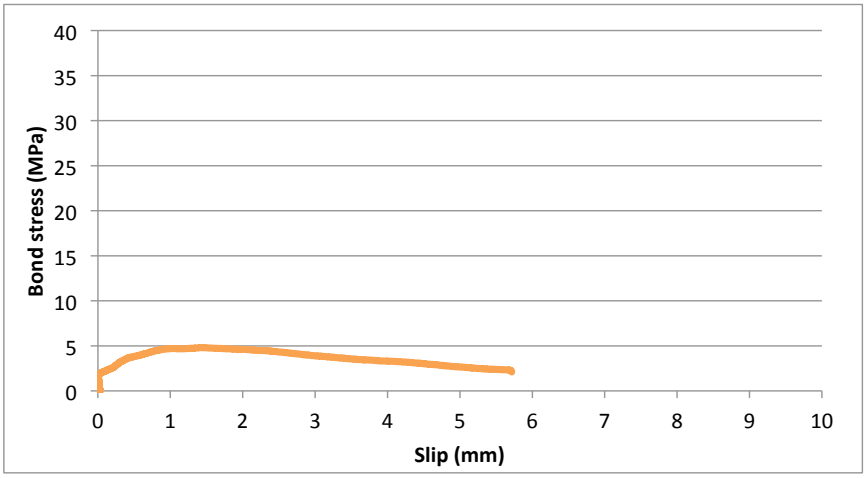

Specimen I L8 3

Descriptors		
Rebar diameter =	16	mm
Cover/Diameter =	5	
Fiber content =	0	kg/m3
Fiber type =		

Bond Parameters		
Bond strength =	6,16	MPa
Area A_peak =	6,88	mmMPa
Area A_80 =	15,40	mmMPa
Area A_50 =	24,80	mmMPa

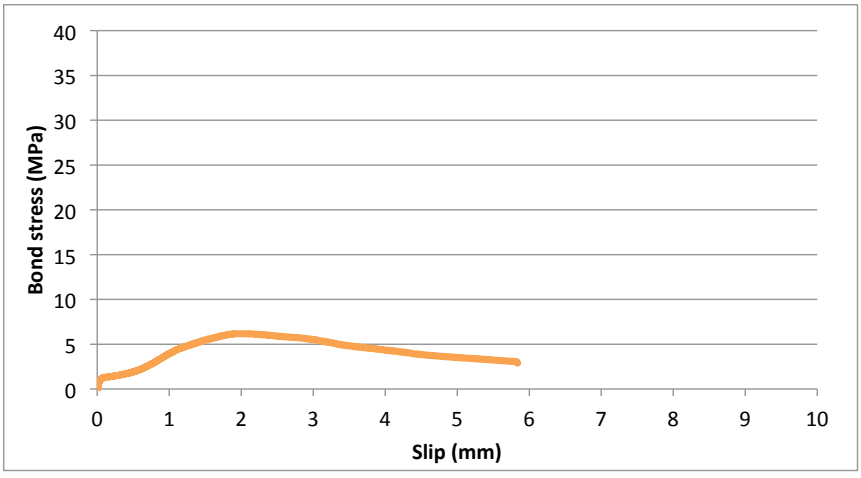

Specimen I L9 1

Descriptors		
Rebar diameter =	8	mm
Cover/Diameter =	3,75	
Fiber content =	70	kg/m3
Fiber type =	80_50	

Bond Parameters		
Bond strength =	5,37	MPa
Area A_peak =	8,51	mmMPa
Area A_80 =	19,20	mmMPa
Area A_50 =	31,35	mmMPa

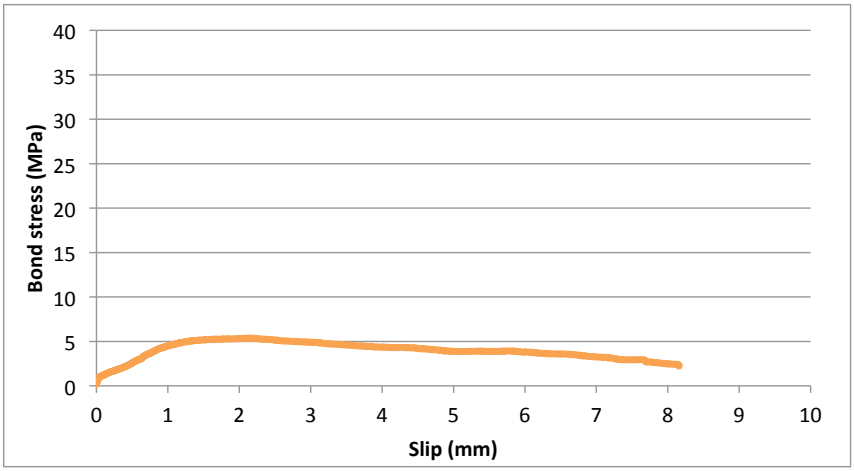

Specimen I L9 2

Descriptors		
Rebar diameter =	8	mm
Cover/Diameter =	3,75	
Fiber content =	70	kg/m3
Fiber type =	80_50	

Bond Parameters		
Bond strength =	6,50	MPa
Area A_peak =	10,73	mmMPa
Area A_80 =	22,30	mmMPa
Area A_50 =	32,50	mmMPa

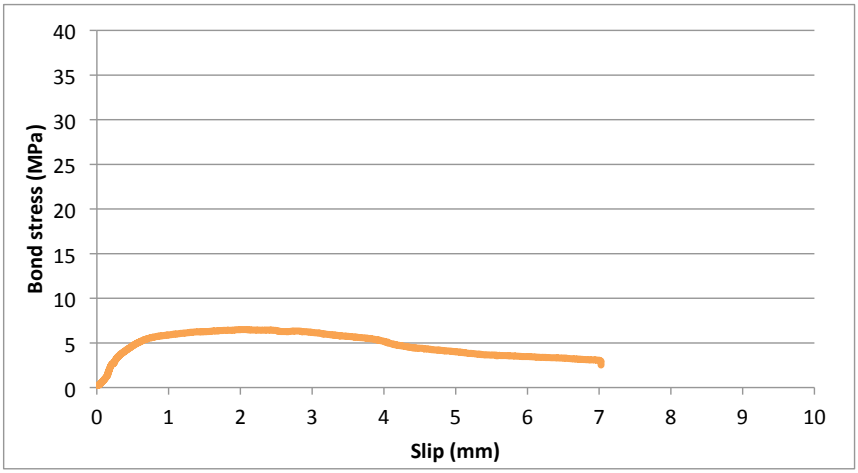

Specimen I L9 3

Descriptors		
Rebar diameter =	8	mm
Cover/Diameter =	3,75	
Fiber content =	70	kg/m3
Fiber type =	80_50	

Bond Parameters		
Bond strength =	5,00	MPa
Area A_peak =	10,10	mmMPa
Area A_80 =	31,10	mmMPa
Area A_50 =	42,30	mmMPa

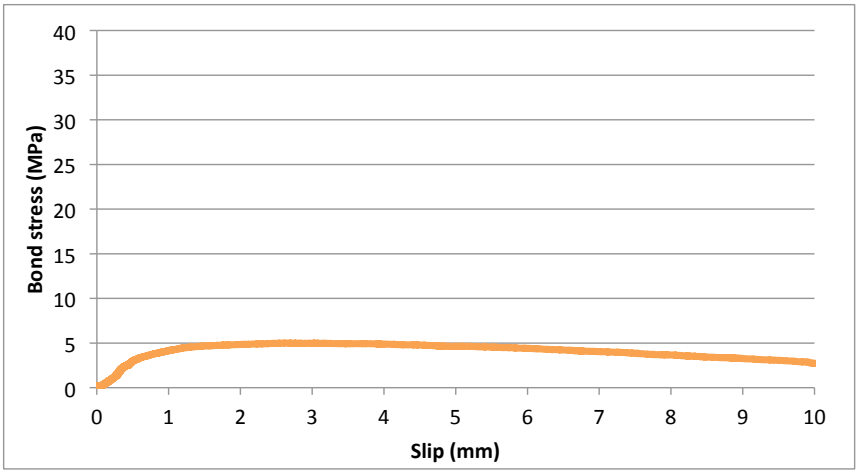

A3| Bond Stress – Slip Curves (Type II Series)

Appendices

Specimen II L1 1

Descriptors		
Rebar diameter =	8	mm
Cover/Diameter =	2,5	
Fiber content =	0	kg/m3
Fiber type =		

Bond Parameters		
Bond strength =	13,79	MPa
Area A_peak =	6,82	mmMPa
Area A_80 =	13,00	mmMPa
Area A_50 =	25,85	mmMPa

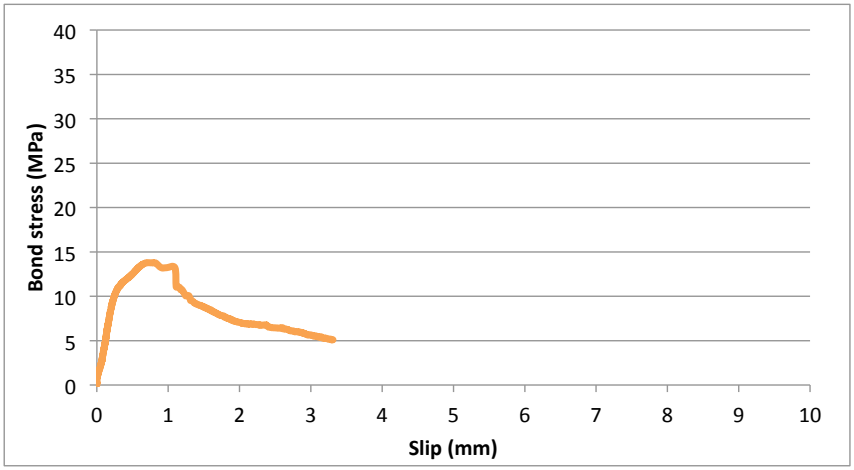

Specimen II L1 2

Descriptors		
Rebar diameter =	8	mm
Cover/Diameter =	2,5	
Fiber content =	0	kg/m3
Fiber type =		

Bond Parameters		
Bond strength =	20,29	MPa
Area A_peak =		mmMPa
Area A_80 =		mmMPa
Area A_50 =		mmMPa

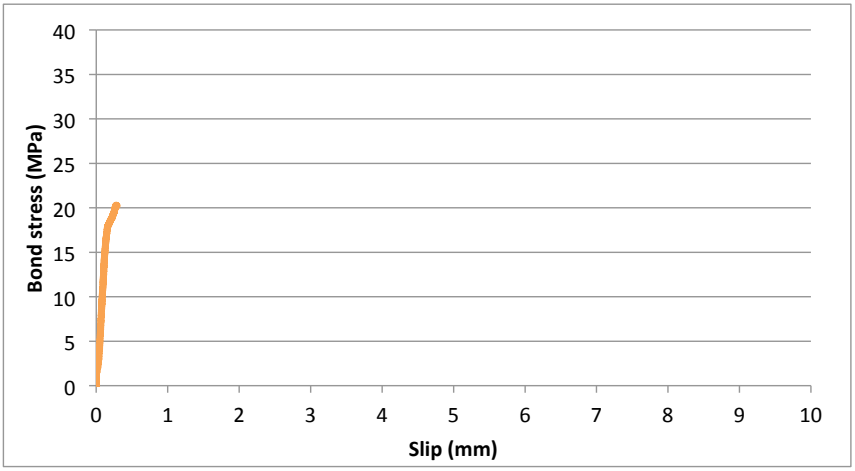

Specimen II L1 3

Descriptors		
Rebar diameter =	8	mm
Cover/Diameter =	2,5	
Fiber content =	0	kg/m3
Fiber type =		

Bond Parameters		
Bond strength =	17,25	MPa
Area A_peak =	3,04	mmMPa
Area A_80 =	13,39	mmMPa
Area A_50 =	18,95	mmMPa

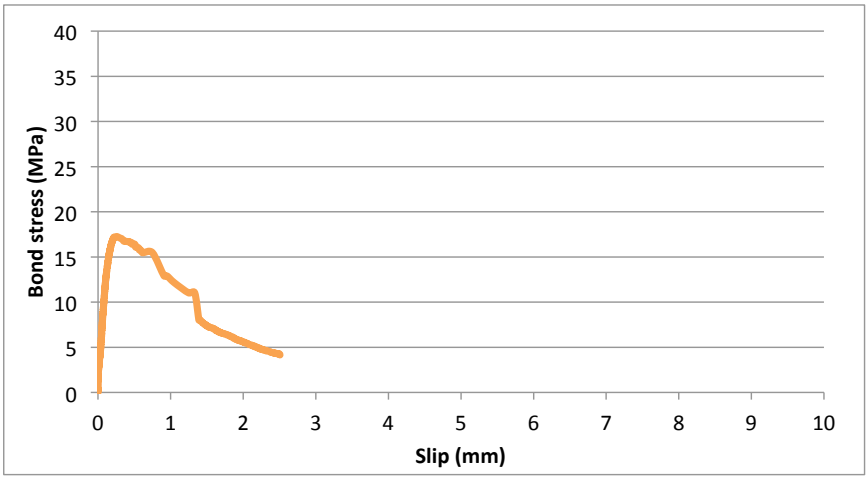

Specimen II L2 1

Descriptors		
Rebar diameter =	8	mm
Cover/Diameter =	3,5	
Fiber content =	60	kg/m3
Fiber type =	80_35	

Bond Parameters		
Bond strength =	36,89	MPa
Area A_peak =	46,54	mmMPa
Area A_80 =	162,46	mmMPa
Area A_50 =	256,54	mmMPa

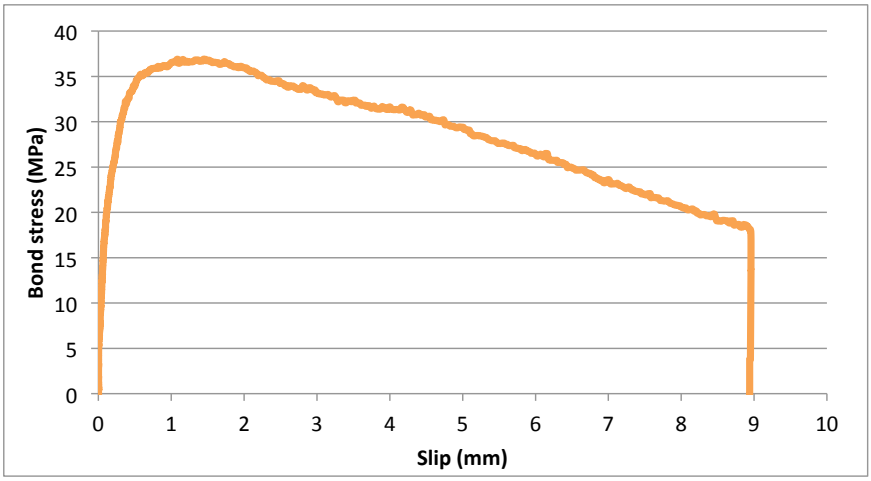

Specimen II L2 2

Descriptors		
Rebar diameter =	8	mm
Cover/Diameter =	3,5	
Fiber content =	60	kg/m3
Fiber type =	80_35	

Bond Parameters		
Bond strength =	25,36	MPa
Area A_peak =	15,09	mmMPa
Area A_80 =	30,06	mmMPa
Area A_50 =	150,22	mmMPa

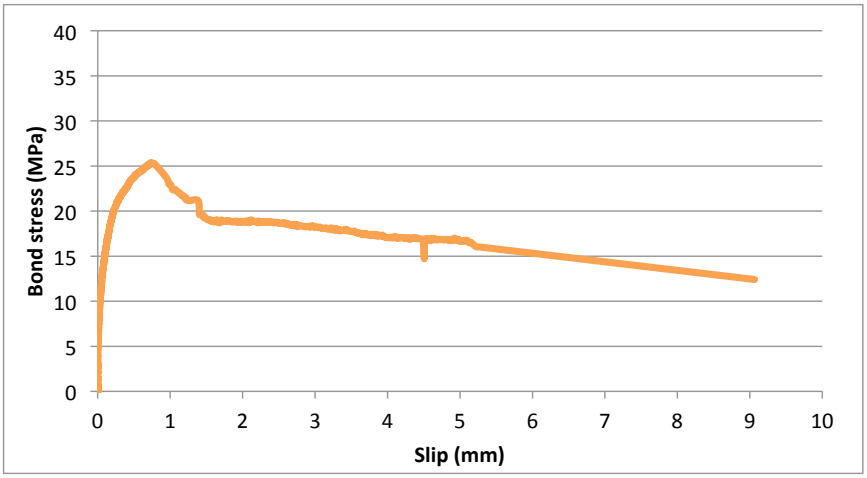

Specimen II L3 1

Descriptors		
Rebar diameter =	8	mm
Cover/Diameter =	5	
Fiber content =	40	kg/m3
Fiber type =	45_50	

Bond Parameters		
Bond strength =	20,90	MPa
Area A_peak =	27,34	mmMPa
Area A_80 =	126,79	mmMPa
Area A_50 =	176,40	mmMPa

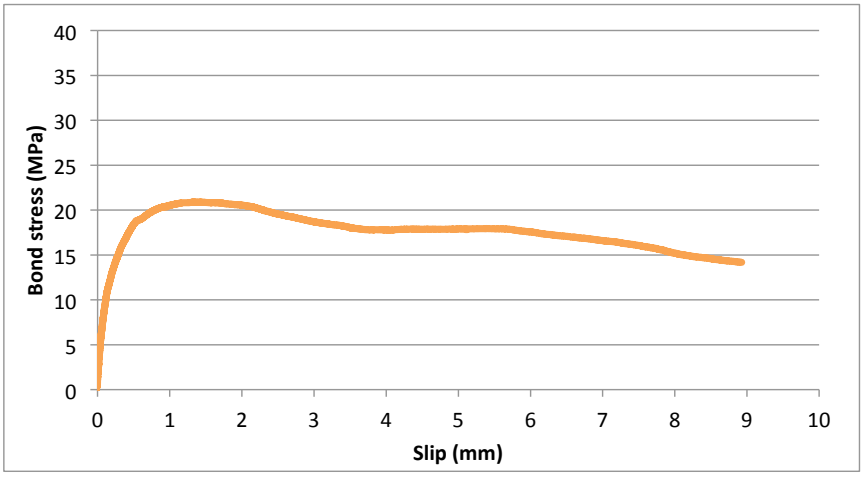

Specimen II L3 2

Descriptors		
Rebar diameter =	8	mm
Cover/Diameter =	5	
Fiber content =	40	kg/m3
Fiber type =	45_50	

Bond Parameters		
Bond strength =	20,16	MPa
Area A_peak =	29,55	mmMPa
Area A_80 =	115,01	mmMPa
Area A_50 =	157,34	mmMPa

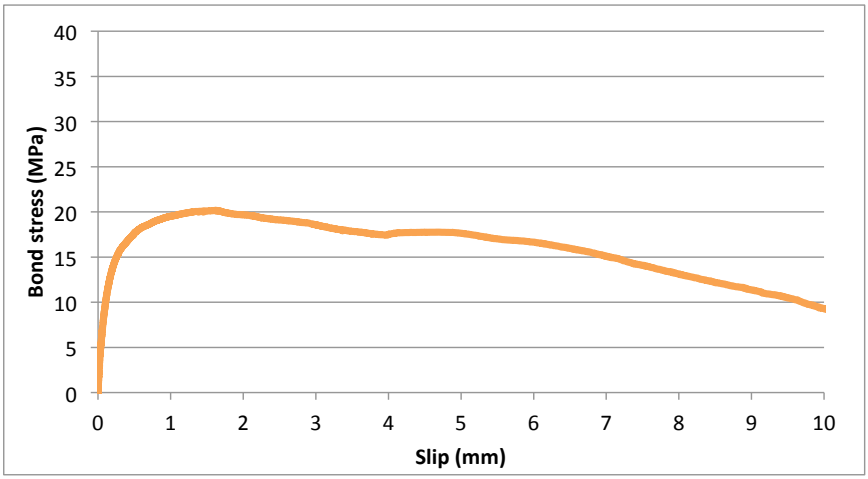

Specimen II L3 3

Descriptors		
Rebar diameter =	8	mm
Cover/Diameter =	5	
Fiber content =	40	kg/m3
Fiber type =	45_50	

Bond Parameters		
Bond strength =	23,00	MPa
Area A_peak =	29,09	mmMPa
Area A_80 =	106,75	mmMPa
Area A_50 =	206,42	mmMPa

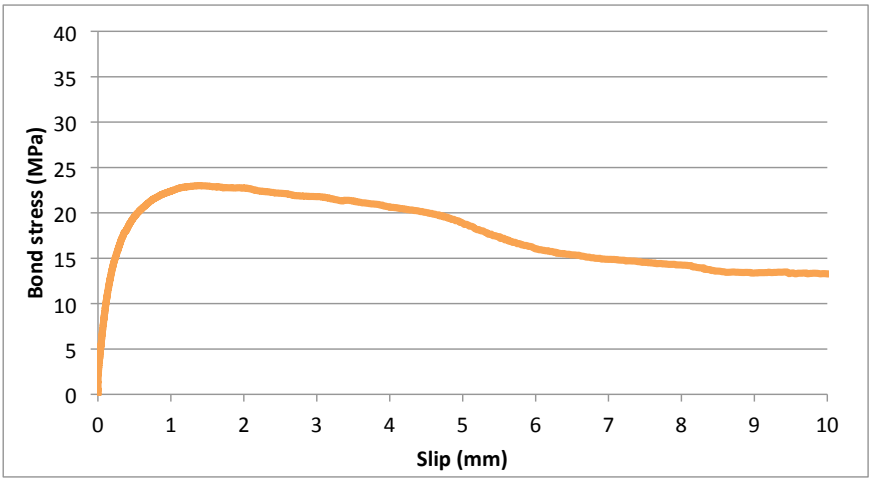

Specimen II L4 1

Descriptors		
Rebar diameter =	12	mm
Cover/Diameter =	2,5	
Fiber content =	60	kg/m3
Fiber type =	45_50	

Bond Parameters		
Bond strength =	18,63	MPa
Area A_peak =		mmMPa
Area A_80 =		mmMPa
Area A_50 =		mmMPa

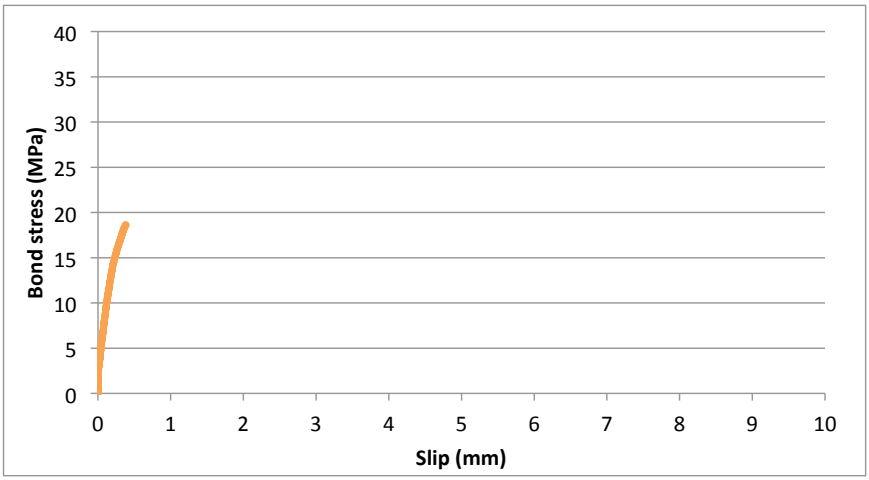

Specimen II L4 2

Descriptors		
Rebar diameter =	12	mm
Cover/Diameter =	2,5	
Fiber content =	60	kg/m3
Fiber type =	45_50	

Bond Parameters		
Bond strength =	18,27	MPa
Area A_peak =		mmMPa
Area A_80 =		mmMPa
Area A_50 =		mmMPa

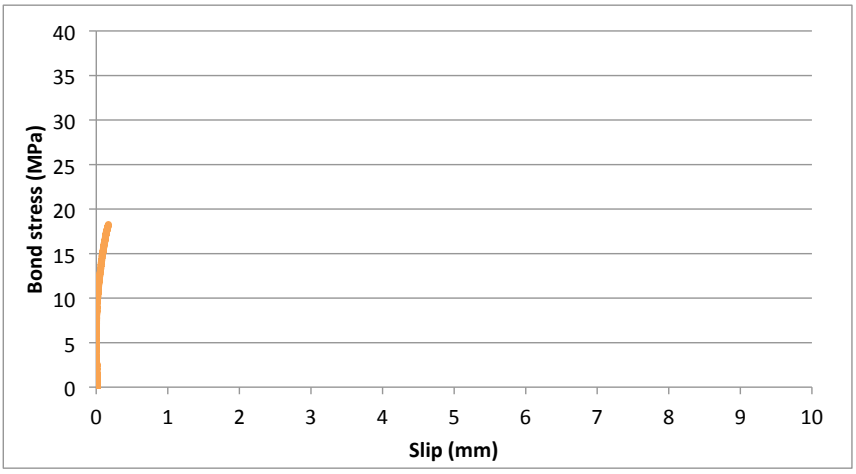

Specimen II L4 3

Descriptors		
Rebar diameter =	12	mm
Cover/Diameter =	2,5	
Fiber content =	60	kg/m3
Fiber type =	45_50	

Bond Parameters		
Bond strength =	17,46	MPa
Area A_peak =		mmMPa
Area A_80 =		mmMPa
Area A_50 =		mmMPa

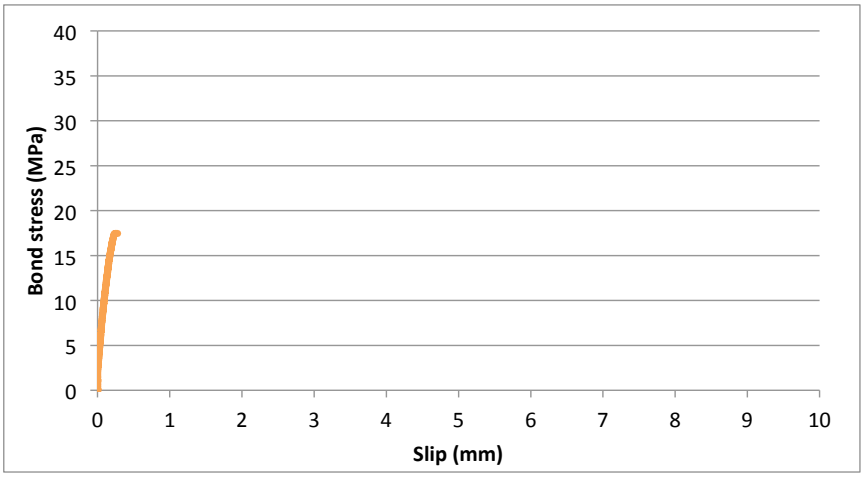

Specimen II L5 1

Descriptors		
Rebar diameter =	12	mm
Cover/Diameter =	3,5	
Fiber content =	40	kg/m3
Fiber type =	80_50	

Bond Parameters		
Bond strength =	27,01	MPa
Area A_peak =		mmMPa
Area A_80 =		mmMPa
Area A_50 =		mmMPa

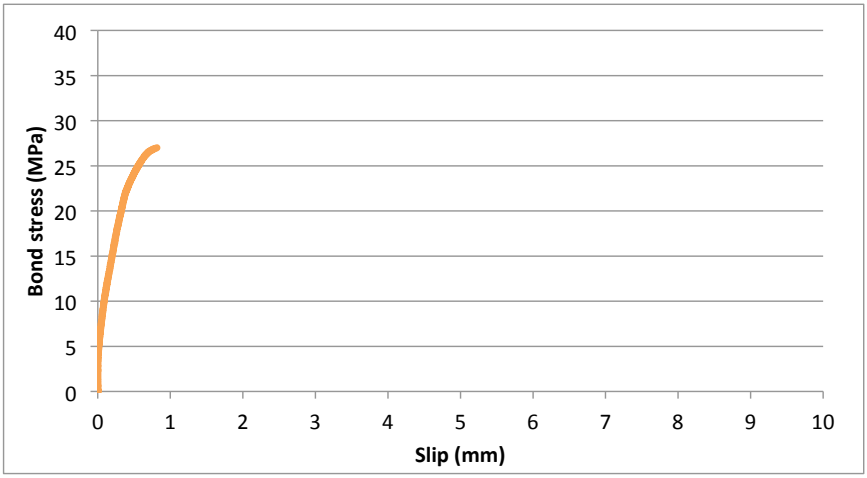

Specimen II L5 2

Descriptors		
Rebar diameter =	12	mm
Cover/Diameter =	3,5	
Fiber content =	40	kg/m3
Fiber type =	80_50	

Bond Parameters		
Bond strength =	24,64	MPa
Area A_peak =		mmMPa
Area A_80 =		mmMPa
Area A_50 =		mmMPa

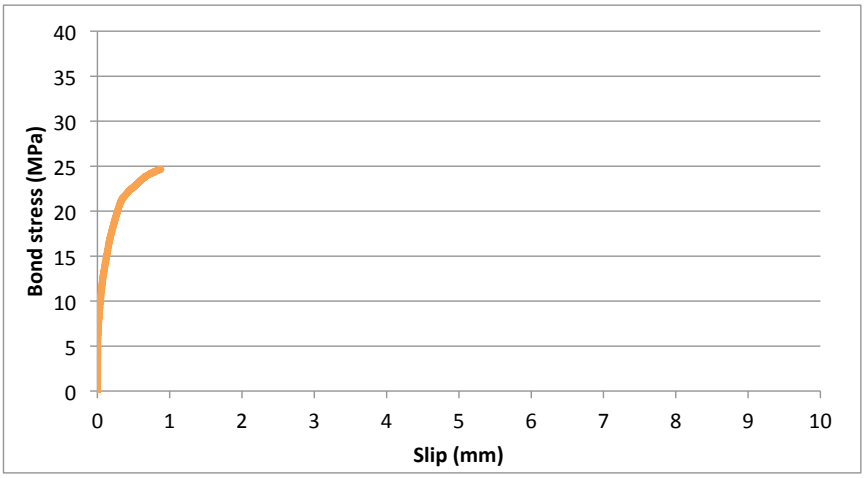

Specimen II L5 3

Descriptors		
Rebar diameter =	12	mm
Cover/Diameter =	3,5	
Fiber content =	40	kg/m3
Fiber type =	80_50	

Bond Parameters		
Bond strength =	23,90	MPa
Area A_peak =	8,97	mmMPa
Area A_80 =	26,52	mmMPa
Area A_50 =	47,62	mmMPa

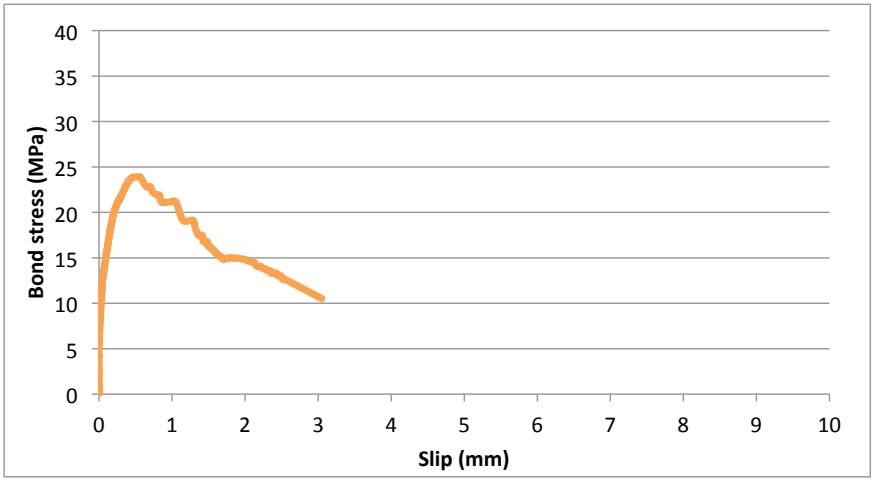

Specimen II L6 1

Descriptors		
Rebar diameter =	12	mm
Cover/Diameter =	5	
Fiber content =	0	kg/m3
Fiber type =		

Bond Parameters		
Bond strength =	27,75	MPa
Area A_peak =	23,50	mmMPa
Area A_80 =	72,90	mmMPa
Area A_50 =	148,98	mmMPa

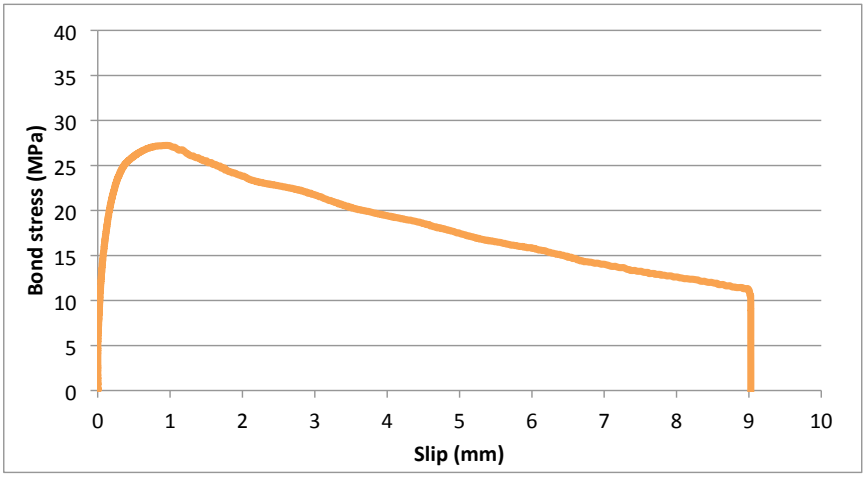

Specimen II L6 2

Descriptors		
Rebar diameter =	12	mm
Cover/Diameter =	5	
Fiber content =	0	kg/m3
Fiber type =		

Bond Parameters		
Bond strength =	24,19	MPa
Area A_peak =	48,66	mmMPa
Area A_80 =	111,00	mmMPa
Area A_50 =	186,14	mmMPa

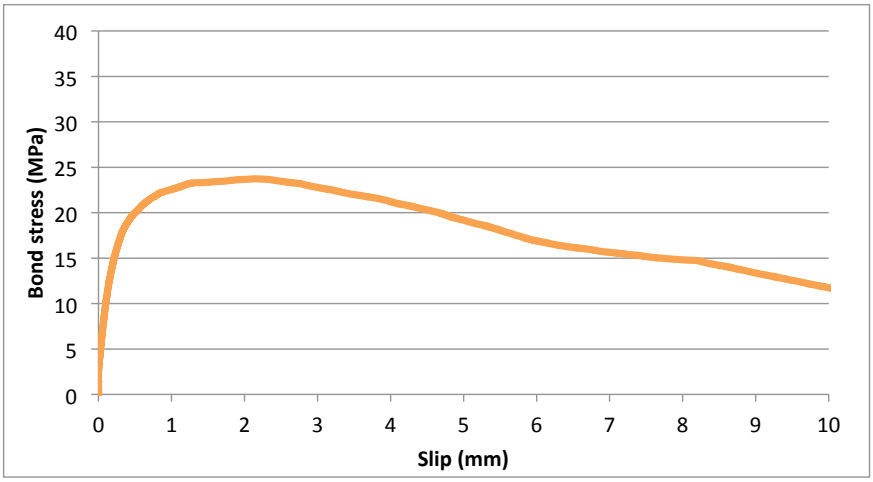

Specimen II L6 3

Descriptors		
Rebar diameter =	12	mm
Cover/Diameter =	5	
Fiber content =	0	kg/m3
Fiber type =		

Bond Parameters		
Bond strength =	23,92	MPa
Area A_peak =	25,32	mmMPa
Area A_80 =	86,30	mmMPa
Area A_50 =	179,84	mmMPa

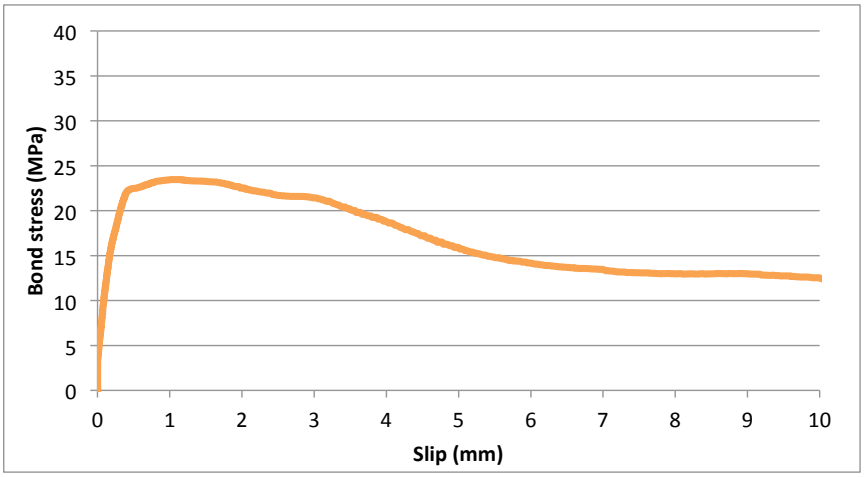

Specimen II L7 1

Descriptors		
Rebar diameter =	16	mm
Cover/Diameter =	2,5	
Fiber content =	40	kg/m3
Fiber type =	80_35	

Bond Parameters		
Bond strength =	22,49	MPa
Area A_peak =		mmMPa
Area A_80 =		mmMPa
Area A_50 =		mmMPa

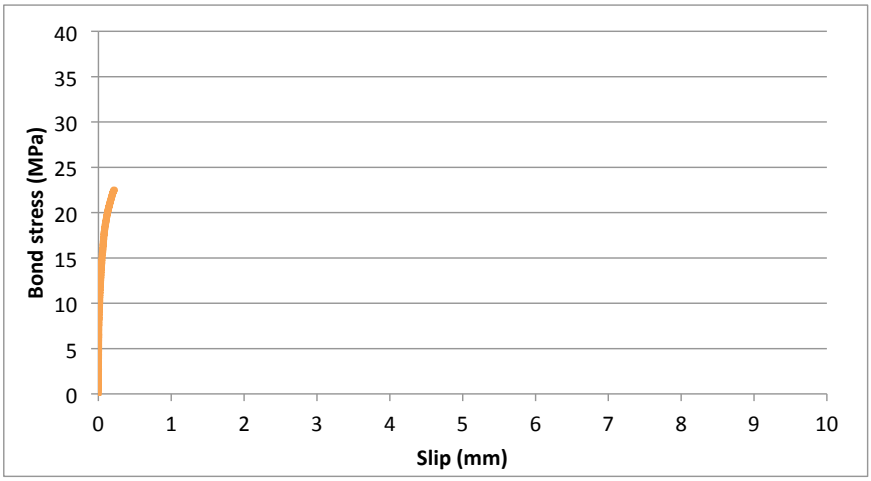

Specimen II L7 2

Descriptors		
Rebar diameter =	16	mm
Cover/Diameter =	2,5	
Fiber content =	40	kg/m3
Fiber type =	80_35	

Bond Parameters		
Bond strength =	23,16	MPa
Area A_peak =		mmMPa
Area A_80 =		mmMPa
Area A_50 =		mmMPa

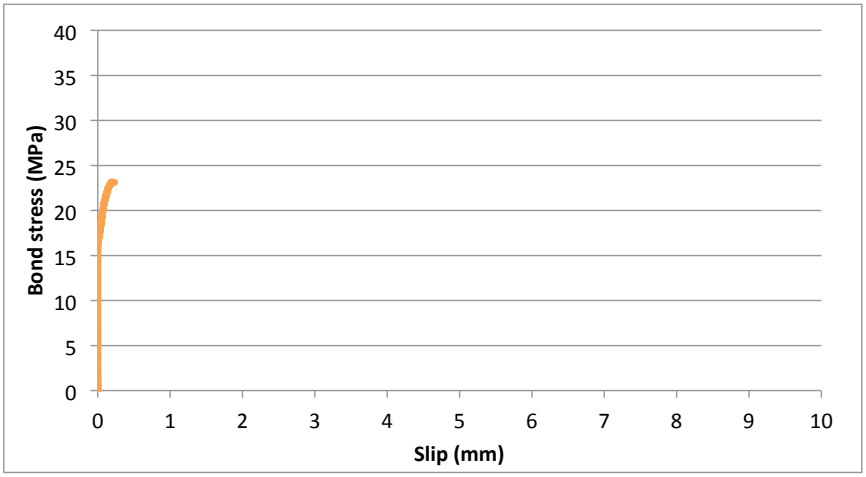

Specimen II L7 3

Descriptors		
Rebar diameter =	16	mm
Cover/Diameter =	2,5	
Fiber content =	40	kg/m3
Fiber type =	80_35	

Bond Parameters		
Bond strength =	20,48	MPa
Area A_peak =		mmMPa
Area A_80 =		mmMPa
Area A_50 =		mmMPa

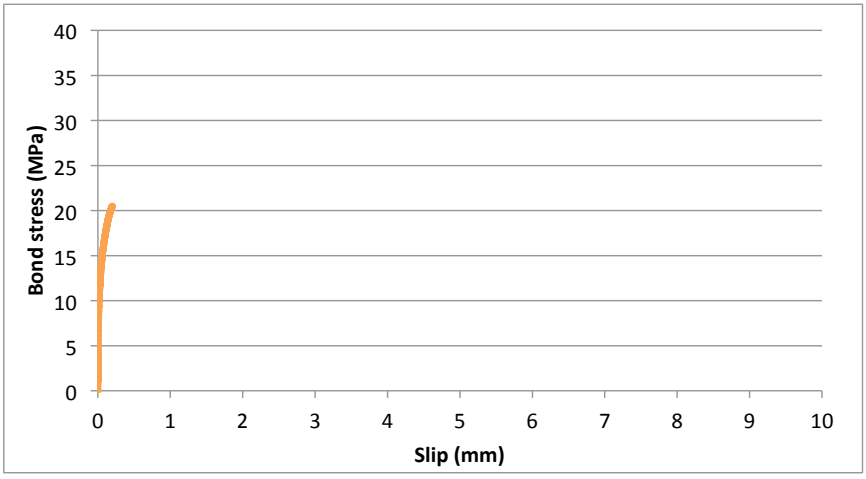

Specimen II L8 1

Descriptors		
Rebar diameter =	16	mm
Cover/Diameter =	3,75	
Fiber content =	0	kg/m3
Fiber type =	no	

Bond Parameters		
Bond strength =	26,49	MPa
Area A_peak =		mmMPa
Area A_80 =		mmMPa
Area A_50 =		mmMPa

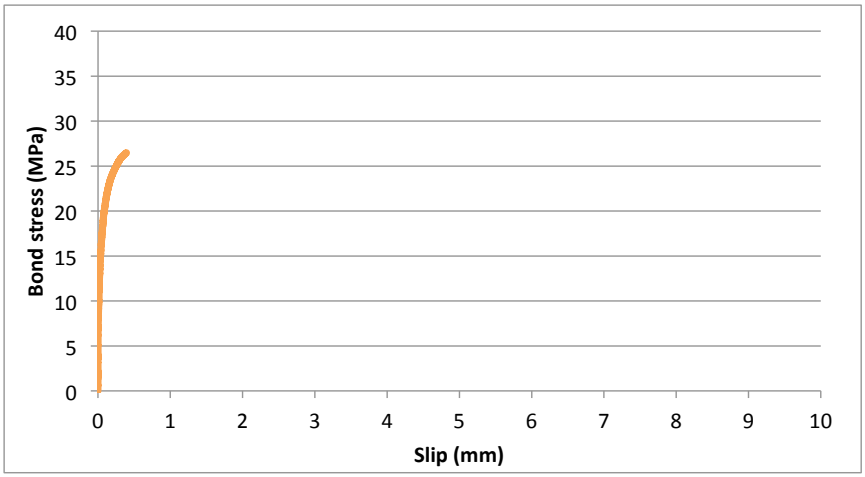

Specimen II L8 3

Descriptors		
Rebar diameter =	16	mm
Cover/Diameter =	3,75	
Fiber content =	0	kg/m3
Fiber type =	no	

Bond Parameters		
Bond strength =	26,86	MPa
Area A_peak =		mmMPa
Area A_80 =		mmMPa
Area A_50 =		mmMPa

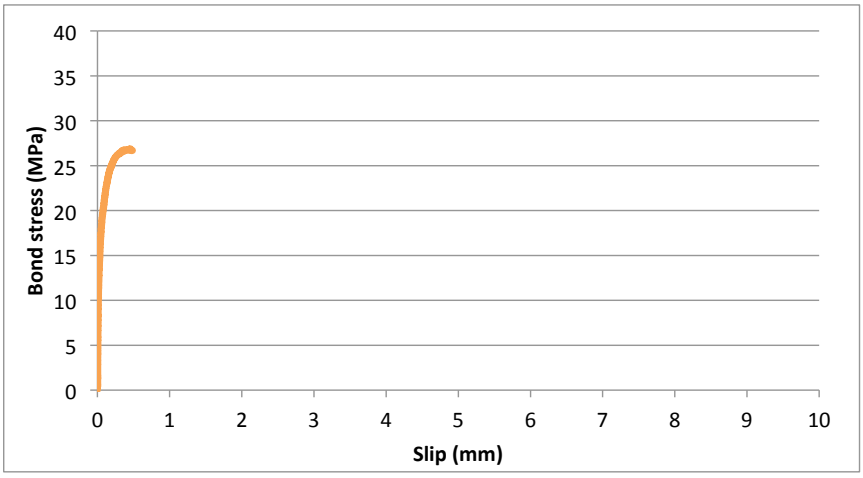

Specimen II L9 2

Descriptors		
Rebar diameter =	16	mm
Cover/Diameter =	5	
Fiber content =	60	kg/m3
Fiber type =	80_50	

Bond Parameters		
Bond strength =	25,83	MPa
Area A_peak =		mmMPa
Area A_80 =		mmMPa
Area A_50 =		mmMPa

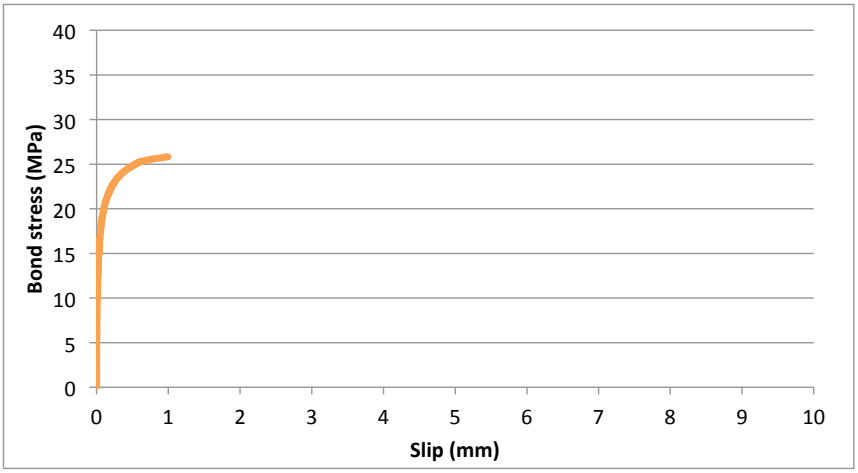

Specimen II L9 3

Descriptors		
Rebar diameter =	16	mm
Cover/Diameter =	5	
Fiber content =	60	kg/m3
Fiber type =	80_50	

Bond Parameters		
Bond strength =	27,39	MPa
Area A_peak =		mmMPa
Area A_80 =		mmMPa
Area A_50 =		mmMPa

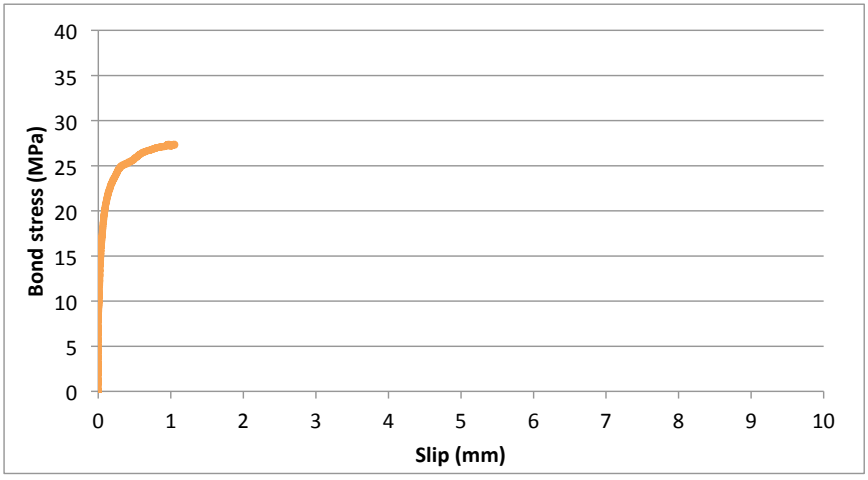

A4| Bond Stress – Slip Curves (Type III Series)

Appendices

Specimen III L1 1

Descriptors		
Rebar diameter =	8	mm
Cover/Diameter =	2,5	
Fiber content =	0	kg/m3
Fiber type =	no fibers	

Bond Parameters		
Bond strength =	21,58	MPa
Area A_peak =		mmMPa
Area A_80 =		mmMPa
Area A_50 =		mmMPa

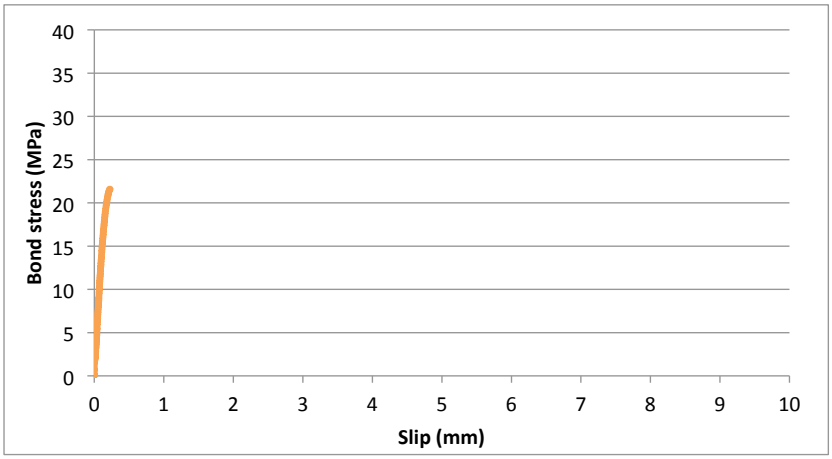

Specimen III L1 2

Descriptors		
Rebar diameter =	8	mm
Cover/Diameter =	2,5	
Fiber content =	0	kg/m3
Fiber type =	no fibers	

Bond Parameters		
Bond strength =	7,81	MPa
Area A_peak =		mmMPa
Area A_80 =		mmMPa
Area A_50 =		mmMPa

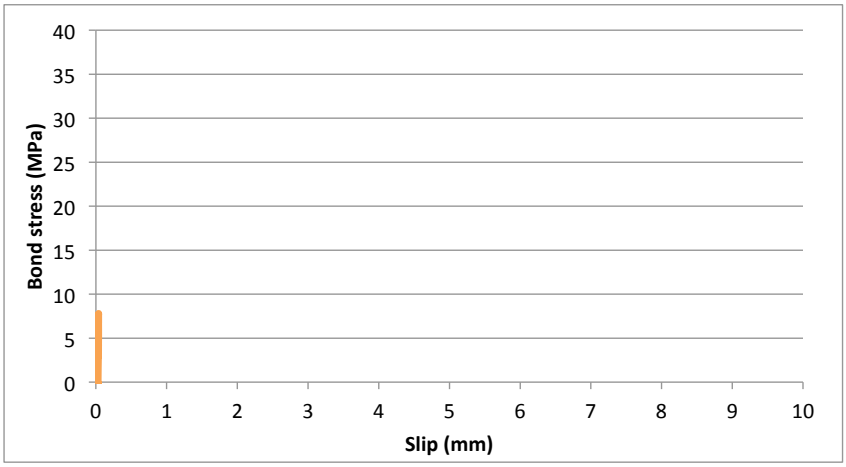

Specimen III L1 3

Descriptors		
Rebar diameter =	8	mm
Cover/Diameter =	2,5	
Fiber content =	0	kg/m3
Fiber type =	no fibers	

Bond Parameters		
Bond strength =	20,66	MPa
Area A_peak =		mmMPa
Area A_80 =		mmMPa
Area A_50 =		mmMPa

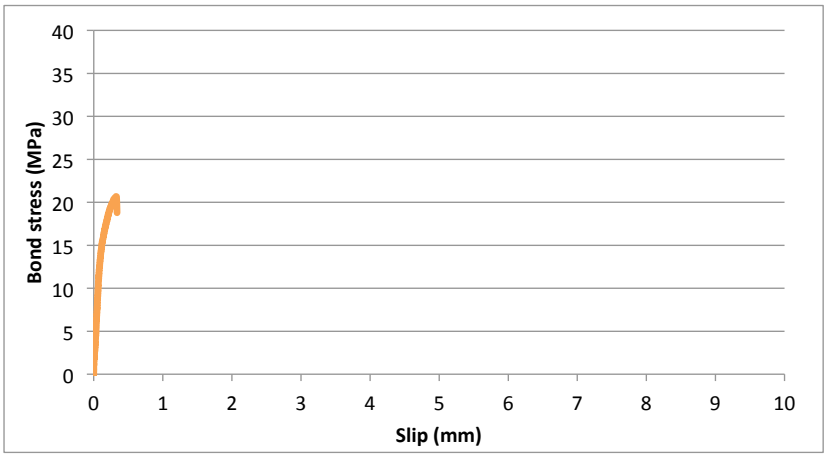

Specimen III L2 1

Descriptors		
Rebar diameter =	12	mm
Cover/Diameter =	3,5	
Fiber content =	40	kg/m3
Fiber type =	80_50	

Bond Parameters		
Bond strength =	15,90	MPa
Area A_peak =	12,19	mmMPa
Area A_80 =	52,60	mmMPa
Area A_50 =	86,70	mmMPa

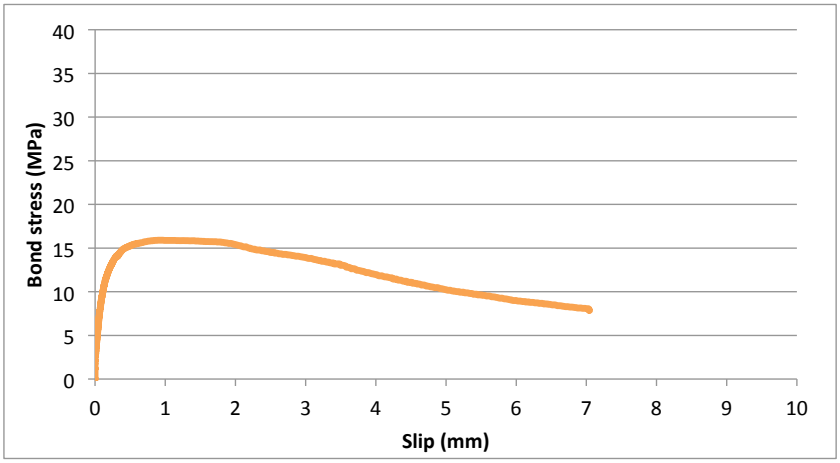

Specimen III L2 2

Descriptors		
Rebar diameter =	12	mm
Cover/Diameter =	3,5	
Fiber content =	40	kg/m3
Fiber type =	80_50	

Bond Parameters		
Bond strength =	12,84	MPa
Area A_peak =	12,23	mmMPa
Area A_80 =	38,50	mmMPa
Area A_50 =	66,50	mmMPa

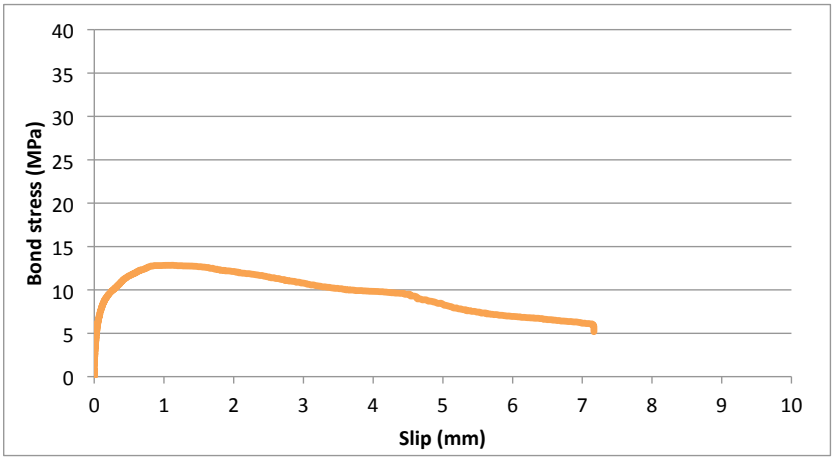

Specimen III L2 3

Descriptors		
Rebar diameter =	12	mm
Cover/Diameter =	3,5	
Fiber content =	40	kg/m3
Fiber type =	80_50	

Bond Parameters		
Bond strength =	14,36	MPa
Area A_peak =	10,47	mmMPa
Area A_80 =	45,80	mmMPa
Area A_50 =	81,00	mmMPa

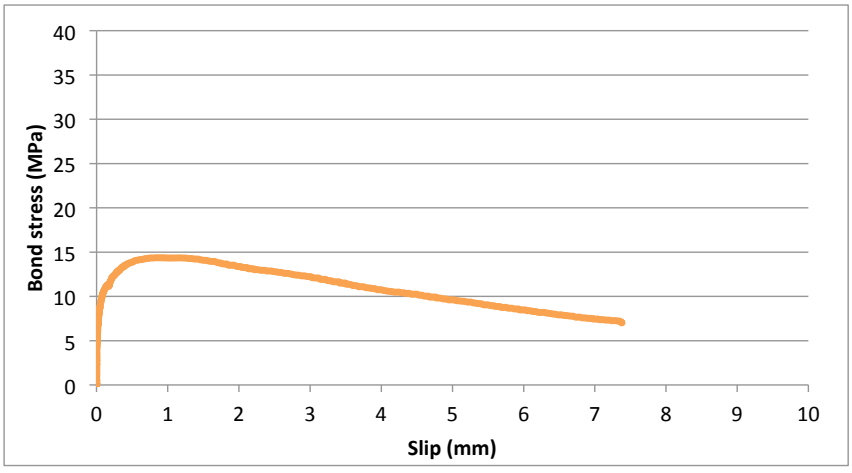

Specimen III L3 1

Descriptors		
Rebar diameter =	16	mm
Cover/Diameter =	5	
Fiber content =	60	kg/m3
Fiber type =	80_50	

Bond Parameters		
Bond strength =	23,17	MPa
Area A_peak =	23,54	mmMPa
Area A_80 =	86,60	mmMPa
Area A_50 =	166,00	mmMPa

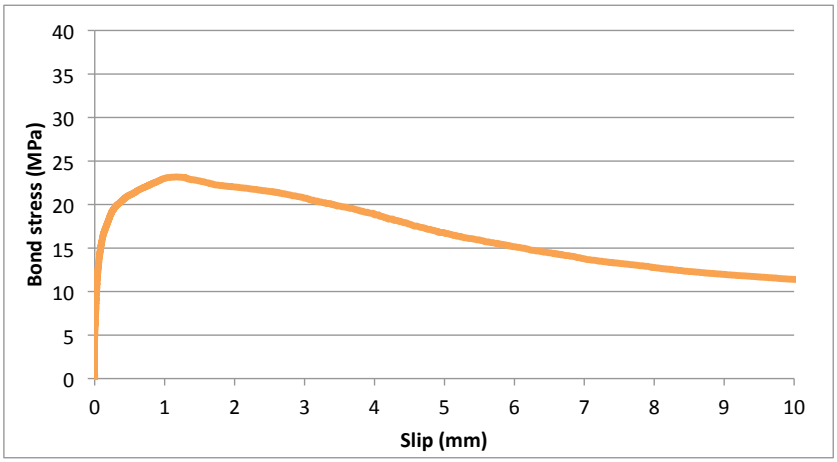

Specimen III L3 2

Descriptors		
Rebar diameter =	16	mm
Cover/Diameter =	5	
Fiber content =	60	kg/m3
Fiber type =	80_50	

Bond Parameters		
Bond strength =	25,08	MPa
Area A_peak =	25,58	mmMPa
Area A_80 =	120,00	mmMPa
Area A_50 =	249,00	mmMPa

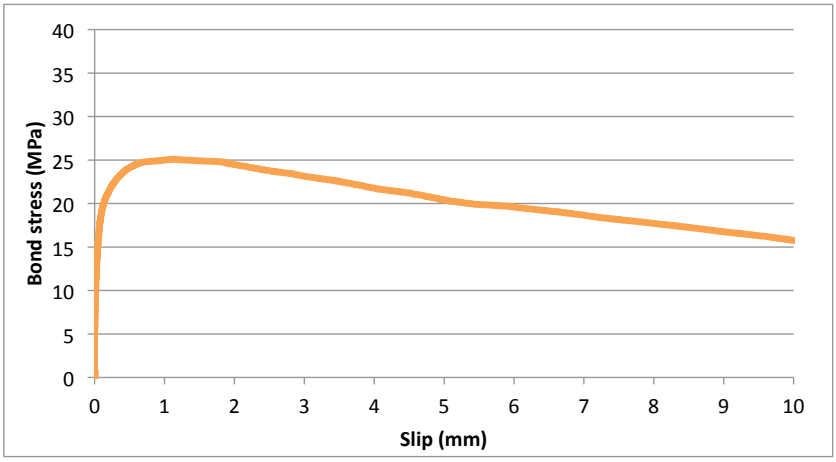

Specimen III L3 3

Descriptors		
Rebar diameter =	16	mm
Cover/Diameter =	5	
Fiber content =	60	kg/m3
Fiber type =	80_50	

Bond Parameters		
Bond strength =	17,60	MPa
Area A_peak =	14,55	mmMPa
Area A_80 =	50,10	mmMPa
Area A_50 =	100,00	mmMPa

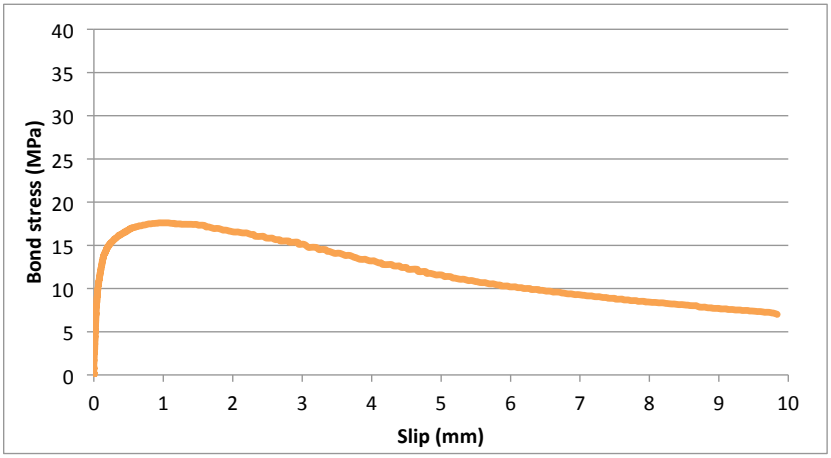

Specimen III L4 1

Descriptors		
Rebar diameter =	12	mm
Cover/Diameter =	5	
Fiber content =	0	kg/m3
Fiber type =	no fibers	

Bond Parameters		
Bond strength =	10,97	MPa
Area A_peak =	8,51	mmMPa
Area A_80 =	23,40	mmMPa
Area A_50 =	47,90	mmMPa

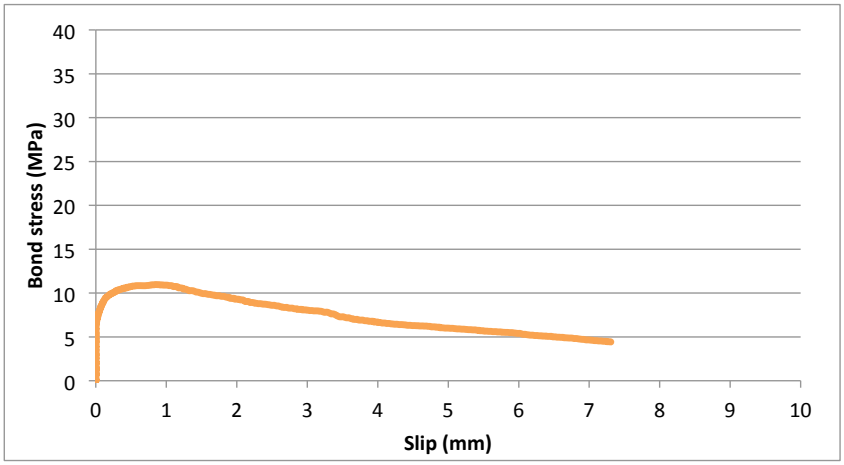

Specimen III L4 2

Descriptors		
Rebar diameter =	12	mm
Cover/Diameter =	5	
Fiber content =	0	kg/m3
Fiber type =	no fibers	

Bond Parameters		
Bond strength =	13,14	MPa
Area A_peak =	15,58	mmMPa
Area A_80 =	34,00	mmMPa
Area A_50 =	55,60	mmMPa

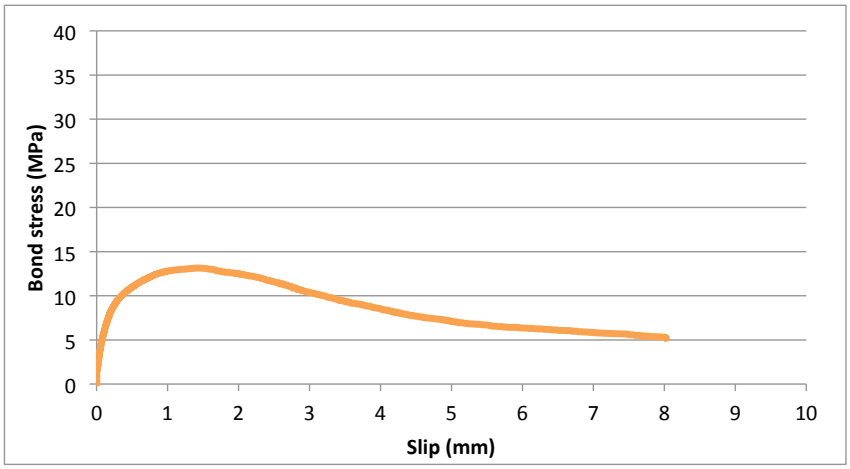

Specimen III L4 3

Descriptors		
Rebar diameter =	12	mm
Cover/Diameter =	5	
Fiber content =	0	kg/m3
Fiber type =	no fibers	

Bond Parameters		
Bond strength =	17,39	MPa
Area A_peak =	8,45	mmMPa
Area A_80 =	23,00	mmMPa
Area A_50 =	61,30	mmMPa

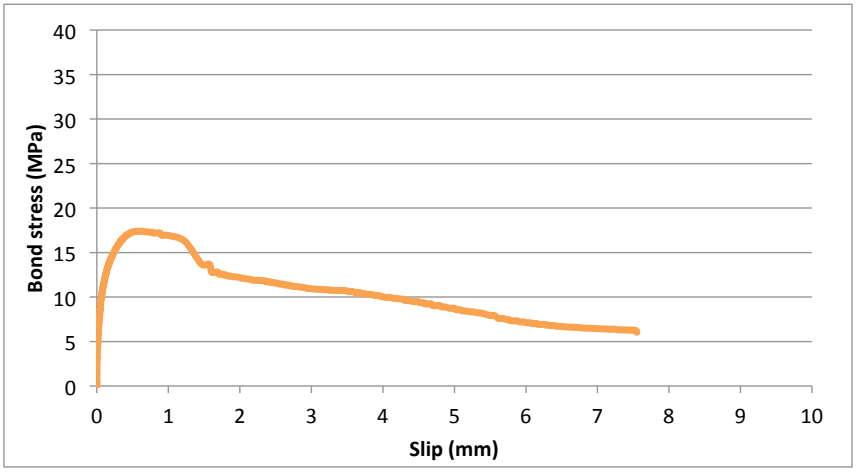

Specimen III L5 1

Descriptors		
Rebar diameter =	16	mm
Cover/Diameter =	2,5	
Fiber content =	40	kg/m3
Fiber type =	45_50	

Bond Parameters		
Bond strength =	17,91	MPa
Area A_peak =		mmMPa
Area A_80 =		mmMPa
Area A_50 =		mmMPa

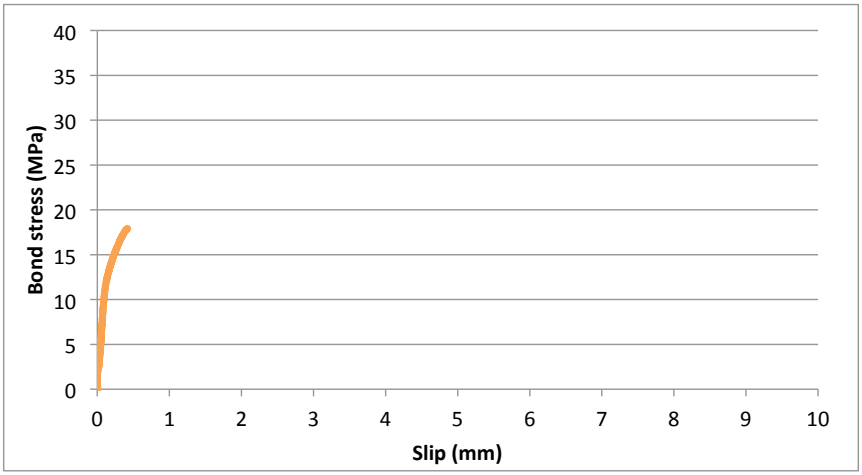

Specimen III L5 2

Descriptors		
Rebar diameter =	16	mm
Cover/Diameter =	2,5	
Fiber content =	40	kg/m3
Fiber type =	45_50	

Bond Parameters		
Bond strength =	19,19	MPa
Area A_peak =		mmMPa
Area A_80 =		mmMPa
Area A_50 =		mmMPa

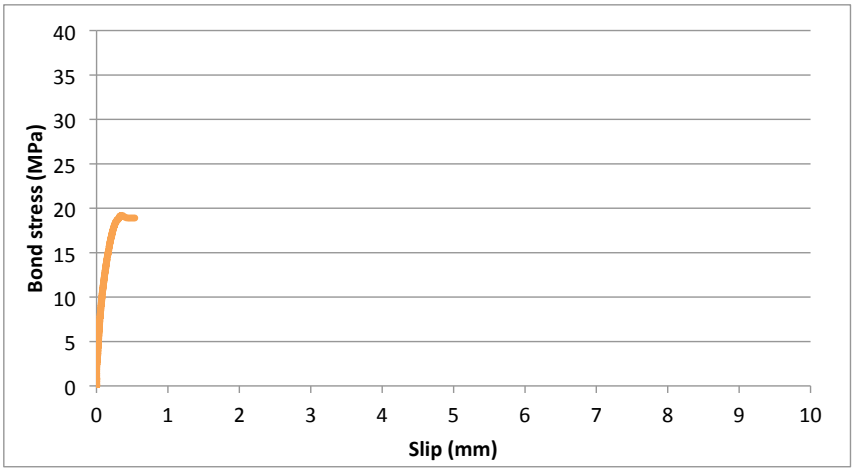

Specimen III L5 3

Descriptors		
Rebar diameter =	16	mm
Cover/Diameter =	2,5	
Fiber content =	40	kg/m3
Fiber type =	45_50	

Bond Parameters		
Bond strength =	19,52	MPa
Area A_peak =		mmMPa
Area A_80 =		mmMPa
Area A_50 =		mmMPa

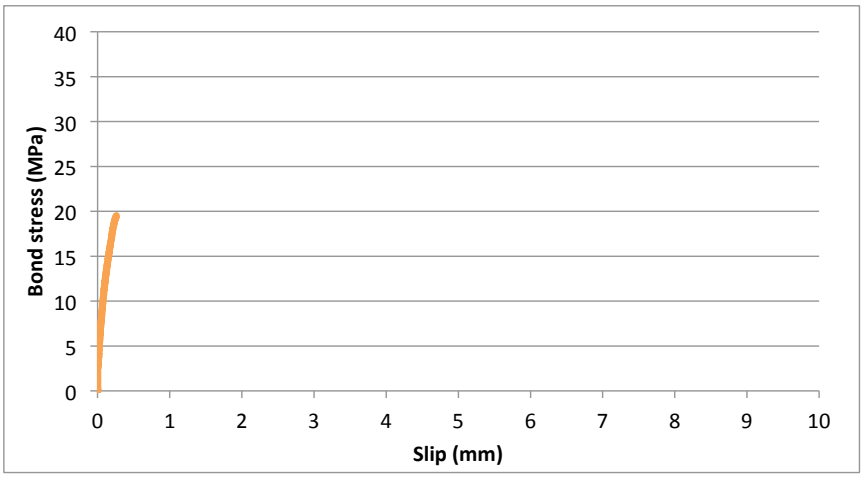

Specimen III L6 1

Descriptors		
Rebar diameter =	8	mm
Cover/Diameter =	3,5	
Fiber content =	60	kg/m3
Fiber type =	45_50	

Bond Parameters		
Bond strength =	21,85	MPa
Area A_peak =	14,15	mmMPa
Area A_80 =	40,60	mmMPa
Area A_50 =	77,70	mmMPa

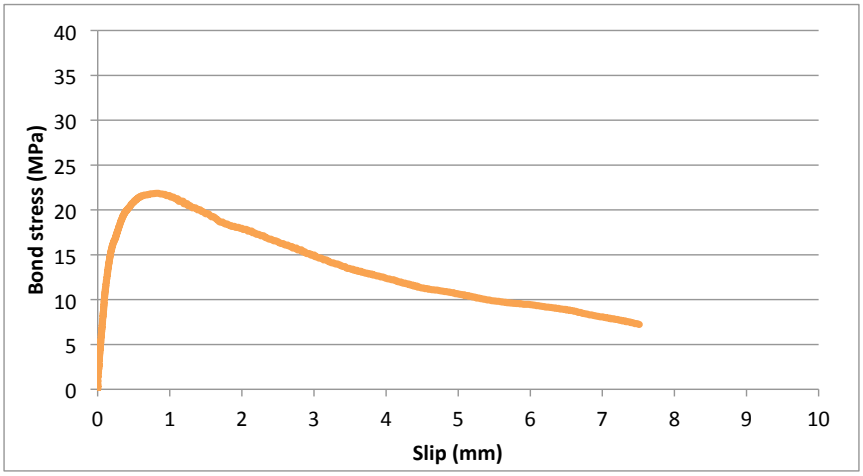

Specimen III L6 2

Descriptors		
Rebar diameter =	8	mm
Cover/Diameter =	3,5	
Fiber content =	60	kg/m3
Fiber type =	45_50	

Bond Parameters		
Bond strength =	20,03	MPa
Area A_peak =	14,94	mmMPa
Area A_80 =	33,90	mmMPa
Area A_50 =	84,50	mmMPa

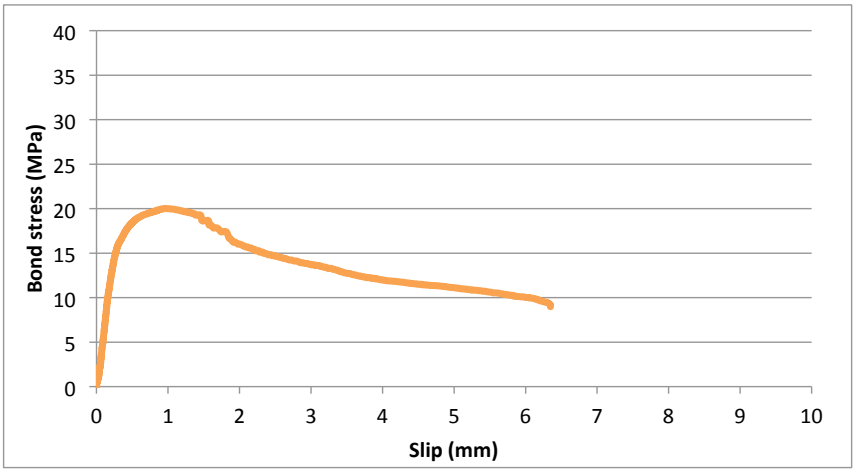

Specimen III L6 3

Descriptors		
Rebar diameter =	8	mm
Cover/Diameter =	3,5	
Fiber content =	60	kg/m3
Fiber type =	45_50	

Bond Parameters		
Bond strength =	24,11	MPa
Area A_peak =	12,84	mmMPa
Area A_80 =	28,40	mmMPa
Area A_50 =	66,10	mmMPa

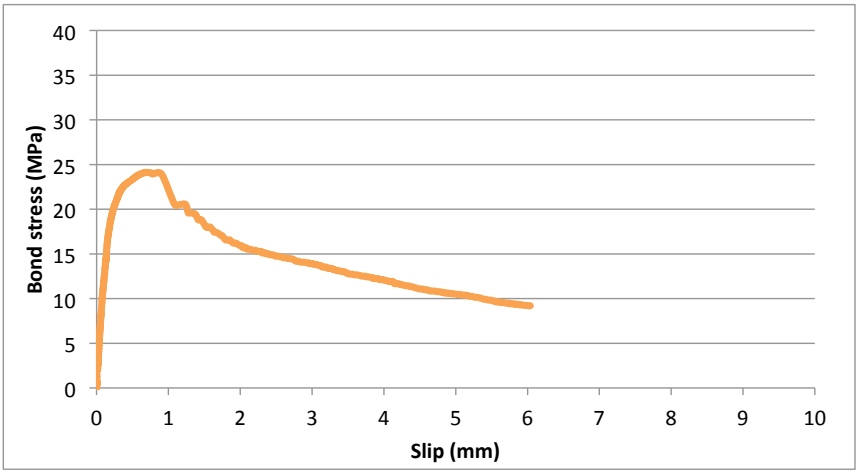

Specimen III L7 1

Descriptors		
Rebar diameter =	16	mm
Cover/Diameter =	3,5	
Fiber content =	0	kg/m3
Fiber type =	no fibers	

Bond Parameters		
Bond strength =	21,22	MPa
Area A_peak =	19,49	mmMPa
Area A_80 =	65,90	mmMPa
Area A_50 =	117,00	mmMPa

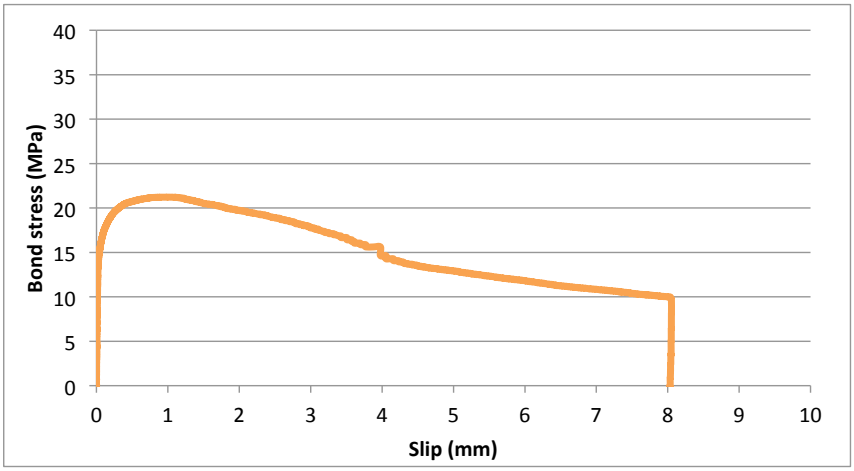

Specimen III L7 2

Descriptors		
Rebar diameter =	16	mm
Cover/Diameter =	3,5	
Fiber content =	0	kg/m3
Fiber type =	no fibers	

Bond Parameters		
Bond strength =	24,24	MPa
Area A_peak =		mmMPa
Area A_80 =		mmMPa
Area A_50 =		mmMPa

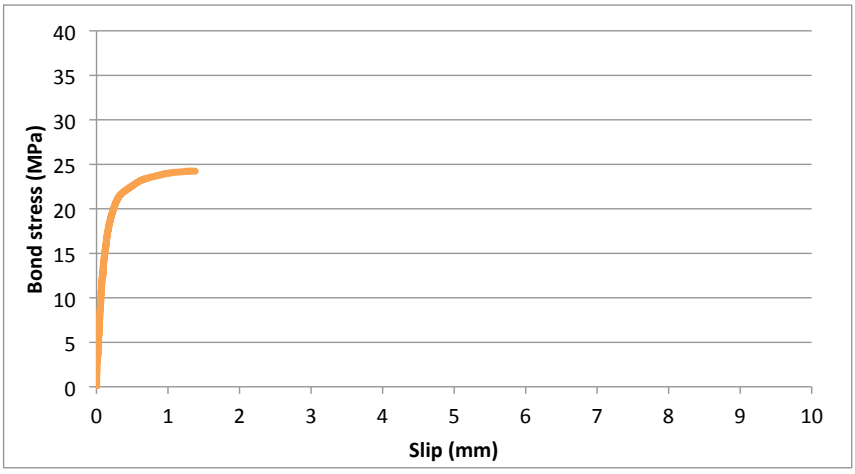

Specimen III L7 3

Descriptors		
Rebar diameter =	16	mm
Cover/Diameter =	3,5	
Fiber content =	0	kg/m3
Fiber type =	no fibers	

Bond Parameters		
Bond strength =	21,08	MPa
Area A_peak =	30,18	mmMPa
Area A_80 =	102,00	mmMPa
Area A_50 =	184,00	mmMPa

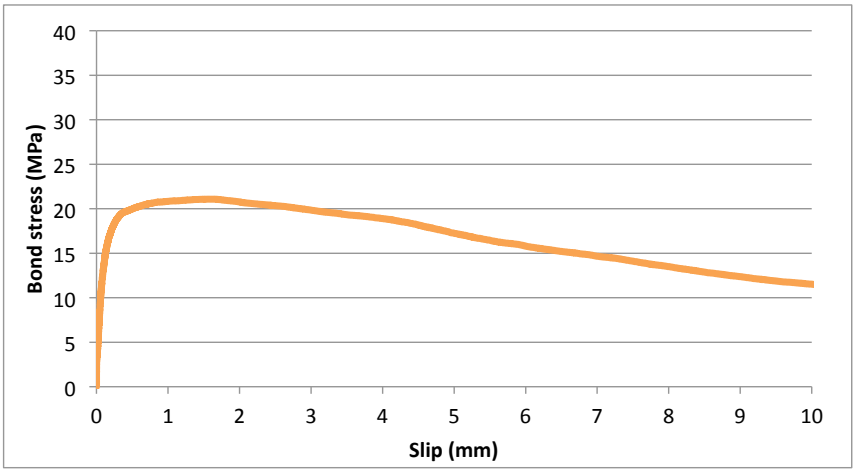

Specimen III L8 1

Descriptors		
Rebar diameter =	8	mm
Cover/Diameter =	5	
Fiber content =	40	kg/m3
Fiber type =	80_35	

Bond Parameters		
Bond strength =	10,41	MPa
Area A_peak =	4,97	mmMPa
Area A_80 =	22,50	mmMPa
Area A_50 =	35,90	mmMPa

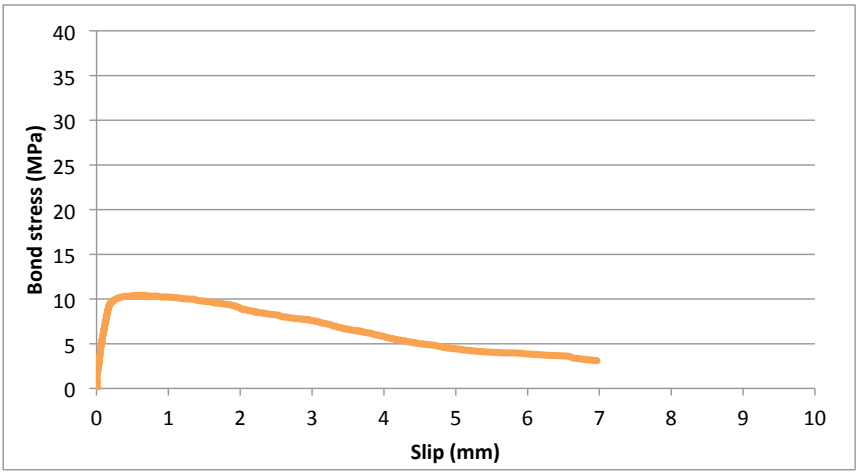

Specimen III L8 2

Descriptors		
Rebar diameter =	8	mm
Cover/Diameter =	5	
Fiber content =	40	kg/m3
Fiber type =	80_35	

Bond Parameters		
Bond strength =	10,99	MPa
Area A_peak =	5,27	mmMPa
Area A_80 =	18,40	mmMPa
Area A_50 =	29,40	mmMPa

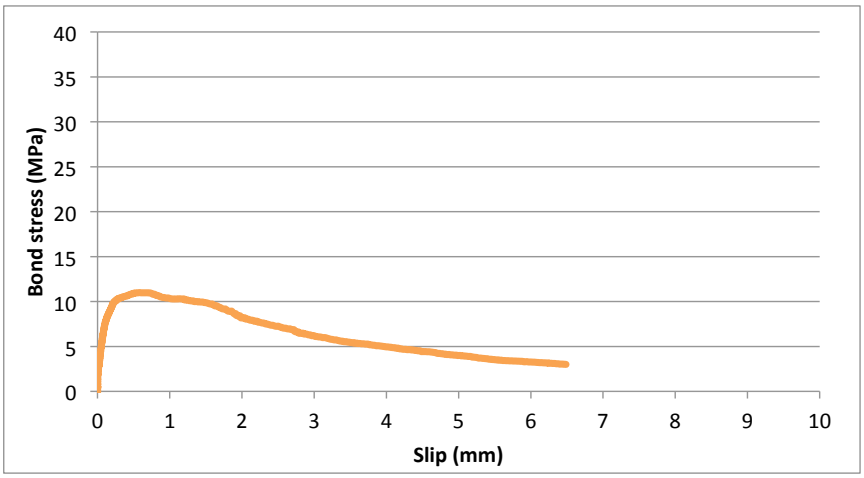

Specimen III L8 3

Descriptors		
Rebar diameter =	8	mm
Cover/Diameter =	5	
Fiber content =	40	kg/m3
Fiber type =	80_35	

Bond Parameters		
Bond strength =	20,70	MPa
Area A_peak =	15,70	mmMPa
Area A_80 =	45,40	mmMPa
Area A_50 =	97,00	mmMPa

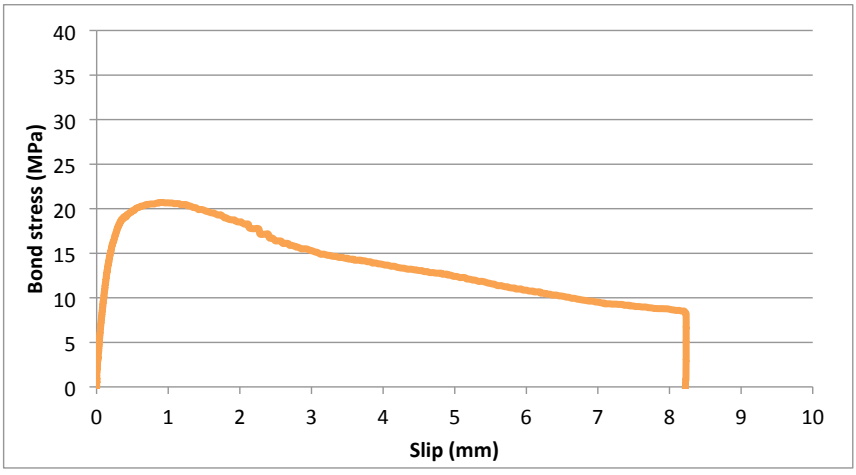

Specimen III L9 1

Descriptors		
Rebar diameter =	12	mm
Cover/Diameter =	2,5	
Fiber content =	60	kg/m3
Fiber type =	80_35	

Bond Parameters		
Bond strength =	20,15	MPa
Area A_peak =	23,05	mmMPa
Area A_80 =	61,70	mmMPa
Area A_50 =	120,00	mmMPa

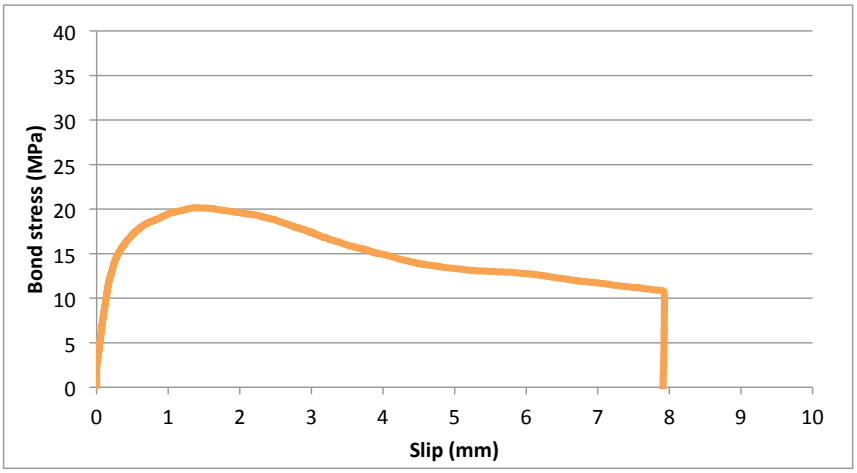

Specimen III L9 2

Descriptors		
Rebar diameter =	12	mm
Cover/Diameter =	2,5	
Fiber content =	60	kg/m3
Fiber type =	80_35	

Bond Parameters		
Bond strength =	21,66	MPa
Area A_peak =	26,46	mmMPa
Area A_80 =	60,90	mmMPa
Area A_50 =	123,00	mmMPa

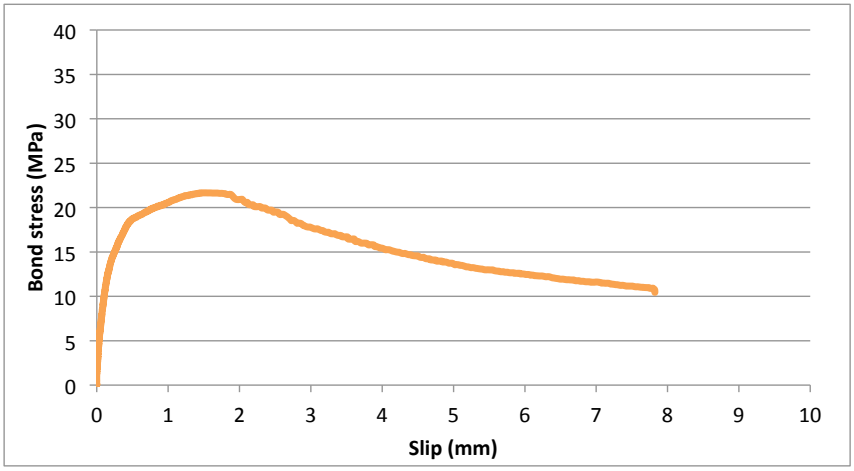

Specimen III L9 3

Descriptors		
Rebar diameter =	12	mm
Cover/Diameter =	2,5	
Fiber content =	60	kg/m3
Fiber type =	80_35	

Bond Parameters		
Bond strength =	21,14	MPa
Area A_peak =	17,81	mmMPa
Area A_80 =	72,20	mmMPa
Area A_50 =	124,00	mmMPa